A high-complexity lentiviral shRNA screen identifies synthetic lethal interactions with deregulated N-Myc in neuroblastoma cells

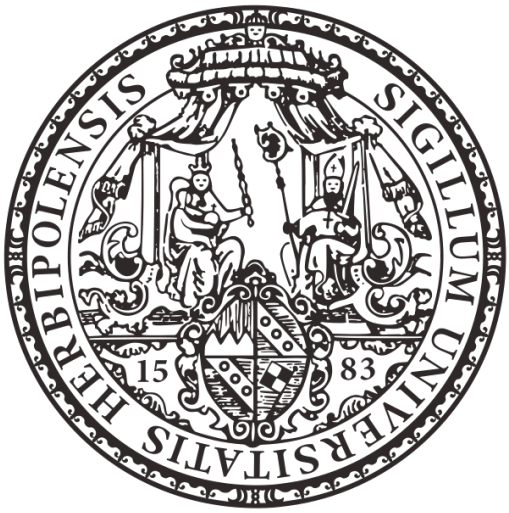

Dissertation zur Erlangung des
Naturwissenschaftlichen Doktorgrades
der Julius-Maximilians-Universität Würzburg

vorgelegt von

Jiajia Xu

aus Shanghai

Würzburg, 2014

Eingereicht am: _____

Mitglieder der Promotionskommission:

Vorsitzender: Prof. Dr. Markus Engstler

Erstgutachter: Prof. Dr. Martin Eilers

Zweitgutachter: Prof. Dr. Manfred Schartl

Tag des Promotionskolloquiums: _____

Doktorurkunde ausgehändigt am: _____

1 Introduction

1.1 Neuroblastoma

1.1.1 Clinical features of neuroblastoma

Neuroblastoma, the most common extracranial solid tumour in children, is derived from primordial neural crest cells that ultimately inhabit the sympathetic ganglia and adrenal medulla. It is associated with quite different patterns of clinical behaviour: life-threatening progression, maturation to ganglio-neuroblastoma or ganglioneuroma and spontaneous regression, so it is enigmatic and unpredictable (Westermann and Schwab, 2002).

Neuroblastomas have heterogeneous clinical hallmarks. At diagnosis, the age and stage are used to predict the development of disease. Tumour progression can vary widely according to anatomic stage and age. Generally, children diagnosed before the age of 1 year with localized disease are curable with surgery and almost no adjuvant therapy. Some of these tumours undergo spontaneous regression or differentiate to benign tumours. There is one distinct subset of infant patients who present an unique pattern of extensive disseminated disease but who reliably have spontaneous disease regression (stage 4S) (D'Angio et al., 1971). In contrast, the high-risk clinical prognostic factors of age over 18 months and advanced stage are closely associated with unfavorable biologic risk factors, including dedifferentiated histopathology, tumour amplification of the *MYCN* oncogene, and loss of heterozygosity of 1p and 11q, or other partial chromosome deletions (Mueller and Matthay, 2009). The 5-year event-free survival (EFS) rate for high-risk neuroblastoma is less than 50% (Cohn et al., 2009). Until recently, the best outcome reported for high-risk neuroblastoma was achieved with intensive combination induction chemotherapy and surgery, followed by myeloablative therapy with hematopoietic stem cell rescue, and then differentiation therapy with isotretinoin (Matthay et al., 1999), the first tumour-targeted therapy with demonstrated activity in neuroblastoma (Matthay et al., 2012).

1.1.2 Genetics of neuroblastoma

The majority of neuroblastoma cell lines show double minute chromosomes (DMs) or homogeneously staining regions (HSRs). Both cytogenetic characterizations represent DNA

amplification and deletions of the short arm of chromosome 1. Both gain and loss of genetic material are common during neuroblastoma evolution (Castel et al., 2007).

DNA content is significantly linked to tumour stage in infants. Diploidy occurs much more frequent in advanced tumour stages being associated with advanced tumour growth and significantly reduced survival probability while hyperdiploidy is mainly observed in low stage tumours of younger patients with a favorable clinical outcomes (Look et al., 1984).

In an analysis of 298 infants, hyperdiploidy mostly is closely associated with lower stage of disease and long-term survival whereas diploidy is always linked to advanced stages and treatment failure treatment. Additionally, in children of 12-24 months of age, diploidy predicted early failure of chemotherapy whereas half of the children with hyperdiploidy achieved long-term disease-free survival. Unfortunately, the DNA content lost its prognostic significance for patients over 2 years of age (Look et al., 1991).

There are four ploidy levels in neuroblastoma: near-diploid, near-triploid, near-tetraploid and near pentaploid tumours (Kaneko et al., 1987). Structural abnormalities and *MYCN* amplification are frequent in near-diploid and near-tetraploid tumours, most commonly involving chromosome 1p deletion. The near-triploid tumours are characterized by three almost complete haploid sets of chromosomes, with few structural abnormalities and were predominantly found in infants with favorable outcome. According to the clinical data, the near-pentaploid tumour patients like the near-triploid tumour patients had favorable clinical and biological factors and high survival rates. In contrast, patients who had either near-diploid or near-tetraploid tumours are always with unfavorable prognostic factors. These patients had always poor outcomes (Kaneko et al., 1987; Hayashi et al., 1989).

Segmental alterations play an important role in prognosis in neuroblastoma. A number of segmental chromosomal alterations have been reported, including deletions of chromosomes 1p, 3p, 4p and 11q, which are thought to harbour tumour suppressor genes, and gains of chromosomes 1q, 2p and 17q, harbouring putative oncogenes. A large number of these segmental alterations have been shown to be of prognostic impact in univariate analyses (Schleiermacher et al., 2012).

Apart from the frequently occurring segmental chromosome alterations such as 17q gains and 1p, 3p and 11q deletions, the discoveries of rare focal genomic imbalances targeting anaplastic lymphoma kinase (*ALK*) provided new insights into the pathogenesis of advanced neuroblastoma. ALK was originally identified as a fusion kinase in a subtype of non-Hodgkin's lymphoma (NPM-ALK) and more recently in adenocarcinoma of the lung (EML4-ALK). It is a

frequent target of genetic alteration in advanced neuroblastoma. Downregulation of ALK through RNA interference suppresses proliferation of neuroblastoma cells harbouring mutated ALK (Chen et al., 2008). Preclinical data support an oncogene addiction of neuroblastoma cells to mutated ALK and demonstrate that ALK inhibitory therapy strongly combats tumour models. Most recently, pediatric phase I testing has been completed for the first approved ALK inhibitor, Crizotinib, showing encouraging antitumoural results in neuroblastoma patient (Schulte et al., 2013).

1.1.2.1 *MYCN*-amplification in neuroblastoma

Amplified *MYCN* in neuroblastomas is a typical example of a proto-oncogene amplification. The amplification is present as either a homogeneously stained region or double minutes (Schwab et al., 1983). Double minutes means an extrachromosomal amplification of *MYCN* and homogeneously stained regions are located on different chromosomes, but not on 2p24 its resident site. Amplification ranges from 50 to 100 folds are generally observed in tumour, but the amplification of *MYCN* in neuroblastoma can range from 10 to 500 folds (Schwab et al., 2003).

There are no mutations found in *MYCN* coding sequence (Stanton et al., 1986). The tumourigenesis is probably initiated by increased expression of the wild-type protein by the amplification. Enhanced expression of wild-type N-Myc is able to transform cells experimentally (Schweigerer et al., 1990).

The proportion of tumours with amplified *MYCN* is about 20–30%, with variations between different studies. Amplified *MYCN* is found in stage 1, 2, 3, 4s, but not significant in stage 4 (Figure 1). In stage 4, *MYCN* amplification is not an important prognostic marker. In some studies, a significant difference has also been found in children with stage 4 tumours with a poor prognosis (Schwab et al., 2003).

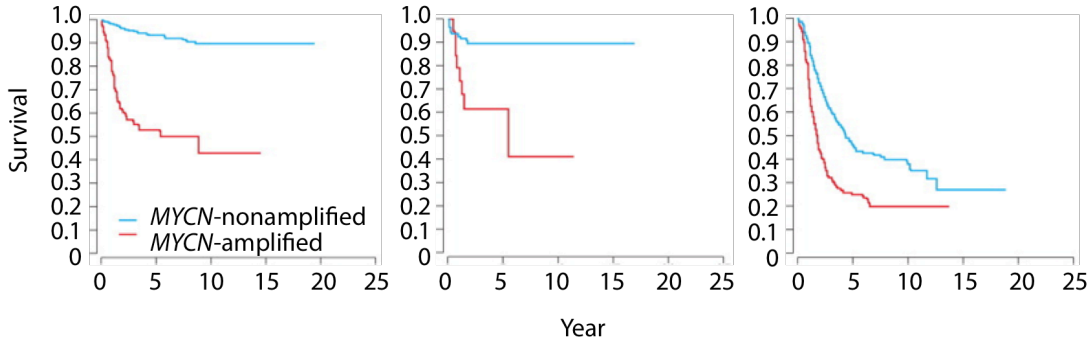

Figure 1: Stage-related overall survival by *MYCN* amplification in 1706 patients with neuroblastoma (Schwab et al., 2003).

Stage 1–3 disease (left). Stage 4s disease (middle). Stage 4 disease (right). p=0.01 for all curves.

1.2 N-Myc

1.2.1 N-Myc protein

N-Myc is a member of the Myc protein family, which are best known for their potent oncogenic activities and association with large numbers of human cancers. Research on Myc family protein reveals their transcriptional function and oncogenic activities. Myc proteins have broad effects on transcription, stimulating a large amount of genes contributing in the tumourigenesis (Hurlin, 2005).

MYCN was identified in 1983 in human neuroblastoma as an amplified gene homologous to *v-myc* but distinct from *c-Myc* (Kohl et al., 1983; Schwab et al., 1983). Both c-Myc and N-Myc are structurally highly homologous. They both heterodimerize with MAX at consensus E-box sequences (CACGTG) and have conserved regions for DNA-protein and protein-protein interactions.

N-Myc is distinct from c-Myc. Although a *Mycn* knock-in can compensate for a *c-Myc* knockout, knockout of either *c-Myc* or *Mycn* results in embryonic lethality at approximately E10.5-E11.5 (Charron et al., 1992; Davis et al., 1993; Sawai et al., 1993). Expression of N-Myc is tissue-specific during early developmental stages, unlike expression of c-Myc, which is more general. In mouse embryo ranging from 6.5 to 16.5 days of gestation, *Mycn*, but not *c-Myc*, is highly expressed. Once somitogenesis and neurulation have commenced, the *MYCN* gene

becomes increasingly restricted in its distribution of expression. Although *c-Myc* transcripts are present in many tissues at low levels, they are notably reduced or absent in neuroepithelium. A tissue like central nervous system (CNS) undergoing considerable proliferation retains high levels of *MYCN* mRNA. *MYCN* transcript levels are highest in the CNS, cranial and spinal ganglia in the peripheral nervous system (PNS) and heart. In the developing brain, there is a notable absence of N-Myc expression in the roof plate neuroepithelium overlying the mesencephalon. *MYCN* transcripts are also found in several epithelial cell types during embryogenesis including developing gut, kidney and lung. The forming gut comprises two cell types of endodermal origin: epithelial cells lining the inner lumen of the intestine and the surrounding mesenchyme. *MYCN* transcripts are found in the inner cells corresponding to the lumen whereas *c-Myc* transcripts are present in the surrounding mesenchyme. *MYCN* transcripts are also present in the luminal cells of branching lung epithelium that later form bronchioles whereas *c-Myc* transcripts are confined to the surrounding connective mesenchymal cells (Stanton et al., 1992).

MYCN is highly expressed in immature cells of newborn mice and reduced in differentiated adult tissues, which is consistent with the finding that differentiation of neuroblastoma cells is associated with reduced *MYCN* expression (Matsumoto et al., 1989; Cinatl et al., 1993). A decrease in *MYCN* expression precedes the retinoic acid (RA)-induced morphological differentiation in human neuroblastoma. Retinoic acid can inhibit neuroblastoma cell growth and clonability and induce extensive neurite outgrowth. They found a decreased level of *MYCN* expression within 6 hours of RA treatment which proceeded both cell cycle arrest and morphological differentiation (Thiele et al., 1985). N-Myc can directly block differentiation pathways and maintain pluripotency (Wakamatsu et al., 1997; Kang et al., 2006). Mice with conditional deletion of *MYCN* in neural progenitor cells show decreased brain size and a substantial increase in neuronal differentiation compared to control mice. The reason is that cyclin-dependent kinase inhibitor p27, which plays a role in differentiation and is normally degraded by E3 ubiquitin ligase SKP2, a N-Myc transcriptional target, is increased in *MYCN* null neural progenitor cells (Casaccia-Bonnefil et al., 1997; Gomez-Casares et al., 2013).

N-Myc and c-Myc have roles in maintaining pluripotency, which were proved in a study of medulloblastoma (Nakagawa et al., 2010; Varlakhanova et al., 2010). When *MYCN* or *c-Myc* were misexpressed in cerebellar granule neural precursors (GNPs) dependent on SHH signalling for survival, N-Myc promotes an expected SHH-driven malignancy, whereas c-Myc transforms these cells to a SHH-independent lineage (Kawauchi et al., 2012; Pei et al., 2012; Roussel and

Robinson, 2013). These data show that N-Myc can transform cells in a committed lineage while c-Myc enable to reprogram to a distinct lineage. Additionally, c-Myc can drive cancer stem cell functionality and enable reprogramming down a distinct lineage. It is likely that N-Myc has this function as well. Swartling et al showed that co-expression of SOX9 with *MYCN* in cerebellar stem and progenitor cells could drive self-renewal, whereas neither SOX9 nor *MYCN* could drive self-renewal individually (Swartling et al., 2012).

1.2.2 N-Myc in neuroblastoma

1.2.2.1 Proliferation and cell cycle

Promoting proliferation and cell cycle progression are the best characterized tumourigenic effect of N-Myc. Myc proteins have been implicated in progression through G1 to S-phase of the cell cycle by cooperating with RAS to induce Cyclin D/CDK4 or Cyclin E/CDK2 complexes that phosphorylate and inactivate Rb proteins, activating E2F transcription factors to induce S-phase (Farrell and Sears, 2014). *RAS* signalling stabilizes Myc proteins by activating AKT, which phosphorylates and blocks glycogen synthase kinase 3ß (GSK-3ß)-mediated degradation of Myc protein. This can further lead to cell cycle progression. Therefore, Yaari et al reported that blockade of *RAS* signalling can induce growth arrest in *MYCN*-amplified neuroblastoma cells (Yaari et al., 2005). mTOR signals, downstream of the RAS/PI3K/AKT pathway, have essential functions in translational control, impacting metabolism, proliferation and tumourigenesis. Allosteric blockade of mTOR with rapamycin or CCI-779 displayed a more pronounced antiproliferative effect in *MYCN*-amplified than in *MYCN*-nonamplified neuroblastoma tumours. Additionally, allosteric mTOR inhibitors also suppressed expression of Cyclin D1 (Johnsen et al., 2008).

Specifically, *MYCN*-amplified neuroblastoma cells show an inability to arrest in G1 in response to irradiation and DNA damage, possibly via down-regulation of p53 induced nuclear protein 1 (TP53INP1) and up-regulation of both CDK4 and SKP2, allowing CDK2 to escape p21 inhibition (Tweddle et al., 2001; Bell et al., 2007; Ma et al., 2010; Muth et al., 2010; Gogolin et al., 2013).

Furthermore, N-Myc upregulation of checkpoint kinase 1 (CHK1) which is an important regulator of S-phase and G2/M checkpoints, has been suggested as a mechanism through which *MYCN*-amplified neuroblastoma becomes refractory to standard chemotherapy (Cole et al.,

2011). Inhibition of CHK1 promoted chemosensitization in various types of tumour cells (Blasina et al., 2008; Zhang et al., 2009).

Generally, N-Myc directly represses expression of anti-proliferative proteins and stimulates genes that drive proliferation. N-Myc represses Dickkopf-1, which disrupts the WNT/ß-catenin signalling pathway (Koppen et al., 2007), CDKL5 which arrests cells between G0/G1 phase (Valli et al., 2012). Additionally, minichromosome maintenance (MCM) gene is also a downstream target of N-Myc, which is responsible for DNA elongation and unwinding during the replication process (Koppen et al., 2007).

1.2.2.2 Apoptosis

N-Myc activates both proliferation and apoptosis (Evan et al., 1992). Loss of caspase-8 function in neuroblastoma has been thought to be a mechanism of apoptosis evasion in *MYCN*-amplified neuroblastoma (Teitz et al., 2000; Gonzalez-Gomez et al., 2003; Iolascon et al., 2003). Multiple groups have reported methylation of the promoter of caspase-8 (Casciano et al., 2004; Banelli et al., 2005; Lazcoz et al., 2006), although Fulda et al did not find correlation between caspase-8 expression and risk in neuroblastoma (Fulda et al., 2006). Loss of caspase-8 promotes resistance to tumour necrosis factor-related ligand-induced apoptosis (Eggert et al., 2001).

Additionally, *MYCN*-amplified neuroblastoma could survive via constitutive activation of prosurvival signalling cascades, such as tropomyosin receptor kinase B (TRKB). TRKB expression levels are low in *MYCN*-nonamplified neuroblastoma but high in *MYCN*-amplified neuroblastoma (Nakagawara et al., 1994). Activation of TRKB is implicated in resistance to chemotherapy and can up-regulate *MYCN* mRNA (Ho et al., 2002; Dewitt et al., 2014). However, N-Myc appears to down-regulate tropomyosin receptor kinase A (TRKA) which is normally found in low-risk neuroblastoma, recruiting HDAC1 to the *TRKA* promoter to induce a repressed chromatin state (Iraci et al., 2011).

Moreover, N-Myc induces p53-dependent apoptosis (Elson et al., 1995; Chesler et al., 2008). p53 mutations are not often found in neuroblastoma suggesting that N-Myc perhaps cooperates with a p53 suppressor like MDM2. Contrastly, p53 mutations or mutations in p53-dependent apoptosis pathway occur commonly in neuroblastoma at relapse which is consistent with the opinion that these mutations driving therapy-resistant disease and probably arise in response to cytotoxic chemotherapy (Slack et al., 2005).

MDM2 is an E3 ubiquitin ligase that targets p53 and also stabilizes the *MYCN* mRNA by binding to the 3'UTR of *MYCN* (Gu et al., 2012). N-Myc can promote transcription of *MDM2* and *p53* (Figure 2), which presents conflicting sensitivities to chemotherapy in *MYCN*-amplified neuroblastoma. Usually, *MYCN*-amplified neuroblastomas respond initially to chemotherapy and p53 apoptosis is induced. Then, these tumours relapse and become resistant through chemotherapy-induced p53 mutations (Slack et al., 2005; Chen et al., 2010).

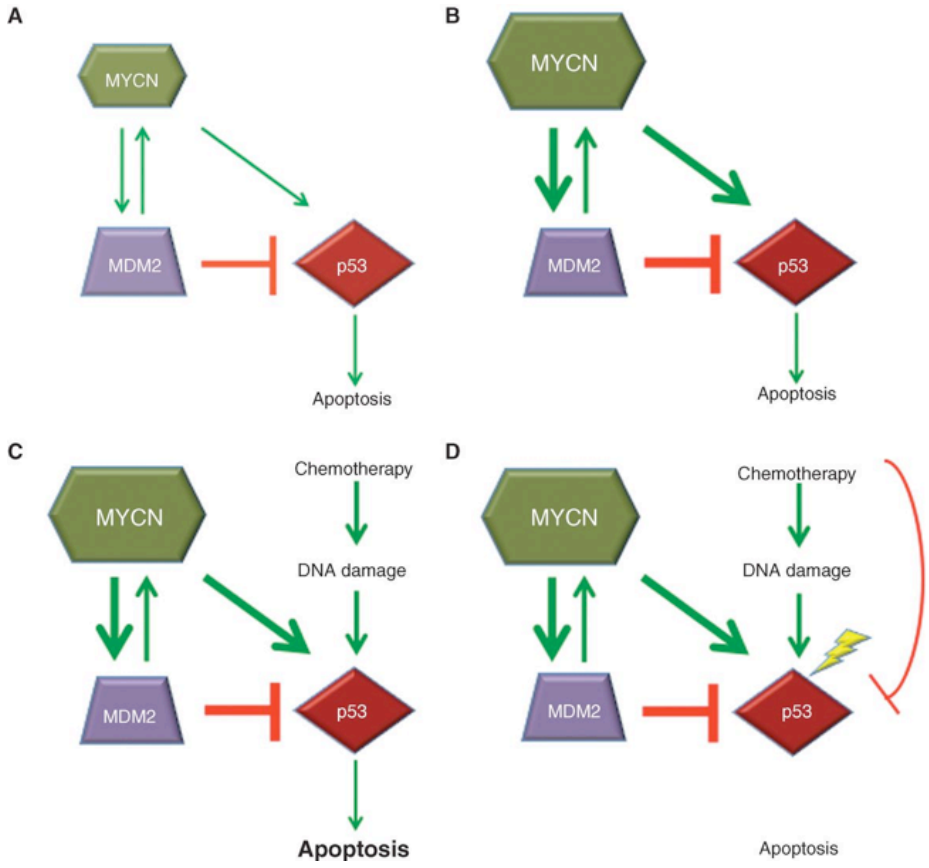

Figure 2: Amplified *MYCN* marks chemoresistance in patients with neuroblastoma (Huang and Weiss, 2013).

(A, B) Amplified *MYCN* results in elevated transcription of MDM2 and p53. High levels of p53 sensitize tumours to apoptosis.

(C) Patients initially respond to chemotherapy as p53 triggers apoptosis.

(D) At relapse, tumours show mutation in p53 or p53 pathways, resulting in therapy resistance.

1.2.2.3 Self-renewal and pluripotency

Neuroblastoma is thought to arise from neural crest cells, which possess the characteristics of self-renewal and multipotency. N-Myc is likely involved in the regulation of both traits, as N-Myc can substitute for c-Myc in reprogramming fibroblasts into induced pluripotent stem cells (iPS) cells. Both c-Myc and N-Myc promote a stem-like state, likely because of blockade of differentiation pathways and expression of self-renewal and pluripotency factors (Nakagawa et al., 2010).

Upregulation of endodermal and mesodermal markers of differentiation such as BMP4, GATA6, as well as activators of lymphocytic differentiation such as STAT1, EFR1, ELK3 were found in *c-Myc* and *Mycn* deleted mouse ESCs suggesting that Myc proteins repress differentiation pathways. Additionally, N-Myc up-regulates expression of the polycomb and self-renewal protein BMI1 in neuroblastoma by directly binding to the E-Box sites within the promoter of *BMI1* (Ochiai et al., 2010; Varlakhanova et al., 2010; Huang et al., 2011). Furthermore, N-Myc mediated expression of *DLL3*, a Notch1 ligand, has been described as a mechanism to maintain neural stem cell fate (Zhao et al., 2009). Lastly, the finding that *MYCN*-amplified neuroblastoma cell lines tend to undergo symmetric cell division whereas *MYCN*-nonamplified lines preferentially divided asymmetrically is a further support for N-Myc promoting self-renewal (Izumi and Kaneko, 2012).

N-Myc also up-regulates the pluripotency genes *KLF2*, *KLF4* and *LIN28B*. Conversely, *c-Myc* and *Mycn* knock-out mESCs also lost expression of the pluripotency marker SSEA-1, although other markers like NANOG, OCT4 and REX-1 were not affected significantly (Varlakhanova et al., 2010).

1.2.2.4 Metastasis

Metastasis occurs in about 50% of neuroblastoma patients at diagnosis (Maris et al., 2007) with frequent spread to bone marrow (70%), bone (55%), lymph nodes (30%), liver (30%) and brain (18%) (DuBois et al., 1999). *MYCN* level correlates with invasive and metastatic behavior. N-Myc contributes to all aspects of metastasis: adhesion, motility, invasion and degradation of surrounding matrices (Zaizen et al., 1993; Benard, 1995; Goodman et al., 1997).

As mentioned above, caspase-8 has been associated mostly with promoting apoptosis, caspase-8 has also a paradoxical role in both promoting and inhibiting metastasis in neuroblastoma depending on cellular context. It has been observed that incidence of spontaneous metastasis is

significantly higher in primary neuroblastoma tumours without caspase-8. NB7 neuroblastoma cell lines with ectopic expression of caspase-8 eventually lost expression of caspase-8 at site of dissemination (Stupack et al., 2006). The lack of caspase-8 triggered integrin-mediated death, a mechanism of apoptosis in cells that have detached from the extracellular matrix and unligated their integrins (Stupack et al., 2001). In the TH-*MYCN* mouse model of neuroblastoma, deletion of caspase-8 did not affect apoptosis, but instead, increased significantly the incidence of metastasis specifically to the bone marrow, possibly caused by upregulation of genes involved in epithelia-mesenchymal-transition (EMT), decreased cell adhesion and increased fibrosis (Teitz et al., 2013).

Additionally, N-Myc-directed downregulation of integrins α1 and ß1 promotes detachment from the extracellular matrix and allow cells to migrate and invade (van Golen et al., 2003; Tanaka and Fukuzawa, 2008). The miR-9 directly targets and suppresses E-cadherin mRNA leading to increased cell motility and invasiveness. Expression of miR-9 is activated by c-Myc and N-Myc, both of which directly bind to the miR-9-3 locus. In human cancer, miR-9 levels correlate with *MYCN* amplification, tumour grade and metastatic status (Ma et al., 2010).

1.2.3 Targeting N-Myc in neuroblastoma

A targeted molecular approach to therapy for the treatment of specific cancers has been widely used (Traxler et al., 2001). However, the pharmacologic inactivation of N-Myc must be achieved in the presence of a background of high-level overexpression associated with gene amplification. Therefore, the ability to target *MYCN* with antisense (AS) oligonucleotides *in vitro* and *in vivo* was examined by Brukhart et al. They found that IMR-32 cells treated with AS oligonucleotides displayed reduced *MYCN* protein and cell proliferation relative to controls; transgenic mice treated with AS oligonucleotides had lower tumour incidence compared to control mice (Burkhart et al., 2003). Although antisense inhibition of *MYCN* expression *in vitro* was shown to decrease neuroblastoma proliferation and promote neuronal differentiation, major clinical limitation of conventional antisense oligonucleotides is that they are rapidly degraded by nucleases (Negroni et al., 1991).

However, the development of inhibitors targeting N-Myc is very challenging, as N-Myc protein is a basic helix-loop-helix zipper protein without obvious surfaces for small molecule binding. There are four suggestions for direct or indirect targeting N-Myc reviewed in Weiss and Huang (Huang and Weiss, 2013).

First, epigenetic regulatory proteins like acetyl-lysine binding motif bromodomains, which activate N-Myc could be targeted. Acetylation marks are placed in the regions of active transcription facilitated by histone acetyltransferases. The recognition of acetylation marks is mediated by bromodomains, e.g BRD2-4 which are the members of bromodomain and extraterminal subfamily (BET). BRD 2-4 mediate the interactions with chromatin-remodeling complex SWI/SNF and pTEFb (Puissant et al., 2013; Sabo and Amati, 2014). N-Myc recruits pTEFb to release RNA polymerase II promoting transcription. BRD2-4 inhibitor JQ1 was shown to block Myc targets and a Myc-dependent malignancy (Delmore et al., 2011). JQ1 also suppresses the growth of *MYCN*-amplified neuroblastoma. Mice treated with JQ1 show a significant increase in survival rate. The treated tumours showed increased apoptosis and decreased proliferation. N-Myc can silence tumour suppressor genes by elevating expression of HDAC, suggesting a possible therapeutic option of HDAC inhibitors. Using HDAC inhibitors in TH-*MYCN* model of neuroblastoma has obtained promising results in several preclinical studies (Delmore et al., 2011; Puissant et al., 2013).

Second, N-Myc is degraded by the proteasome after a series of sequential phosphorylation events, so targeting regulators of protein stability is also an option. Initially, N-Myc is phosphorylated at S62 by CDK1 (Sjostrom et al., 2005). Then, N-Myc is phosphorylated at T58 via GSK-3ß (Pulverer et al., 1994), and dephosphorylation of S62 via PP2A a phosphatase sensitizes T58 phosphorylated N-Myc to bind FBW7 resulting in ubiquitination and proteasomal degradation (Sears et al., 2000; Welcker et al., 2004; Yada et al., 2004). PI3K drives an inhibitory phosphorylation on GSK-3ß, thereby, inhibition of PIK3 could indirectly promote the N-Myc phosphorylation (Figure 3) (Gustafson and Weiss, 2010). Aurora A from a shRNA screen of genes highly expressed in *MYCN*-amplified tumours was proved important for N-Myc stabilization. Aurora A binds to N-Myc and prevents FBW7-mediated proteasomal degradation of N-Myc. Aurora A has a ligand binding sites for small molecule inhibitors, so targeting Aurora A became a strategy to treat *MYCN*-amplified tumours. However, the ability of Aurora A to stabilize N-Myc has been shown to be independent of kinase activity (Otto et al., 2009). Brockmann et al showed that two Aurora A inhibitors, MLN8054 and MLN8237 (currently in phase 2 clinical evaluations for childhood neuroblastoma), disrupt the Aurora A/N-Myc complex and promote degradation of N-Myc mediated by the FBW7 ubiquitin ligase. Disruption of Aurora A/N-Myc complex inhibits N-Myc-dependent transcription, correlating with tumour regression and prolonged survival in a mouse model of *MYCN*-driven neuroblastoma. Aurora A forms a complex with N-Myc and leads to N-Myc stabilization so that N-Myc does not get phosphorylated by Cyclin B/CDK1 and degraded during mitosis suggesting a stabilizing activity

of Aurora A recruitment. Both inhibitors are allosteric drugs, disrupt the Aurora A/N-Myc complex and inhibit the kinase activity of Aurora A to promote entry into mitosis (Brockmann et al., 2013).

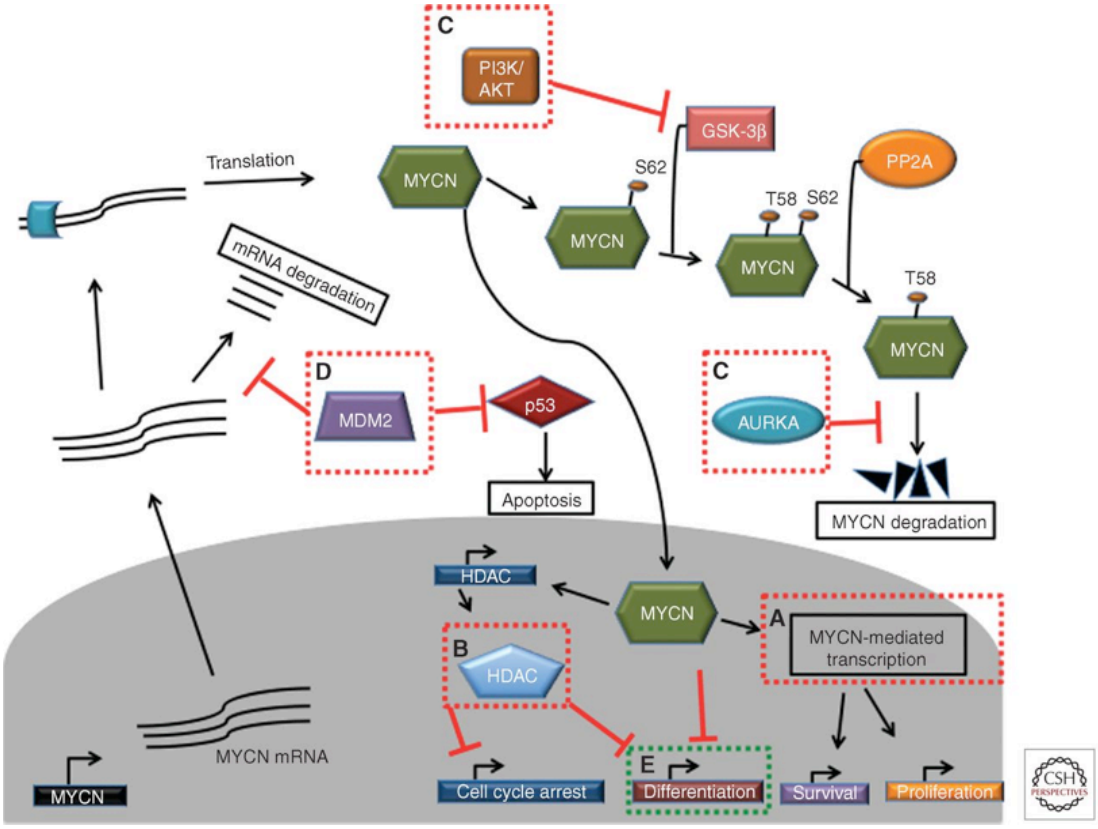

Figure 3: Therapeutic strategies to target *MYCN* in neuroblastoma. Possible strategies to treat *MYCN*-amplified neuroblastoma patients include (Huang and Weiss, 2013).

(A) blocking *MYCN*-dependent transcription with BET-bromodomain inhibitors,

(B) inhibiting HDACs,

(C) antagonizing proteins involved in stabilizing *MYCN* protein,

(D) suppressing MDM2 (which stabilizes *MYCN* mRNA and disrupts p53-mediated apoptosis), and (E) inducing differentiation.

Third, targeting p53-dependent apoptosis is also an option for therapy. Inhibition of MDM2 is supposed to have two effects on *MYCN*-amplified neuroblastoma. First, *MYCN* mRNA is destabilized via MDM2 silencing because MDM2 binding to 3'UTR of *MYCN* could stabilize *MYCN* mRNA (Gu et al., 2012). Second, p53 is increased with decreased MDM2 level, which increases the possibility of p53-dependent apoptosis.

Fourth, neuroblastoma is originated from immature neural crest cells, so they are less differentiated and more proliferative. Triggering differentiation in these cells could reduce

proliferation and increase apoptosis. So targeting differentiation is also an option for therapy (Huang and Weiss, 2013).

1.3 Synthetic lethality

1.3.1 The concept of synthetic lethality

The development of safe and effective anticancer drugs is still a challenge. Most of the chemotherapeutic agents used today have low therapeutic indices and narrow therapeutic windows. Most anticancer drugs in use were discovered based on their ability to kill rapidly dividing cancer cells *in vitro*. Many of these drugs also injure rapidly dividing normal cells, such as bone-marrow haematopoietic precursors and gastrointestinal mucosal epithelial cells. Additionally, many of these drugs are toxic to normal cells that are not rapidly dividing, e.g. doxorubicin (toxic to the heart), bleomycin (toxic to the lung) and cytarabine (toxic to the cerebellum) (Kaelin, 2005). So the dose-settings of these drugs become quite important and difficult to avoid organ damage. Altogether, it is imperative to develop anticancer drugs that can kill cancer cells at clinically achievable concentrations with therapeutic indices that are higher than those of classic cytotoxic agents. There are two ways to design new anticancer drug. The first is to find drug targets that are essential for the viability of cancer cells but not present in normal cells. The second is to achieve enhanced cancer-cell selectivity. This implies the requirement for a particular target, which is enhanced in the context of cancer cells compared to normal cells. The requirement for a particular target might be increased because of changes that are significant to the cancer cell, e.g. genetic changes (Kaelin, 2005).

Therefore, a conceptual framework for the development of cancer-specific cytotoxic agents mentioned above is provided by synthetic lethality (Hartwell et al., 1997; Friend and Oliff, 1998; Kaelin, 1999). Two genes *A* and *B* are synthetic lethal if mutation of either gene alone is compatible with viability while the simultaneous mutation of both genes causes death (Figure 4) (Guarente, 1993; Friend and Oliff, 1998; Hartman et al., 2001; Kamb, 2003). This means that simultaneous mutations of two genes impair cellular fitness more than mutation of either gene alone. Gene *A* can buffer the consequence of defects in gene *B* and vice-versa, whereas this buffering effect is lost when both genes are mutated (Hartman et al., 2001; Kamb, 2003; Sharom et al., 2004). Loss-of-function alleles are most commonly described by synthetic lethal

interactions, but gain-of-function alleles can also be involved. The concept of synthetic lethality is a good approach to choose anticancer drug targets. For example, the protein product of a gene synthetic lethal to known cancer-causing mutations, which is druggable, could be potentially an excellent target for anticancer therapy. Many cancer-related mutations carry a loss of function, so it is quite unclear how to pharmacologically approach these cancer cells containing mutation of tumour suppressor genes. Therefore, targeting a protein that is synthetic lethal to such loss-of-function protein is quite efficient. Moreover, the selectivity of drug by inhibiting protein, which is important for cellular homeostasis is quite difficult to achieve. If *A* and *B* are synthetic lethal, inhibition of *B* should selectively kill cancer cells with *A* mutation. Ideally, inhibition of *B* should have no effect on normal cells while even partial inhibition of *B* in cancer would cause death because of mutant *A*. In the cancer cell context, a mutation may increase the dependency of *B* for cell fitness so that keeping *B* activity below a certain threshold selectively impairs cells with A mutation (Kaelin, 2005).

Gene A	Gene B	
A	B	Viable
a	B	Viable
A	b	Viable
a	b	Lethal

Figure 4: The concept of synthetic lethality

Two genes *A* and *B* are synthetic lethal if mutation of either gene alone is compatible with viability but simultaneous mutation of both genes causes death.

1.3.2 *Myc* synthetic lethal genes

In 2004 Wang et al showed that the agonists of the TRAIL death receptor DR5 potently induce apoptosis in human cells overexpressing the Myc oncogene, both *in vitro* and as tumour xenografts *in vivo*. Myc sensitizes cells to DR5 in a p53-independent manner by up-regulating

DR5 cell surface levels and stimulating autocatalytic processing of procaspase-8. These results identify a mechanism by which Myc sensitizes cells to apoptosis and validate DR5 agonists as potential Myc-selective cancer therapeutics (Wang et al., 2004).

In 2005 Rottmann et al published that they identified glycogen synthase kinase 3ß (GSK3ß) by screening a kinase-directed library of small inhibitory RNAs whose inactivation potentiates TNF-related apoptosis-inducing ligand (TRAIL) death receptor-mediated apoptosis specifically in Myc-overexpressing cells. Knockdown of GSK3ß prevents phosphorylation of Myc on T58, thereby inhibiting recognition of Myc by the E3 ubiquitin ligase FBW7. Attenuating the GSK3ß-FBW7 axis results in stabilization of Myc, upregulation of surface levels of TNF-related apoptosis-inducing ligand death receptor 5 (DR5), the potentiation of DR5 induced apoptosis *in vitro* and *in vivo*. These results identify GSK3ß and FBW7 as potential cancer therapeutic targets and Myc as a critical substrate in the GSK3ß survival-signalling pathway (Rottmann et al., 2005).

Molenaar et al detected in 2009 a synthetic lethal relationship between CDK2 inhibition and N-Myc indicating CDK2 inhibitors as potential *MYCN*-selective cancer therapeutics. They found after CDK2 silencing *MYCN*-induced apoptosis was accompanied by nuclear stabilization of p53. Silencing of p53 rescued the cells from Myc-driven apoptosis (Molenaar et al., 2009).

In the following year Yang et al reported that a circumscribed exposure to the aurora kinase inhibitor VX-680 selectively killed cells overexpressing Myc. This synthetic lethal interaction results from inhibition of Aurora B kinase, with consequent disabling the chromosomal passenger protein complex (CPPC) and ensuing DNA replication in the absence of cell division, executed by sequential apoptosis and autophagy, not reliant on the tumour suppressor p53 (Yang et al., 2010).

In 2012 Liu et al published that oncogenic levels of Myc established a dependence on AMPK-related kinase 5 (ARK5) for maintaining metabolic homeostasis and for cell survival. ARK5 is an upstream regulator of AMPK and limits protein synthesis via inhibition of the mammalian target of rapamycin (mTORC1) signalling pathway. ARK5 also maintains expression of mitochondrial respiratory chain complexes and respiratory capacity, which is required for efficient glutamine metabolism. Inhibition of ARK5 leads to a collapse of cellular ATP levels in cells expressing deregulated Myc, inducing multiple pro-apoptotic responses as a secondary consequence. Depletion of ARK5 prolongs survival in Myc-driven mouse models of hepatocellular carcinoma demonstrating that targeting cellular energy homeostasis is a valid therapeutic strategy to eliminate tumour cells with deregulated Myc (Liu et al., 2012).

Also in 2012 Kessler et al identified a SAE1/2 mediated SUMOylation pathway supporting the Myc oncogenic program via a genome-wide RNA interference screen to search for Myc synthetic lethal genes. They uncovered a role for SUMO-activating enzyme SAE1/2. Loss of SAE1/2 enzymatic activity drives synthetic lethality with Myc. Inactivation of SAE2 leads to mitotic catastrophe and cell death upon Myc hyperactivation. Mechanistically, SAE2 inhibition switches a transcriptional subprogram of Myc from being activated to repressed. A subset of these SUMOylation-dependent Myc switches is required for mitotic spindle function and support the Myc oncogenic program. They also showed that SAE2 was required for growth of Myc-dependent tumours in mice. Gene expression analysis of Myc-high human breast cancers suggests that low SAE1/2 abundance in the tumours correlates with longer metastasis-free survival of the patients (Kessler et al., 2012).

Targeting CDK1 but not CDK4/6 or CDK2 is selectively lethal to Myc-dependent human breast cancer cells. Myc-dependent breast cancer cells were not sensitive to CDK4/6 inhibitor PD332991. Cell cycle arrest induced by Myc knockdown was accompanied by a decrease in CDK2 activity, but inactivation of CDK2 did not selectively affect the viability of Myc-dependent breast cancer cells. Contrastly, CDK1 inactivation significantly induced apoptosis and reduced viability of Myc-dependent cells but not of Myc-independent cells. This selective induction of apoptosis by CDK1 inhibitors was associated with upregulation of the pro-apoptotic molecule BIM and p53-independent (Kang et al., 2014).

Romero et al reported in small cell lung cancers (SCLC) a tumour specific inactivation of MAX disrupted Myc-SWI/SNF programs and was synthetic lethal with BRG1. MAX inactivation is mutually exclusive with alterations of Myc and BRG1. BRG1 codes for an ATPase of switch/sucrose nonfermentable (SWI/SNF) complex. They demonstrated that BRG1 regulated the expression of MAX through direct recruitment to the MAX promoter, and that depletion of BRG1 strongly hindered cell growth, specifically in MAX-deficient cells, leading to a synthetic lethal interaction (Romero et al., 2014).

1.3.3 Synthetic lethality in the clinic

The only clinical application of synthetic lethality so far is the use of poly (ADP-ribose) polymerase (PARP) inhibitors in patients with mammary tumours carrying a BRCA1 or BRCA2 mutation (Farmer et al., 2005). PARP is involved in base excision repair (BER), which is responsible for the repair of breaks that frequently occur in single strand DNA. PARP can detect single strand breaks, catalyze the formation of poly (ADP-ribose) polymers and recruit a number

of substrates for DNA repair. If PARP activity is inhibited, single-strand DNA breaks are not repaired and these single-strand DNA breaks lead to replication forks stalling or collapse. In normal cells, the consequence of PARP inhibition can be compensated by homologous recombination which repairs the resultant double-strand breaks. Homologous recombination needs functional BRCA1 and BRCA2. In patient with BRCA1 and BRCA2 mutation, this kind of homologous recombination can not occur to compensate the effect of PARP inhibition which leads to tumour cell deaths and spares the normal cells (Rehman et al., 2010).

1.4 Objectives of the thesis

Expression of *MYCN* gene is deregulated in several human neuroendocrine tumours. In neuroblastoma, amplification of the *MYCN* gene predicts poor prognosis and resistance to therapy. The inability to target the N-Myc protein directly necessitates the search for alternative targets.

This project aims at identifying genes, which are specifically required for growth and survival of cells that express high levels of N-Myc using high-throughput genome-wide shRNA screening combined with next generation sequencing. The identification and analysis of these genes will shed light on functional interaction partners of N-Myc and uncover mechanism of synthetic lethal interaction with N-Myc.

2 Materials

2.1 Strains and cell lines

2.1.1 Human cell lines

HEK293T

Human embryonic kidney cell line (ATCC)

SHEP

MYCN-nonamplified human neuroblastoma cell line, original from bone marrow, provided by Manfred Schwab

SKN-AS

MYCN-nonamplified human neuroblastoma cell line, original from bone marrow, provided by Manfred Schwab

NB69

MYCN-nonamplified human neuroblastoma cell line, original from lung liver sternum, provided by Angelika Eggert

IMR5

MYCN-amplified human neuroblastoma cell line, provided by Angelika Eggert

IMR32

MYCN-amplified human neuroblastoma cell line, original from abdomen, provided by Manfred Schwab

SMS-KCN

MYCN-amplified human neuroblastoma cell line, original from adrenal, provided by Angelika Eggert

Kelly

MYCN-amplified human neuroblastoma cell line

SHEP-N-MycER

SHEP cell line stably expresses MycER with neomycin resistance, stably expresses murine ecotrophic receptor with hygromycin resistance.

2.1.2 Bacterial strains

XL1 blue

Escherichia coli, recA1, endA1, gyrA96, thi-1, hsdR17 supE44, relA1, lac [F'proAB lacIqZ_M15Tn10 (Tetr)]; for generation and amplification of plasmids

2.2 Cultivation media and supplements

2.2.1 Media for mammalian cell culture

Basal medium DMEM containing L-glutamine (584 mg/ml) was purchased by Sigma.

Fetal bovine serum (FBS; from PAA) was heat-inactivated for 30 min at 56 °C before use.

Basal medium

DMEM 10% (v/v) FBS 1% (v/v) penicillin/ streptomycin (100,000 U/ml; from PAA)

Freezing medium

90% (v/v) FBS 10% (v/v) DMSO

2.2.2 Antibiotics for mammalian cell culture

For selection of transfected or infected cells they were treated with the antibiotics given below. A resistance to neomycine was selected with G418, a bleomycine resistance with zeocine.

Blasticidin S (InvivoGen)	5-10 mg/ml
G418 (PAA)	800 mg/ml
Puromycin (InvivoGen)	2 mg/ml
Hygromycin (Merck)	100 mg/ml
Zeocin (InvivoGen)	50-500 mg/ml

2.2.3 Media and antibiotics for bacterial cell culture

Media

LB-medium

10% (w/v) bacto tryptone

0.5% (w/v) yeast extract

1% (w/v) NaCl

LB-agar

LB-medium

1.2% (w/v) Bacto-Agar autoclaved, cooled down to 50 °C before adding ampicillin, 20 ml poured into 10 cm dishes, antibiotics depending on the resistance marker on the corresponding DNA plasmid, the following antibiotics were added to the LB-medium or LB-agar:

Ampicillin	100 mg/ml
Kanamycin	100 mg/ml
Chloramphenicol	25 mg/ml

2.3 Nucleic acids

2.3.1 Primers

DNA-primers were synthesized either by Sigma (f, fw, for = forward; r, rv, rev = reverse). Primers for quantitative qRT-PCR were designed with the Universal Probe Library by Roche and are all intron-spanning to avoid amplification of genomic DNA.

Table 1: List of Primers

Name	Amplication	Sequence 5'-3'
Mncul3_age_f	cloning	CGCACCGGTATGTCGAATCTGAGCAAAGGCAC
Mncul3_spe_r	cloning	CGCACTAGTTTATGCTACATATGTGTATACTTTGCGATCCTC
Mncul3_3xFLAG_spe_r	cloning	CGCACTAGTATTCTTGTCGTCATCGTCCTTGTAATCGATGTCATGATCTTTATAATCACCGTCATGGTCTTTGTAGTCTGCTACATATGTGTATACTTTGCGATCCTC
Mncul3_strepII_spe_r	cloning	CGCACTAGTATTCTTCTCGAACTGTGGATGTGACCATGCTACATATGTGTATACTT
Mncul3_strepII_spe_r	cloning	CGCACTAGTATTCTTCTCGAACTGTGGATGTGACCATGCTACATATGTGTATACTT

xj_mc3_age_ΔN30f	cloning	CGCACCGGTATGAGCATTTGGGACCTTC TGAAAAATGC
xj_mc3_age_ΔN150f	cloning	CGCACCGGTATGGTACGGTATGGGTGTA TTAGGGATCATC
xj_mc3_Δ24r	cloning	TCTCAGAGTCATCAGAAACACTTTTATT TGTGACCATTGCCTTATCCAATATTGTTT CTACTTC
xj_mc3_Δ24f	cloning	ACAAATAAAAGTGTTTCTGATGACTCTG AGA
xj_mc3_Δ_roc1r	cloning	TCTTTCAGGGATATCTGTCTCTTGTTGA ATAGTGGAGACTTGCAGTATGTGCTT
xj_mc3_Δ_roc1f	cloning	ATTCAACAAGAGACAGATATCCCTGAA AGA
xj_mc3_spe_ΔC20r	cloning	CGCACTAGTTTATCCTTCAATACGTTTCT TAATAACAACTGGACTT
cul3 seq left	sequencing	AAGAATCCTGTTGACTATATCCAGGGC
cul3 seq right	sequencing	AGATGCTCATATCCCTAAACATTCCTTC C
cul3 seq right 2	sequencing	TTGATGATCATTCCAAGCTTGATTTAG
cul3 seq right3	sequencing	TCATTAACATCTGGCAAGCATTTCTTAT TG
pLKO seq primer	sequencing	GACTATCATATGCTTACCGT
pGIPZ seq primer	sequencing	GCATTAAAGCAGCGTATC
KW_SFFV_seq	sequencing	CTTCTGCTTCCCGAGCTCTA

KW_SFFV_seq	sequencing for pRRL	CTTCTGCTTCCCGAGCTCTA
[illegible]	[illegible]	[illegible]

2.3.2 Oligos for pLKO cloning

Table 2: List of oligos for pLKO cloning

Name	Sequence 5'-3'
GTP_da_1849_f	CCGGTGAAGAATGCTCAGAAGAACTCGAGTTCTTCTGAGCATTCTTCATTTTTG
GTP_da_1849_r	AATTCAAAAATGAAGAATGCTCAGAAGAACTCGAGTTCTTCTGAGCATTCTTCA
GTP_dk_1040_f	CCGGGACTGAGGAAGGTGTTATTACTCGAGTAATAACACCTTCCTCAGTCTTTTTG
GTP_dk_1040_r	AATTCAAAAAGACTGAGGAAGGTGTTATTACTCGAGTAATAACACCTTCCTCAGTC
GTP_dk_1375_f	CCGGGCCATAATATAGCTGATTATCTCGAGATAATCAGCTATATTATGGCTTTTTG
GTP_dk_1375_r	AATTCAAAAAGCCATAATATAGCTGATTATCTCGAGATAATCAGCTATATTATGGC
EXO_dk_318_f	CCGGGCCCTAGTGAACTGTCAATACTCGAGTATTGACAGTTCACTAGGGCTTTTTG
EXO_dk_318_r	AATTCAAAAAGCCCTAGTGAACTGTCAATACTCGAGTATTGACAGTTCACTAGGGC

EXO_dk_857_f	CCGGCCACCCATGTCCAGAATAAACTCGAGTTTATTCTGGACATGGGTGGTTTTTG
EXO_dk_857_r	AATTCAAAAACCACCCATGTCCAGAATAAACTCGAGTTTATTCTGGACATGGGTGG
EXO_dk_856_f	CCGGGCCACCCATGTCCAGAATAACTCGAGTTATTCTGGACATGGGTGGCTTTTTG
EXO_dk_856_r	AATTCAAAAAGCCACCCATGTCCAGAATAACTCGAGTTATTCTGGACATGGGTGGC
CSE_dk_1339_f	CCGGCAGGAATCTTCTCTGGTTATCTCGAGATAACCAGAGAAGATTCCTGTTTTTG
CSE_dk_1339_r	AATTCAAAAACAGGAATCTTCTCTGGTTATCTCGAGATAACCAGAGAAGATTCCTG
CSE_dk_585_f	CCGGCGTACAGCACATTCATTATTCTCGAGAATAATGAATGTGCTGTACGTTTTTG
CSE_dk_585_r	AATTCAAAAACGTACAGCACATTCATTATTCTCGAGAATAATGAATGTGCTGTACG
CSE_da_2666_f	CCGGTGGCATAACCAAATTACTACTCGAGTAGTAATTTGGTTATGCCATTTTTG
CSE_da_2666_r	AATTCAAAAATGGCATAACCAAATTACTACTCGAGTAGTAATTTGGTTATGCCA
DDX_da_491_f	CCGGAGTATAAAGAAGATCCGCTCTCGAGAGCGGATCTTCTTTATACT TTTTTG
DDX_da_491_r	AATTCAAAAAAGTATAAAGAAGATCCGCTCTCGAGAGCGGATCTTCTTTATACT

DDX_dk_793_f	CCGGCACGAGGACTGGTCCATTATCTCGAGATAATGGACCAGTCCTCGTGTTTTTG
DDX_dk_793_r	AATTCAAAAACACGAGGACTGGTCCATTATCTCGAGATAATGGACCAGTCCTCGTG
DDX_dk_1781_f	CCGGGCATACAGGAGGTGCTTAATCTCGAGATTAAGCACCTCCTGTATGCTTTTTG
DDX_dk_1781_r	AATTCAAAAAGCATACAGGAGGTGCTTAATCTCGAGATTAAGCACCTCCTGTATGC
RBB_dk_158_f	CCGGGCCTTACCCGTGTGAGAATACTCGAGTATTCTCACACGGGTAAGGCTTTTTG
RBB_dk_158_r	AATTCAAAAAGCCTTACCCGTGTGAGAATACTCGAGTATTCTCACACGGGTAAGGC
RBB_ir_1321_f	CCGGAAGACTCCTCCTCAAGAAGAATTCTCGAGAATTCTTCTTGAGGAGGAGTCTTTTTTTG
RBB_ir_1321_r	AATTCAAAAAAAGACTCCTCCTCAAGAAGAATTCTCGAGAATTCTTCTTGAGGAGGAGTCTT
RBB_ir_2961_f	CCGGAAGGAGCAGAAGACATAGACGTTCTCGAGAACGTCTATGTCTTCTGCTCCTTTTTTTG
RBB_ir_2961_r	AATTCAAAAAAAGGAGCAGAAGACATAGACGTTCTCGAGAACGTCTATGTCTTCTGCTCCTT
RPS_t1_dk_940_f	CCGGCCAGCACTTGTATTGATTATCTCGAGATAATCAATACAAGTGCTGGTTTTTG
RPS_t1_dk_940_r	AATTCAAAAACCAGCACTTGTATTGATTATCTCGAGATAATCAATACAAGTGCTGG

RPS_t1_dk_941_f	CCGGCAGCACTTGTATTGATTATTCTCGAGAATAATCAATACAAGTGCTGTTTTTG
RPS_t1_dk_941_r	AATTCAAAAACAGCACTTGTATTGATTATTCTCGAGAATAATCAATACAAGTGCTG
RPS_dk_268_f	CCGGCTAACAAGCCGCAACGTAAACTCGAGTTTACGTTGCGGCTTGTTAGTTTTTG
RPS_dk_268_r	AATTCAAAAACTAACAAGCCGCAACGTAAACTCGAGTTTACGTTGCGGCTTGTTAG
RPS_dk_30_f	CCGGCGGATGCAAGCGTGCTATATCTCGAGATATAGCACGCTTGCATCCGTTTTTG
RPS_dk_30_r	AATTCAAAAACGGATGCAAGCGTGCTATATATATAGCACGCTTGCATCCG
RPS_dk_32_f	CCGGGATGCAAGCGTGCTATATAACTCGAGTTATATAGCACGCTTGCATCTTTTTG
RPS_dk_32_r	AATTCAAAAAGATGCAAGCGTGCTATATAACTCGAGTTATATAGCACGCTTGCATC
MCM_ir_2351_f	CCGGAAGGTGGCCCTCTTGGATGTGTTCTCGAGAACACATCCAAGAGGGCCACCTTTTTTTG
MCM_ir_2351_r	AATTCAAAAAAAGGTGGCCCTCTTGGATGTGTTCTCGAGAACACATCCAAGAGGGCCACCTT
MCM_dk_2751_f	CCGGGGGAGAGGACAATGACTATTCTCGAGAATAGTCATTGTCCTCTCCCTTTTTG
MCM_dk_2751_r	AATTCAAAAAGGGAGAGGACAATGACTATTCTCGAGAATAGTCATTGTCCTCTCCC

MCM_dk_2054_f	CCGGGGTCCAGTATGCTTACTTTACTCGAGTAAAGTAAGCATACTGGACCTTTTTG
MCM_dk_2054_r	AATTCAAAAAGGTCCAGTATGCTTACTTTACTCGAGTAAAGTAAGCATACTGGACC
NAE1_dk_1148_f	CCGGGGGTAATCATGTTGCCAAATCTCGAGATTTGGCAACATGATTACCCTTTTTG
NAE1_dk_1148_r	AATTCAAAAAGGGTAATCATGTTGCCAAATCTCGAGATTTGGCAACATGATTACCC
NAE1_dk_199_f	CCGGCAGGAACTGAAATTCTTAAACTCGAGTTTAAGAATTTCAGTTCCTGTTTTTG
NAE1_dk_199_r	AATTCAAAAACAGGAACTGAAATTCTTAAACTCGAGTTTAAGAATTTCAGTTCCTG
NAE1_dk_1469_f	CCGGCCTTCAGGAATATGGTTTATCTCGAGATAAACCATATTCCTGAAGGTTTTTG
NAE1_dk_1469_r	AATTCAAAAACCTTCAGGAATATGGTTTATCTCGAGATAAACCATATTCCTGAAGG
NAE1_dk_922_f	CCGGCAAGCAGTATTGAAGATATACTCGAGTATATCTTCAATACTGCTTGTTTTTG
NAE1_dk_922_r	AATTCAAAAACAAGCAGTATTGAAGATATACTCGAGTATATCTTCAATACTGCTTG
CUL5_dk_1205_f	CCGGGTAAGAGAATCCTATGTTAACTCGAGTTAACATAGGATTCTCTTACTTTTTG
CUL5_dk_1205_r	AATTCAAAAAGTAAGAGAATCCTATGTTAACTCGAGTTAACATAGGATTCTCTTAC

CUL5_dk_71_f	CCGGGGACAATGCACCTCCCTTAACTCGAGTTAAGGGAGGTGCATTGTCCTTTTTG
CUL5_dk_71_r	AATTCAAAAAGGACAATGCACCTCCCTTAACTCGAGTTAAGGGAGGTGCATTGTCC
CUL5_dk_1360_f	CCGGGAAATATGCAGATGCTAAATCTCGAGATTTAGCATCTGCATATTTCTTTTTG
CUL5_dk_1360_r	AATTCAAAAAGAAATATGCAGATGCTAAATCTCGAGATTTAGCATCTGCATATTTC
CUL5_dk_1606_f	CCGGCTTGGAGGAACATATCATTACTCGAGTAATGATATGTTCCTCCAAGTTTTTG
CUL5_dk_1606_r	AATTCAAAAACTTGGAGGAACATATCATTACTCGAGTAATGATATGTTCCTCCAAG
CUL3_1694_f	CCGGCAAGGAGACTTCTCACAAATCTCGAGATTTGTGAGAAGTCTCCTTGTTTTTG
CUL3_1694_r	AATTCAAAAACAAGGAGACTTCTCACAAATCTCGAGATTTGTGAGAAGTCTCCTTG
CUL3_5884_f	CCGGGCCAGATACTATTCTGAATACTCGAGTATTCAGAATAGTATCTGGCTTTTTG
CUL3_5884_r	AATTCAAAAAGCCAGATACTATTCTGAATACTCGAGTATTCAGAATAGTATCTGGC
CUL3_552_f	CCGGGCTCTATAGAAATGCATATACTCGAGTATATGCATTTCTATAGAGCTTTTTG
CUL3_552_r	AATTCAAAAAGCTCTATAGAAATGCATATACTCGAGTATATGCATTTCTATAGAGC

CUL3_868_f	CCGGCGGCAAACTCTATTGGATATCTCGAGATATCCAATAGAGTTTGCCGTTTTTG
CUL3_868_r	AATTCAAAAACGGCAAACTCTATTGGATATCTCGAGATATCCAATAGAGTTTGCCG
PWP2_1521_f	CCGGGCAGGACTCCTTTGAGATTTCTCGAGAAATCTCAAAGGAGTCCTGCTTTTTG
PWP2_1521_r	AATTCAAAAAGCAGGACTCCTTTGAGATTTCTCGAGAAATCTCAAAGGAGTCCTGC
PWP2_191_f	CCGGGCAATAGAGTCACTGTATTTCTCGAGAAATACAGTGACTCTATTGCTTTTTG
PWP2_191_r	AATTCAAAAAGCAATAGAGTCACTGTATTTCTCGAGAAATACAGTGACTCTATTGC
PWP2_921_f	CCGGGGCCAAGTACTTCTTCAATACTCGAGTATTGAAGAAGTACTTGGCCTTTTTG
PWP2_921_r	AATTCAAAAAGGCCAAGTACTTCTTCAATACTCGAGTATTGAAGAAGTACTTGGCC
PWP2_1863_f	CCGGGAAGGAGCTGGACAAGATTACTCGAGTAATCTTGTCCAGCTCCTTCTTTTTG
PWP2_1863_r	AATTCAAAAAGAAGGAGCTGGACAAGATTACTCGAGTAATCTTGTCCAGCTCCTTC
KIF11_4840_f	CCGGCGATGAGTTTAGTGTGTAAACTCGAGTTTACACACTAAACTCATCGTTTTTG
KIF11_4840_r	AATTCAAAAACGATGAGTTTAGTGTGTAAACTCGAGTTTACACACTAAACTCATCG

KIF11_929_f	CCGGGGATGAAGTCTATCAAATTTCTCGAGAAATTTGATAGACTTCATCCTTTTTG
KIF11_929_r	AATTCAAAAAGGATGAAGTCTATCAAATTTCTCGAGAAATTTGATAGACTTCATCC
KIF11_1287_f	CCGGCGTACAAGAACATCTATAATCTCGAGATTATAGATGTTCTTGTACGTTTTTG
KIF11_1287_r	AATTCAAAAACGTACAAGAACATCTATAATCTCGAGATTATAGATGTTCTTGTACG
KIF11_1345_f	CCGGCTCTGAGTACATTGGAATATCTCGAGATATTCCAATGTACTCAGAGTTTTTG
KIF11_1345_r	AATTCAAAAACTCTGAGTACATTGGAATATCTCGAGATATTCCAATGTACTCAGAG
ALDOA_da_804_f	CCGGTGAGTGACCACCACATCTACTCGAGTAGATGTGGTGGTCACTCATTTTTG
ALDOA_da_804_r	AATTCAAAAATGAGTGACCACCACATCTACTCGAGTAGATGTGGTGGTCACTCA
ALDOA_da_1164_f	CCGGTTGCCTGTCAAGGAAAGTACTCGAGTACTTTCCTTGACAGGCAATTTTTG
ALDOA_da_1164_r	AATTCAAAAATTGCCTGTCAAGGAAAGTACTCGAGTACTTTCCTTGACAGGCAA
ALDOA_da_995_f	CCGGTCCATCAACCTCAATGCCACTCGAGTGGCATTGAGGTTGATGGATTTTTG
ALDOA_da_995_r	AATTCAAAAATCCATCAACCTCAATGCCACTCGAGTGGCATTGAGGTTGATGGA

PIK3_da_1011_f	CCGGGGTTAAGGGAAATAAACTTCTCGAGAAGTTTATTTCCCTTAACCTTTTTG
PIK3_da_1011_r	AATTCAAAAAGGTTAAGGGAAATAAACTTCTCGAGAAGTTTATTTCCCTTAACC
PIK3_da_1408_f	CCGGGAAGAAATGTTGAATCCAACTCGAGTTGGATTCAACATTTCTTCTTTTTG
PIK3_da_1408_r	AATTCAAAAAGAAGAAATGTTGAATCCAACTCGAGTTGGATTCAACATTTCTTC
PIK3_da_1563_f	CCGGTGATAGTGCTAATGTGTCACTCGAGTGACACATTAGCACTATCATTTTTG
PIK3_da_1563_r	AATTCAAAAATGATAGTGCTAATGTGTCACTCGAGTGACACATTAGCACTATCA
MCL1_dk_748_f	CCGGGATTATCTCTCGGTACCTTCTCGAGAAGGTACCGAGAGATAATCTTTTTG
MCL1_dk_748_r	AATTCAAAAAGATTATCTCTCGGTACCTTCTCGAGAAGGTACCGAGAGATAATC
MCL1_dk_911_f	CCGGGTTCTTCCATGTAGAGGACCTCGAGGTCCTCTACATGGAAGAACTTTTTG
MCL1_dk_911_r	AATTCAAAAAGTTCTTCCATGTAGAGGACCTCGAGGTCCTCTACATGGAAGAAC
MCL1_dk_222_f	CCGGAAAGAAACGCGGTAATCGGCTCGAGCCGATTACCGCGTTTCTTTTTTTTG
MCL1_dk_222_r	AATTCAAAAAAAAGAAACGCGGTAATCGGCTCGAGCCGATTACCGCGTTTCTTT

SENP1_1051_f	CCGGCAGGGAAACAGTTTACTATACTCGAGTATAGTAAACTGTTTCCCTGTTTTTG
SENP1_1051_r	AATTCAAAAACAGGGAAACAGTTTACTATACTCGAGTATAGTAAACTGTTTCCCTG
SENP1_2927_f	CCGGCCTCCAGGACCTTTCCTATTCTCGAGAATAGGAAAGGTCCTGGAGGTTTTTG
SENP1_2927_r	AATTCAAAAACCTCCAGGACCTTTCCTATTCTCGAGAATAGGAAAGGTCCTGGAGG
SENP1_3058_f	CCGGCAAGCAGTCCTTTCCGTAAACTCGAGTTTACGGAAAGGACTGCTTGTTTTTG
SENP1_3058_r	AATTCAAAAACAAGCAGTCCTTTCCGTAAACTCGAGTTTACGGAAAGGACTGCTTG
CDK11A_dk_2586_f	CCGGGTAAATTTGTAGAATTAAATCTCGAGATTTAATTCTACAAATTTACTTTTTG
CDK11A_dk_2586_r	AATTCAAAAAGTAAATTTGTAGAATTAAATCTCGAGATTTAATTCTACAAATTTAC
CDK11A_da_306_f	CCGGGTATAGAAGAGAAGACTCACTCGAGTGAGTCTTCTCTTCTATACTTTTTG
CDK11A_da_306_r	AATTCAAAAAGTATAGAAGAGAAGACTCACTCGAGTGAGTCTTCTCTTCTATAC
CDK11A_da_324_f	CCGGAATGGAAGACAGAGGAGAACTCGAGTTCTCCTCTGTCTTCCATTTTTTTG
CDK11A_da_324_r	AATTCAAAAAAATGGAAGACAGAGGAGAACTCGAGTTCTCCTCTGTCTTCCATT

CDK11A_da_520_f	CCGGAGACAGAAGAGAAGGGAAACTCGAGAGACAGAAGAGAAGGGAAATTTTTG
CDK11A_da_520_r	AATTCAAAAAAGACAGAAGAGAAGGGAAACTCGAGAGACAGAAGAGAAGGGAAA
USP7_da_1942_f	CCGGTGACATGTACGATGAAGAACTCGAGTTCTTCATCGTACATGTCATTTTTG
USP7_da_1942_r	AATTCAAAAATGACATGTACGATGAAGAACTCGAGTTCTTCATCGTACATGTCA
USP7_da_2099_f	CCGGCGACCAGCAATGTTAGATACTCGAGTATCTAACATTGCTGGTCGTTTTTG
USP7_da_2099_r	AATTCAAAAACGACCAGCAATGTTAGATACTCGAGTATCTAACATTGCTGGTCG
USP7_da_2103_f	CCGGCAGCAATGTTAGATAATGACTCGAGTCATTATCTAACATTGCTGTTTTTG
USP7_da_2103_r	AATTCAAAAACAGCAATGTTAGATAATGACTCGAGTCATTATCTAACATTGCTG
USP7_da_3141_f	CCGGACATAGACAAAGAGAATGACTCGAGTCATTCTCTTTGTCTATGTTTTTTG
USP7_da_3141_r	AATTCAAAAAACATAGACAAAGAGAATGACTCGAGTCATTCTCTTTGTCTATGT
TOR1AIP1_2328_f	CCGGCACTAAGTTTCCTGAGTTATCTCGAGATAACTCAGGAAACTTAGTGTTTTTG
TOR1AIP1_2328_r	AATTCAAAAACACTAAGTTTCCTGAGTTATCTCGAGATAACTCAGGAAACTTAGTG

TOR1AIP1_2434_f	CCGGCCTATAGGAACATAAGTAATCTCGAGATTACTTATGTTCCTATAGGTTTTTG
TOR1AIP1_2434_r	AATTCAAAAACCTATAGGAACATAAGTAATCTCGAGATTACTTATGTTCCTATAGG
TOR1AIP1_2621_f	CCGGGGTGGATTCCGTTGGGATTTCTCGAGAAATCCCAACGGAATCCACCTTTTTG
TOR1AIP1_2621_r	AATTCAAAAAGGTGGATTCCGTTGGGATTTCTCGAGAAATCCCAACGGAATCCACC
TOR1AIP1_3479_f	CCGGGTGGTAGTAGAGTGGTTTAACTCGAGTTAAACCACTCTACTACCACTTTTTG
TOR1AIP1_3479_r	AATTCAAAAAGTGGTAGTAGAGTGGTTTAACTCGAGTTAAACCACTCTACTACCAC
PKM2_2400_f	CCGGCCTCCAGGCCTGTTGCTATACTCGAGTATAGCAACAGGCCTGGAGGTTTTTG
PKM2_2400_r	AATTCAAAAACCTCCAGGCCTGTTGCTATACTCGAGTATAGCAACAGGCCTGGAGG
PKM2_1403_f	CCGGGCCATCTACCACTTGCAATTCTCGAGAATTGCAAGTGGTAGATGGCTTTTTG
PKM2_1403_r	AATTCAAAAAGCCATCTACCACTTGCAATTCTCGAGAATTGCAAGTGGTAGATGGC
PKM2_1404_f	CCGGCCATCTACCACTTGCAATTACTCGAGTAATTGCAAGTGGTAGATGGTTTTTG
PKM2_1404_r	AATTCAAAAACCATCTACCACTTGCAATTACTCGAGTAATTGCAAGTGGTAGATGG

PKM2_2423_f	CCGGCCTACCTGTATGTCAATAAACTCGAGTTTATTGACA TACAGGTAGGTTTTTG
PKM2_2423_r	AATTCAAAAACCTACCTGTATGTCAATAAACTCGAGTTTA TTGACATACAGGTAGG
MYCN_dk_1754_f	CCGGCAAACATTGTGTTGACATTACTCGAGTAATGTCAAC ACAATGTTTGTTTTTG
MYCN_dk_1754_r	AATTCAAAAACAAACATTGTGTTGACATTACTCGAGTAA TGTCAACACAATGTTTG
MYCN_dk_2083_f	CCGGGGTGCATAGAACTGGGTAAACTCGAGTTTACCCAG TTCTATGCACCTTTTTG
MYCN_dk_2083_r	AATTCAAAAAGGTGCATAGAACTGGGTAAACTCGAGTTT ACCCAGTTCTATGCACC
scramble_plko_f	CCGGAGGCTCGCATGTATACAGACTCGAGTCTGTATACA TGCGAGCCTTTTTTG
scramble_plko_r	AATTCAAAAAAGGCTCGCATGTATACAGACTCGAGTCTG TATACATGCGAGCCT
shRLuc_pLKO_f	CCGGGTAGCGCGGTGTATTATACCTCGAGGTATAATACA CCGCGCTACTTTTTG
shRLuc_pLKO_r	AATTCAAAAAGTAGCGCGGTGTATTATACCTCGAGGTAT AATACACCGCGCTAC
THOC1_358_f	CCGGGGATCAGTGTGACACAATATCTCGAGATATTGTGT CACACTGATCCTTTTTG
THOC1_358_r	AATTCAAAAAGGATCAGTGTGACACAATATCTCGAGATA TTGTGTCACACTGATCC

THOC1_1164_f	CCGGCAAAGATGGTAGAGCATATACTCGAGTATATGCTC TACCATCTTTGTTTTTG
THOC1_1164_r	AATTCAAAAACAAAGATGGTAGAGCATATACTCGAGTAT ATGCTCTACCATCTTTG
THOC1_1569_f	CCGGCAACCAACCAGCAGTTTAAACTCGAGTTTAAACTG CTGGTTGGTTGTTTTTG
THOC1_1569_r	AATTCAAAAACAACCAACCAGCAGTTTAAACTCGAGTTT AAACTGCTGGTTGGTTG
PIK3_ir_612_f	CCGGCTGCCAGGACGTGTTTAGCTCTCGAGAGCTAAACA CGTCCTGGCAGTTTTTG
PIK3_ir_612_r	AATTCAAAAACTGCCAGGACGTGTTTAGCTCTCGAGAGC TAAACACGTCCTGGCAG
PIK3_ir_1998_f	CCGGTCGGAGGATAGGGCAGTTTCCTCGAGGAAACTGCC CTATCCTCCGATTTTTG
PIK3_ir_1998_r	AATTCAAAAATCGGAGGATAGGGCAGTTTCCTCGAGGAA ACTGCCCTATCCTCCGA
PIK3_ir_2349_f	CCGGGCCTTTGTGGCTGGTATACACTCGAGTGTATACCAG CCACAAAGGCTTTTTG
PIK3_ir_2349_r	AATTCAAAAAGCCTTTGTGGCTGGTATACACTCGAGTGTA TACCAGCCACAAAGGC
UBE2M_da_729_f	CCGGAGACGTGTGATATCAGCTTCTCGAGAAGCTGATAT CACACGTCTTTTTTG
UBE2M_da_729_r	AATTCAAAAAAGACGTGTGATATCAGCTTCTCGAGAAGC TGATATCACACGTCT

UBE2M_da_737_f	CCGGGATATCAGCTTCTCAGATCCTCGAGGATCTGAGAAGCTGATATCTTTTTG
UBE2M_da_737_r	AATTCAAAAAGATATCAGCTTCTCAGATCCTCGAGGATCTGAGAAGCTGATATC
UBE2M_da_804_f	CCGGTCTACAAGAGTGGGAAGTTCTCGAGAACTTCCCACTCTTGTAGATTTTTG
UBE2M_da_804_r	AATTCAAAAATCTACAAGAGTGGGAAGTTCTCGAGAACTTCCCACTCTTGTAGA
ccne1_1270_f	CCGGCACAGAGACAGCTTGGATTTCTCGAGAAATCCAAGCTGTCTCTGTGTTTTTG
ccne1_1270_r	AATTCAAAAACACAGAGACAGCTTGGATTTCTCGAGAAATCCAAGCTGTCTCTGTG
ccne1_1177_f	CCGG GTTCCATTTGCCATGGTTATCTCGAGATAACCATGGCAAATGGAACTTTTTG
ccne1_1177_r	AATTCAAAAA GTTCCATTTGCCATGGTTATCTCGAGATAACCATGGCAAATGGAAC
ccne1_1099_f	CCGG CACAGAGACAGCTTGGATTTCTCGAGAAATCCAAGCTGTCTCTGTGTTTTTG
ccne1_1099_r	AATTCAAAAA CACAGAGACAGCTTGGATTTCTCGAGAAATCCAAGCTGTCTCTGTG
ccne2_661_f	CCGG GCTTCAACTCATTGGAATTCTCGAGAATTCCAATGAGTTGAAGCTTTTTG
ccne2_661_r	AATTCAAAAA GCTTCAACTCATTGGAATTCTCGAGAATTCCAATGAGTTGAAGC

ccne2_1023_f	CCGG CCTCCATTGAAGTGGTTAACTCGAG TTAACCACTTCAATGGAGGTTTTTG
ccne2_1023_r	AATTCAAAAA CCTCCATTGAAGTGGTTAACTCGAG TTAACCACTTCAATGGAGG
TCEB1_512_f	CCGGCCTGTATGCAGTTGAACTATCTCGAGATAGTTCAAC TGCATACAGGTTTTTG
TCEB1_512_r	AATTCAAAAACCTGTATGCAGTTGAACTATCTCGAGATA GTTCAACTGCATACAGG
TCEB1_161_f	CCGGGGCCATGAATTTATTGTAAACTCGAGTTTACAATAA ATTCATGGCCTTTTTG
TCEB1_161_r	AATTCAAAAAGGCCATGAATTTATTGTAAACTCGAGTTTA CAATAAATTCATGGCC
TCEB1_405_f	CCGGCGAACTTCTTAGATTGTTAACTCGAGTTAACAATCT AAGAAGTTCGTTTTTG
TCEB1_405_r	AATTCAAAAACGAACTTCTTAGATTGTTAACTCGAGTTAA CAATCTAAGAAGTTCG
nup153_4098_f	CCGGGCAGGATCCTCCTTTGTATTCTCGAGAATACAAAG GAGGATCCTGCTTTTTG
nup153_4098_r	AATTCAAAAAGCAGGATCCTCCTTTGTATTCTCGAGAATA CAAAGGAGGATCCTGC
nup153_1759_f	CCGGCTGGCAGTCCCATGTTTAAACTCGAGTTTAAACATG GGACTGCCAGTTTTTG
nup153_1759_r	AATTCAAAAACTGGCAGTCCCATGTTTAAACTCGAGTTTA AACATGGGACTGCCAG

nup153_2092_f	CCGGCAACAAGCCCAGTAGTTTATCTCGAGATAAACTACTGGGCTTGTTGTTTTTG
nup153_2092_r	AATTCAAAAACAACAAGCCCAGTAGTTTATCTCGAGATAAACTACTGGGCTTGTTG
eny2_294_f	CCGGCTGGTACCTGACAGTGTAAACTCGAGTTTACACTGTCAGGTACCAGTTTTTG
eny2_294_r	AATTCAAAAACTGGTACCTGACAGTGTAAACTCGAGTTTACACTGTCAGGTACCAG
eny2_155_f	CCGGGTTGCTGAGAGCTAAATTAACTCGAGTTAATTTAGCTCTCAGCAACTTTTTG
eny2_155_r	AATTCAAAAAGTTGCTGAGAGCTAAATTAACTCGAGTTAATTTAGCTCTCAGCAAC
eny2_359_f	CCGGCAGCCTTTAAGATTGAATTACTCGAGTAATTCAATCTTAAAGGCTGTTTTTG
eny2_359_r	AATTCAAAAACAGCCTTTAAGATTGAATTACTCGAGTAATTCAATCTTAAAGGCTG
ell_1989_f	CCGGGTGAGAGAGGATTTATTTAACTCGAGTTAAATAAATCCTCTCTCACTTTTTG
ell_1989_r	AATTCAAAAAGTGAGAGAGGATTTATTTAACTCGAGTTAAATAAATCCTCTCTCAC
ell_1987_f	CCGGCGGTGAGAGAGGATTTATTTCTCGAGAAATAAATCCTCTCTCACCGTTTTTG
ell_1987_r	AATTCAAAAACGGTGAGAGAGGATTTATTTCTCGAGAAATAAATCCTCTCTCACCG

ell_3260_f	CCGGCAGGCAGGGAGAACAGAAATCTCGAGATTTCTGTTCTCCCTGCCTGTTTTTG
ell_3260_r	AATTCAAAAACAGGCAGGGAGAACAGAAATCTCGAGATTTCTGTTCTCCCTGCCTG
larp7_549_f	CCGGGCCAGAGCATTGAGAAGTTCTCGAGAACTTCTCAATGCTCTGGCTTTTTG
larp7_549_r	AATTCAAAAAGCCAGAGCATTGAGAAGTTCTCGAGAACTTCTCAATGCTCTGGC
larp7_570_f	CCGGGCTGTTGTAGAGCTTGATTCTCGAGAATCAAGCTCTACAACAGCTTTTTG
larp7_570_r	AATTCAAAAAGCTGTTGTAGAGCTTGATTCTCGAGAATCAAGCTCTACAACAGC
larp7_1386_f	CCGGGGAGAAGAAGTTATACCATCTCGAGATGGTATAACTTCTTCTCCTTTTTG
larp7_1386_r	AATTCAAAAAGGAGAAGAAGTTATACCATCTCGAGATGGTATAACTTCTTCTCC
ncapg2_497_f	CCGGGCCCTACTGGAATGTGTTATCTCGAGATAACACATTCCAGTAGGGCTTTTTG
ncapg2_497_r	AATTCAAAAAGCCCTACTGGAATGTGTTATCTCGAGATAACACATTCCAGTAGGGC
ncapg2_240_f	CCGGCTTTCAGCCTAAATGAATTACTCGAGTAATTCATTTAGGCTGAAAGTTTTTG
ncapg2_240_r	AATTCAAAAACTTTCAGCCTAAATGAATTACTCGAGTAATTCATTTAGGCTGAAAG

ncapg2_297_f	CCGGGGCAAAGGCTGAAGAATTTACTCGAGTAAATTCTTCAGCCTTTGCCTTTTTG
ncapg2_297_r	AATTCAAAAAGGCAAAGGCTGAAGAATTTACTCGAGTAAATTCTTCAGCCTTTGCC
nipbl_609_f	CCGGCAAAGAGCCTTCTCTTTAATCTCGAGATTAAAGAGAAGGCTCTTTGTTTTTG
nipbl_609_r	AATTCAAAAACAAAGAGCCTTCTCTTTAATCTCGAGATTAAAGAGAAGGCTCTTTG
nipbl_6035_f	CCGGGCTGAACAGTATTATGATATCTCGAGATATCATAATACTGTTCAGCTTTTTG
nipbl_6035_r	AATTCAAAAAGCTGAACAGTATTATGATATCTCGAGATATCATAATACTGTTCAGC
nipbl_9206_f	CCGGGTTGGAAATTAGTCTGTTAACTCGAGTTAACAGACTAATTTCCAACTTTTTG
nipbl_9206_r	AATTCAAAAAGTTGGAAATTAGTCTGTTAACTCGAGTTAACAGACTAATTTCCAAC
nipbl_9328_f	CCGGGGCAGAATCTCCTGGATATACTCGAGTATATCCAGGAGATTCTGCCTTTTTG
nipbl_9328_r	AATTCAAAAAGGCAGAATCTCCTGGATATACTCGAGTATATCCAGGAGATTCTGCC
nipbl_1612_f	CCGGCCAGCAAGAGGATATGATTTCTCGAGAAATCATATCCTCTTGCTGGTTTTTG
nipbl_1612_r	AATTCAAAAACCAGCAAGAGGATATGATTTCTCGAGAAATCATATCCTCTTGCTGG

nipbl_5036_f	CCGGGCAGAAGAAGATTCAAATAACTCGAGTTATTTGAATCTTCTTCTGCTTTTTG
nipbl_5036_r	AATTCAAAAAGCAGAAGAAGATTCAAATAACTCGAGTTATTTGAATCTTCTTCTGC
ncapg2_297_f	CCGGGGCAAAGGCTGAAGAATTTACTCGAGTAAATTCTTCAGCCTTTGCCTTTTTG
ncapg2_297_r	AATTCAAAAAGGCAAAGGCTGAAGAATTTACTCGAGTAAATTCTTCAGCCTTTGCC
ncapg2_745_f	CCGGGGAGGAAAGTGGAGAAATTACTCGAGTAATTTCTCCACTTTCCTCCTTTTTG
ncapg2_745_r	AATTCAAAAAGGAGGAAAGTGGAGAAATTACTCGAGTAATTTCTCCACTTTCCTCC
ncapg2_922_f	CCGGGGTATACATTGCAGAAATTTCTCGAGAAATTTCTGCAATGTATACCTTTTTG
ncapg2_922_r	AATTCAAAAAGGTATACATTGCAGAAATTTCTCGAGAAATTTCTGCAATGTATACC

2.4 Plasmids

2.4.1 Empty vectors

Table 3: List of empty vectors

pLKO	Mammalian Expression, Lentiviral, RNAi, human U6 promoter

pGIPZ	Mammalian Expression, Lentiviral, RNAi, CMV promoter (Lars Zender)
pRRL	Mammalian Expression, Lentiviral, RNAi, human U6 promoter (Addgene)

2.4.2 Expression vectors

pLKO lentiviral vector was used for all the shRNA expression with RNA polymerase III-dependent promoter and puromycin resistance. pRRL lentiviral vector was used for overexpressing of murine CUL3.

Table 4: List of expression vectors

pLKO_sh scramble	Mammalian Expression, Lentiviral, RNAi,human U6 promoter with a non-targeting shRNA
pLKO_sh nae1-1	Mammalian Expression, Lentiviral, RNAi,human U6 promoter with sh RNA targeting NAE1
pLKO_sh nae1-2	Mammalian Expression, Lentiviral, RNAi,human U6 promoter with sh RNA targeting NAE1
pLKO_sh nae1-3	Mammalian Expression, Lentiviral, RNAi,human U6 promoter with sh RNA targeting NAE1
pLKO_sh cul5-1	Mammalian Expression, Lentiviral, RNAi,human U6 promoter with sh RNA targeting CUL5
pLKO_sh cul5-2	Mammalian Expression, Lentiviral, RNAi,human U6 promoter with sh RNA targeting CUL5
pLKO_sh cul5-3	Mammalian Expression, Lentiviral, RNAi,human U6 promoter with sh

	RNA targeting CUL5
pLKO_sh cul3-1	Mammalian Expression, Lentiviral, RNAi,human U6 promoter with sh RNA targeting CUL3
pLKO_sh cul3-2	Mammalian Expression, Lentiviral, RNAi,human U6 promoter with sh RNA targeting CUL3
pLKO_sh cul3-3	Mammalian Expression, Lentiviral, RNAi,human U6 promoter with sh RNA targeting CUL3
pLKO_sh tceb-1	Mammalian Expression, Lentiviral, RNAi,human U6 promoter with sh RNA targeting TCEB
pLKO_sh tceb-2	Mammalian Expression, Lentiviral, RNAi,human U6 promoter with sh RNA targeting TCEB
pLKO_sh tceb-3	Mammalian Expression, Lentiviral, RNAi,human U6 promoter with sh RNA targeting TCEB
pLKO_sh ell-1	Mammalian Expression, Lentiviral, RNAi,human U6 promoter with sh RNA targeting ELL
pLKO_sh ell-2	Mammalian Expression, Lentiviral, RNAi,human U6 promoter with sh RNA targeting ELL
pLKO_sh ell-3	Mammalian Expression, Lentiviral, RNAi,human U6 promoter with sh RNA targeting ELL
pLKO_sh eny2-1	Mammalian Expression, Lentiviral, RNAi,human U6 promoter with sh RNA targeting ENY2
pLKO_sh eny2-2	Mammalian Expression, Lentiviral, RNAi,human U6 promoter with sh RNA targeting ENY2
pLKO_sh eny2-3	Mammalian Expression, Lentiviral, RNAi,human U6 promoter with sh

	RNA targeting ENY2
pLKO_sh nup153-1	Mammalian Expression, Lentiviral, RNAi,human U6 promoter with sh RNA targeting NUP153
pLKO_sh nup153-2	Mammalian Expression, Lentiviral, RNAi,human U6 promoter with sh RNA targeting NUP153
pLKO_sh nup153-3	Mammalian Expression, Lentiviral, RNAi,human U6 promoter with sh RNA targeting NUP153
pLKO_sh larp7-1	Mammalian Expression, Lentiviral, RNAi,human U6 promoter with sh RNA targeting LARP7
pLKO_sh larp7-2	Mammalian Expression, Lentiviral, RNAi,human U6 promoter with sh RNA targeting LARP7
pLKO_sh larp7-3	Mammalian Expression, Lentiviral, RNAi,human U6 promoter with sh RNA targeting LARP7
pLKO_sh nipbl-1	Mammalian Expression, Lentiviral, RNAi,human U6 promoter with sh RNA targeting NIPBL
pLKO_sh nipbl-2	Mammalian Expression, Lentiviral, RNAi,human U6 promoter with sh RNA targeting NIPBL
pLKO_sh nipbl-3	Mammalian Expression, Lentiviral, RNAi,human U6 promoter with sh RNA targeting NIPBL
pLKO_sh ncapg2-1	Mammalian Expression, Lentiviral, RNAi,human U6 promoter with sh RNA targeting NCAPG2
pLKO_sh ncapg2-2	Mammalian Expression, Lentiviral, RNAi,human U6 promoter with sh RNA targeting NCAPG2
pLKO_sh ncapg2-3	Mammalian Expression, Lentiviral, RNAi,human U6 promoter with sh

	RNA targeting NCAPG2
pLKO_sh thoc1-1	Mammalian Expression, Lentiviral, RNAi,human U6 promoter with sh RNA targeting THOC1
pLKO_sh thoc1-2	Mammalian Expression, Lentiviral, RNAi,human U6 promoter with sh RNA targeting THOC1
pLKO_sh thoc1-3	Mammalian Expression, Lentiviral, RNAi,human U6 promoter with sh RNA targeting THOC1
pRRL_murine cul3	Mammalian Expression, Lentiviral, RNAi,human U6 promoter with overexpression of murine *CUL3* CDS

2.4.3 Packaging plasmids for producing lentivirus

The packaging plasmids were obtained from Manfred Gessler.

Table 5: List of packaging plasmids

psPAX2	packaging vector containing all required genes for packaging
pMD2-VsVg	envelope plasmid encoding for the VsVg surface protein resulting in a higher virus stability

2.4.4 Lentiviral shRNA library

The pGIPZ lentiviral shRNAmir Library (releases 6.1-6.12) is based on pGIPZ vector with RNA polymerase II-dependent CMV promoter, turbo-GFP to track shRNAmir expression, IRES-puro

as a mammalian selectable marker.

The GIPZ lentiviral shRNAmir library was kindly provided by Lars Zender, which was developed by Open Biosystems in collaboration with Greg Hannon (Cold Spring Harbor Lab) and Steve Elledge (Harvard). This library combines the design advantages of microRNA-adapted shRNA (shRNAmir) with the pGIPZ lentiviral vector to create a RNAi trigger capable of producing RNAi in most cell types including primary and non-dividing cells.

Two pools were used for screening. Pool1 was constructed with numbers 4801-14389 and pool2 was constructed with 44100-53800 (without the constructs with number 46000-47000).

2.5 Antibodies

WB: western blot; IP: Immunoprecipitation; IF; Immunofluorescence; ChIP: chromatin immunoprecipation

Mono: monoclonal; poly: polyclonal

H: human; M: mouse; R: rabbit; MK: monkey

2.5.1 First antibodies

Table 6: List of primary antibodies

Protein	Species reactivity	Application	Antibody type	Description
RNA POL2	M, R, H	WB, IP	R poly IgG	N-20 santa cruz
CUL3	M, R, H	WB, ChIP	M mono IgG1	CUL3-9 sigma
CUL5	M, H	WB	R poly IgG	A302-173A bethyl lab
NAE1	H	WB	M mono IgG2a	AB56420 abcam

Histon H2B	M, R, H	WB	R poly IgG	ab1790 abcam
r-H2Ax (ser139)	H, M, R, MK	WB,IF	R poly IgG	2577 cell signaling
Vincullin	H, M, R, MK	WB	M mono IgG1	v913 sigma
ß-actin	M, R, H, Rabbit	WB	M mono IgG1	AC-15 sigma
a-Tubulin	mammalian	WB	R poly IgG	sc-12462-R santa cruz
HELLS	H	WB	R poly IgG	produced by Dr.Björn von Eyss
CHK2	M, R, H	WB	R ploy igG1	ab8108 abcam
ER-a	M, R, H	WB	R poly IgG	M-20/sc#542 santa cruz
p53	H	WB	M mono IgG2a	Do-1 santa cruz
p-p53(ser15)	H, M, R, MK	WB	R poly IgG	9284 cell signaling
CHK1	H	WB	G poly IgG	sc-7234 santa cruz
p14ARF	H, M	WB	R ploy igG1	NB200-111 Novus
cleaved PARP (Asp214)	H	WB	R	51-9000017 BD
cyclin E	H, M, R	WB	R ploy igG1	M-20 santa cruz
NEDD8	H, M, R, MK	WB	R	2745 cell signaling

p21	H	WB	R poly IgG	N-20 santa cruz
p21	H	WB	R poly IgG	sc-397 santa cruz
p-CHK1(Ser 345)	H, M, R, MK	WB	R poly IgG	2341 cell signaling
p-CHK2(Thr68)	H, MK	WB	R poly IgG	2661 cell signaling
THOC1	H, M	WB	M poly IgG	ab487 abcam
p-ATM(Ser1981)	H, M	WB	M mono IgG1k	MAB38062 millipore
c-myc	M, R, H	WB	R poly IgG	ab32072 abcam
n-myc	H	WB	M mono IgG2a	sc-53993 santa cruz
RPA32	H	WB	M mono IgG1	sc-53496 santa cruz
p-RPA32 (Ser33)	H	WB	R poly IgG	A300-246A Bethyl
p-RPA32 (Ser4/Ser8)	H	WB	R poly IgG	A300-245A Bethyl

2.5.2 Second antibodies

Table 7: List of secondary antibodies

Name	Application	Description
a-rabbit-HRP	WB	donkey-anti-rabbit-immunoglobulin coupled with

		horseradish peroxidase (Amersham, NA 934)
a-mouse-HRP	WB	donkey-anti-mouse-immunglobulin coupled with horseradish peroxidase (Amersham, NA 931)
a-goat-HRP	WB	donkey-anti-goat-immunoglobulin coupled with horseradish peroxidase (santa cruz)
a-rabbit-Alexa488	IF	goat-anti-rabbit-immunglobulin conjugated with Alexa Fluor 488
a-rabbit-Alexa647	IF	goat-anti-rabbit-immunglobulin conjugated with Alexa Fluor 488

2.6 Chemicals

All chemicals were purchased from the companies Sigma, Merck, Roth, Acors Organics, Active Biochem, Invitrogen and Applichem and used without further purification.

2.7 Media

2.7.1 Bacterial culture media

LB-medium
1% (w/v) Bactotrypton 0,5% (w/v) yeast extract 1% (w/v) NaCl

LB-Amp-medium
LB-Medium with100 µg/ml ampicillin

LB-Amp-agar
LB-medium with 1.2% (w/v) bacto-Agar, cool down after heating at 50°C, add 100 µg/ml ampicillin, pour 20 ml on a 10 cm-dish.

2.7.2 Media and chemicals for mammalian cells

Neuroblastoma cells: RPMI-1640 (Sigma), 10% (v/v) FBS (Sigma), 1% (v/v) Penicillin/Streptomycin (100.000 U/ml, Invitrogene)

HEK 293T: DMEM (Sigma), 10% (v/v) FBS (Sigma), 1% (v/v) penicillin/streptomycin (100.000 U/ml, Sigma)

Freez medium 90% (v/v) FBS, 10% (v/v) DMSO

The chemicals following are used for selecting the infected cells and keeping the resistance in the cells.

4-Hydroxytamoxifen (Sigma) 200 nM in ethanol

Cycloheximid (Sigma) 50 µg/ml in ethanol

G418 (PAA) 500 µg/ml

Hygromycin B (Merck) 100 µg/ml

Puromycin (Invivogen) 1 µg/ml

MLN4924 (Active Biochem)

2.8 Buffers and solutions

Annealing buffer
10 mM Tris, pH 7.5–8.0, 50 mM NaCl, 1 mM EDTA

AnnexinV binding buffer
10 mM HEPES, pH 7.4, 140 mM NaCl, 2.5 mM $CaCl_2$

Bacterial lysis buffer

50 mM NaCl, 50 mM Tris base, 5 mM EDTA

Bacterial wash buffer

50 mM Tris base, 5 mM EDTA, adjust to pH 8 with 6 M HCl, 1:1000 proteinase inhibitors (freshly added)

Blocking solution for PVDF membrane

5% (w/v) skim milk powder in TBS-T

Crystal violet solution

0.1% (w/v) crystal violet, 20% (v/v) ethanol

DNA loading buffer

40% (w/v) saccharose (pH 8.0), 0.2% (w/v) bromphenol blue, 0.2% (w/v) xylene cyanol, 10 mM EDTA

PBS

137 mM NaCl, 2.7 mM KCl, 10.1 mM Na_2HPO_4, 1.76 mM KH_2PO_4 autoclaved

PI-FACS-buffer

38 mM sodium citrate, 54 mM propidium iodide, 24 mg/ml RNAse A

SDS sample buffer (3x)

187.5 mM Tris (pH 6.8), 30% (v/v) glycerine, 6% SDS (sodium dodecyl sulfate), 0.03%, (w/v) bromphenol blue, 2 M ß-mercaptoethanol

TBS (20x)

500 mM Tris Base, 2.8 M NaCl, adjusted to pH 7.4

TBS-T

0.2% Tween-20, 25 mM Tris, 140 mM NaCl, adjusted to pH 7.4

TBS-T

0.2% Tween-20, 25mM Tris, 140mM NaCl, adjusted to pH 7.4

TE

10 mM Tris, 1 mM EDTA, adjusted to pH 8.0

TAE

40 mM Tris, 0.114% (v/v) acetic acid, 1 mM EDTA, adjusted to pH 8.0

Trypsin solution

0.25% trypsin, 5 mM EDTA, 22.3 mM Tris pH 7.4, 125 mM NaCl

Bradford-solution 8.5% (v/v) Ortho-phosphoric acid

4.75% (v/v) ethanol, 0.01 (w/v) Coomassie Brilliant Blue G-250, filtered with filterpaper

5x high-MW running buffer
250 mM MOPs, 250 mM Tris, 5 mM EDTA, 0.5% SDS, add sodium bisulfite to 5 mM fresh

10% Bis-Tris gel

4x Bis-Tris buffer 2.5 ml, 30% acrylamid 3.3 ml, 10% APS 50ul, VE water 4.2 ml, TEMED 5 µl

BCA

Reagent a: Reagent b is 50:1, Reagent a: bicinchoninic acid, Reagent b: 4% $CuSO_4$ $5H_2O$

20x Transfer buffer

500 mM bis-tris, 500 mM Bicine, pH 7.2

1x Transfer buffer

25 mM bis-tris, 25 mM bis-tris, 20% Ethanol

Nuclear extraction buffer

20 mM HEPES-KOH pH 7.9, 400 mM NaCl, 1.5 mM MgCl2, 0.5 mM DTT, 0.2 mM EDTA, 15% glycrol

Cytoplasm extraction buffer

10 mM HEPES pH7.9, 1.5 mM MgCl2, 10 mM KCl, 0.5 mM DTT, 0.05% NP40

RIPA buffer

50 mM HEPES pH7.9, 140 mM NaCl, 1 mM EDTA, 1% Triton x-100, 0.1% Na-deoxycholate, 0.1% SDS

DNAzol reagent for isolating DNA from more than 10^7 cells

Trizol for isolating RNA

2.9 Consumables and equipment

Consumables such as reaction tubes, cell culture and other plastic products were purchased from Applied Biosystems, Eppendorf, Greiner, Kimberley-Clark, Nunc, Sarstedt, B. Braun, Schleicher und Schuell, Millipore and VWR international.

Chemiluminescence imaging

LAS-4000 mini (Fujifilm)

Cell culture incubator

BBD 6220 (Heraeus)

Cell counter

CASY cell counter (Innovatis)

Centrifuges

Galaxy MiniStar (VWR International)

Eppendorf 5417 R (Eppendorf)

Eppendorf 542 (Eppendorf)

Multifuge 1S-R (Heraeus)

Avanti J-26 XP (Beckman Coulter)

Fluorcytometer

BD FACS Canto II (BD Biosciences)

Heating block

Dry Bath System (STARLAB)

Incubator shaker

Model G25 (New Brunswick Scientific)

Illumina Genome Analyzer IIx

Microscope for immunofluorescence

PerkinElmer Operetta® High Content Imaging System

Microscope for cell culture

Axiovert 40CFL (Zeiss)

Nucleic acid analysis

Experion™ Automated Electrophoresis System (BIO-RAD)

PCR thermal cycler

Mastercycler pro S (Eppendorf)

Power supply

PowerPac HC (BIO-RAD)

Sterile bench

HeraSafe (Heraeus)

Ultrasonifier

W-250 D (Heinemann)

Universal shaker

SM-30 (Edmund Buehler GmbH)

UV fluorescent table

Maxi UV fluorescent table (PEQLAB)

UV filtered lamp

VL-6.MC with 312nm and 254nm (Vilber Lourmat)

Western blot transfer chamber

PEQLAB

2.10 Software

Ape plasmid editor

M. Wayne Davis

Bowtie (version 0.12.8)

Johns Hopkins University

Convert the .sam file into a .bam file

Samtools (version 0.1.18) (Li et al., 2009)

Convert the .bam file into a .bed file

Bedtools (version 2.17.0) (Quinlan and Hall, 2010)

GraphPad Prism

GraphPad Software

MxPro qPCR Software

Stratagene

Multi Gauge

Fujifilm

Mac OS X

Apple Inc.

Illustrator™, Photoshop™, Acrobat™

Adobe Inc.

R

Created by Ross Ihaka and Robert Gentleman

2.11 Dataset

Reference dataset used for the alignments

The human transcriptome “homo_sapiens.GRCh37.74.cDNA.all”

3 Methods

3.1 Molecular biology methods

3.1.1 Transfection of bacteria with plasmid DNA and plasmid amplification

Circular DNA can be transformed into bacteria to amplify the plasmid. Competent bacteria were thawed on ice and mixed with 200 ng plasmid DNA or ligation mix, then incubated on ice for 10 min followed by a 45 s heat shock at 42 °C. The bacteria were plated on an LB agar plate to pick clones from the next day or directly cultivated in 200 ml LB medium to amplify the plasmid on a larger scale. Both procedures were conducted at 37 °C using the appropriate antibiotic to select for bacteria that had been successfully transformed.

3.1.2 Isolation of plasmid DNA from bacteria

A large-scale purification of plasmid DNA was performed with the Plasmid Purifcation Maxi Kit (Invitrogen) according to the manufacturer's instructions. The purified plasmid was dissolved in B. Braun water, diluted to a concentration of 1 µg/µl and stored at -20 °C. For the isolation of small amounts of plasmid (mini prep), 2 ml of cultivated bacteria were transferred to a reaction tube, spun down and resuspended in 200 µl plasmid prep buffer 1 to lyse the cells. After a five-minute incubation at room temperature 200 µl plasmid prep buffer 2 was added to denature the protein components, these were spun down subsequently (8000 rpm, 5 min, 4 °C). The supernatant was vigorously mixed with 200 µl isopropanol to precipitate the DNA, which was then pelleted through centrifugation (8000 rpm, 10 min, 4 °C). The DNA was washed one with 70% Ethanol, then dried and resuspended in 50 µl B. Braun water.

3.1.3 Nucleid acid quantitation

The concentration of DNA and RNA in solution was determined with NanoDrop 1000. Purity was determined by assessing the ratio of absorbance at 260 and 280 nm. For pure DNA, A260/280 is ~ 1.8, for RNA ~ 2.

3.1.4 Sequence specific hydrolysis of DNA (restriction digest)

DNA was hydrolyzed in a sequence-specific manner with restriction endonucleases (Fermentas) using the recommended reaction buffers. The digestions were set up according to the table below and incubated at 37 °C for 1 h.

Table 8: Restriction digest mix

2 µg	DNA
1 µl	restriction endonuclease 1
1 µl	restriction endonuclease 2 (if applicable)
2 µl	10 x reaction buffer
Ad to 20 µl	aqua bidest.

3.1.5 Separation of DNA fragments via gel electrophoresis

DNA fragments of different sizes were separated by agarose gel electrophoresis. Depending on the fragment size, a solution of 1-3% agarose was boiled in TAE buffer. The size of the nucleotide fragments was determined using 1.5 µl of the 1 kb DNA Ladder. The gel was run at 120 V for one hour.

3.1.6 DNA extraction and purification from agarose gels

After separating the DNA by gel electrophoresis the fragment of interest was cut out of the gel with a scalpel. The DNA was extracted from the gel using the Gel Extraction Kit (Fermentas) following the manufacturer's protocol.

3.1.7 Ligation of DNA fragments

Insert and plasmid were incubated in a molar ration of 3:1 in the ligation mix according to the table below and incubated for 2 h at RT or overnight at 16 °C.

Table 9: Ligation mix

100ng	linearized plasmid
x ng	DNA fragment (insert)
2 µl	T4 DNA ligase buffer (Fermentas)
1 µl	T4 DNA ligase (Fermentas)
ad to 20 µl	aqua bidest.

3.1.8 Isolation of genomic DNA from mammalian cells with DNAzol reagent

1-3x10^7 cells were pelleted. 1 ml reagent (for 100 µl pellet) was added to lyse the cells by gently pipetting with a wide bore pipette tip. Centrifuged 10 minutes at 10000 rcf 4°C. The resulting viscous supernatant was transferred to a fresh tube to get rid of RNA. 0.5ml 100% ethanol was added, mixed by inversion and stored at RT for 1-3 minutes (a cloudy precipitate would be seen at this step). The DNA precipitate was transferred by spooling with a pipette tip into a clean tube. The precipitate was washed twice with 1 ml 75% ethanol by inverting the tube 3-6 times. Centrifuged 1 minute at 1000 rcf and 4°C and the ethanol was removed by pipetting. After second wash, the big DNA precipitate was transferred carefully into a new tube with fresh 8 mM NaOH already prepared. This step should be done within only 5-15 seconds. DNA was dissolved by slowly pipetting.

3.1.9 Isolation of RNA

For the isolation of total RNA from cultured cells TriFast reagent (Peqlab) was used. Cells were pelleted by centrifugation (5 min, 1500 rpm, 4 °C) and resuspended in 1 ml TriFast. After 5 minutes 200 ml chloroform was added and the mixture was vortexed for 15 seconds. After 10 minutes of incubation the solution was separated into aqueous and organic phase by centrifugation (10 min, 11400 rpm, RT). The upper aqueous phase was transferred into a new reaction tube, and the RNA was precipitated by adding an equal volume of isopropanol. The samples were stored at -20 °C for 30 minutes, then centrifuged (10 min, 11400 rpm, 4 °C) and the pellet was washed in 75% Ethanol and dried, then resuspended in 20 µl B. Braun water,

frozen at -20 °C, then thawed again and the RNA concentration was determined by NanoDrop measurement..

3.1.10 DNAse digestion and cDNA synthesis

To remove any residual traces of DNA from the RNA preparations, a DNAse digestion was performed on the total RNA isolated from the cells. 2 mg of RNA were diluted in 8 ml of B. Braun water and mixed with 1 ml of 10x digestion buffer containing $MgCl_2$, 1 ml of RNAse-free DNAse (Qiagen) and 0.2 ml of RNAse inhibitor Ribolock (Fermentas). This mix was incubated for 30 minutes at 37 °C, then 1 ml of 25 mM EDTA was added and incubated at 65 °C for 10 minutes to stop the digestion. To quantify specific mRNAs, the RNA was then transcribed into complementary DNA (cDNA) by reverse transcription, using random hexanucleotide primers. For that, 2 mg total RNA in a volume of 10 ml were heated up to 65 °C. The cDNA synthesis mix according to the table below was added and incubated for 10 min at RT, 50 min at 37 °C and 15 min at 70 °C.

Table 10: mix of cDNA synthesis

10 µl	5 x First Strand Buffer (Invitrogen)
5 µl	dNTPs (2.5 mM, Roth)
2 µl	random primer p (dN)6 (2 mg/ml)
0.2 µl	Ribolock (Fermentas)
1 µl	M-MLV reverse transcriptase (200 U/ml, Promega)
ad to 40 µl	B. Braun water

3.1.11 Polymerase chain reaction (PCR)

PCR to amplify cDNA for cloning

To generate new expression vectors the gene of interest was amplified based on existing expression vectors, which allowed the addition of new restriction sites.

Table 11: standard PCR setup

10 µl	5 x phusion polymerase buffer H (Fermentas)
1 µl	Phusion High Fidelity Polymerase (Fermentas)
100 ng	cDNA template
10 pmol	forward primer
10 pmol	reverse primer
1 µl	DMSO
1 µl	dNTPs (10mM)
ad to 50 µl	B. Braun water

PCR based site directed mutagenesis

To mutate single base in a PCR template primers were chosen as such to fit the desired target sequence. As such, a product mostly containing the modified bases was generated.

Table 12: Standard PCR thermal cycling profile

Temperature	Time	
98 °C	1 min	
98 °C 53-65 °C (template dependent) 68 °C	30 sec 60 sec 3 min	30 cycles
72 °C	10 min	

To remove residual wild type template DNA, the PCR product was digested with the enzyme DpnI (1 h, 37 °C), which hydrolyses only methylated DNA.

Table 13: Mutagenesis PCR setup

10 µl	5 x Phusion buffer H (Fermentas)
1 µl	Phusion High Fidelity Polymerase (Fermentas)
100 ng	cDNA template
0.25 pmol	forward primer
0.25 pmol	reverse primer
1 µl	dNTPs (10 mM)
ad to 50 µl	B. Braun water

Table 14: Mutagenesis PCR thermal cycling profile

Temperature	Time	
98 °C	1 min	
98 °C 55 °C 72 °C	30 sec 60 sec 2 min	18 cycles
72 °C	10 min	

Quantitative reverse transcriptase PCR (qRT-PCR)

To quantify specific mRNA levels the cDNA synthesized by reverse transcription was amplified by real time PCR. The qPCR SYBR Green Mix (Thermo Scientific) was used to set up a reaction mix as described in the table below. Finally, 10 ml of a 1:10 dilution of cDNA was added to each well, the measurement was carried out with the Mx3000P qPCR system (Stratagene).

Table 15: qRT PCR setup

5 µl	SYBR Green Mix (Thermo Scientific)
0.6 µl	0.6 µl forward primer (10 pmol/ ml)
0.6 µl	0.6 µl reverse primer (10 pmol/ ml)
1 µl	cDNA
ad to 20 µl	B. Braun water

Table 16: qRT PCR thermal cycling profile

Temperature	Time	
95 °C		
95 °C 60 °C (template dependent) 72 °C	30 sec 20 sec 15-60 sec (primer dependent)	38 cycles
95 °C	1 min	
60 °C	30 sec	
95 °C	30 sec	

The basis of real time PCR is fluorescent monitoring of DNA amplification, from which target DNA concentration can be determined from the fractional cycle at which a threshold amount of amplicon DNA is produced. The calculation was performed using the relative CT method (Applied Biosystems User Bulletin 2); the housekeeping gene beta-2-microglobulin (ß2M) was used for normalization. The measurements were performed in triplicates to calculate the standard deviation according to the Gaussian law of error.

3.2 Cell biology methods

All cell culture work was performed at a sterile workbench. Cells were cultivated in CO_2 incubators at 37 °C, 95% relative humidity and 5% CO_2.

3.2.1 Passaging of cells

Adherent cells were passaged before completely covering the surface to avoid contact inhibition of growth. The cultivation medium was removed and the cells were washed with PBS. An appropriate amount of trypsin solution was added and incubated for 5 minutes at 37 °C to detach the cells. By resuspending the cells in fresh medium the enzymatic activity of trypsin was stopped and a single cell solution was generated. For S2 cells the cell count was determined with a Neubauer counting chamber, for S1 cells with the CASY cell counter. The cells were then plated for experiments according to their size and proliferation rate in relation to the length of the experiment.

3.2.2 Freezing and thawing cells

For long-term freezer storage cells were detached with trypsin solution as described above, resuspended in fresh medium and then pelleted (5 min, 1200 rpm, RT). The cells were resuspended in 1 ml freezing medium containing DMSO, transferred to a cryo vial and then slowly frozen at -80 °C using a Mr FROSTY freezing container. After 24 h the cells were stored in a liquid nitrogen storage tank. To thaw cells stored in cryo vials these were quickly heated up in a 37 °C water bath, then transferred onto a 10 cm dish containing 10 ml fresh medium.

3.2.3 Production of lentivirus

$6x10^6$ HEK 293T cells were seeded in a 10 cm dish one day before transfection. The cells were starved for 2 hours with 2% serum before transfection. Packaging vector psPAX.2, envelope vector pMD2G and the gene of interest in a lentiviral vector, such as pRRL, pLKO, pGIPZ were first incubated 15 min with PEI (mass : volume =1:1) at RT. Then the mixture of DNA and PEI were added to cells drop by drop. The medium was replaced by full medium after 4 hours. First harvest was at 24 hours after changing medium, than the second and third harvests were done every 12 hours. The virus was filtered with 45 µm filter and stored at -80°C.

Table 17: Transfection setup with pLKO

pLKO	5 µg
psPAX.2	2.5 µg
pMD2G	1.25 µg
PEI	8.75 µl

Table 18: Transfection setup with pGIPZ

pGIPZ	3.5 µg
psPAX.2	2.7 µg
pMD2G	1.8 µg
PEI	8 µl

Table 19: Transfection setup with pRRL

pRRL	5 µg
psPAX.2	2.5 µg
pMD2G	1.25 µg
PEI	8.75 µl

3.2.4 Infection of mammalian cells with lentivirus

Lentivirus can efficiently mediate integration of transgenes in dividing and non-dividing cells. HEK 293T cells were used to generate lentivector particles by transfecting them with separate plasmids coding for the virion packaging system, the envelope, and the gene of interest. The structural and enzymatic components of the virion came from HIV-1, the envelope from vesicular stomatitis virus (VSV), using a second generation lentivirus packaging system.

Cells were seeded one day before infection. The high titer lentivirus was 1:7 diluted in pure medium for infection and supplied with 8 ng/µl polybrene. After 3-5 hours, the virus was removed and replaced by full medium. Appropriate antibiotic was used for selection 2 days after infection.

3.2.5 Colony formation Assay

The proliferation behavior of cells was determined by colony assay. Cells were infected with different genes of interest and a control and selected with antibiotics if necessary. After selection, the cells from each condition were counted and a defined number was plated on 6 cm dishes using medium without the selection agent. The cells were grown for 5 to 6 days until 80% confluent. Formaldehyde was directly added to medium to a final concentration of 3.7%. The cells were incubated with formaldehyde for 15 min at RT. After aspirating the formaldehyde the crystal violet was added to the cells and stay for half an hour, the superfluous dye was washed away with desalted water and the cell culture dishes were dried at room temperature.

3.2.6 Propidium iodide staining for flow cytometry (PI FACS)

FACS (fluorescence-activated cell sorting) was used to analyze cells based on detection of a fluorescent intercalating agent. The cell cycle stage was determined by measuring fluorescence emission of the intercalating dye propidium iodide (PI), which relates to the DNA content as follows: G0/G1 (2N), S (>2N, <4N) and G2/M (4N). Polyploid cells (>4N) and apoptotic or necrotic cells (subG1, <2N) could thus be identified as well.

Cells should not be confluent for checking cell cycle and were harvested by trypsinisation including floating cells from the medium supernatant. After resuspension in 1 ml cold PBS the cells were fixed by adding 4 ml ice-cold absolute ethanol while vortexing. The cells were stored at least one night at -20 °C, then washed with PBS and resuspended in FACS buffer containing propidium iodide solution. After at least 1 hour of staining in the dark at RT the cells were transferred into FACS tubes and measured with the BD FACSCanto II with the following measurement settings: excitation wavelength of 488nm using a 556 nm longpass- and a 585/42 nm bandpassfilter for propidium idodide (emission at 617 nm). The cell cycle distribution was analysed using the BD FACSDiva 6.1.2 software and flowjo 8.8.6.

3.2.7 AnnexinV/Propidium iodide assay for apoptosis (AV/PI FACS)

Cells from a 6-well dish were harvested by trypsinisation including the floating dead cells to a 15ml falcon and always kept on ice. The plate was washed with PBS adding to harvested cells. The cells were pelleted by centrifugation (300 g, 4 °C). The supernatant is aspirated down to the last 50 µl and vortex gently to loosen cell pellets. 100 µl AnnexinV binding buffer was added to the cell and vortex again to suspend cells. Then, 5 µl AnnexinV-488 was added to each falcon and incubate 15 minutes at RT. After incubation 300 µl chilled AnnexinV binding buffer was added to the falcon to stop the staining. 5 µl of PI stock solution (1 mg/ml) was added to each tube immediately prior to placement on the FACS.

3.2.8 Bromodeoxyuridine/Propidium iodide assay for apoptosis (BrdU/PI FACS)

BrdU is added directly to the culture medium to achieve a final concentration of 10 µM. The cells were incubated for 60 minutes in the CO_2 incubator. The cells were trypsinized and washed with PBS and spun down at 1500rpm for 5 minutes at 4 °C. The pellet was resuspended in 1 ml cold PBS. Cells should be added slowly, a few drops at a time, into the 4 ml ethanol while maintaining a vortex and stored at -20°C to fix the cells.

On the day of FACS cells were centrifuged at 2000 rpm for 10 minutes at 4 °C. The supernatant was aspirated carefully. The cells were washed once with 5 ml PBS and spun down at 1500 rpm for 10 minutes at 4 °C. 1 ml of 2 N HCl/Triton X-100 was slowly added to the cells, a few drops at a time, while maintaining a vortex and incubated at RT for an additional 30 minutes, gently vortexed every 10 minutes. This denatures the DNA to produce single-stranded molecules. The cells were centrifuged at 2000 rpm for 10 minutes. Supernatant was aspirated and the cells were resuspended in 1 ml of 0.1 M $Na_2B_4O_7{\cdot}10H_2O$, pH 8.5, to neutralize the acid. The cells were centrifuged at 2000rpm for 10 minutes. The supernatant was aspirated and the cells resuspended with 100 µl of 0.5% Tween 20/ 1%BSA/ PBS. 20 µl BrdU-FITC antibody was added and incubated in dark for 30 minutes. Cells were centrifuged at 2000 rpm for 5 minutes at 4°C and the supernatant was aspirated. The cells were washed once with 200 µl 0.5% Tween 20/ 1%BSA/ PBS. Pellet was resuspended with 38mM sodium citrate (400 µl) supplied with 54 µM propidium iodide (15 µl) and 24 µg/ml RNaseA (1 µl from stock solution) and incubated for 30 minutes at 37 °C in the dark. Cells were transferred into FACS tube mix with pipette and continue with FACS measurement (PI : FL2-A LIN, BrdU : FL1-H Log).

3.3 Protein biochemistry methods

3.3.1 Cell lysis for Western blot

To isolate total protein cells were washed in ice cold PBS, scraped of the cell culture dish and pelleted (1500 rpm, 5 min, 4 °C). The cell pellet was either frozen in liquid nitrogen to be stored at -80 °C or directly lysed by resuspending cells in TNN-, NP40-, RIPA-r or SDS sample buffer with freshly added proteinase inhibitors (1:1000) or phosphatase inhibitor (1:100). The cells were incubated for 30 minutes on ice, then the cell debris was pelleted (14000 rpm, 10 min, 4 °C) and the supernatant transferred to a fresh tube. Alternatively, cells grown in 24- or 6-well plates were lysed directly in hot SDS sample buffer, transferred to a reaction tube and boiled for 15 minutes. The lysates were then used for Western blot analysis or stored at -20 °C.

3.3.2 Protein determination by the Bradford method

Protein concentrations were determined according to Bradford (Bradford, 1976). 100 µl 0.15 M NaCl was pipetted into cuvette, 1 µl of the protein sample solution was added and mixed with 900 µl Bradford dye reagent. After vortex the absorption was measured at a wavelength of 595 nm using an appropriate reference. The measured values were compared to a previously obtained calibration curve to calculate the protein concentration of the sample solution.

3.3.3 Protein determination by the BCA (Bicinchoninic acid assay)

The BCA Protein Assay is a detergent-compatible formulation based on bicinchoninic acid (BCA) for the colorimetric detection and quantitation of total protein. 200 µl mixture of bicinchoninic acid and $CuSO_4$ (50:1) was pipetted into a 96-well plate. 3 µl protein lysate was added to the mixture. After incubation 30 minutes at 37 °C, the absorption was measured at 550 nm (instead of 632 nm) using an appropriate reference. The measured values were compared to a previously obtained standard curve to calculate the protein concentration of the sample solution.

3.3.4 SDS polyacrylamide gel electrophoresis (SDS-PAGE) with Bis-Tris gels

Bis-Tris SDS-PAGE (Sodium dodecyl sulfate polyacrylamide gel electrophoresis) was used to separate proteins according to size (Laemmli et al., 1970). Protein lysates as described in 3.3.1

were filled up with lysis buffer to an equal volume and mixed with half the volume of 3 x SDS sample buffer. These samples were incubated for 5 minutes at 95 °C and spun down afterwards. The protein samples were then transferred into the wells of an SDS polyacrylamide gel consisting of a 7.5-15% stacking gel and a 4% resolving gel. The PageRuler Pre-Stained Protein Ladder (Fermentas) was used for monitoring the running.

3.3.5 Western blot

Proteins were separated by SDS-PAGE (3.3.3), followed by blotting onto a PVDF membrane using a transfer blot system. A PVDF membrane the size of the SDS gel was incubated first in methanol for at least 30s. Gel was first calibrated in transfer blot buffer for 10 minutes on a shaker. Gel and membrane were neatly layered on top of each other and fixed between Whatman filter papers in a Western blot transfer chamber (Peqlab). The electrophoretic protein transfer was carried out at 250 mA for 3 h. All following incubation steps were performed with gentle shaking. The membrane with immobilized proteins was blocked in blocking solution 5% milk solved in TBS-T for at least 30 min, then cut into pieces if several proteins from the same membrane were to be visualized. The membrane pieces were incubated overnight with a dilution of primary antibody in blocking solution, then washed (3 x 10 min in TBS-T), incubated with secondary antibody in blocking solution for 1 hour at RT, then again washed (3 x 10 min in TBS-T). Finally, the proteins of interest were visualized via chemiluminescence, To trigger a specific chemiluminescent signal the Immobilon Western Chemiluminescent HRP Substrate from Millipore was used according to the manufacturer's instructions, the signal was detected with the ImageQuant LAS 4000 imager.

3.3.6 Indirect immunofluorescence imaged by confocal fluorescence microscope (Leica)

Cells were cultivated and transfected on cover slips to be processed for indirect immunofluorescence. To fix the cells they were incubated in 3.7% paraformaldehyde or methanol for 15 min at RT after an initial wash with ice cold PBS. To permeabilized the cells they were washed with PBS/ 0.1M glycin (3x 10min, RT) and PBS/ 0.1% NP-40 (3x 10min, RT), to be blocked with PBS/ 0.5 % NP-40/ 5 % FCS (blocking buffer) for 45 min at 37 °C. The cover slips were transferred into a wet chamber with the cells facing upward and 40 µl of primary antibody diluted in blocking buffer was pipetted on top. After an incubation time of 45

min at 37 °C the cells were washed three times with blocking buffer. Next the cells were incubated with a 40 µl dilution of secondary antibody and Hoechst nuclear stain (1:5000) in blocking solution, again for 45 min at 37 °C in the dark. Unbound antibody was removed by washing three times with blocking buffer. Finally the cover slips were washed with distilled water and mounted on a glass slide using a small drop of mounting medium, the slides could be stored in the dark at 4 °C before analyzing them with the fluorescence microscope.

3.3.7 Indirect immunofluorescence imaged by high content fluorescence microscope

If the staining is imaged and quantified by high content fluorescence microscope the cells were plated in 96-well plate and fixed on the plate. The following procedure is the same as 3.3.6

3.3.8 UV treatment of cells

Before irradiation of attached cells, the medium supernatant was completely removed. The cells were irradiated for 60 s at 254nm after which the medium was restored. Cells on 6 cm or 10 cm dishes were treated with a dose of 500 J/m2 UV-B all at the same time and then harvested at different time points by trypsinisation, including floating cells in the medium supernatant.

3.3.9 Histone extraction

Cells were harvested and washed twice with ice-cold PBS. PBS can be supplemented with 5 mM Sodium Butyrate to retain levels of histone acetylation. Cells were resuspended in Triton Extraction Buffer (TEB: PBS containing 0.5% Triton X-100 (v/v), 2 mM PMSF, 0.02% (w/v) NaN_3) at a cell density of 10^7 cells per ml. Cells were lysed on ice for 10 minutes with gentle stirring and spun down at 2000 rpm for 10 minutes at 4 °C. Supernatant was removed and discarded. The cells were washed in half the volume of TEB and centrifuged like before. The pellet was resuspended in 0.2 N HCl at a cell density of $4x10^7$ cells per ml to acid extract the histones over night at 4 °C. Centrifuged samples at 2000rpm for 10 minutes at 4 °C. The supernatant was removed and the protein content was determined using the Bradford assay. Aliquots were stored at -20°C.

3.3.10 Nuclear fractionation

Buffer A (10 mM HEPES, 1.5 mM MgCl2, 10 mM KCl, 0.5 mM DTT, 0.05% NP40 pH 7.9) was prepared with adding cocktail of usual inhibitors from frozen stock and stored on ice. 500 µl of buffer A was added per large petri dish on ice and scraped thoroughly. The lysate was left on ice for 10 minutes and centrifuged at 4°C at 3000 rpm for 10 minutes. Supernatant was removed and kept (this will contain everything except large plasma membrane pieces, DNA, nucleoli). Pellet was resuspended in 374 µl of buffer B (5 mM HEPES, 1.5 mM MgCl2, 0.2 mM EDTA, 0.5mM DTT, 26% glycerol (v/v), pH 7.9) on ice and 26 µl of 4.6 M NaCl to give 300 mM NaCl (high salt helps lyse membrans and forces DNA into solution) was added. The extract was homogenized with 20 full strokes in Dounce or glass homogenizer on ice if necessary. The extact was left on ice for 30 minutes. Centrifuged at 24,000 rcf for 20 minutes at 4 °C. Supernatant was aliquoted and stored at -80 °C.

3.3.11 Chromatin immunoprecipitation (ChIP)

Chromatin preparation

Cells were plated on five 15 cm dishes. Formaldehyde was added to the medium to a final concentration 1% to crosslink the protein to DNA and incubated for 10 minutes at RT. 1 ml 1 M glycine was added to medium for 5 min at RT on a shaker to stop the formaldehyde. The medium was removed and cells were washed twice with ice cold PBS. 1 ml ice cold PBS containing protease inhibitor cocktail was added to the cells. The cells were scraped off the plate to 15 ml falcon and pelleted at 1200 rpm, 4 °C, then resuspend in 3 ml lysis buffer 1 (5 mM PIPES pH 8, 85 mM KCl, 0.5% NP40) containing protease inhibitors, incubated on ice for 20 minutes. The cells were centrifuged at 1200 rpm for 5 min at 4 °C, resuspend in 2 ml lysis buffer 2 (RIPA buffer: 50 mM HEPES pH 7.9, 140 mM NaCl, 1 mM EDTA, 1% Triton-X-100, 0,1% Nadeoxycholate, 0,1% SDS), incubated on ice for 10 minutes. Cell lysate was sonicated in a program according to your requirement. After sonication the cell lysate was transferred to an tube and centrifuged at max speed for 15 minutes at 4 °C. The supernatant (chromatin) was transferred to a new tube, kept at 4 °C for a few days or frozen in liquid nitrogen and stored at -80 °C.

Check fragment size after sonication

25 µl chromatin was added to 475 µl TE buffer used for checking fragment. NaCl to a final concentration of 160 mM and RNAse A to a final concentration of 20 µg/ml were added to the chromatin. The chromatin was incubated at 37 °C for 1 hour for reverting the crosslink. EDTA to a final concentration of 5 mM and Proteinase K to 200 µg/ml were added to chromatin, then incubate for 2 h at 45 °C. 300 µl chloroform/ phenol/ isoamyalcohol (25:24:1) was added to the DNA and vortex well. The sample was centrifuged for 5 minutes at max speed at RT. The upper phase was transferred to a new reaction tube. 1 µl glycoblue, 50 µl 3 M NaAc pH 5.2, 1 ml ice cold 100% ethanol were added to the sample and incubated for 30 minutes at -20 °C, then centrifuge at max speed at 4 °C for 30 min. The supernatant was removed. The pellet was washed with 500 µl ice cold 70% ethanol, centrifuged at max speed for 10 minutes at 4 °C and dried at RT, resuspended in 25 µl TE. 10 µl sample was loaded on 2% agarose gel.

Chromatin immunoprecipitation

30 µl dynabeads was used for antibody, washed 3 times with 1ml BSA-PBS (5 mg/ml). 1 ml BSA-PBS and 3 µg antibody were added to the beads and incubated overnight at 4 °C on rotating wheel. The beads were washed for 3 times with 1 ml BSA-PBS and resuspended in 30 µl BSA-PBS. Appropriate amount of chromatin was added to the beads and keep 1% chromatin as input. The beads were incubated at 4 °C for 6 hours on rotating wheel and washed with wash buffer I (20 mM Tris HCl pH 8,1, 150 mM NaCl , 2 mM EDTA, 0,1% SDS, 1% Triton-X-100), wash buffer II (10 mM Tris HCl pH 8,1, 500 mM NaCl, 2 mM EDTA, 0,1% SDS, 1% Triton X-100), wash buffer III (10 mM Tris HCl pH 8 , 250 mM LiCl, 1 mM EDTA, 1% NP40, 1% sodium deoxycholate) for 3 times by incubating each time for 5 minutes at 4°C, respectively. The beads were denn washed once with TE buffer. The chromatin was eluted twice with 250 µl elution buffer (50 mM Tris pH 7.5, 1 mM EDTA, add freshly SDS to a final concentration 1%) by incubating at RT on rotating wheel for 15 minutes. The two eluates were merged.

16 µl 5 M NaCl and 1 µl RNase A (10 mg/ml) were added to eluate and incubated 1 hour at 37 °C and 6 hours at 65 °C. Afterwards 7 µl 0.5 M EDTA and 10 µl proteinase K (10 mg/ml) were added to the eluate and the eluate was incubated 2 hours at 45 °C. The DNA was purified with phenol/ chloroform.

3.4 Screening of pGIPZ Lentiviral library

3.4.1 Preparation of pooled plasmids

The lentiviral library was obtained from Lars Zender as 60 pools, each of which contains 1000 individual plasmids. To prepare plasmid DNA it is important to take care of sufficient colonies on agar plates after bacterial transformation. For 1000 individual plasmids the number of colonies being inoculated for an overnight culture has to be, due to variations of individual plasmid concentrations, 10,000 or higher (the higher the better).

The bacteria competence had to be checked first: 1 µg of plasmid DNA should create more than 10^6 colonies. To check, dilute DNA and/or bacteria to get information on competence and total yield of bacteria.

3.4.1.1 Transformation of suitable bacterial strain

1 µg of plasmid DNA was added to 200 µl of freshly thaw DH5α competent cells and incubated for 30 minutes on ice. After a 2 minutes heat shock at 42 °C 800 µl of LB medium was added to the cells. The bacteria were incubated for 45 minutes at 37 °C. After incubation the bacteria were spun down at 6000 rpm for 3 minutes in an eppendorf centrifuge. Supernatant was then reduced to 500 µl. The pellet was resuspended and bacterial suspension was plated out in LB agar plates containing 100 µl/ml ampicillin. Colonies were grown overnight at 37 °C. At the next day the plates should yield more than 10,000 colonies.

3.4.1.2 Overnight culture

Bacteria were transferred into 200 ml of LB-Amp medium. The bacterial culture was incubated overnight on a rotary shaker at 37 °C.

3.4.1.3 Plasmid preparation

Bacteria were harvested by centrifugation at 8000 rpm for 30 minutes at 4 °C in a sorvall or Beckman centrifuge. Plasmid DNA was prepared from bacteria with maxi prep kit (Jetstar) according to the supplier's protocol.

3.4.2 Preparation of lentiviruses

HEK 293T cells were grown in DMEM medium containing 10% FCS and 1% penicillin/streptomycin on 10 cm plates. At the day of transfection cells should be grown to 50%-70% confluence. Cells were transfected with the following vectors:

pGIPZ	library vector containing mammalian puromycin resistance gene, GFP, sh RNA coding sequences driven by CMV promoter
psPAX2	packaging vector containing all required genes for packaging
pMD2-VsVg	envelope plasmid encoding for the VsVg surface protein resulting in a higher virus stability

Total 8 µg of plasmids were incubated with 16 µl polyethyleneimin (PEI) for 15 minutes then transfected to HEK 293T cells (3.5 µg of pGIPZ, 2.7 µg of psPAX2, and 1.8 µg of pMD2-VsVg). The DNA ratio/amounts were adapted from a protocol of Manfred Gessler. Fluorophore expression was checked 24 hours after transfection. The transfection efficiency was determined to be close to 100% as seen by GFP expression, but the fluorescense only proofs the presence and functionally of the library vector but not the generation of viruses.

Virus containing supernatant was harvested 36 hours, 48 hours and 72 hours post transfection. Supernatant was passed through a 0.22 µm filter to get rid of cell debris and stored at -80°C.

3.4.3 Checking the virus titer

Since the virus expresses GFP, the titer can be easily determined by FACS analysis. This has to be done for each cell line you want to infect, since some cell lines are more difficult to infect than others.

Dilute virus (example, 5-fold 20-fold 100-fold diluted) in DMEM supplemented with 8 µg/ml polybrene (sequabrene^{TM}, Sigma). Polybrene is a cation that is often pre-incubated with the virus particles to give it a net positive charge, which helps to counteract the negatively-charged cell surface membrane. Cells were infected at 50% confluency with diluted virus solutions. One plate was kept uninfected as negative control.

6 plates of HEK cells were used to produce lentiviruses. As library vector a pool of 10000 individual pGIPZ plasmids were used. After 24 hours post-infection, the virus was harvested every 12 hours up to 72 hours. The viruses harvested at different time points were combined.

A 10 cm plate of SHEP-N-MycER cells at 50% confluency were infected by adding the diluted virus solutions quantitatively. 48 hours after infection cells were fixed with 3.7% formaldehyde and subjected to FACS analysis. Green cells appeared dependent on the dilution of the virus with a frequency of 0.5, 1.5 or 7.5%, respectively.

3.4.4 Infecting SHEP-N-MycER cells with pool of 10000 individual viruses

Ideally there should be an equal distribution of all individual plasmids in such a pool. In reality there can be a big difference between one individual plasmid being the most under- or over-represented. If one plasmid is underrepresented more than 10 times if compared to the average, you would not find this plasmid anymore if you would analyze 10^5 sequences. Since nothing is known about the quality of the pools received from Lars Zender in terms of distribution of individual clones. Finally, 10^7 sequences should be obtained by high-throughput sequencing using a Genome analyzer IIx (Illumina). This important number 10^7 should be kept throughout the experiment.

As a start a huge number of lentiviruses were generated. The aim is to have sufficient virus to obtain 10^7 green cells after infection. To avoid multiple infections the multiplicity of infection (MOI) should be kept quite low (0.1). Therefore, 10^8 cells have to be infected to achieve 10^7 infected cells. To generate a 10000-pool 10 of the 1000 pools were combined. It is important to have the correct concentrations of each 1000 pool and it should be done with one and the same pipet. 5 µg of each 1000 pool were combined (pool 51-150, pool 461-560) and the concentration determined. Viruses were generated and the titer determined in SHEP-N-MycER cells (see 3.4.3). 15 cm plates with these cells at 50% confluency were infected with the virus pool. SHEP-N-MycER cells at confluency in 15 cm plates are $1.2x10^7$. $6x10^6$ cells (50% of confluency is $6x10^6$, to keep MOI 0.1, $6x10^5$ cells were infected) were seeded for infection for the next day. To keep redundancy 1000, minimal 17 plates were required. Two days after infection puromycin was added (1 µg/ml final concentration) to select the infected cells for 2 days. After 2 days selection all positive cells (should at least 10^7 cells) from 17 plates were combined and distributed to 3 plates (redundancy). The cells were grown to confluency ($1.2x10^7$), split (while splitting always first combine and split to keep redundancy!!) 1:3 into new 15cm plates, now

there were 9 plates altogether. Every 3 plates ($1.2x10^7$ altogether) was one unit kept for the redundancy 1000. So until now there were 3 units. One unit was kept as control, one was treated with ethanol and one was treated with 100 nM tamoxifen. Until the 3 units were grown to confluency, they were split 1:3 (at least 9 plates in all). One unit (3 plates) was used for propagation. The other two (6 plates) were used for isolating genomic DNA.

3.4.5 PCR amplification of shRNA coding sequences

Since shRNA coding sequences were introduced into the genome via the same vector, they can be amplified in an equal distribution by flanking primers. The shRNA coding sequences were embedded in a sequence coding for the mir30 micro RNA. To avoid primer annealing the mir30 sequence in the human genome (chromosome 6) the sense primer was designed to anneal outside of the mir30 sequence on the pGIPZ vector. The antisense primer anneals within the mir30 sequence but the vector sequence is interrupted by an EcoRI site, which is not present in the original mir30 sequence. This design was chosen to keep the resulting PCR-product below 300bp. Both sense and antisense primer were introduced a grafting sequence being required for cluster formation on an illumina single read sequencing flow cell.

To keep the redundancy of 1000 copies of each individual clone, the genomic DNA of 10^7 cells was required for the first PCR step. The genomic DNA of one cell contains one shRNA.

Bp (660g/mol) x $6.4x10^9$ (diploid human cell) = 7 pg DNA/ cell

Using 10^7 cells: 70 µg of genomic DNA had to be subjected to PCR

Typically 1 µg of genomic DNA was used in 50 µl PCR reactions. Therefore up to 70 reactions had to be performed. The amount of PCR product being produced was much lower:

Bp (660g/mol) x 300bp (fragment length) = 3.3×10^{-19} g

At 10^7 sequences: 3.3pg of PCR product are required to keep the redundancy.

Table 20: PCR mix

98°C 1min 64°C 1min	30 cycles

72°C 1min	

The PCR reactions of the 70 reactions were pooled and the DNA precipitated using 1/10 vol of 3 M NaAc pH 5.2 and an equal volume of isopropanol. After centrifugation the pellet was washed once with 70% ethanol, again centrifuged and the supernatant discarded. The pellet was air dried and resolved in 150 µl TE buffer pH 7.6. 30 µl of 6x agarose loading dye was added and the mixture loaded onto a 1.8% LMP agarose gel. After electrophoresis the bands were excised and the DNA extracted by columns. The DNA concentration was determined.

3.5 Sequencing DNA template

The DNA sample preparation part used the single-read cluster generation kit v2 on the cluster station according to the illumina standard protocol. The DNA template was prepared at a concentration of 10 nM in Tris-Cl 10 mM, pH 8.5 and denatured with 2 N NaOH to a final DNA concentration of 1 nM, diluted with pre-chilled hybridization buffer to a volume of 1000 µl to concentration of 5 pM and 8 pM. The DNA samples were ready in an eight-tube strip and loaded to the cluster station for cluster amplification, linearization, blocking and primer hybridization. Afterwards the sequencing reagents were prepared and the flow cell with clusters was transferred and loaded on to genome analyzer following the reagent preparation instructions described in using the SBS sequencing kit v3 36 cycles on the genome analyzer and the standard sequencing protocol described in the sequencing user guide.

Table 21: Flow cell 2011.01.19

Lane	1	2	3	4	5	6	7	8
Sample	EU	LU	LS	EU	phix	LU	LS	
Concentration	5 pM	5 pM	5 pM	8 pM	8 pM	8 pM	8 pM	

Table 22: Flow cell 2011.02.11

Lane	1	2	3	4	5	6	7	8
Sample	EU	LU	LS	EU	LU	LS	phix	
Concentration	5 pM	5 pM	5 pM	8 pM	8 pM	8 pM	8 pM	

3.6 Sequencing data analysis

The sequencing data converting, alignment, statistical analyses were done by Mark Onyango and Carsten Ade.

A total of 18290 unique shRNAmir constructs cloned in the lentiviral RNAi vector pGIPZ were used to carry out two negative selection screens in SHEP-N-MycER cells. Both screens were done in an equal format, one with a pool of 9589 and the other one with a pool of 8701 constructs. Both screens were done in two biological replicates.

To guarantee a sufficient redundancy for all sequenced shRNAs, at least 8 million reads were generated by next generation sequencing (Illumina GAIIx) for each sample. The raw-sequences were filtered for high quality reads using the Illumina CASAVA software. For each sample, all reads with a reliable quality score were extracted and written in a FASTQ file. To allow for a combined analysis of the changes in frequency of all screened shRNAs, the sequencing data generated for corresponding conditions (EU, LU or LS) of corresponding biological replicates (replicate 1 or replicate 2) of both screens were combined in joint FASTQ files. Adjusting the sizes of all initial FASTQ files prior to their fusion guaranteed that subsequent normalizations of the joint dataset do not result in an unequal weighting of the sequencing data generated in the separate screens.

The alignment of FASQ files was performed in Bowtie tool. The criteria used for the alignment to the reference was the default settings except for discarding all shRNAs that did not align 100%, only 0 mismatch was allowed. After the data was aligned, a custom tool designed by Mark Onyango was used to create the count matrix (Onyango et al., 2013). The tool creates a matrix with the target shRNAs as rows and the individual samples/replicates as columns. Each

alignment in the alignment file was counted and summed up in the count matrix. The count matrix was then used to run DESeq analysis tool with the default routine under R environment, calculating the different sequencing depth to get the size factors. The variance in the data was then calculated. The differential expression was analyzed using a cutoff value of 0.05 for the p-value which is quite standard.

To identify annotated and protein encoding target genes, all 18290 constructs were mapped against the most recent human transcriptome (GRCh37) resulting in 13406 unique combinations of shRNA sequences and target genes. This new list of shRNA-sequences was used as a reference for the alignment of the raw-sequences generated for each sample. Based on these alignments, the abundances of all shRNAs targeting annotated genes were determined for each condition.

4 Results

4.1 Genome-wide lentiviral shRNA screen

4.1.1 Work flow of screen

For screening, we used the neuroblastoma cell line SHEP with an inducible N-MycER construct that can be activated by tamoxifen (4-OHT). Western blot analysis shows N-Myc is activated upon tamoxifen treatment (Figure 5A). SHEP is a *MYCN*-nonamplified neuroblastoma cell line which carrys a single copy of *MYCN*. Briefly, shRNA screens were conducted in a pooled format using a total of 18290 unique pGIPZ based shRNAmir constructs. These 18290 constructs constitute largely the releases 6.2, 6.3, 6.10, 6.11 and 6.12 of the commercial genome-wide Open-Biosystems shRNA pGIPZ-library as described in materials chapter. The screen was done in two independent experiments, one with a pool of 9589 and the other one with a pool of 8701 constructs. For both screens, two biological replicates were done, including infection of the cells with independently prepared lentivirus-pools.

Figure 5B shows how the screens were performed. For each screen, a large population of SHEP-N-MycER cells were infected with the pooled shRNA library and selected with puromycin. This assured a multiplicity of infection (MOI) of < 0.1 and consequently the integration of not more than a single shRNA construct into the targeted cell genome. Further more, the theoretical redundancy per shRNA in the infected cell population was > 1000. After selection, the cells were splited into three populations. Cells of the first population were immediately harvested and defined as the early unstimulated condition (EU). The other two populations were treated with ethanol or with 100nM tamoxifen (4-OHT) to activate N-Myc and cultured for approximately two weeks. Cells of the control population were harvested and defined as late unstimulated condition (LU) while cells of the 4-OHT treated population were harvested and defined as late stimulated condition (LS). After isolating genomic DNA, the shRNA cassettes were PCR amplified using primers referred as grafting-primer-3' and grafting-primer-5' (Figure 5C). These primers introduced adapter sequences ("graft sequence") required for the amplification products to bind to the Illumina flowcell for next generation sequencing. The quality and quantity of PCR product were determined by Experion chip electrophoresis. Figure 5D shows the PCR product of a length of 340bp. Afterwards the standard Illumina protocol was used for the next generation sequencing of PCR products on a genome Analyzer IIX. Changes in frequencies of individual

shRNAs were calculated from their relative abundances in the cell populations of the three different conditions.

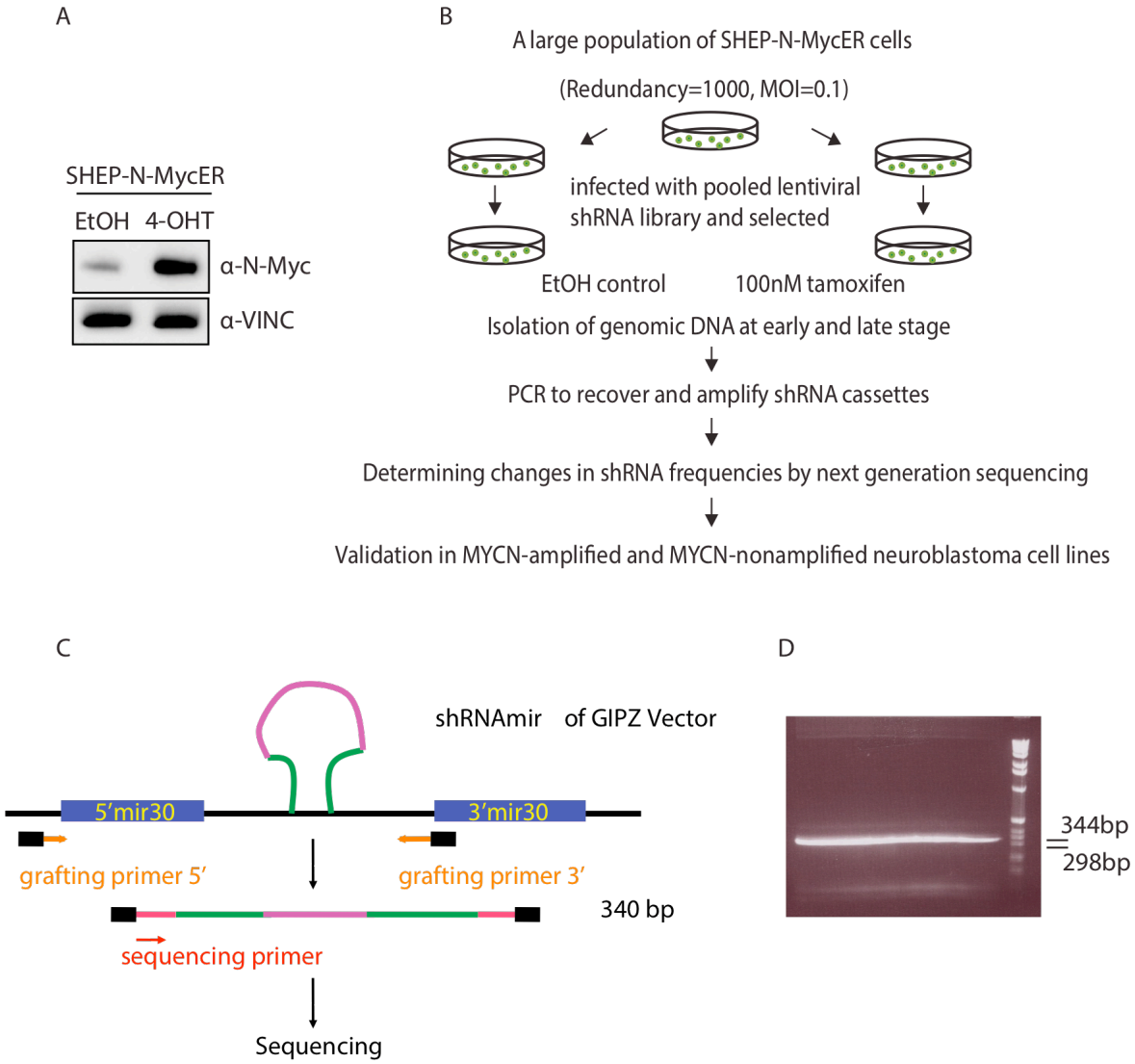

Figure 5: Workflow of screen

(A) SHEP-N-MycER cells were treated with 100nM 4-OHT for 24 hours and lysed with RIPA buffer. The protein extracts were analysed by western blot.

(B) Flow chart of the screening procedure. A large population of SHEP-N-MycER cells were infected with a pooled lentiviral shRNA library. After selection with puromycin, the cells were split into three populations, one was harvested immediately after selection, one treated with 100nM tamoxifen to activate N-MycER while the other population was treated with ethanol used as reference. The genomic DNA was isolated from cells two weeks after tamoxifen treatment and subjected to PCR to amplify the shRNA cassettes. The frequencies of shRNAs were determined by next generation sequencing.

(C) Schematic of shRNAmir sequence of GIPZ vector and primer binding sites. Two blue bars indicate the start and end of mir30 region. Green-red-green line indicates the stem-loop-stem structure. Grafting primers have a grafting sequence at 3' end representing the adaptor sequence required for binding to the flow cell. 5'grafting primer binds to a region outside of 5'mir30 whereas 3'grafting primer binds within the 3'mir30 sequence. The primer pair amplifies a length of 340bp long product.

(D) The PCR products were pooled, precipitated, then dissolved in TE buffer and subsequently purified by gel electrophoresis using a 0.8% agarose gel.

4.1.2 Polo-like kinase 1 (PLK1) is a positive control for the lethal effect

For the screen shRNAs of interest are strongly depleted after activation of N-Myc. In this context, two important questions have to be answered prior the conduction of a large-scale screen. First, how fast does a lethal shRNA disappear completely from the cell population as a result of apoptosis induction? Second, how long after the start of the screen will a pGIPZ-based shRNA be functional? To answer these questions, we used shRNAs targeting PLK1 as "proof of principle". To exclude apoptosis, we used PLK1 as positive control to mimic the lethal effects. Depletion of PLK1 induces apoptosis and growth arrest, which leads to a strong lethal effect. Three PLK1 shRNAs based on pGIPZ vector backbone were used. All of the shRNAs show good knockdown efficiency (Figure 6A) and the depletion of PLK1 over 7 days clarly shows a delay in proliferation but no complete loss of growth (Figure 6B). The sh #711 reduces mRNA level for 70% while sh #709 and sh #708 reduce mRNA level for more than 80%. Additionally, all shRNAs show growth arrest in SHEP-N-MycER cells (Figure 6B).

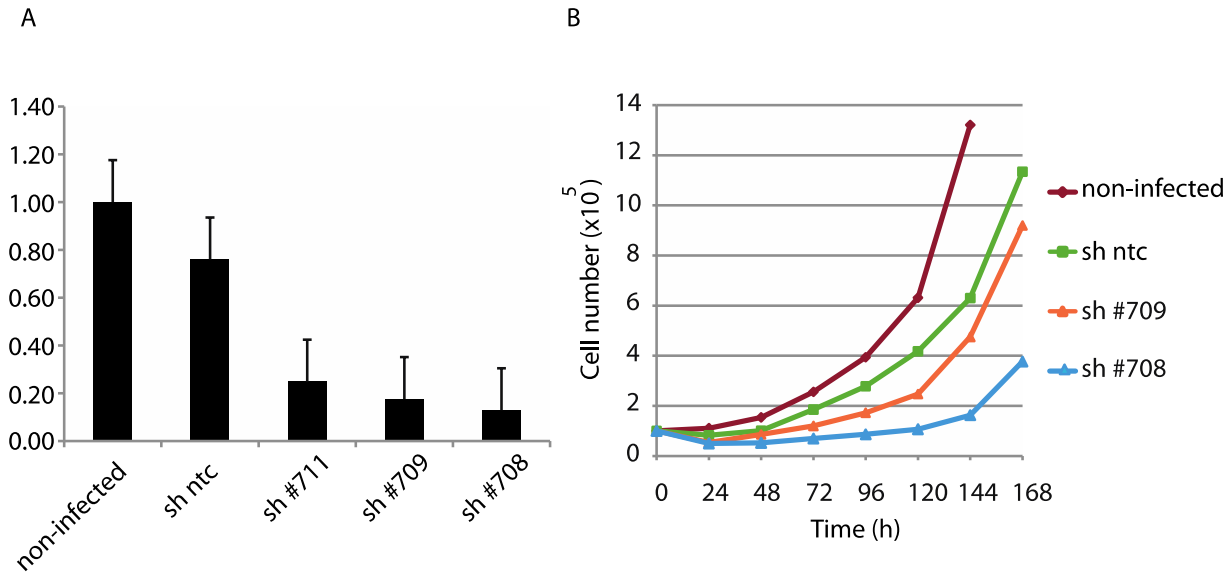

Figure 6: SHEP-N-MycER cells infected with PLK-1 shRNAs have a growth disadvantage.

(A) RT-PCR determines the knockdown efficiency of PLK1 shRNAs.

(B) SHEP-N-MycER cells infected with PLK1 shRNAs have a proliferation delay. Cells with different PLK1 shRNAs were plated on day 0 and counted on every 24 h until 168 h.

To better visualize the behaviour of PLK1 shRNAs, a dual-colour competition assay was performed. The vector's GFP marker was exchanged for RFP marker to obtain a shRNA targeting *PLK1* with red fluorescence. Equal amounts of sh ntc (a non-targeting shRNA as control) in green and sh plk1 in red were plated on day 0. The cells were harvested at regular intervals. The ratio of green and red cells was determined by flow cytometry (Figure 7A). The assays were conducted with sh #709 and sh #708, both of which have a good knockdown efficiency (Figure 6A). The assay showed until day 9 the sh #708 decreases from 51% to 8.5% indicating a 6-fold reduction.

From day 9 onwards, the two curves stay parallel meaning the ratio between red and green cells remains unchanged (Figure 7B). The sh #709 shows a similar effect as sh #708 with a 2.7-fold decrease (Figure 7C). The result leads us to the conclusion that sh plk1 is depleted in the mixed population only over the course of the first 9 days.

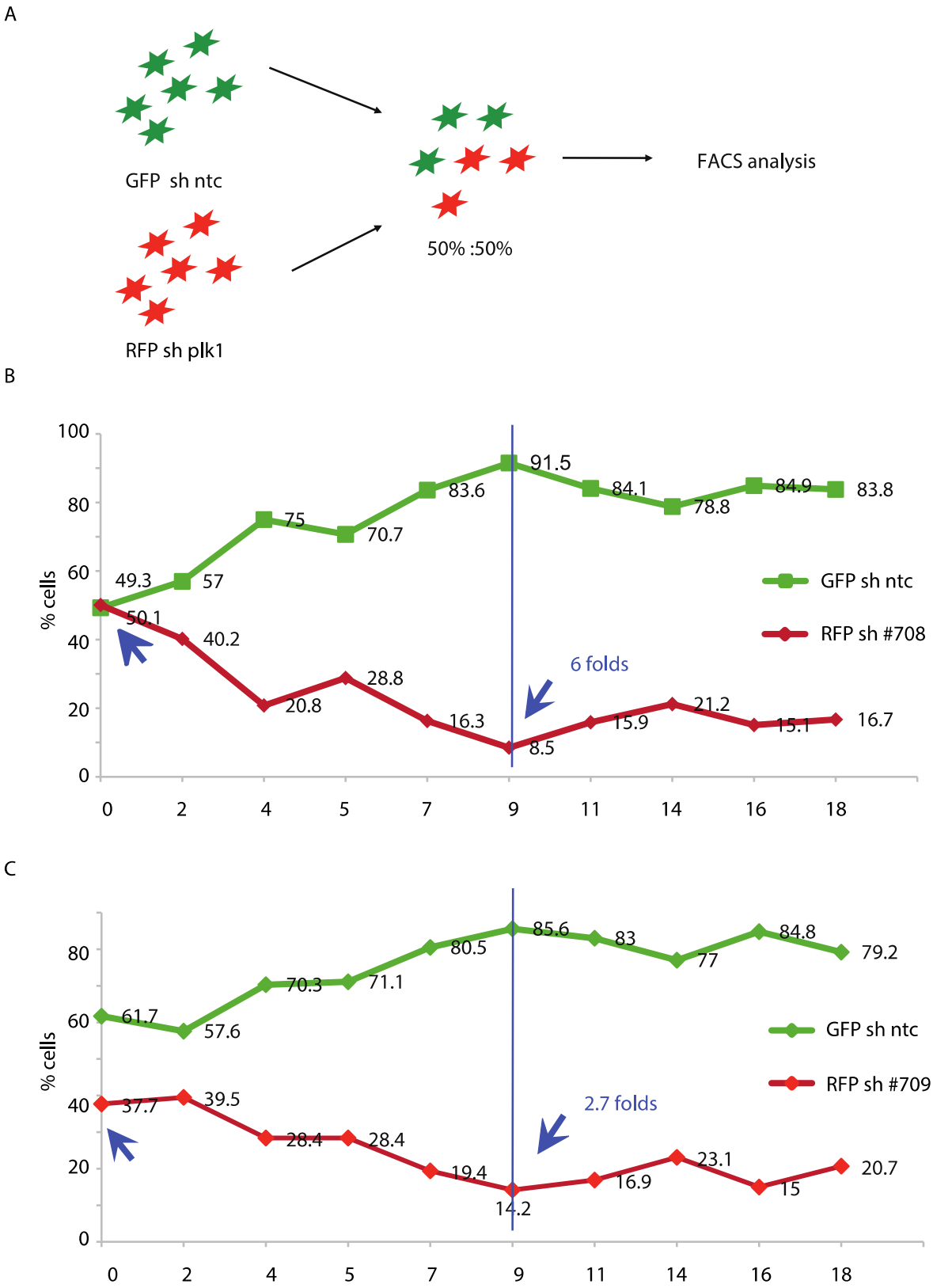

Figure 7: Dual-colour competition assay in SHEP-N-MycER cells stably expressing GFP or RFP.

(A) Schematic illustrates dual-colour competition assay. Equal numbers of control cells expressing GFP and sh plk1 cells expressing RFP were plated on day 0. The ratio between green and red cells was analyzed at regular intervals by flow cytometry.

(B) The assay was set up according to (A). Green line indicates the relative frequency of cells infected with sh ntc (stably expressing GFP) and the red line indicates the relative frequency of cells infected with the shRNA targeting PLK1 sh #708 that stably expresses RFP. The cells were harvested at indicated time points and subjected to FACS analysis to determine the ratio.

(C) PLK1 sh709 was used for cells stably expressing RFP. The experiment was described in (B).

Since the sustained function of shRNAs is quite important, the knockdown effect of all sh plk1 were checked via RT-PCR at post infection day6, 10, 13, 18 and 21 (Figure 8). The diagram shows that on day 13 the knockdown efficiency of all shRNAs was still strong with a decrease of *PLK1* mRNA levels of more than 70%. However, on day 18, the knockdown efficiencies were already strongly reduced showing no more than 50% reduction in *PLK1* mRNA levels. The combined results from the dual-colour competition assays and from the RT-PCR showed that shRNA activity and consequently a depletion of lethal shRNAs could be expected over a course of approximately 9 to 18 days. As a result of these studies, we decided to screen the shRNA libraries in the SHEP-N-MycER cells over a period of 14 days.

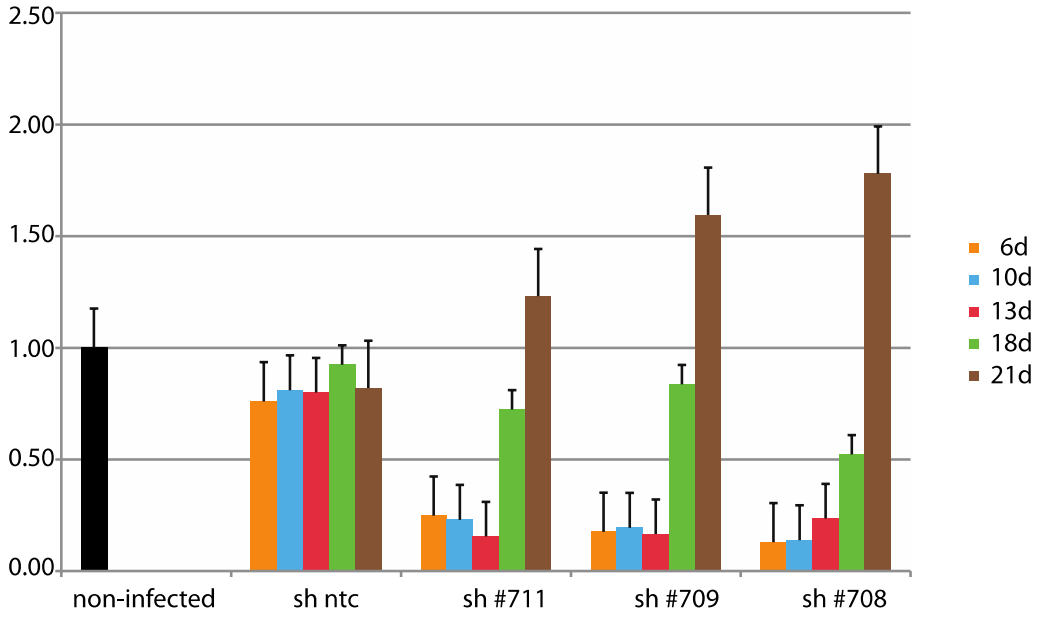

Figure 8: Time course of *plk1* mRNA level in SHEP-N-MycER cells infected with PLK1 shRNAs.

SHEP-N-MycER cells were infected with different lentiviral PLK1 shRNAs and selected. The mRNA level of *plk1* was analysed at indicated timepoints after infection.

4.2 Data analyses

As described above, 18290 shRNAs were used to carry out two screens in SHEP-N-MycER cells. Both screens were done in an equal format, one with a pool of 9589 and the other one with a pool of 8701 constructs and in two biological replicates.

To guarantee a sufficient redundancy for all sequenced shRNAs, at least 8 million reads were generated by the sequencer for each sample. The raw-sequences were filtered for high quality reads using the Illumina CASAVA software. For each sample, all reads with a reliable quality score were extracted and written in a FASTQ file. To allow for a combined analysis of the changes in frequency of all screened shRNAs, the sequencing data generated for corresponding conditions (EU, LU or LS) of corresponding biological replicates (replicate 1 or replicate 2) of both screens were combined in joint FASTQ files. Adjusting the sizes of all initial FASTQ files prior to their fusion guaranteed that subsequent normalizations of the joint dataset do not result in an unequal weighting of the sequencing data generated in the separate screens.

The focus of the present study was on identifying annotated and protein encoding target genes that show a synthetic lethal interaction with N-Myc. Unfortunately, the annotations of shRNA-sequences used in the present study are outdated. Consequently, all 18290 constructs were mapped against the most recent human transcriptome (GRCh37), resulting in 13406 unique combinations of shRNA sequences and target genes. This new list of shRNA-sequences was used as a reference for the alignment of the raw-sequences generated for each sample. Based on these alignments, the abundances of all shRNAs targeting annotated genes were determined for each condition.

The correlations for the counts detected for each shRNA in the various different conditions between the two independently conducted replicate experiments are shown in Figure 9. Correlation coefficients of 0.71 – 0.75 show effects of biological variability in all conditions. Consequently, reliable effects during the screening process, including depletion and enrichment of shRNAs, can only be expected for sufficiently strong changes in shRNA frequencies.

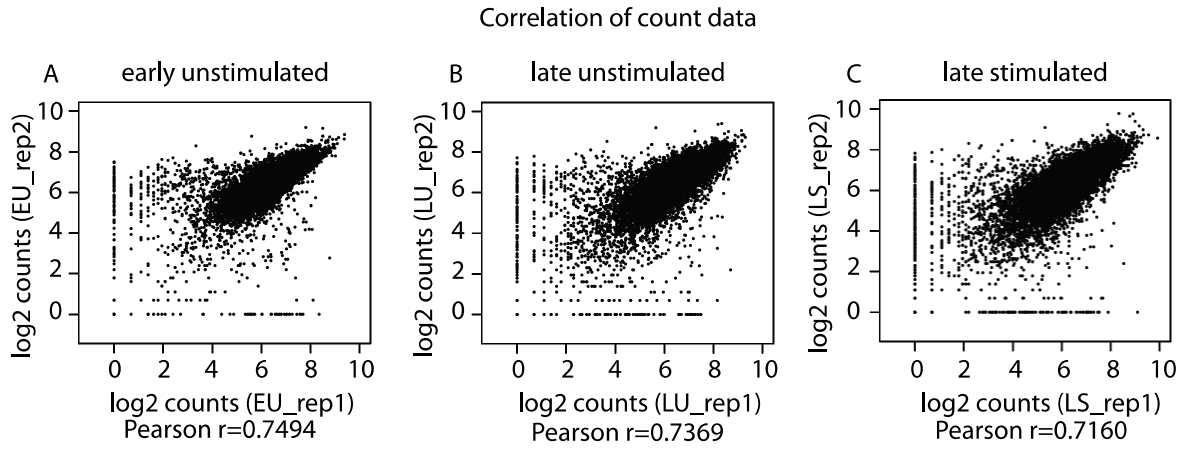

Figure 9: Two biological replicates are well correlated in either EU, LU or LS condition.

The correlations for the counts detected for each shRNA in EU, LU, LS conditions between the two independently conducted replicate experiments. The Pearson value indicates the correlation level of two biological replicates. The plots were generated by Carsten Ade.

Means of counts were calculated from the counts determined in the two biological replicates for each shRNA. Changes in shRNA frequencies were then calculated as log2 fold changes between the conditions “EU” and “LU”, “EU” and “LS” and “LU” and “LS”. Statistical inference, using the R implemented program edgeR (Mark D. Robinson, 2010), allowed us to determine the significance of the calculated fold changes. The red coloured population in Figure 10 shows shRNAs significantly depleted (padj< 0.1) only after OHT treatment and with a strong synthetic lethal effect represented by an at least 4-fold reduced frequency in the OHT treated population compared to the reference population (log2 FC LS/LU< -2).

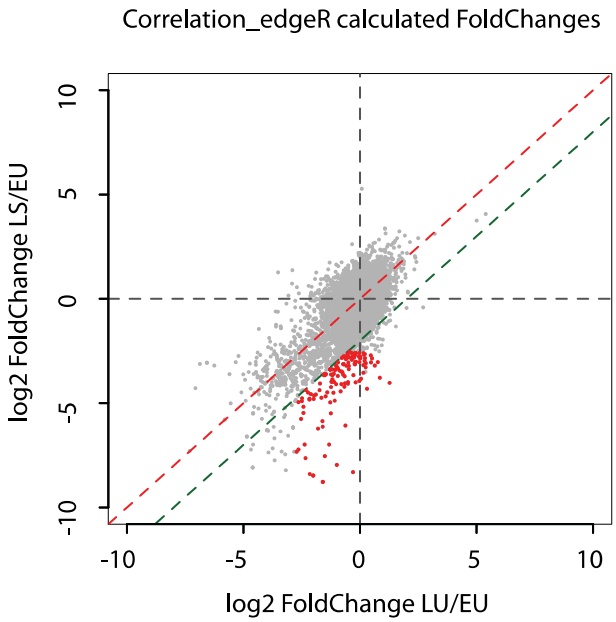

Figure 10: Dot-plot showing correlation_edgeR between fold changes of LS/EU and LU/EU

In this dot-plot, the log2 fold changes of the counts of all 13408 unique combinations of shRNAs for the conditions EU/LU and EU/LS are plotted. The population indicated in red represents shRNAs significantly depleted (p-adj < 0.1) only after N-Myc activation (LU) and with the a strong synthetic lethal effect of log2 fold change LS/LU < -2 (green line). The plot was generated by Carsten Ade.

Genes whose knockdown shows a synthetic lethal interaction with activated N-Myc in the SHEP-N-MycER cells were identified from this dataset applying the following series of criteria: 1) shRNAs significantly depleted (p-adjusted > 0.1) during the screening process independently of N-Myc activation were considered drop-outs and ignored in all further analyses. Target genes of these shRNAs can be expected to be involved in essential cellular processes in SHEP-N-MycER cells and their knockdown strongly effect the viability of the cells. 2) Conversely, shRNAs that were significantly depleted (p-adjusted < 0.1) only after activation of N-Myc and 3) showed a strong synthetic lethal net effect at the end of the screening procedure (log2 fold change for conditions “LU” versus “LS” > 2) were considered as targeting genes that are essential for SHEP-N-MycER cells after N-Myc activation (Table 23).

Of the total 13408 unique combinations of shRNAs and target genes screened in our approach, 148 were selected based on the above criteria. Knockdown of the target genes of these shRNAs shows a strong and significant synthetic lethal interaction with active N-Myc in SHEP-N-MycER cells.

This gene-set was found to be enriched for genes involved in a number of important biological processes. DAVID analysis revealed the ubiquitin mediated proteolysis pathway to be the top enriched pathway (Table 24)(Sherman et al., 2007). Overall, processes significantly enriched in the gene-set include protein ubiquitination and assembly of the RNA polymerase II complex. Genes from the gene-set involved in protein neddylation and RNA polymerase II mediated transcriptional elongation were selected for further analyses, including *NAE1*, *CUL3*, *CUL5*, *UBE2M* and members of the COP9 signalosome and *NUP153*, *NCAPG2*, *ELL*, *TCEB1*, *LARP7*, *THOC1*, respectively (Figure 11).

Table 23: A candidate list of 148 shRNAs

The shRNAs were selected with the criteria that padj of log2 FC (LU/EU)>0.1, padj of log2<0.1, log2 FC (LS/LU)<-2. The list was sorted after ascending value of log2 FC (LS/LU). The genes involved in neddylation pathway (labeled in red), RNAII-mediated transcription elongation (labeled in green), chromosome integrity (labeled in orange), replication and checkpoint (labeled in brown), p53, ARF-mediated apoptosis (labeled in blue) are indicated.

gene_symbo	logFC LU/EU	padj	logFC LS/EU	padj	logFC LS/LU	padj		gene_symbo	logFC LU/EU	padj	logFC LS/EU	padj	logFC LS/LU	padj
NAE1	-0.30	1.00	-8.30	0.00	-7.96	0.00		ATP6V0D1	-2.43	0.22	-5.17	0.00	-2.70	0.70
ALDOA	-1.59	1.00	-8.77	0.00	-7.13	0.00		EXOSC4	-0.95	1.00	-3.69	0.01	-2.70	0.70
ALDOAP1	-1.59	1.00	-8.77	0.00	-7.13	0.00		TRIP12	-0.48	1.00	-3.21	0.02	-2.69	0.67
RRS1	-1.00	1.00	-7.96	0.00	-6.91	0.00		BAZ1B	-0.05	1.00	-2.76	0.09	-2.67	0.88
BIRC5	-2.01	0.60	-8.47	0.00	-6.41	0.00		POLDIP2	-0.78	1.00	-3.48	0.01	-2.65	0.75
uncharacteri	-2.01	0.60	-8.47	0.00	-6.41	0.00		ZNF562	-1.89	0.69	-4.58	0.00	-2.65	0.76
RBM27	-2.16	0.43	-8.39	0.00	-6.19	0.00		RMND1	-1.18	1.00	-3.85	0.01	-2.63	0.83
ZNF271	-1.51	1.00	-7.54	0.00	-5.98	0.00		CCT5	-1.98	0.57	-4.63	0.00	-2.61	0.76
RPL36	-1.33	1.00	-6.98	0.00	-5.61	0.01		PPWD1	-2.17	0.38	-4.83	0.00	-2.61	0.74
ATL1	-0.63	1.00	-6.07	0.00	-5.40	0.01		UBE2I	-1.74	0.85	-4.37	0.00	-2.59	0.76
BRCA1	-2.34	0.30	-7.64	0.00	-5.25	0.04		TEX19	-0.59	1.00	-3.21	0.02	-2.58	0.73
CLEC4G	1.27	1.00	-4.03	0.03	-5.25	0.04		MCM6	-2.17	0.38	-4.78	0.00	-2.57	0.76
PIK3CB	0.85	1.00	-3.78	0.01	-4.59	0.04		POLR2K	-0.87	1.00	-3.45	0.01	-2.54	0.75
MUC22	0.30	1.00	-4.31	0.00	-4.57	0.02		KIF23	-0.35	1.00	-2.92	0.05	-2.53	0.92
BCLAF1	-2.72	0.11	-7.33	0.00	-4.56	0.18		ZNF717	-0.04	1.00	-2.60	0.09	-2.51	0.77
TUBG1	-2.37	0.29	-6.98	0.00	-4.56	0.15		GPATCH1	-0.26	1.00	-2.82	0.06	-2.51	0.83
NKAP	-2.64	0.15	-7.22	0.00	-4.53	0.17		KIF11	-0.50	1.00	-3.05	0.03	-2.50	0.92
RCC1	-1.60	1.00	-6.13	0.00	-4.48	0.18		GAPDHP41	-0.25	1.00	-2.76	0.07	-2.47	0.92
POP7	-1.80	0.77	-6.22	0.00	-4.38	0.04		PBRM1	-0.21	1.00	-2.69	0.07	-2.44	0.92
SCFD1	-1.61	1.00	-5.86	0.00	-4.21	0.32		ERI2	-1.18	1.00	-3.66	0.01	-2.43	1.00
HMGN2P13	-1.25	1.00	-5.48	0.00	-4.19	0.05		SEPT7	-0.37	1.00	-2.83	0.04	-2.42	0.92
THOC1	-0.03	1.00	-3.93	0.00	-3.86	0.08		SEPT7P5	-0.37	1.00	-2.83	0.04	-2.42	0.92
TMEM207	0.04	1.00	-3.83	0.06	-3.83	0.60		SEPT7P4	-0.37	1.00	-2.83	0.04	-2.42	0.92
PHB	0.64	1.00	-3.20	0.03	-3.79	0.14		SEPT7P6	-0.37	1.00	-2.83	0.04	-2.42	0.92
TRIP12	-0.19	1.00	-4.01	0.00	-3.78	0.11		MCM3	-1.12	1.00	-3.59	0.01	-2.42	0.92
TOP1	0.77	1.00	-3.03	0.04	-3.75	0.12		COPS4	-2.11	0.43	-4.56	0.00	-2.41	0.92
WISP2	-1.08	1.00	-4.88	0.00	-3.75	0.15		STRBP	-0.32	1.00	-2.75	0.06	-2.39	0.93
KAZN	0.15	1.00	-3.54	0.02	-3.65	0.18		PSMA6	-0.71	1.00	-3.13	0.04	-2.38	1.00
EXOSC4	-1.28	1.00	-4.96	0.00	-3.64	0.19		PSMA6P1	-0.71	1.00	-3.13	0.04	-2.38	1.00
ORC1	-0.83	1.00	-4.43	0.00	-3.56	0.15		PSMA6P2	-0.71	1.00	-3.13	0.04	-2.38	1.00
PPL	-0.52	1.00	-4.06	0.00	-3.50	0.19		uncharacteri	-0.71	1.00	-3.13	0.04	-2.38	1.00
CUL5	-0.67	1.00	-4.21	0.00	-3.49	0.19		GEMIN4	-2.49	0.17	-4.90	0.00	-2.37	0.97
COPS5	0.24	1.00	-3.28	0.02	-3.48	0.18		AAGAB	-0.94	1.00	-3.35	0.02	-2.37	0.99
NAA15	0.47	1.00	-3.05	0.03	-3.47	0.19		RB1	-0.28	1.00	-2.68	0.09	-2.36	1.00
KLHL29	-0.51	1.00	-3.99	0.04	-3.43	0.92		FBXL5	-0.20	1.00	-2.58	0.09	-2.34	0.99
PPWD1	-0.64	1.00	-4.04	0.00	-3.36	0.25		TMEM126B	-0.22	1.00	-2.60	0.08	-2.34	0.98
EYS	-0.28	1.00	-3.66	0.01	-3.33	0.25		INIP	-1.24	1.00	-3.62	0.01	-2.33	1.00
ZNF853	0.51	1.00	-2.85	0.05	-3.32	0.23		UTP20	-1.07	1.00	-3.42	0.01	-2.30	1.00
USP9X	-1.14	1.00	-4.50	0.00	-3.32	0.32		DDX27	-1.72	0.95	-4.06	0.00	-2.29	1.00
SLC25A51	0.25	1.00	-3.09	0.03	-3.30	0.24		PARP12	-1.03	1.00	-3.36	0.01	-2.29	1.00
TOPBP1	0.14	1.00	-3.18	0.03	-3.28	0.30		SNRPFP1	-0.48	1.00	-2.81	0.08	-2.28	1.00
UBA3	-0.80	1.00	-4.09	0.00	-3.25	0.28		HTATSF1	-2.64	0.11	-4.95	0.00	-2.27	1.00
SGSM3	-2.53	0.21	-5.76	0.00	-3.18	1.00		SUDS3	-0.97	1.00	-3.28	0.02	-2.26	1.00
NUP153	-1.48	1.00	-4.67	0.00	-3.15	0.36		SUDS3P1	-0.97	1.00	-3.28	0.02	-2.26	1.00
AP2M1	0.46	1.00	-2.71	0.08	-3.13	0.31		OR7C2	-0.60	1.00	-2.89	0.05	-2.25	1.00
COPS4	0.19	1.00	-2.98	0.04	-3.13	0.31		TCF3	-2.49	0.19	-4.76	0.00	-2.23	1.00
CHTF18	-1.65	1.00	-4.74	0.00	-3.04	0.39		VPRBP	-2.23	0.36	-4.49	0.00	-2.22	1.00
CDKN2D	-1.40	1.00	-4.48	0.00	-3.03	0.66		POLR3K	-0.61	1.00	-2.87	0.05	-2.21	1.00
YIPF5	0.22	1.00	-2.84	0.05	-3.02	0.43		DTL	-0.51	1.00	-2.75	0.07	-2.21	1.00
EFTUD1	-1.03	1.00	-4.09	0.00	-3.02	0.39		ZNF480	-0.35	1.00	-2.60	0.09	-2.20	1.00
POLR2K	-0.66	1.00	-3.71	0.01	-3.01	0.39		RFX2	-0.61	1.00	-2.83	0.05	-2.18	1.00
DHX15	-2.43	0.21	-5.47	0.00	-3.00	0.50		ACTBL2	-1.19	1.00	-3.38	0.01	-2.15	1.00
uncharacteri	-0.03	1.00	-3.04	0.03	-2.96	0.39		FRYL	-0.39	1.00	-2.58	0.09	-2.14	1.00
SUPT6H	-1.24	1.00	-4.23	0.00	-2.94	0.47		TOX4	-1.02	1.00	-3.21	0.02	-2.14	1.00
CUL3	-0.22	1.00	-3.14	0.02	-2.88	0.50		TOX4P1	-1.02	1.00	-3.21	0.02	-2.14	1.00
LARP7	-0.72	1.00	-3.64	0.01	-2.88	0.50		FLAD1	-0.54	1.00	-2.71	0.08	-2.13	1.00
MLC1	-0.48	1.00	-3.37	0.01	-2.85	0.51		NCAPG2	-1.45	1.00	-3.61	0.01	-2.11	1.00
CXorf48	-0.23	1.00	-3.12	0.03	-2.84	0.52		XPO5	-1.50	1.00	-3.65	0.01	-2.11	1.00
TCOF1	-1.12	1.00	-3.98	0.00	-2.82	0.69		PDZK1IP1	-1.55	1.00	-3.66	0.01	-2.07	1.00
RABGEF1	0.01	1.00	-2.85	0.05	-2.81	0.51		PKN2	-1.28	1.00	-3.38	0.02	-2.06	1.00
KCTD7	0.01	1.00	-2.85	0.05	-2.81	0.51		TCEB1	-1.28	1.00	-3.38	0.02	-2.06	1.00
WWP2	0.21	1.00	-2.65	0.09	-2.81	0.57		TCEB1P20	-1.28	1.00	-3.38	0.02	-2.06	1.00
SMC5	0.17	1.00	-2.68	0.06	-2.80	0.51		TCEB1P19	-1.28	1.00	-3.38	0.02	-2.06	1.00
SGCD	-0.17	1.00	-3.02	0.06	-2.80	0.76		TCEB1P22	-1.28	1.00	-3.38	0.02	-2.06	1.00
ELL	-0.21	1.00	-3.02	0.03	-2.77	0.59		TCEB1P33	-1.28	1.00	-3.38	0.02	-2.06	1.00
NCAPH	-1.99	0.56	-4.79	0.00	-2.76	0.63		TCEB1P21	-1.28	1.00	-3.38	0.02	-2.06	1.00
CBLC	0.01	1.00	-2.79	0.06	-2.76	0.63		SOX10	-0.54	1.00	-2.64	0.09	-2.06	1.00
NKAPL	-0.75	1.00	-3.53	0.01	-2.74	0.60		OR8G7P	-0.94	1.00	-3.04	0.04	-2.05	1.00
HYALP1	0.01	1.00	-2.77	0.09	-2.73	0.76		GTF2E2	-1.52	1.00	-3.59	0.01	-2.03	1.00
COPS8	-1.22	1.00	-3.97	0.00	-2.71	0.70		CA7	-0.45	1.00	-2.52	0.10	-2.02	1.00
COPS8P2	-1.22	1.00	-3.97	0.00	-2.71	0.70		DNASE1L3	-0.68	1.00	-2.74	0.07	-2.02	1.00
SNRPA	-1.18	1.00	-3.93	0.00	-2.70	0.67		OR1J1	-2.32	0.37	-4.37	0.00	-2.01	1.00
C19orf54	-1.18	1.00	-3.93	0.00	-2.70	0.67		OIP5	-0.72	1.00	-2.77	0.06	-2.01	1.00
SLC4A1	0.15	1.00	-2.60	0.09	-2.70	0.66		C14orf93	-0.78	1.00	-2.83	0.05	-2.00	1.00

Table 24: DAVID pathway analysis

The final list of 148 candidates (log2FCLS/LU <-2) was subjected to DAVID pathway analysis using 13408 shRNAs list as background.

Top enriched pathways		
NAME	p-value	q-value
Ubiquitin mediated proteolysis	6.71E-05	0.004
HIV infection	4.44E-04	0.016
General transcription by RNA polymerase I	0.0092	0.249
Pausing and recovery of Tat-mediated HIV-mediated elongation	0.026	0.384
Pausing and recovery of elongation	0.026	0.384
Elongation pausing and recovery	0.029	0.304

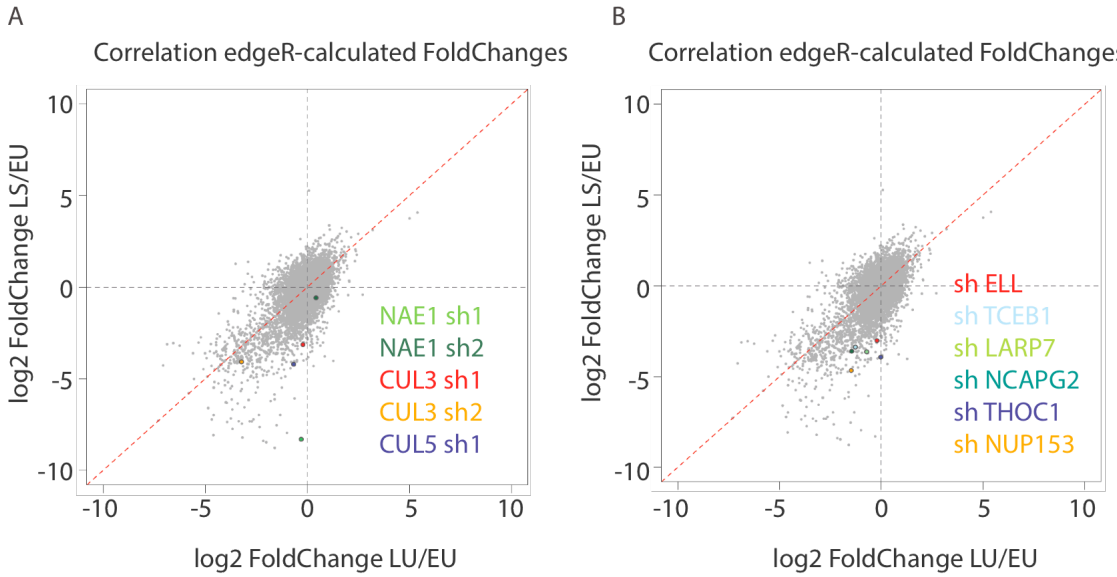

Figure 11: Dot-plot showing correlation_edgeR between fold changes of LS/EU and LU/EU

The plots were described in figure 6. The shRNA involved in neddylation (A) and RNAPII mediated transcription elongation (B) were labelled.

4.3 NAE1

4.3.1 Validation of NAE1 in SHEP-N-MycER

NAE1 is not only a candidate involved in neddylation pathway but also top ranked. To verify synthetic lethal effect of NAE1, three pLKO NAE1 shRNAs were designed. Western blot analysis shows that all shRNAs have knockdown efficiency (Figure 12A). The sh #2 has almost

100% knockdown efficiency while sh1 and sh #3 have more than 50% knockdown efficiency. The colony formation assay shows that NAE1 depletion alone has in general weak effects but combined with N-My activation leads to a lethal effect on cells (Figure 12A). The effect in the colony assay is correlated with knockdown efficiency.

Regarding the short period of colony assay because of confluency, a dual colour competition assay was performed in order to keep cells longer in cell culture and enlarge the difference between OHT treated and untreated cells (Figure 12B). SHEP-N-MycER stably expressing GFP and mCherry were generated. Cells with GFP were infected with sh nae1 while cells with mCherry were infected with sh scramble. The same amounts of GFP and mCherry expressing cells were plated in a dish on day 0. Cells were harvested at indicated time points and the ratio between GFP and mCherry cells was determined by flow cytometry. The diagram shows only the bar of GFP. On day 8 the sh #2 without OHT decreases from 46.8% to 19.9% indicating 2.4 fold decrease while the sh #2 with OHT decreases from 46.8% to 4.2% indicating a 11-fold reduction. The sh #1 and sh#3 present the same effect as sh #2.

With the colony assay and dual-colour competition assay we verify that NAE1 depletion with N-Myc activation leads to cell growth arrest.

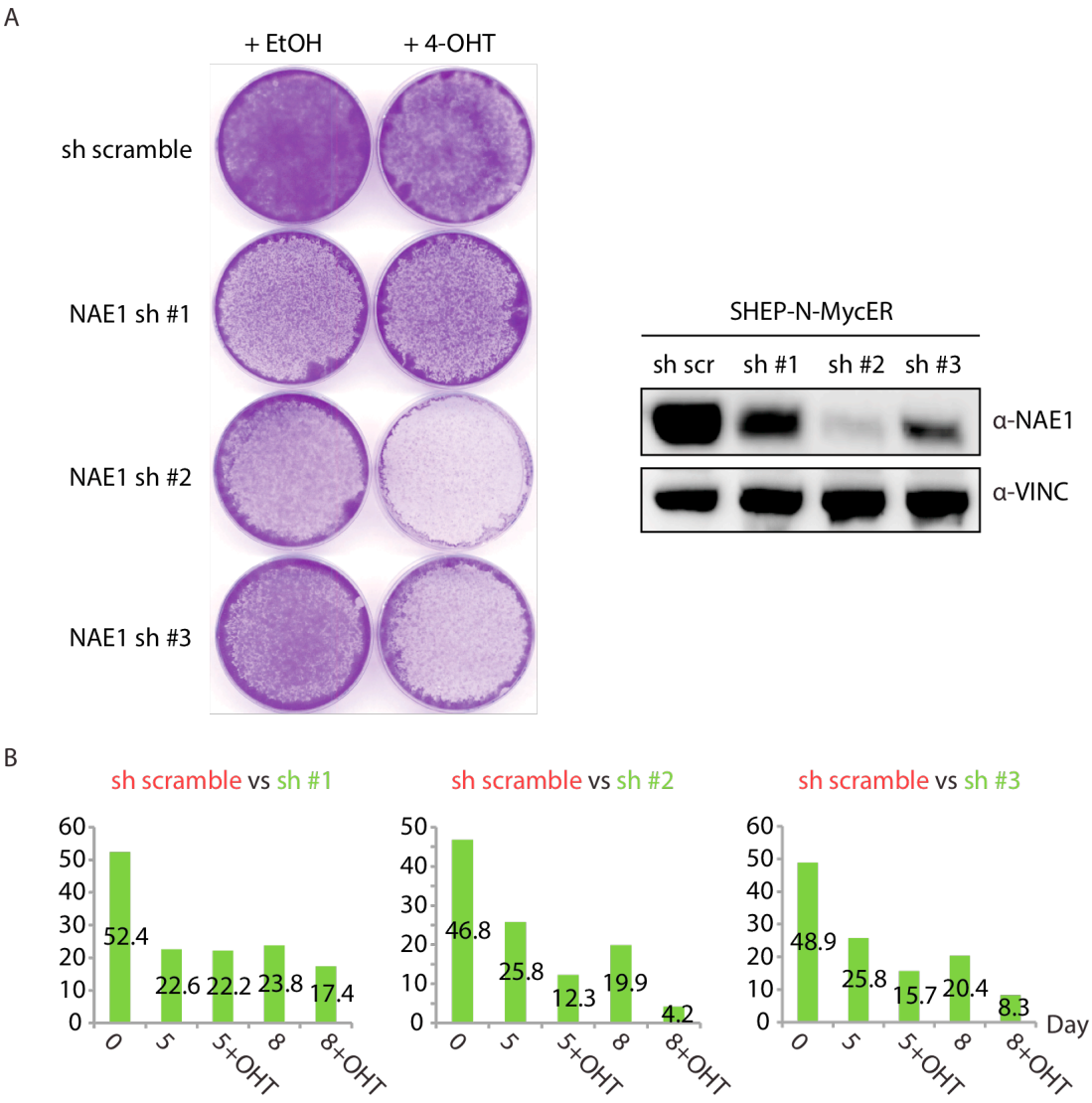

Figure 12: SHEP-N-MycER cells with NAE1 depletion and N-Myc activation have a strong growth disadvantage.

(A) $5x10^4$ of SHEP-N-MycER cells infected with pLKO sh nae1 or sh scramble were plated on a 6cm dish on day 0. 200nM 4-OHT was added on day 2. Cells were harvested and fixed, subsequently stained with crystal violet. The knockdown efficiency of pLKO sh nae1 was analysed by western blot.

(B) Equal number of SHEP-N-MycER cells expressing RFP infected with sh scramble and cells expressing GFP infected sh nae1 were plated on day 0. The ratio of green and red cells was determined by flow cytometry.

4.3.2 NAE1 depletion induces S-phase arrest and apoptosis with N-Myc

To confirm the effect in colony assay results from cell cycle arrest or apoptosis, BrdU/PI assay and Annexin/PI assay were performed. In BrdU/PI plots, the population in blue frame indicates BrdU positive cells (Figure 13A) while the population in red frame indicates the BrdU negative cells with intermediate DNA content. The cells in red frame are considered in S-phase according to the DNA content but not able to incorporate BrdU. The total S-phase is an addition of the population from blue frame and red frame. Cells with sh scramble show a normal cell distribution. 45.5% of the cells are BrdU positive, only 3% are BrdU negative indicating that replication in S-phase is ongoing. After 4-OHT-treatment BrdU positive cells are increased from 45.5% to 59.8% indicating that N-Myc activation promotes S-phase entry. The change of BrdU negative cells is not pronounced and decreased from 3% to 2.3%. The dot-plot of NAE1 sh #2, which has the best knockdown efficiency shows that 44.9% cells are BrdU positive and 11.5% cells are BrdU negative. The population in red frame increases from 11.5% to 17.1% upon N-Myc activation meaning a number of S-phase cells are not able to incorporate BrdU. The sh #1 and sh #3 show similar effects as sh #2 and the effects are correlated with shRNA knockdown efficiency.

AnnexinV/PI FACS is an efficient method to detect early apoptotic cells (Vermes et al., 1995). Early apoptotic cells are AnnexinV positive and late apoptotic cells are AnnexinV PI double positive. Cells with sh scramble show 1.5% early apoptosis and 3% total apoptosis. The early and total apoptosis cells increase to 3% and 6% upon OHT-treatment indicating N-Myc activation induces apoptosis. The diagram shows that NAE1 depletion with sh #2 induces 7% early apoptosis (Figure 13B black bar) and 15% total apoptosis whereas combined with N-Myc 19% early apoptosis and 30% total apoptosis were induced. The sh #1 and sh #3 without OHT induce 6% and 12% total apoptosis, respectively whereas with OHT 8% and 25% total apoptosis were induced (Figure 13B). The amount of apoptosis is correlated with shRNA knockdown efficiency.

Taken together, the NAE1 depletion with N-Myc activation leads to S-phase arrest and induces strong apoptosis.

A

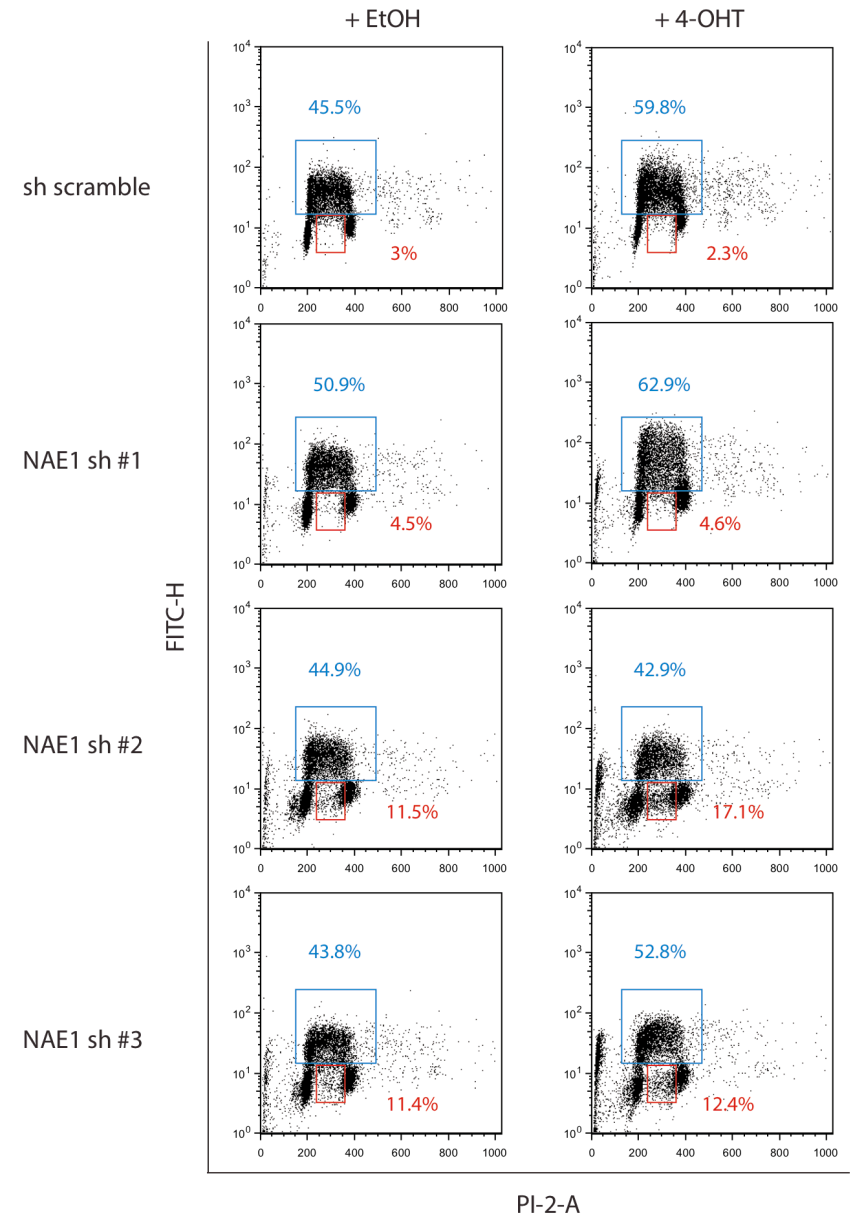
+ EtOH
+ 4-OHT
sh scramble
NAE1 sh #1
NAE1 sh #2
NAE1 sh #3
45.5%
3%
59.8%
2.3%
50.9%
4.5%
62.9%
4.6%
44.9%
11.5%
42.9%
17.1%
43.8%
11.4%
52.8%
12.4%
FITC-H
PI-2-A

B

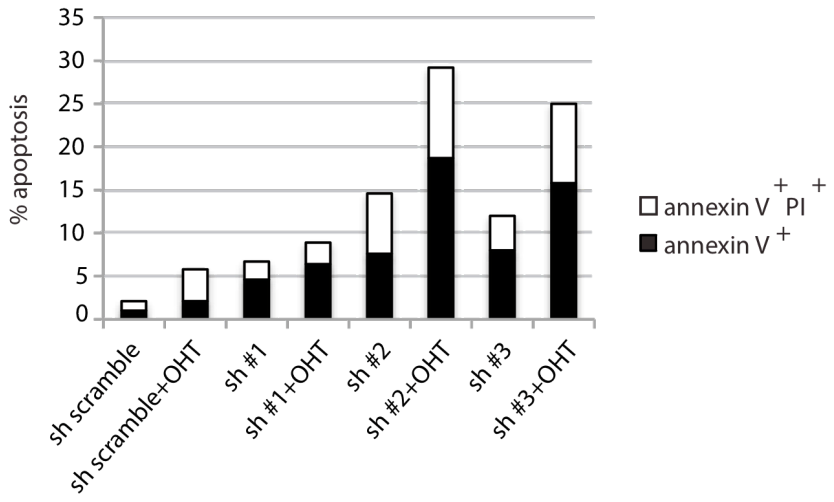
% apoptosis
35
30
25
20
15
10
5
0
sh scramble
sh scramble+OHT
sh #1
sh #1+OHT
sh #2
sh #2+OHT
sh #3
sh #3+OHT
annexin V+ PI+
annexin V+

Figure 13: NAE1 depletion with N-Myc activation in SHEP-N-MycER cells induces S-phase arrest and apoptosis.

(A) NAE1 depletion with N-Myc activation leads to S-phase arrest. SHEP-N-MycER cells were infected with sh nae1 and treated with 200nM 4-OHT for 3 days. Before being harvested, 10μM BrdU was added to the medium and incubated for 1 hour. Then the cells were harvested and fixed in 80% ethanol at -20°C for 1 day then stained with anti-BrdU antibody and propidium iodide and measured by flow cytometry. The population of BrdU positive cells are enclosed in blue frame and the population of BrdU negative cells with intermediate DNA content are enclosed in red frame.

(B) The cells were treated like in (A). They were harvested, stained with AnnexinV and propidium iodide and measured by flow cytometry.

4.3.3 Validation of NAE1 in neuroblastoma cell lines

To ensure the synthetic lethality of NAE1 and N-Myc not only in an inducible cell system but also in *MYCN*-amplified cell lines, three *MYCN*-nonamplified and four *MYCN*-amplified neuroblastoma cell lines were used for colony assays (Figure 14). Although RT-PCR shows the knockdown efficiencies of NAE1 shRNAs in neuroblastoma cell lines are heterogeneous, except in SKN-AS all the shRNAs have more than 50% knockdown efficiency (Figure 14B). The *MYCN*-nonamplified cell lines do not show any evident effect. *MYCN*-amplified neuroblastoma cell lines present a lethal effect except LAN-1 (Figure 14A).

In sum, the depletion of NAE1 is lethal in most of the *MYCN*-amplified neuroblastoma cell line.

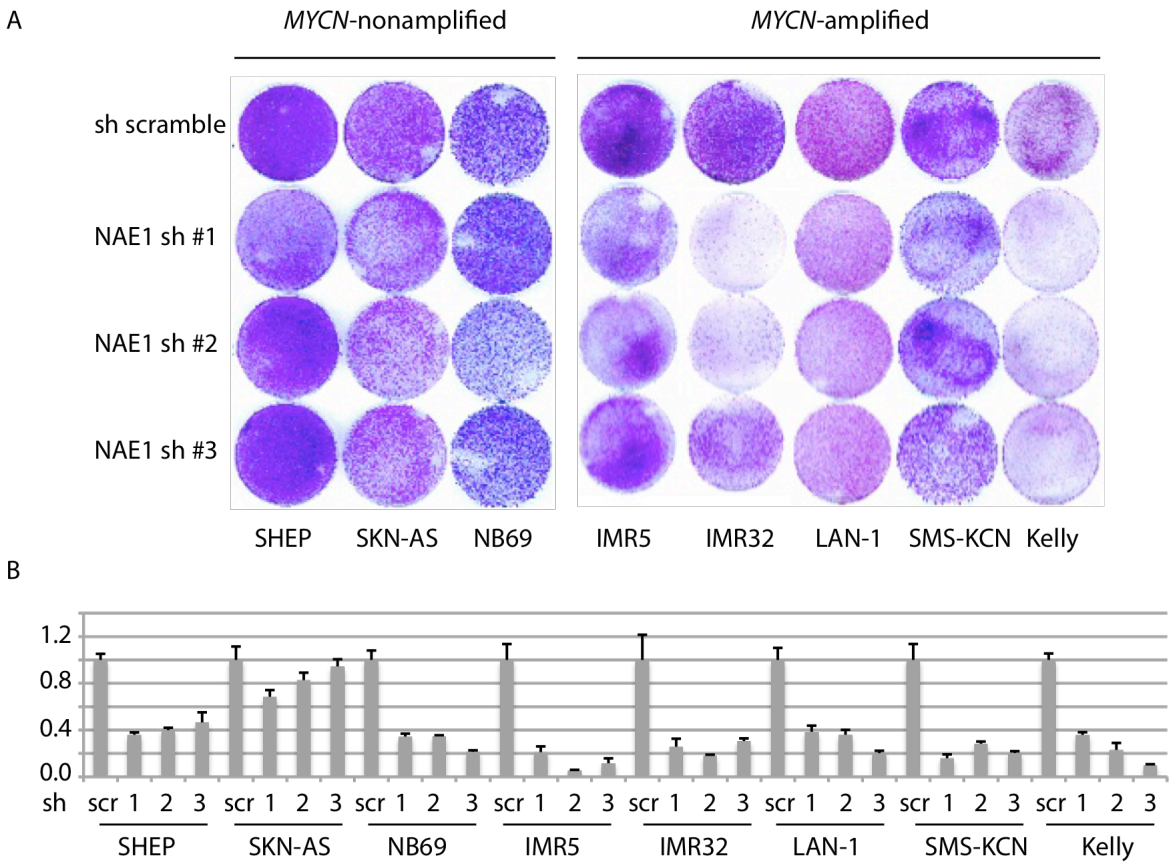

Figure 14: NAE1 is required more for survival of *MYCN*-amplified neuroblastoma cell lines than *MYCN*-nonamplified neuroblastoma cell lines.

(A) Three MYCN-nonamplifed neuroblastoma cell lines show less dependency on NAE1 whereas four MYCN-amplified neuroblastoma cell lines have a growth disadvantage without NAE1 expression. Colony assay procedure was described in Figure 12.

(B) The knockdown efficiencies of shRNAs were analysed by RT-PCR.

4.4 CUL5

4.4.1 Validation of CUL5

Well-characterized substrates of NAE are members of Cullin gene family. Two proteins from this family are on the candidate list: CUL5 and CUL3 (Table 23). To validate CUL5, three pLKO CUL5 shRNAs were designed. Western blot analysis shows sh #1 and sh #3 have a good knockdown efficiency whereas sh #2 does not have any knockdown efficiency but a strong effect

on cell growth (Figure 15A), so it is considered as an off-target. The colony formation assay shows a strong effect of CUL5 depletion alone and a stronger effect of CUL5 depletion with N-Myc activation.

As described in 4.3.1 (Figure 15A), a dual-colour competition assay was performed. The diagram shows on day 8 the sh #1 without OHT decreases from 54.3% to 13.5% indicating a 4-fold reduction whereas the sh #1 with OHT decreases from 54.3% to 4.2% indicating 13-fold reduction. The sh #3 presents the same effect as sh #1.

The colony formation assay and dual-colour competition assay lead us to conclude that CUL5 depletion with N-Myc activation leads to cell growth arrest.

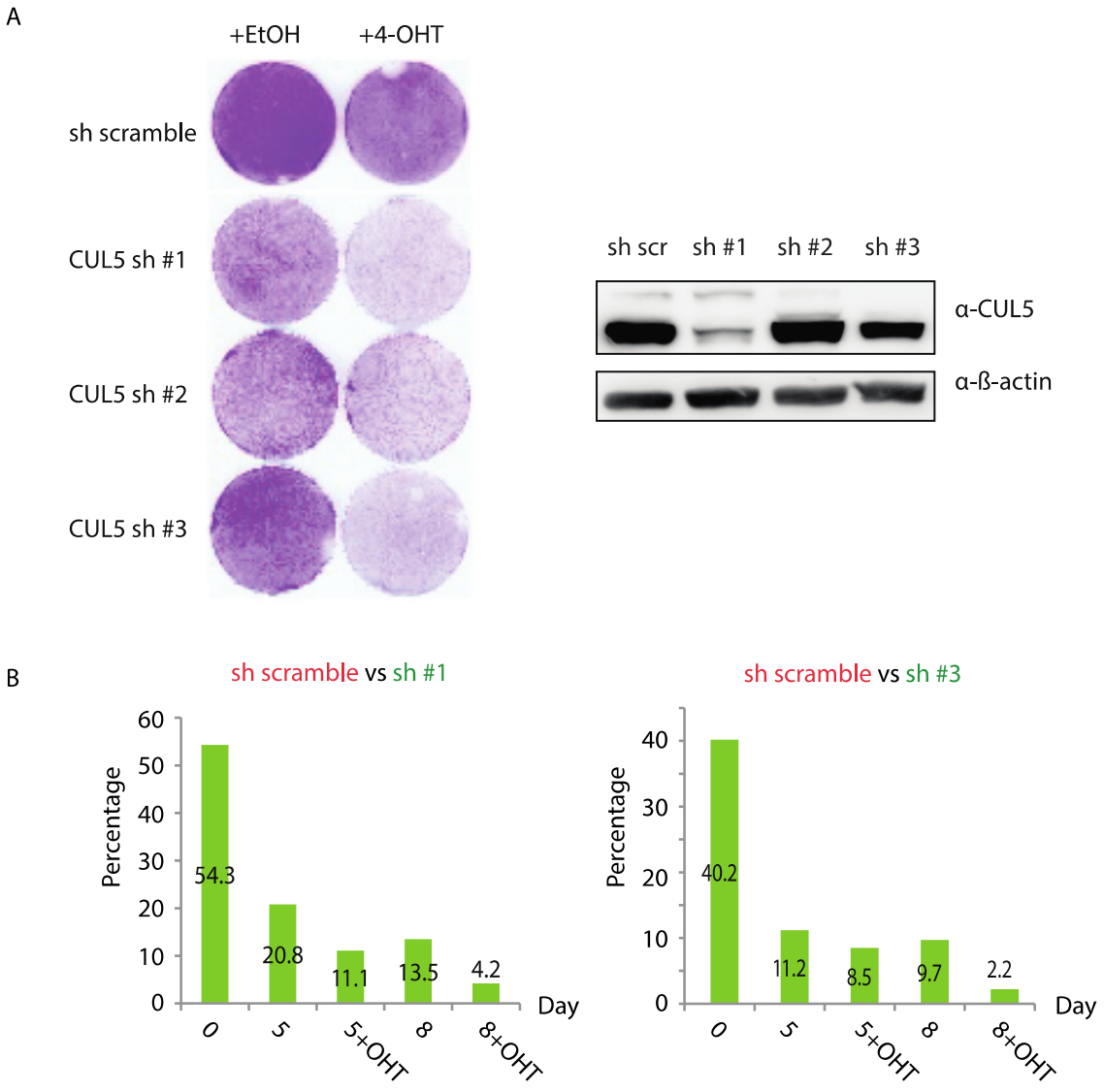

Figure 15: SHEP-N-MycER cells with CUL5 depletion and N-Myc activation have a strong growth disadvantage. The experiments were conducted with pLKO backbone based lentiviral vector.

(A) The colony assay was performed as in Figure 12.

(B) The dual-colour competition assay was performed as in Figure 12.

4.4.2 CUL5 depletion induces S-phase arrest and apoptosis with N-Myc

In the previous chapter 4.3.2, BrdU/PI assay and Annexin/PI assay were performed to reveal the mechanism of growth arrest (Figure 16). To figure out the consequence of the CUL5 depletion and N-Myc activation, the experiments were repeated. The cells with sh scramble show a normal distribution with 45.5% BrdU positive and 3% BrdU negative indicating that replication in S-phase is ongoing. After 4-OHT-treatment BrdU positive cells are increased from 45.5% to 59.8% while BrdU negative cells are decreased from 3% to 2.3%. The increase in BrdU positive cells indicates that N-Myc functions as a cell cycle driver. The dot-plot of CUL5 sh #1 which has the best knockdown efficiency shows that 37.4% cells are BrdU positive and 12.1% cells are BrdU negative but in S-phase (Figure 16, red frame). The population in red frame increases from 12.1% to 14.5% upon N-Myc activation indicating more cells in S-phase are not able to incorporate BrdU. The sh #2 and sh #3 show similar effect as sh #1 and this effect is correlated with shRNA knockdown efficiency (Figure 16A).

Analog to 4.3.2, Annexin/PI FACS was performed to check the apoptosis caused by CUL5 depletion and N-Myc activation. The diagram shows that CUL5 depletion with sh #1 induces 4% early apoptosis and 8% total apoptosis whereas combined with N-Myc 12% early apoptosis and 22% apoptosis are induced. The sh #2 and sh #3 without OHT induce 11% and 13% total apoptosis, respectively where with OHT 24% and 17% total apoptosis were induced (Figure 16B).

In sum, these results suggest a S-phase arrest followed by apoptosis induction.

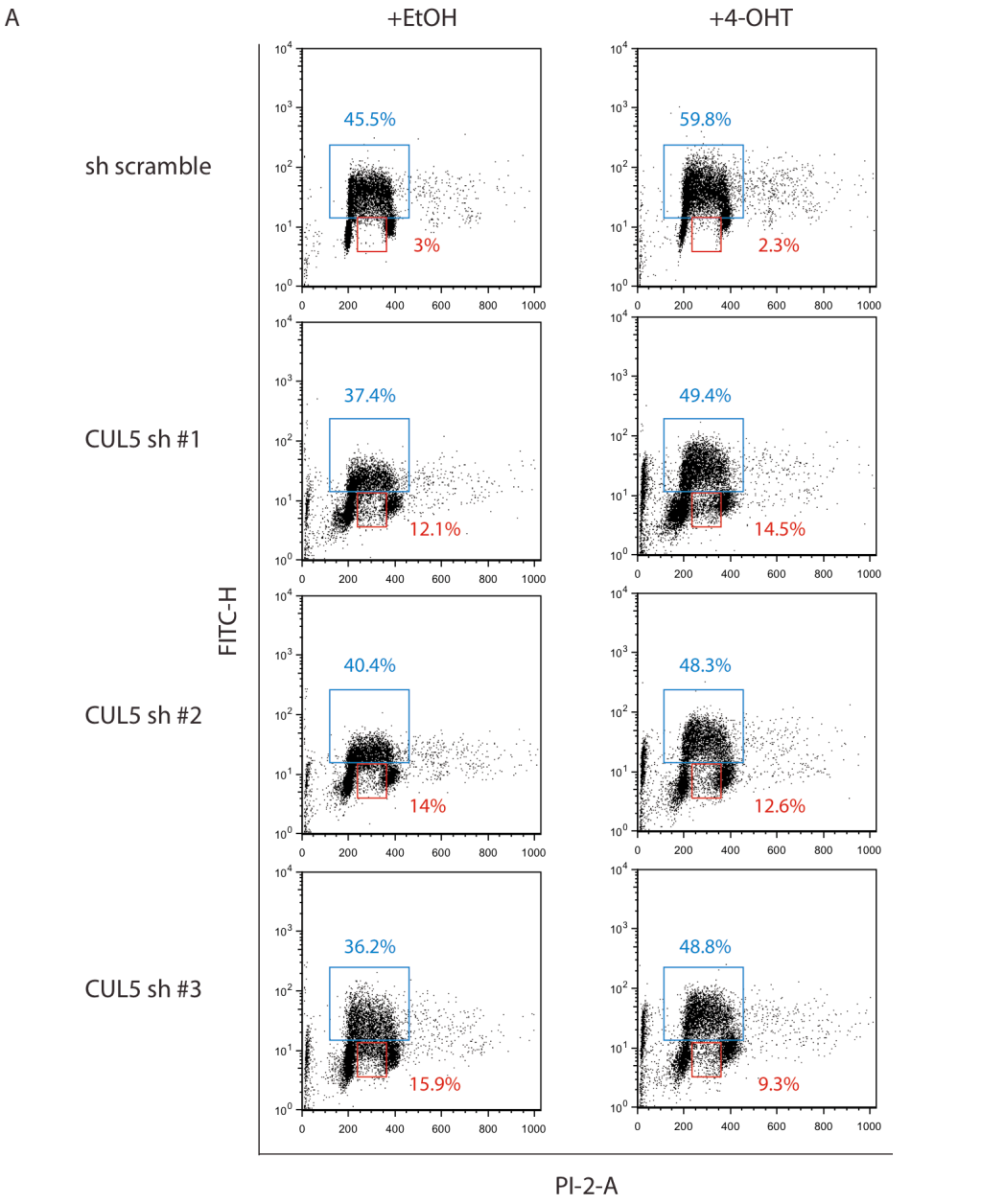
A
+EtOH
+4-OHT
sh scramble
CUL5 sh #1
CUL5 sh #2
CUL5 sh #3
45.5%
3%
59.8%
2.3%
37.4%
12.1%
49.4%
14.5%
40.4%
14%
48.3%
12.6%
36.2%
15.9%
48.8%
9.3%
FITC-H
PI-2-A

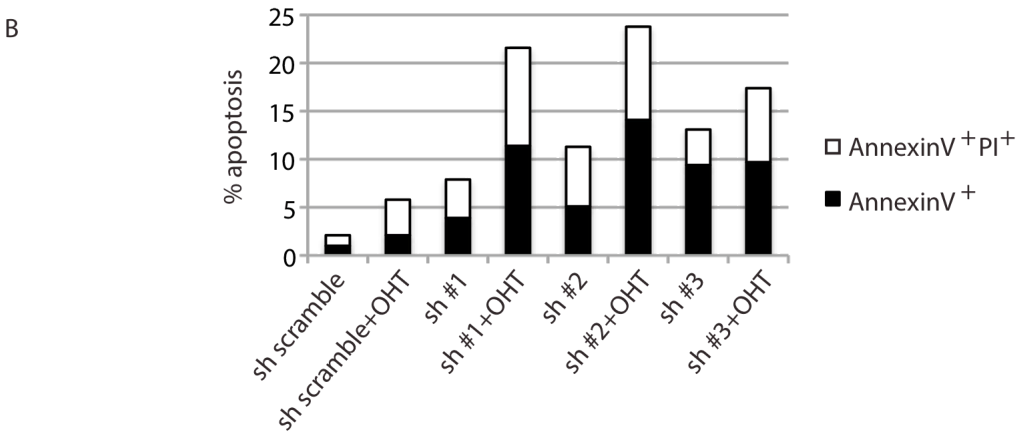
B
% apoptosis
25
20
15
10
5
0
sh scramble
sh scramble+OHT
sh #1
sh #1+OHT
sh #2
sh #2+OHT
sh #3
sh #3+OHT
AnnexinV +PI+
AnnexinV +

Figure 16: CUL5 depletion with N-Myc activation in SHEP-N-MycER cells induces S-phase arrest and strong apoptosis.

(A) The cells were treated as described in Figure 13. The population of BrdU positive cells are enclosed in blue frame and the population of BrdU negative cells are enclosed in red frame.

(B) The cells were treated as in (A). The AnnexinV/PI FACS was performed as in Figure 13.

4.4.3 Validation of CUL5 in neuroblastoma cell lines

To confirm the synthetic lethal effect of CUL5 depletion and *MYCN*-amplification, experiment described in 4.3.3 was repeated (Figure 17). Western blot analysis shows that the CUL5 sh #1 has a better knockdown efficiency than sh #3 whereas sh #2 shows no functional knockdown (Figure 17B). All three *MYCN*-nonamplified neuroblastoma cell lines do not show evident effect whereas all four *MYCN*-amplified neuroblastoma cell lines present a lethal effect (Figure 17A). On the whole, these results indicate CUL5 depletion is lethal in *MYCN*-amplified neuroblastoma cell lines.

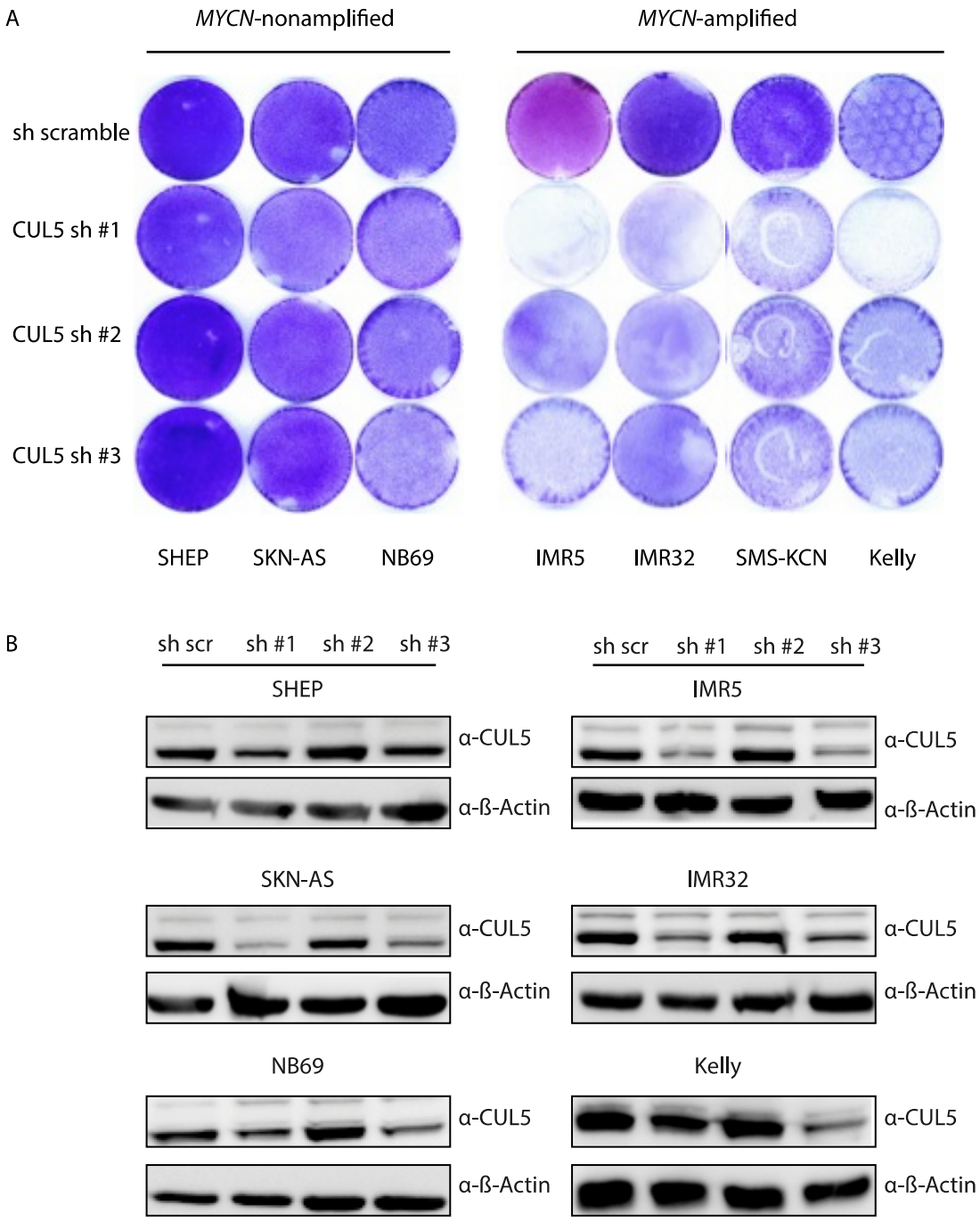

Figure 17: CUL5 is required more for survival of MYCN-amplified neuroblastoma cell lines than *MYCN*-nonamplified neuroblastoma cell lines.

(A) Three *MYCN*-nonamplifed neuroblastoma cell lines do not show lethal effect upon CUL5 depletion whereas four *MYCN*-amplified neuroblastoma cell lines have a strong growth disadvantage upon CUL5 depletion. The colony assay was performed as in Figure 14.

(B) The knockdown efficiency of sh cul5 was analysed by western blot. ß-actin was used as a loading control.

4.5 CUL3

4.5.1 Validation of CUL3

CUL3 is one of the top candidates from the screen (Table 23). The protein belongs to the cullin family and serves as an E3-Ring-ligase (Furukawa et al., 2003).

To verify the synthetic lethal effect of CUL3, a CUL3 shRNAs was designed. Western blot analysis indicates knockdown efficiency of nearly 100% (Figure 18A left panel). The colony formation assay shows that CUL3 depletion with N-Myc activation leads to cell growth arrest. CUL3 depletion alone shows a weak effect. Furthermore, a growth curve was performed to reproduce the effect from colony assays (Figure 18B). The upper and lower black lines indicate the cells with sh scramble and sh scramble with OHT-treatment. Cells with sh scramble and N-Myc activation proliferate slightly than cells with sh scramble. The upper red curve of CUL3 depletion shows a delay in proliferation. The lower red curve indicating CUL3 depletion and N-Myc activation shows much slower proliferation. The cell number decreases continuously from day 3 until day 5 but from day 6 they start to grow again. This could be explained by loss of shRNA function. To exclude off-target effects of sh cul3, a murine CUL3 was overexpressed in the SHEP-N-MycER cells (Figure 18C). Murine Cul3 is similar to human CUL3 and they share 98% homologous protein sequences. Western blots analysis shows the overexpression of murine CUL3. Compared to the cells infected with empty vector, the cells with overexpressed murine CUL3 were completely rescued (Figure 18C).

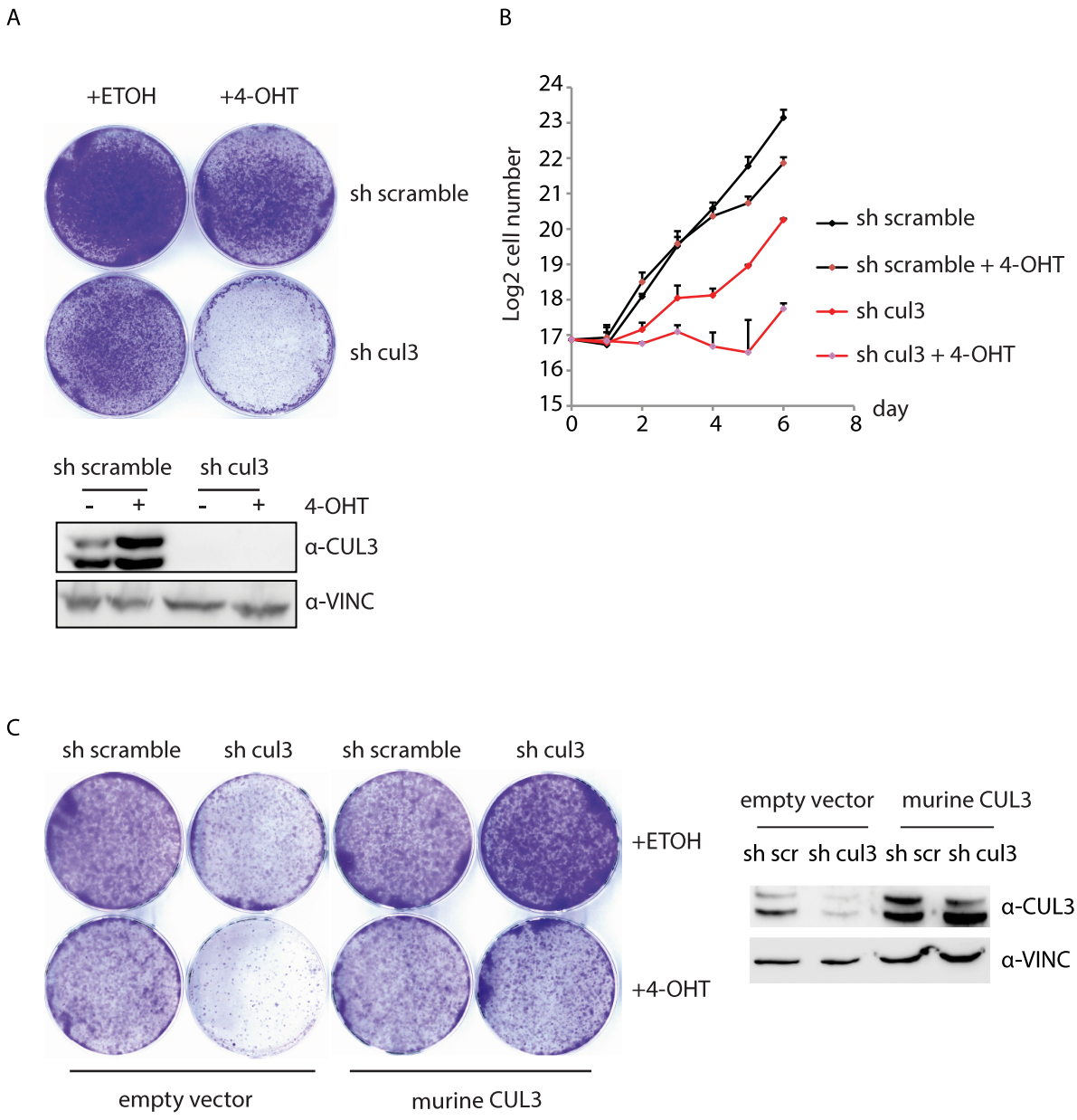

Figure 18: SHEP-N-MycER cells with CUL3 depletion and N-Myc activation have a growth disadvantage. The experiments were conducted with pLKO backbone based lentiviral vector.

(A) CUL3 depletion has a strong lethal effect on SHEP-N-MycER cells upon N-Myc activation. Colony assay was performed as in Figure 12. The knockdown efficiency of pLKO sh cul3 was analysed by western blot.

(B) Growth curve shows a constant result as (A). $5x10^4$ cells were plated as on day 0 and counted every second day. On day 5 cells were split because of confluency.

(C) Murine CUL3 rescues the lethal effect caused by sh cul3 and N-Myc activation. SHEP-N-MycER cells were infected with pRRL empty vector or pRRL cul3 and selected with puromycin for 2 days. Subsequently, the cells were infected with pLKO sh cul3 and sh scramble and plated for colony assay. The overexpression of murine CUL3 was analysed by western blot.

To further confirm the synthetic lethality of CUL3 and N-Myc, two CUL3 shRNAs (sh #412 and sh #784) based on the library vector backbone were used for colony formation assay, growth curve and rescue experiment (Figure 19). Western blot analysis verifies a good knockdown efficiency (Figure 19A lower panel). The curves of sh #412 and sh #784 without OHT shift to the curve of sh scramble indicating CUL3 depletion alone has a weak effect based on pGIPZ vector. The curves of sh #412 and sh #784 with OHT show a delay in proliferation. The cells from day 10 of growth curve were taken for colony formation assay and also show a growth disadvantage more pronounced in sh #412 and sh #784 with OHT (Figure 19B). To exclude an off-target effect of sh #412 and sh #784, a murine CUL3 protein was overexpressed in the SHEP-N-MycER cells. The cell growth arrest can be completely rescued upon murine CUL3 overexpression (Figure 19C). We confirm that CUL3 depletion leads to a proliferation delay upon N-Myc activation.

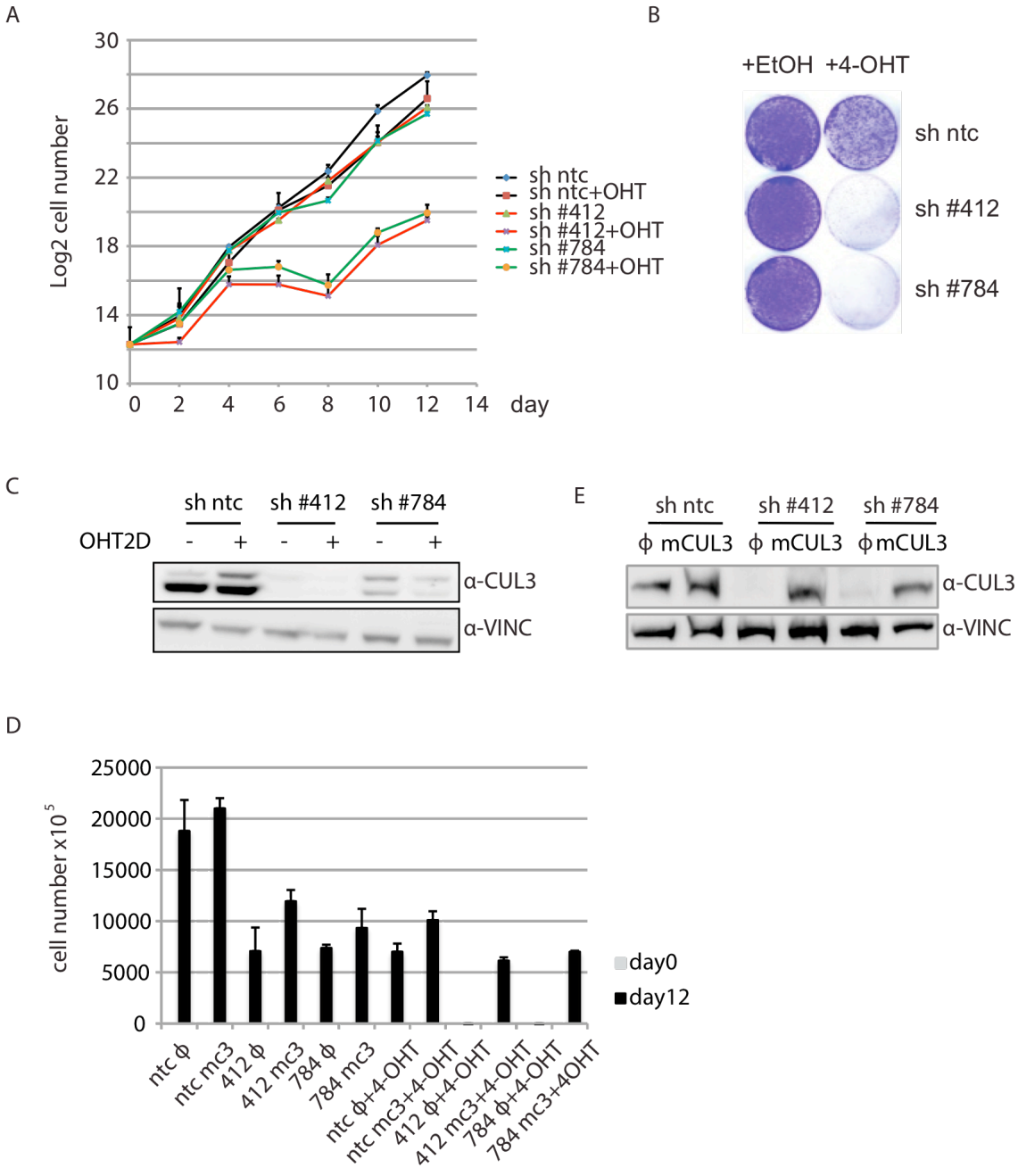

Figure 19: SHEP-N-MycER cells infected with pGIPZ CUL3 with N-Myc activation have a strong growth disadvantage.

(A) $5x10^4$ of SHEP-N-MycER cells infected with pGIPZ CUL3 sh #412, sh #784, sh ntc respectively were plated on a 6cm dish on day 0. 200nM OHT was added to cells on day 1. The cells were counted every second day for 12 days.

(B) Cells from day 10 are seeded for colony assay. The colony assay was performed as in Figure 12

(C) Western blots indicate the knockdown efficiency of pGIPZ CUL3 shRNAs.

(D) Murine CUL3 was overexpressed in SHEP-N-MycER with and without sh cul3 via a lentiviral overexpression vector pRRL. Cells were counted on the day of plating and day 12.

(E) Western blots indicate the overexpression of murine CUL3.

4.5.2 CUL3 in neuroblastoma cell lines

As described in 4.3.3, to ensure the synthetic lethality of CUL3 and N-Myc, three *MYCN*-nonamplified and four *MYCN*-amplified neuroblastoma cell lines were used. Only CUL3 sh #1 and sh #3 were shown, as sh #2 has an off-target effect (Figure 20 lower panel). The SHEP cells and SKN-AS cells show a growth arrest. As expected the NB69 cells are not influenced by knockdown of CUL3 while the four *MYCN*-amplified neuroblastoma cell lines present a lethal effect (Figure 20 upper panel). IMR5, IMR32 and SMS-KCN cells infected with sh #3 show no growth disadvantage, which correlates with the low knockdown efficiency of this shRNA. This result suggests a requirement of CUL3 for proliferation of *MYCN*-amplified neuroblastoma.

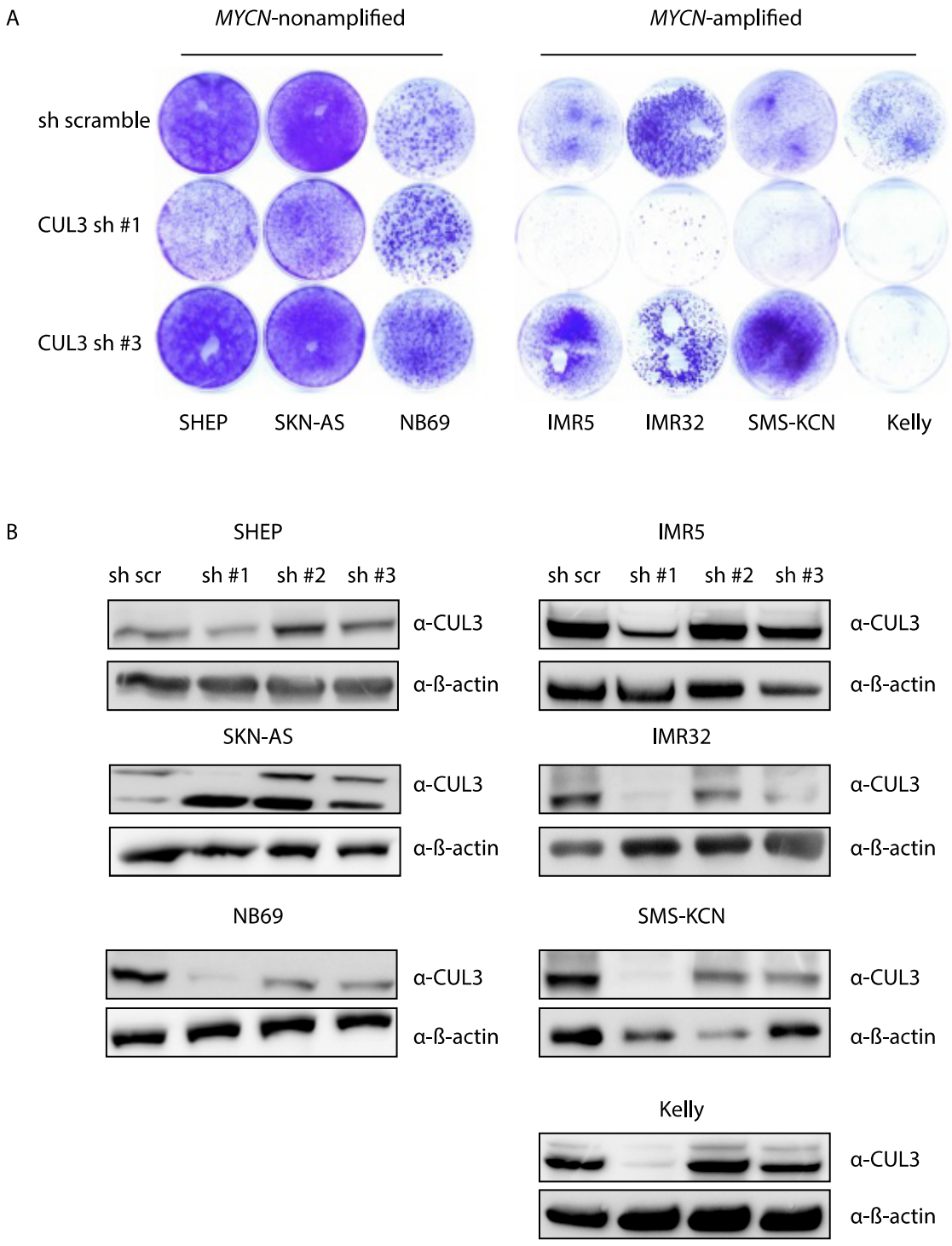

Figure 20: CUL3 is required more for survival of *MYCN*-amplified neuroblastoma cell lines than *MYCN*-nonamplified neuroblastoma cell lines.

A) pLKO CUL3 sh #1 and sh #3 (sh #2 has an off-target effect, not shown) were used for colony assay. Three *MYCN*-nonamplifed neuroblastoma cell lines show less dependency on CUL3 whereas four *MYCN*-amplified neuroblastoma cells lines have a strong growth disadvantage without CUL3 expression. The colony assay was performed as in Figure 14.

B) Western blot analysis indicates the knockdown efficiency of sh cul3.

4.5.3 CUL3 depletion induces apoptosis upon N-Myc activation

As concluded in 4.5.1, CUL3 depletion with N-Myc activation leads to cell growth arrest. To confirm the notion that depletion of CUL3 with N-Myc overexpression induces apoptosis, an AnnexinV/PI FACS was performed to investigate if the growth arrest is caused by apoptosis. The diagram in Figure 21 shows that CUL3 depletion induces 7% early apoptosis and 15% total apoptosis comparable with apoptosis induced by N-Myc. CUL3 depletion with N-Myc activation induces 25% early apoptosis and 40% total apoptosis which is more than the first three conditions (Figure 21). We confirm that CUL3 depletion with N-Myc activation highly induces apoptosis.

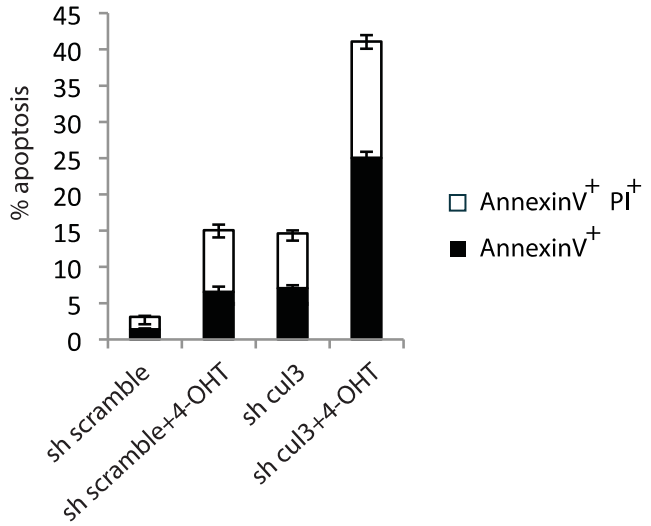

Figure 21: Depletion of CUL3 with N-Myc activation induces strong apoptosis.

Depletion of CUL3 with N-Myc activation highly induces apoptosis. AnnexinV/PI FACS was performed as in Figure 13.

The ability of p53 to control apoptosis in response to abnormal proliferative signal and stress including DNA damage is important for its tumour suppression function (Levine, 1997). BCL2 is a member of BCL2 family that regulates apoptosis by either inducing pro-apoptotic member or inhibiting anti-apoptotic member and it meditates intrinsic apoptosis (Tsujimoto et al., 1984; Cleary et al., 1986). To check whether the apoptosis is p53-dependent or BCL2-related, the cells were infected with sh RNA against *p53* or a BCL2-overexpression vector. Western blot analyses

show a p53 depletion and Bcl2 overexpression in SHEP-N-MycER cells (Figure 22A right panel, C right panel). Cells infected with shRNA against CUL3 and treated with OHT show 5% early apoptosis and 18% total apoptosis when p53 is depleted early apoptosis and total apoptosis are 10% and 25% indicating that p53 depletion does not rescue apoptosis (Figure 22A left panel). The depletion of CUL3 in either p53 wild type IMR5 cells or p53 mutant Kelly cells, both are *MYCN*-amplified neuroblastoma cell lines, lead to a cell growth arrest, but Kelly cells show a weaker effect than IMR5 cells suggesting there might be a p53-dependent apoptosis in *MYCN*-amplified neuroblastoma cell lines (Figure 22B).

In addition, cells infected with shRNA against CUL3 and treated with OHT have around 27% apoptosis whereas BCL2-overexpressed cells show 24% apoptosis indicating BCL2 overexpression does not rescue apoptosis (Figure 22C left panel). In sum, apoptosis induced by CUL3 depletion and N-Myc activation is neither p53-dependent nor BCL2-dependent in SHEP-N-MycER cells, but p53-dependent in some other *MYCN*-amplified neuroblastoma cell lines.

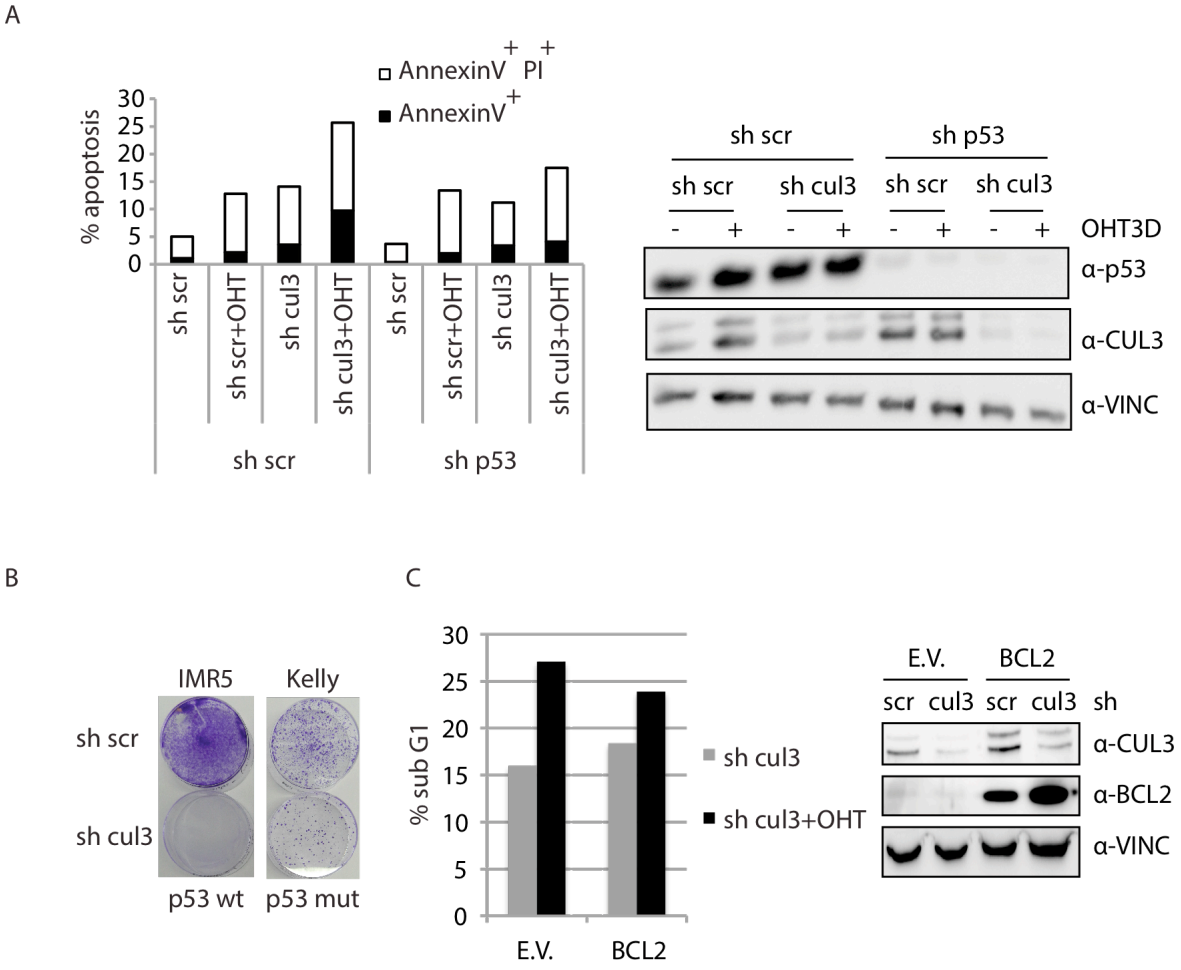

Figure 22: Analysing the p53- and BCL2-dependency of apoptosis induced by CUL3 depletion and N-Myc activation in SHEP-N-MycER and other *MYCN*-amplified neuroblastoma cells

(A) Depletion p53 does not rescue the apoptosis induced by CUL3 depletion and N-Myc activation. AnnexinV/PI was performed as in Figure 13. Western blots (right panel) indicate the knockdown efficiency of sh p53 and sh cul3.

(B) Apoptosis is induced stronger in p53 wt IMR5 cells than p53 mutant Kelly cells upon CUL3 depletion. The colony assay was performed as in Figure 12

(C) BCL2 overexpression in SHEP-N-MycER shows no apoptosis rescue. The cells were infected with pWZL-BCL2 or pWZL empty vector and selected, afterwards infected with sh cul3 or sh scramble. The cells were plated on day 0. 200nM OHT was added on day1. After 3 days OHT-treatment the cells were harvested and fixed in ethanol at -20°C for 1 day and stained with propidium iodide. The sub G1 cells were determined by flow cytometry. Western blots indicate the overexpression of BCL2.

4.5.4 CUL3 depletion with N-Myc activation leads to S-phase arrest

To investigate the reason of growth arrest besides apoptosis, BrdU/PI FACS was performed. N-Myc activation increases the BrdU positive cells from 35% to 48% (Figure 23A). CUL3 depletion without and with OHT has no change. The red frame in dot plot of sh cul3 with OHT

encloses 12% cells which are BrdU negative but in S-phase. This population is 2% in sh scramble, 3.5% in sh scramble with OHT, 5% in sh cul3 (Figure 23 right panel). Here gives us a hint that CUL3 depletion with N-Myc activation leads to S-phase arrest.

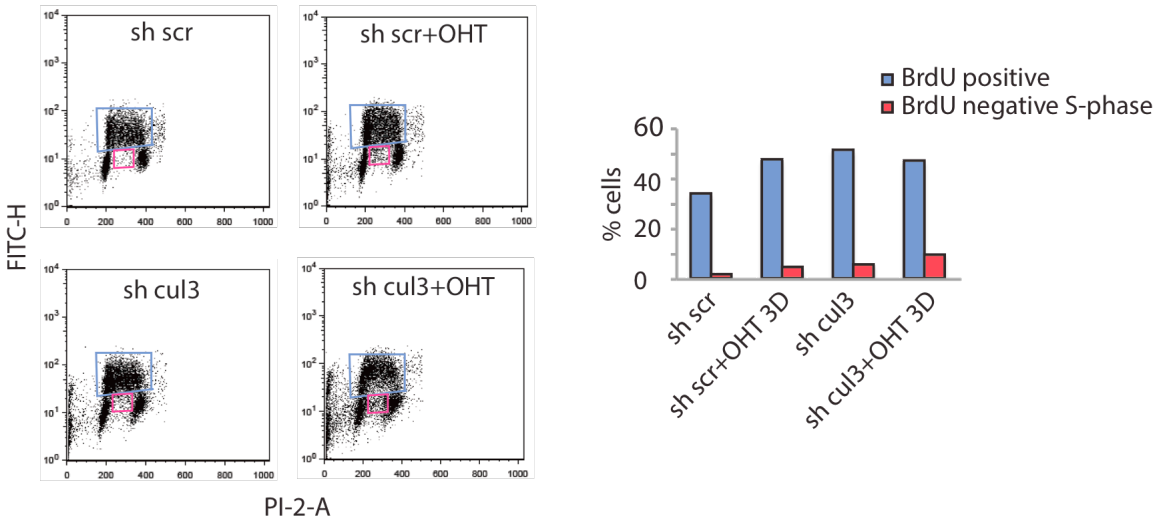

Figure 23: Depletion of CUL3 with N-Myc activation lead to S-phase arrest.

BrdU/PI FACS described in Figure 13 shows a S-phase problem. Blue frame enclosed the population of BrdU positive cells while the red frame enclosed the population of BrdU negative S-phase cells. Right panel shows the quantification of population of in blue and red frames.

To monitor S-phase progression, a BrdU pulse-chase experiment was performed (Figure 24). SHEP-N-MycER cells were pulse-labeled with BrdU for one hour and pulse-chased thereafter. The cells were harvested at the indicated time points after BrdU pulse. Cells infected with sh scramble without or with OHT progress efficiently through all phases of the cell cycle while cells infected with sh cul3 without or with OHT cycle more slowly. In fact, at 4 h, BrdU-labeled/high PI cells from control cells already appear in G1 phase after completion of mitosis. In contrast, only a small percentage of CUL3-depleted BrdU-labeled cells recycle to G1 while the majority of these cells still being in S-phase at 4 h. In CUL3-depleted N-Myc activated cells, the BrdU-labeled population recycle to G1 first at 6 h indicating a slower progression compared to CUL3-depleted cells. At 6 h the CUL3-depleted N-Myc activated cells do not show clear separation of each cell phase. BrdU pulse-chase label demonstrates that CUL3 depletion with N-Myc activation decreases the rates of cell progression through the cell cycle.

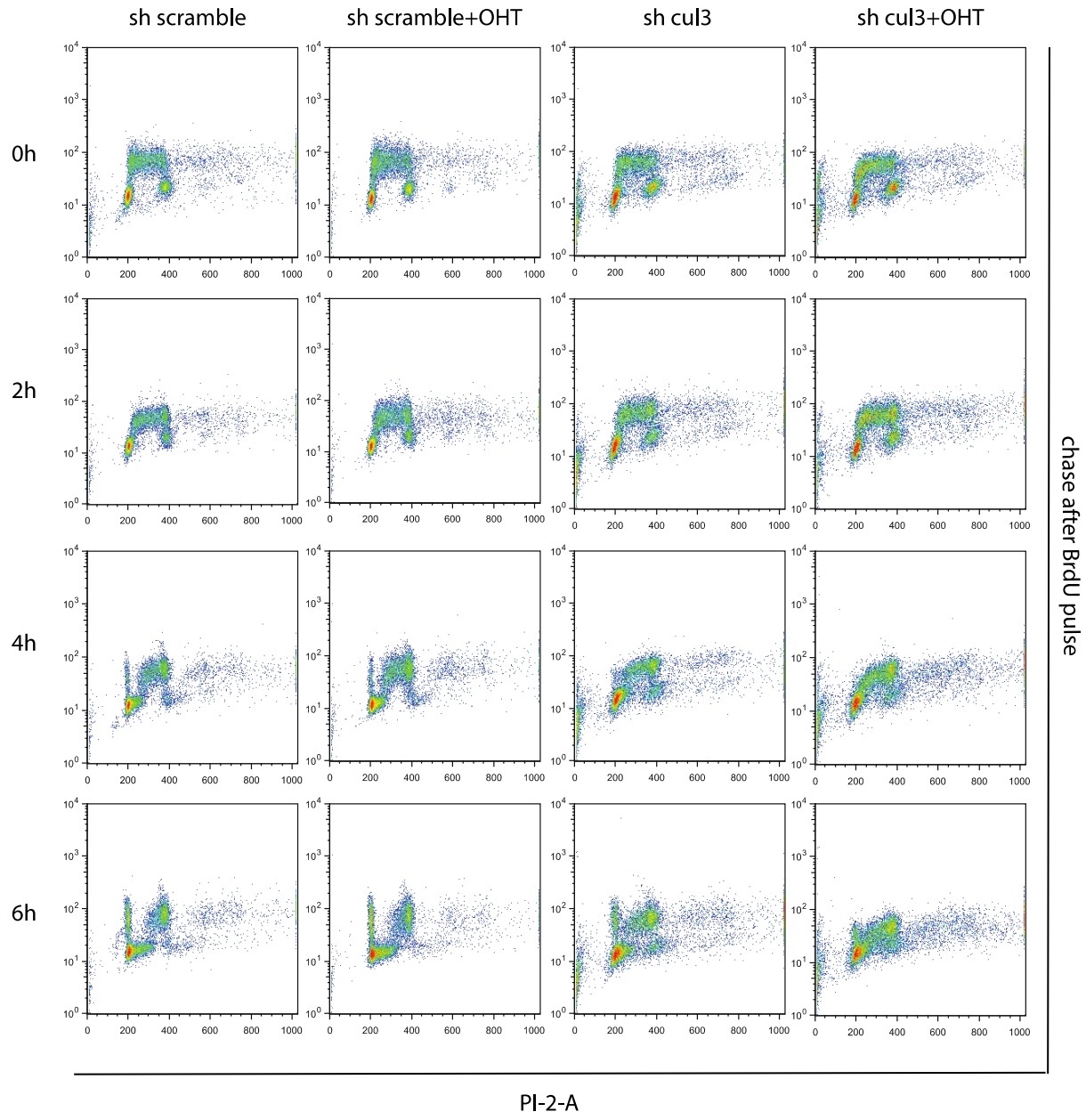

Figure 24: BrdU pulse-chase further detects S-phase problems.

BrdU was pulsed for 1 hour and washed away, subsequently chased for 2, 4, 6 hours. BrdU/PI FACS described in Figure 13 was performed to analyze the cell cycle and BrdU incorporation.

4.5.5 N-Myc does not transcriptionally regulate CUL3

As in Figure 18A shown, CUL3 protein level is increased after OHT-treatment. mRNA expression and DNA-binding studies, *in vitro* and *in vivo*, have nominated an increasing number of genes as Myc targets (Shaffer et al., 2006; Margolin et al., 2009; Wasylishen and Penn, 2010;

Ji et al., 2011) Therefore, we checked whether N-Myc transcriptionally regulates CUL3. To exclude the possibility that the increase of CUL3 protein level is due to tamoxifen by its own, the parental cell line SHEP was treated with tamoxifen for two days. The western blot analysis shows the CUL3 level is not increased upon treatment (Figure 25B). N-Myc activation upregulates slightly *CUL3* mRNA level (Figure 25C). To check whether N-Myc binds to *CUL3* promoter region, chromatin immunoprecipitation (ChIP) with N-Myc from IMR5 cells was performed. The positive controls *FASN*, *CCNE2*, *FBW8* which are known Myc targets have an enrichment of 0.6, 0.4, 0.8 folds compared to the control IgG and the negative control *chr11* does not show an enrichment indicating the ChIP experiment worked (Figure 25D). Two primer pairs were designed binding to the transcription start site while one primer pair binds to an E-box region. The primer pair of tss_1 does not show any enrichment whereas primer pair of tss_1 and E-box have an enrichment for N-Myc of 0.6 and 0.15 folds, but the enrichment of IgG are 0.3 and 0.1 folds suggesting that N-Myc does not bind to *CUL3* mRNA. The Chip experiment leads to the conclusion that N-Myc does not transcriptionally regulate CUL3.

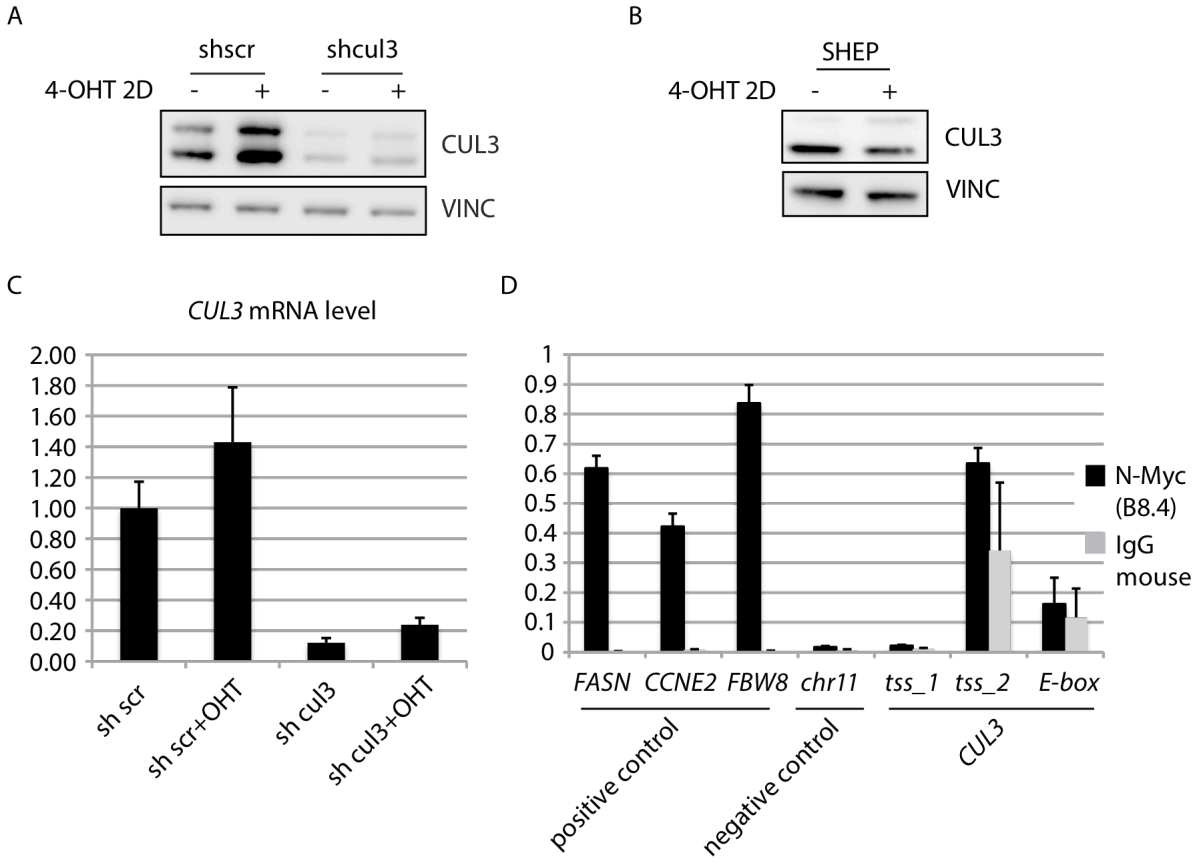

Figure 25: N-Myc does not bind to *CUL3* promoter region but upregulates the CUL3 protein level.

(A) 4-OHT-treatment increased CUL3 protein level in SHEP-N-MycER cells. SHEP-N-MycER infected with sh cul3 and sh scramble were treated with 4-OHT for 2 days and harvested for western blot.

(B) 4-OHT-treatment does not increase the CUL3 protein level in SHEP cells. SHEP cells were treated with 4-OHT for 2 days and harvested for western blot.

(C) 4-OHT-treatment increased *CUL3* mRNA level. SHEP-N-MycER cells infected with sh cul3 and sh scramble were treated with 4-OHT for 2 days. The RNA was isolated and subjected to cDNA synthesis for RT-PCR.

(D) Chromatin immunoprecipitation shows that transcription start site 1, 2 and E-box region are not enriched in N-Myc precipitation. The chromatin was precipitated by N-Myc antibody.

4.5.6 CUL3 depletion with N-Myc activation synergistically increases Cyclin E protein level

Cyclin E is a target of CUL3-Ring-ligase (Kossatz et al., 2010) and regulates the G1- to S-phase transition (Weinberg, 2007). Therefore, Cyclin E expression level upon CUL3 depletion and N-Myc activation was checked. The diagram of RT-PCR shows that after N-Myc activation the *Cyclin E* mRNA level is nearly 2-fold increased compared to control and 2.5-fold increased after CUL3 depletion and N-Myc activation (Figure 26A). CUL3 depletion alone does not change the *Cyclin E* mRNA level evidently. The quantification of western blots from 6 biological replicates shows that CUL3 depletion with N-Myc activation increases Cyclin E level nearly 9 folds indicating that the upregulation of Cyclin E protein level is more post-translational rather than transcriptional regulation (Figure 26B, C). So CUL3 depletion with N-Myc activation synergistically increases Cyclin E protein level.

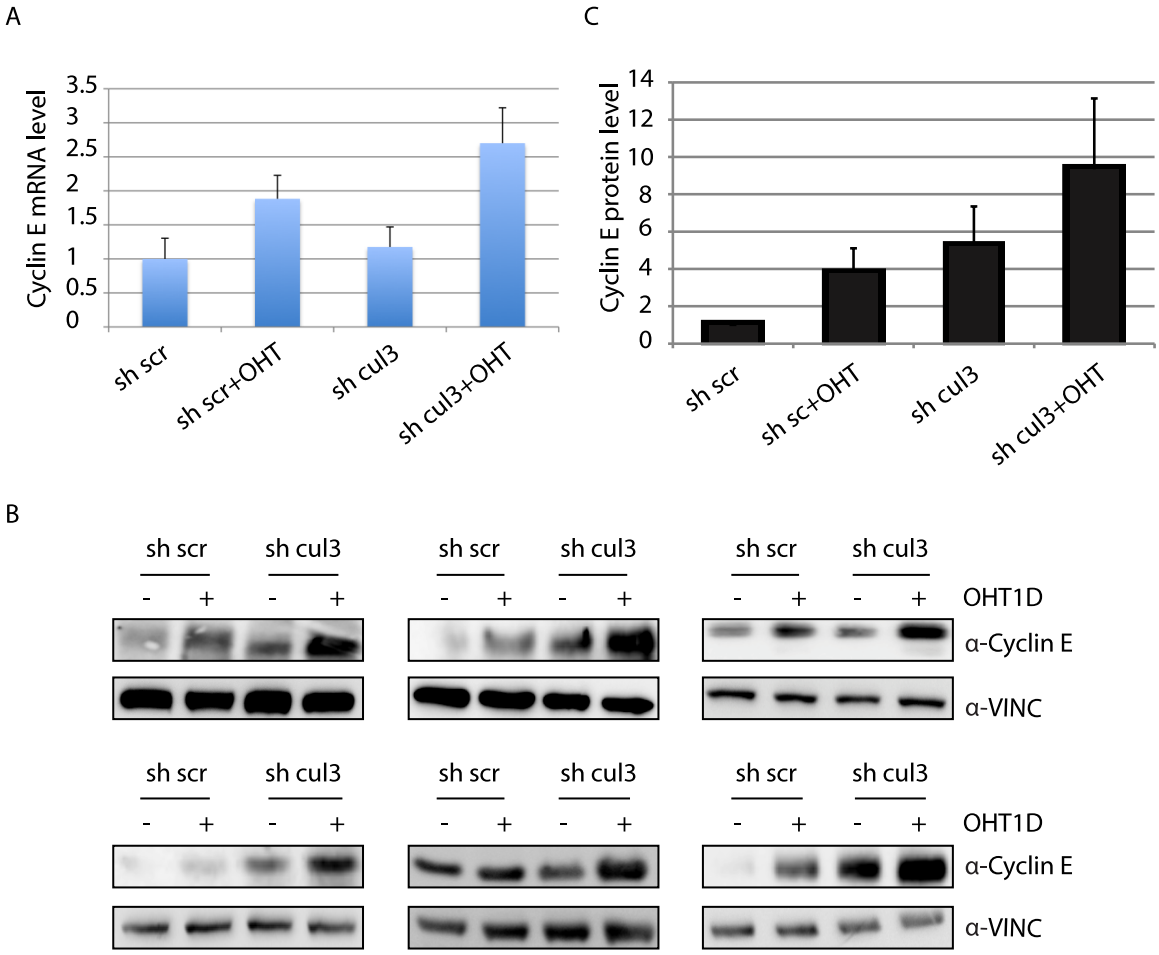

Figure 26: CUL3 depletion and N-Myc activation synergistically increases Cyclin E protein level.

(A) RT-PCR shows that *Cyclin E* mRNA levels are slightly increased via 4-OHT-treatment. SHEP-N-MycER cells infected with sh cul3 and sh scramble were treated with 4-OHT for one day. The total RNA was isolated for RT-PCR. Error bars indicate standard deviation (n=3).

(B) Cyclin E western blots of biological replicates determined the synergistically increase of Cyclin E protein level upon CUL3 depletion and 4-OHT-treatment. SHEP-N-MycER cells infected with sh cul3 and sh scramble were treated with 4-OHT for one day.

(C) Quantification of Cyclin E western blots. Error bars indicate mean of standard deviation (n=6).

4.5.7 CUL3 depletion with N-Myc activation induces pan-nuclear γ-H2Ax formation

Deregulated Cyclin E induces chromosome instability presented by DNA damage response (Spruck et al., 1999). Normally, DNA lesions are immediately recognized by DNA damage response factors, which activate cell cycle checkpoints followed by direct DNA repair. Depending on type of damage, different DNA repair pathways response. γ-H2Ax foci are usually

formed after DNA lesions occur (Bouwman and Jonkers, 2012). Strong DNA damage response induced by checkpoint defect is presented by a pan-nuclear γ-H2Ax (Neelsen et al., 2013). An indirect immunofluorescent staining was performed to check γ-H2Ax expression (Figure 27A). After 24 h OHT-treatment upon CUL3 depletion, a large amount of pan-nuclear γ-H2Ax positive cells are accumulated (Figure 27A black dashed circle). Pan-nuclear γ-H2Ax stained cells are increased 12-fold in CUL3 depleted cells whereas the staining is 20-fold increased in CUL3-depleted N-Myc activated cells (Figure 27B). The pan-nuclear γ-H2Ax cells upon CUL3 depletion with N-Myc activation are significantly more than without N-Myc. To check γ-H2Ax protein level upon CUL3 depletion and N-Myc activation, histone extraction was performed and shows a consistent result with the staining (Figure 27C). We confirm that CUL3 depletion with N-Myc activation leads to formation of pan-nuclear γ-H2Ax.

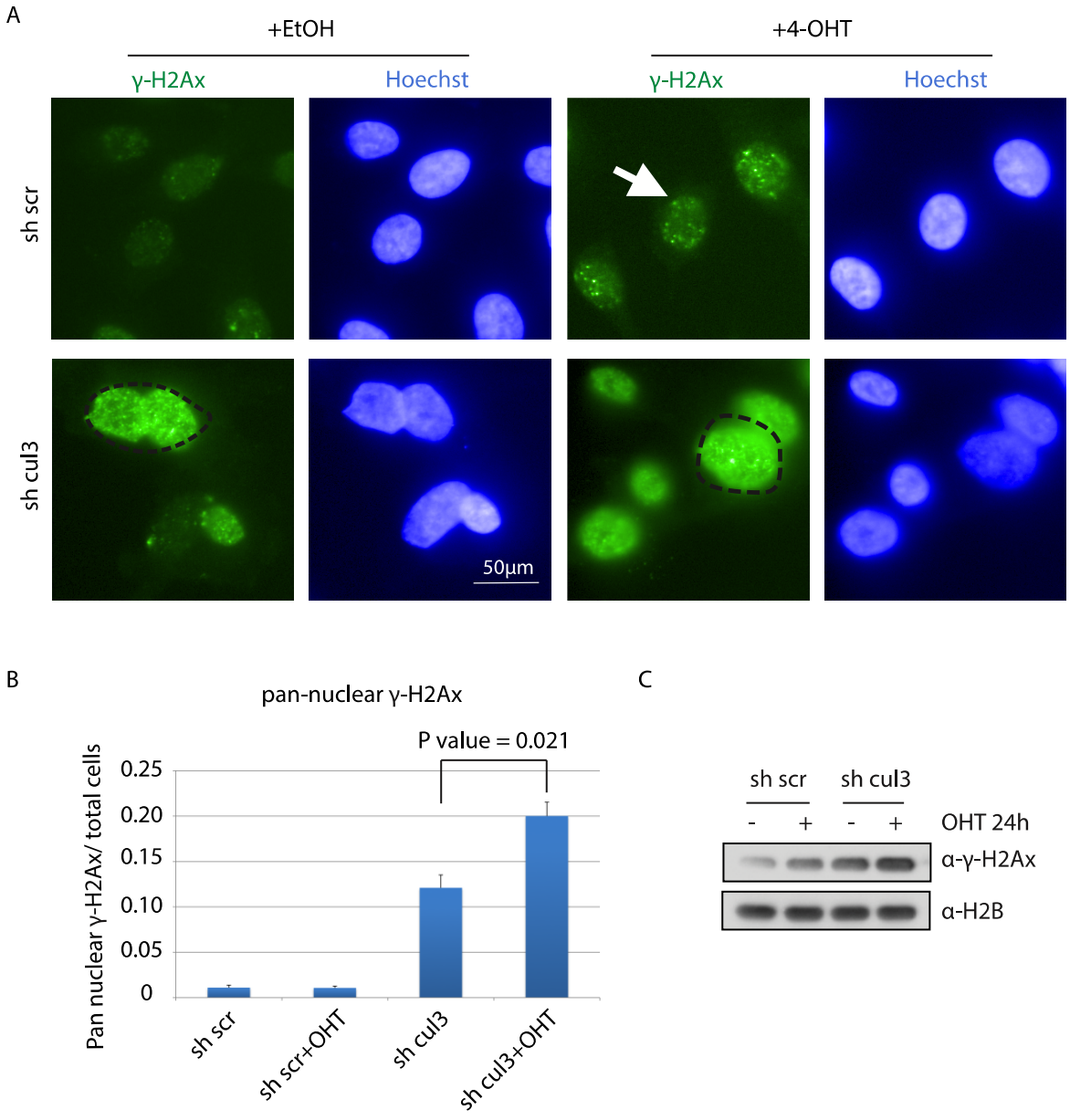

Figure 27: CUL3 depletion with N-Myc activation induces synthetic DNA damage.

(A) Pan-nuclear γ-H2Ax is induced upon CUL3 depletion with and without N-Myc activation. CUL3 depleted SHEP-N-MycER cells were treated with 4-OHT for 24 hour and fixed, stained with γ-H2Ax antibody and related second antibody, afterwards Hoechst for nuclei. γ-H2Ax foci were indicated with a white arrow. Pan-nuclear γ-H2Ax (black dashed circle) was seen in CUL3 depleted cells. The images were captured with 40x magnification. Scale bar=50µm. The staining was performed by Ursula Eilers and Christina Schuelein-Voelk.

(B) Quantification of the staining shows that CUL3 depleted and N-Myc activated cells have significantly higher pan-nuclear γ-H2Ax than only CUL3 depleted cells. P value was calculated with Mann-Whitney U-test.

(C) Histone extraction shows γ-H2Ax protein level is increased more in CUL3-depleted N-Myc activated cells than CUL3 depleted cells. H2B was used as a loading control.

4.5.8 CUL3 depletion with N-Myc activation induces synergistic DNA damage response

To clarify the upstream mechanism of DNA damage response, western blots for p-ATM, p-CHK1 and p-CHK2 were performed (Figure 28). ATM is the major regulator of DNA damage response, which targets a set of substrates that promote cell cycle arrest and DNA repair (Cimprich and Cortez, 2008). ATM is activated through auto- or trans-phosphorylation on serine 1981 (Bakkenist and Kastan, 2003), so we examined the protein level of p-ATM at this phosphosite. The p-ATM (Ser1981) is induced more in CUL3-depleted N-Myc activated cells than CUL3-depleted cells (Figure 28A). CHK1 checkpoint is downstream of ATR and p-CHK1 (Ser 345) is a marker of DNA replication fork stalling (Bouwman and Jonkers, 2012). p-CHK1 is synergistically activated upon CUL3 depletion and N-Myc activation (Figure 28B C). CHK2 checkpoint a downstream factor of ATM, is also synergistically activated (Figure 28C). Replication protein A (RPA) binds to single strand DNA which is a template of replication (Cimprich and Cortez, 2008). RPA gets phosphorylated at serine 33 after the DNA replication stalls and recruits ATR-ATRIP protein complex and RAD17 9-1-1 complex separately, then further activates CHK1 checkpoints (Cimprich and Cortez, 2008). Therefore, phospho-RPA (Ser33) is a more direct marker for stalled replication forks. A robust phosphorylation of RPA in CUL3-depleted N-Myc activated cells was detected by western blot analysis (Figure 28C).

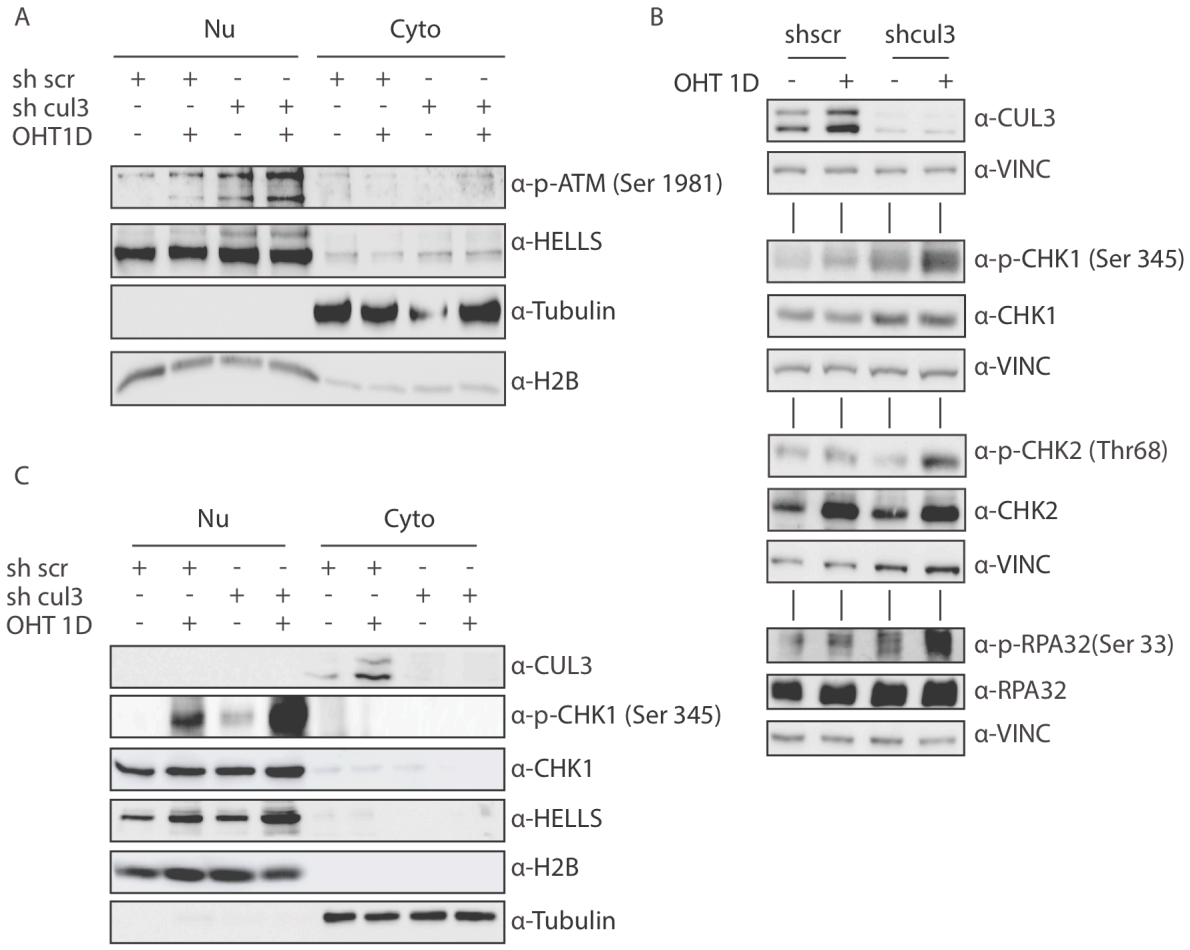

Figure 28: CUL3 depletion with N-Myc activation leads to synthetic activation of checkpoint protein.

(A) Checkpoint protein ATR is activated via phosphorylation at serine 1981 upon CUL3 depletion. SHEP-N-MycER infected with sh scramble or sh cul3 were treated with 4-OHT for one day and subjected to nuclear extraction. HELLS and H2B are used as loading control for nuclear fraction while tubulin for cytoplasmic fraction. The nuclear and cytoplasm extracts were analysed by western blot.

(B) CHK1, CHK2 and RPA32 are activated upon CUL3 depletion with N-Myc activation. Cells described in (A) were lysed directly with SDS sample buffer and analysed by western blot. Vinculin was used as a loading control.

(C) p-CHK1 is activated upon CUL3 depletion with N-Myc activation. SHEP-N-MycER was treated like (A) and subjected to nuclear extraction. Loading controls were described in (B).

4.5.9 DNA damage response induced by CUL3 depletion and N-Myc activation is mediated by synergistic accumulation of Cyclin E

To confirm whether CHK1 activation is caused by Cyclin E accumulation, roscovitine is used to indirectly inhibit the Cyclin E binding partner CDK2 (Figure 29). Roscovitine is a cell

permeable reversible selective inhibitor of CDK1, CDK2 and CDK5. It is a purine analog competing for binding site of ATP in the catalytic cleft (Meijer et al., 1997). In the early S-phase Cyclin E forms an active heterodimer with CDK2 to drive the cell cycle progression from G1 to S-phase (Weinberg, 2007). Inhibition of CDK2 keeps Cyclin E inactive. Phosphorylation of CHK1 is completely inhibited and the total CHK1 level remains unchanged after CUL3 depletion with and without OHT (Figure 29).

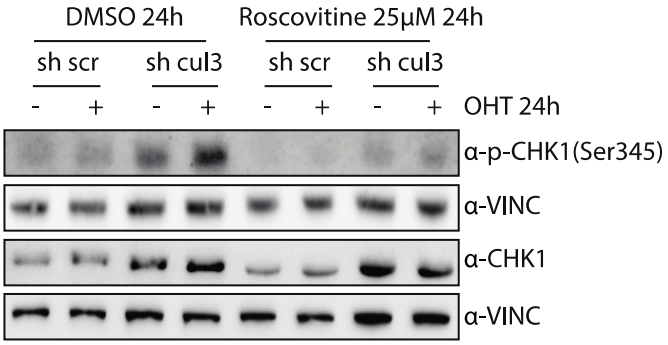

Figure 29: Roscovitin inhibits p-CHK1 activation upon CUL3 depletion with N-Myc activation.

Roscovitin inhibits the activation of p-CHK1. SHEP-N-MycER cells infected with sh cul3 or sh scramble are plated on day 0. 200nM OHT and 25µM roscovintin were added to the cells on day1 for 24 h. The cells were lysed directly with SDS sample buffer and analysed by western blot. Vinculin was used as a loading control.

As roscovitine inhibits also other members of the CDK family, the experiment was repeated with the more specific CDK2 inhibitor cvt-313 (Figure 30). Consistently, cvt-313 rescues the cells from apoptotic appearance after 22 h treatment (Figure 31). CDC25A checkpoint defect combines CDK2 deregulation with impaired cell cycle control, two key steps in tumourigenesis. Additionally, the phosphatase CDC25A, which control the transition of G2- to M-phase, is at the same time a CDK1 activator and a key effector of the DNA damage response (Mailand et al., 2000; Bartkova et al., 2006; Di Micco et al., 2006). As Cyclin B forms a heterodimer with CDK1 bringing the onset of mitosis, we used a specific CDK1 inhibitor Ro-3306 which blocks the entrance to mitosis (Weinberg, 2007). Ro-3306 rescues the CUL3 depleted cells either with or without OHT treatment from apoptotic appearance after 5 h treatment (Figure 30). We conclude that inhibition of Cyclin E can inhibit the synergistic DNA damage response induced by CUL3 depletion and N-Myc activation.

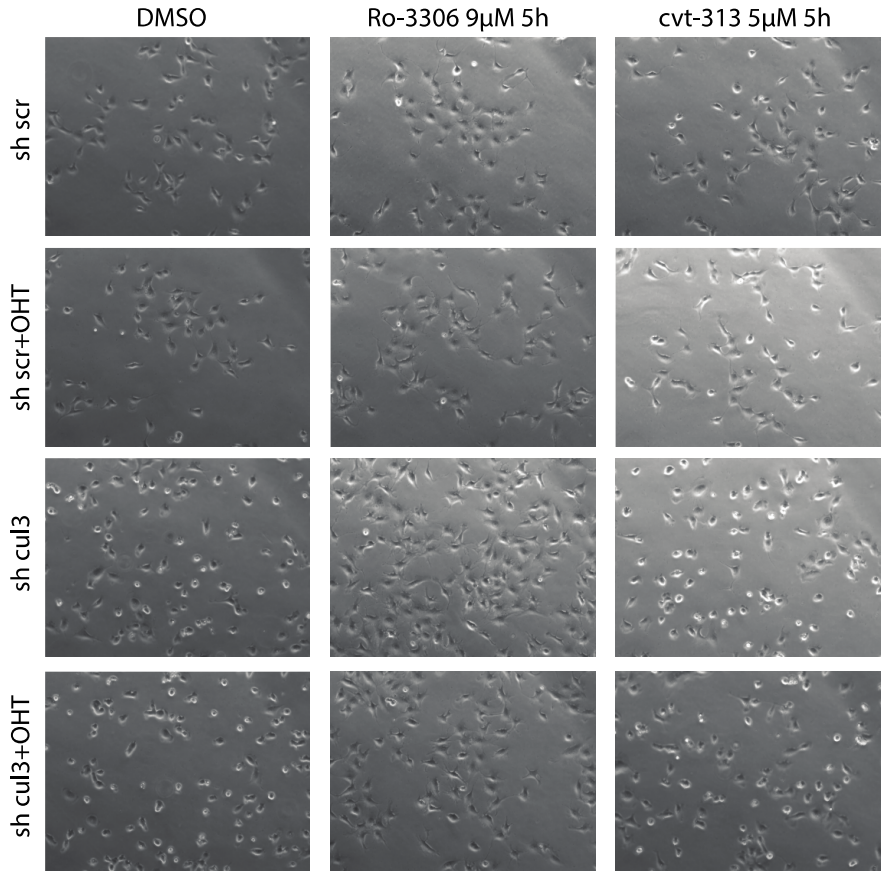

Figure 30: Ro-3306 and cvt-313 can rescue the apoptotic morphology of CUL3-depleted N-Myc-overexpressed cell.

SHEP-N-MycER cells with and without CUL3 depletion were starved with 0.5% FCS for 24 hours and released with 10% FCS and 200nM OHT. After 2-hour OHT-treatment CDK1 inhibitor Ro-3306 and CDK2 inhibitor cvt-313 were added. 5-hour Ro-3306 treatment can rescue the apoptotic cell morphology of CUL3 depletion and N-Myc activation.

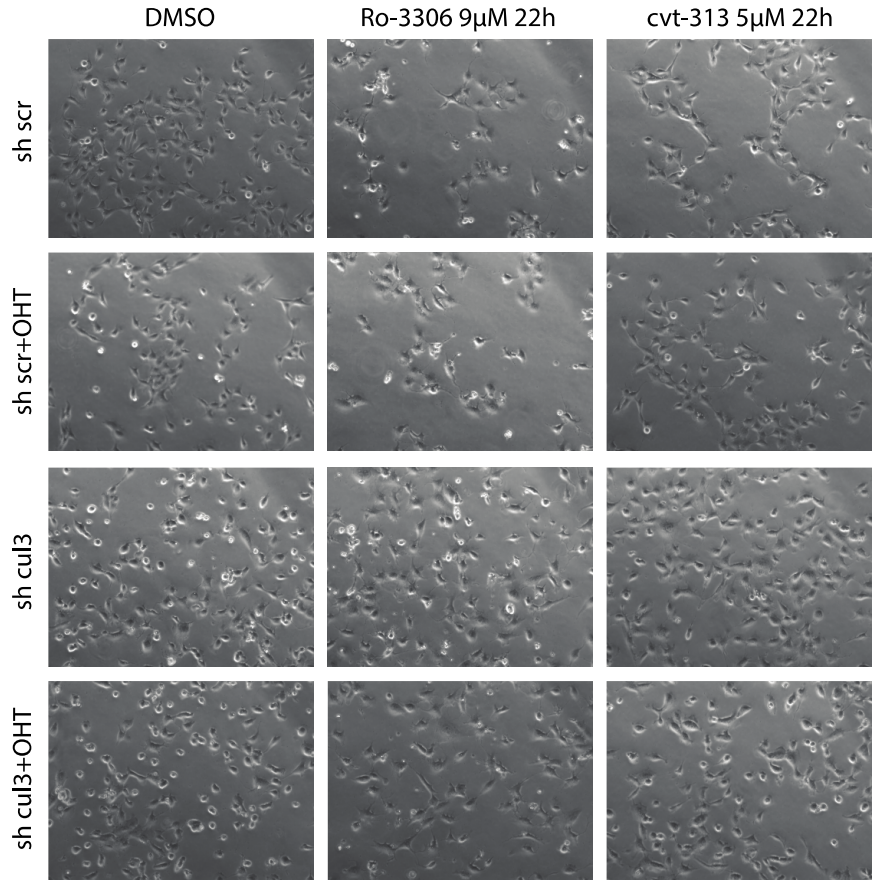

Figure 31: Ro-3306 and cvt-313 can rescue the apoptotic morphology of CUL3-depleted N-My-overexpressed cell.

The cells described in Figure 30 were treated with inhibitors for 22 hours. The apoptotic cell morphology could be rescued by both inhibitors after 22-hour treatment.

4.6 Candidates involved in other biological processes

4.6.1 Validation of the candidate genes

On the candidate list, a group of shRNAs involved in regulating important biological processes: transcription elongation, mRNA export and chromosome segregation. ELL, NUP153, LARP7, TCEB1, THOC1, NCAPG2, NIPBL were chosen for validation.

ELL (elevennineteen lysine-rich leukemia) is an elongation factor for RNA polymerase II, which works as a TFIIH partner (Mourgues et al., 2013). Three shRNAs targeting *ELL* were designed for validation. The sh #1 and sh #3 show around 40% knockdown efficiencies and sh #2 shows a

more than 60% knockdown efficiency (Figure 32B). Colony assay shows a lethal effect from ELL depletion alone rather than synthetic lethal effect (Figure 32A).

NUP153 belongs to the nuclear pore complex, which mediates the nascent mRNA transport from nucleus to cytoplasm. NUP153 interacts with the ENY2/TREX complex, which couples transcription and mRNA processing with nuclear mRNA export. Depletion of any component involved in this pathway inhibits mRNA export (Jani et al., 2012). Three shRNAs targeting *NUP153* were designed for validation. The colony formation assay shows depletion of NUP153 with sh #1 and sh #3 has a pronounced synthetic lethal effect on cells with N-Myc activation (Figure 32A). RT-PCR shows that sh #1 has 70% knockdown efficiency and sh #3 has more than 80% knockdown efficiency (Figure 32B). Although sh #2 has 80% knockdown efficiency, it does not show synthetic lethal effect. In sum, NUP153 depletion with N-Myc activation leads to cell growth arrest.

It has been reported that LARP7, BCDIN3 and noncoding 7SK small nuclear RNA are vital for the formation and stability of 7SK snRNP, which suppresses the positive transcription elongation factor b (P-TEFb) kinase (Barboric et al., 2009). The LARP7 sh #1 has more than 80% knockdown efficiency and show a synthetic lethal effect. The LARP7 sh #3 has also more than 80% knockdown efficiency but shows growth arrest alone. The sh #2 has an off-target effect because it has no knockdown efficiency but a strong growth disadvantage (Figure 32). We conclude that LARP7 depletion with N-Myc activation leads to cell growth arrest.

TCEB1 (Elongin C) is the adaptor of CUL5 E3 ligase complex, which interacts with Elongin B, VHL and targeted protein. Mutation of TCEB1 abolishes the Elongin C VHL binding (Sato et al., 2013). The homolog protein of CUL5 in yeast is CUL3, which mediates the ubiquitination of stalled RNA polymerase II (Harreman et al., 2009). The colony assay does not show a synthetic lethal effect (Figure 4.29).

THOC1 is involved in THO/TREX complex mediating the mRNA processing and export. Mutations in any of the THO/TREX structural genes cause pleiotropic phenotypes such as transcription impairment, mRNA export defects. (Rondon et al., 2003) The THOC1 sh #1 and sh #3 have 60% and 30% knockdown efficiencies, respectively, but the colony formation assay does not show any synthetic lethal effect.

Condensins are multi-subunit protein complexes that play a central role in mitotic chromosome assembly and segregation (Hirano, 2005). All the shRNAs against *NCAPG2* show more than

60% knockdown efficiency. Depletion of condensin alone has a strong lethal effect and together with N-Myc activation the effect is not stronger (Figure 32).

NIPBL is a cohesin loading factor and is one of the several factors, which determine the localization of chromosome. Cohesin tethers two sister chromatids together from S-phase on, allowing for their proper segregation in mitosis (Zuin et al., 2014). The sh #2 has only 20% knockdown efficiency but it has a stronger lethal effect alone compared to sh #1 and sh#3 which have 40% and more than 60% knockdown efficiencies, respectively.

Depletion of NIPBL with sh #1 or sh#3 alone does not show a lethal effect also no synthetic lethal effect with N-Myc. This is reasonable because NIPBL is not on the final list due to its log FoldChange LS/LU more than -2. It was chosen for validation because of functional interests.

In sum, only NUP153 and LARP7 show a synthetic lethal effect in the colony assays and the rest of the candidates show a lethal effect on their own.

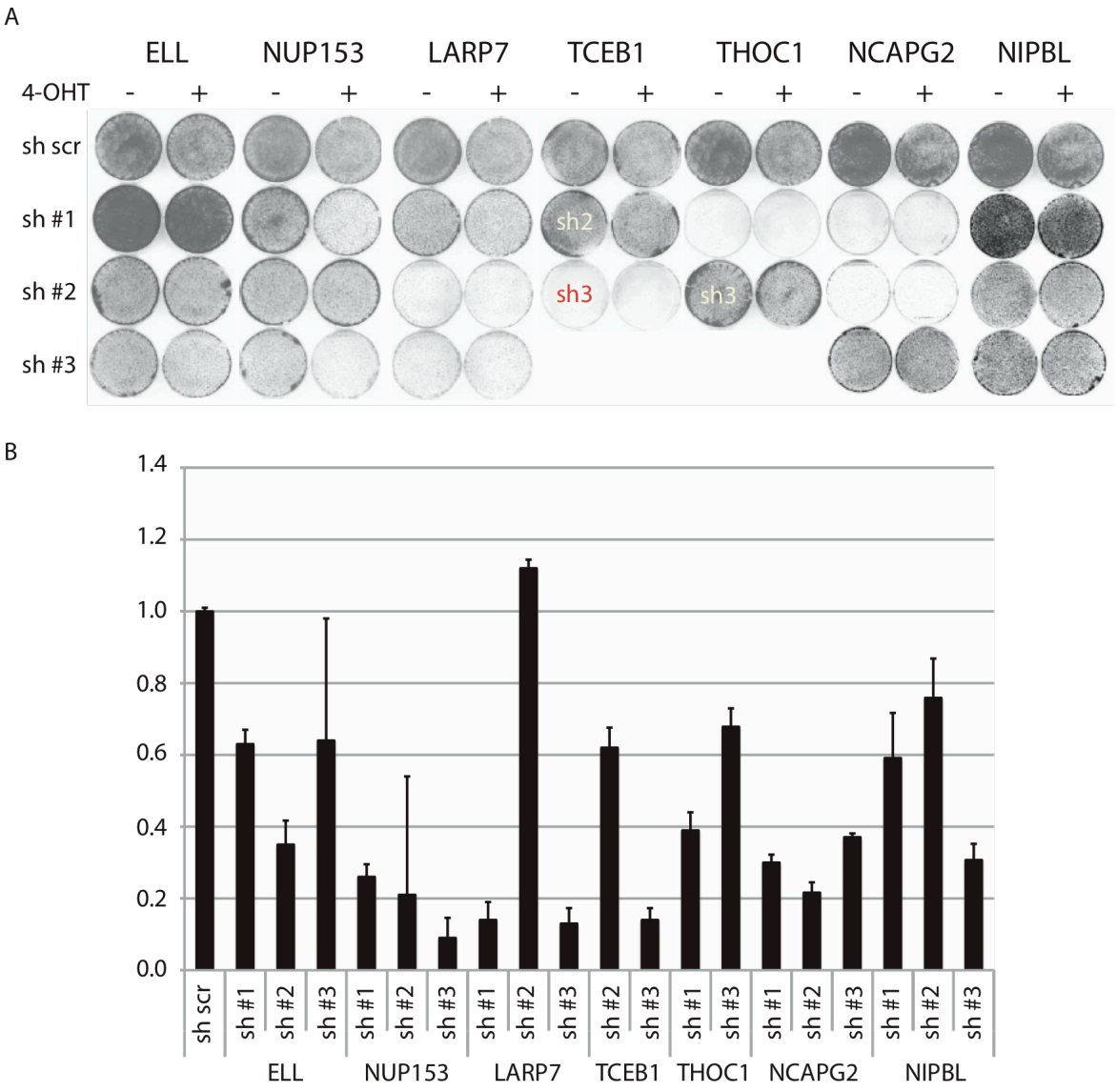

Figure 32: Validation of candidates involved in elongation process by RNA polymerase II

Colony assay described in Figure 12 was performed with indicated shRNAs (upper panel). The knockdown efficiencies of indicated shRNAs were determined by RT-PCR (lower panel).

4.6.2 Investigation of S-phase problem resulted from depletion of candidate genes with N-Myc activation

To address reasons of growth disadvantage from colony assay, BrdU/PI FACs assays were performed to check subG1 and S-phase. The shRNAs with the best knockdown efficiency of each candidate were chosen for BrdU/PI assays. They show heterogeneous S-phase problems (Figure 33). shRNA control has 43% BrdU positive and 4.2% BrdU negative cells while after

OHT-treatment this increased to 51% BrdU positive and decreased to 3.4% BrdU negative cells. SubG1 population of these control cells are comparable without- and with OHT-treatment, 1.1% and 1.3%, respectively. BrdU positive cells increased from 36.8% to 39.2% in ELL-depleted cells upon N-Myc activation whereas BrdU negative cells with intermediate DNA content increased from 5.2% to 10.3%. In addition, with ELL depletion apoptosis increased from 8.0% to 14.9%. NUP153-depleted cells have 45% BrdU positive cells whereas NUP153-depleted N-Myc-activated cells have 50% BrdU positive cells. Compared to NUP153 depletion alone, with OHT-treatment there is a much stronger apoptosis induction. LARP7-depleted cells were 65.6% BrdU positive, 3.4% BrdU negative whereas combined with N-Myc activation there were 72.6% BrdU positive, 3.5% BrdU negative. BrdU positive cells in TCEB1-depleted cells without- and with OHT-treatment are comparable 47% and 45%, respectively, but BrdU negative and apoptosis cells are largely increased from 10.4% to 14.7%, 41.5% to 53.5%, respectively. THOC1 depletion increases BrdU positive cells from 32.1% to 38%, BrdU negative cells from 11.9% to 20.8% and apoptosis cells from 24.5% to 56.9%. NCAPG2 depletion either without- or with 4-OHT shows a larger population of BrdU negative S-phase cells, 10.6% and 15.1%, respectively. BrdU positive cell population increases from 44.2% to 50.1% upon N-Myc activation. NCAPG2 depletion with N-Myc activation induces 53.6% apoptosis, 18.7% more than without N-Myc. BrdU/PI FACS shows generally a synthetic lethal effect according to the apoptosis induction, although the colony assays do not show a synthetic growth disadvantage. NIPBL depletion increased BrdU positive cells from 44.8% to 52.9% upon N-Myc activation but the change in BrdU negative cells and apoptosis cells were marginally, from 4.4% to 5%, from 3.8% to 4.5%, respectively.

Taken together, except NUP153 and LARP7 BrdU negative cells with ELL, TCEB, THOC1 or NCAPG2 depletion are largely increased upon OHT-treatment indicating S-phase arrest.

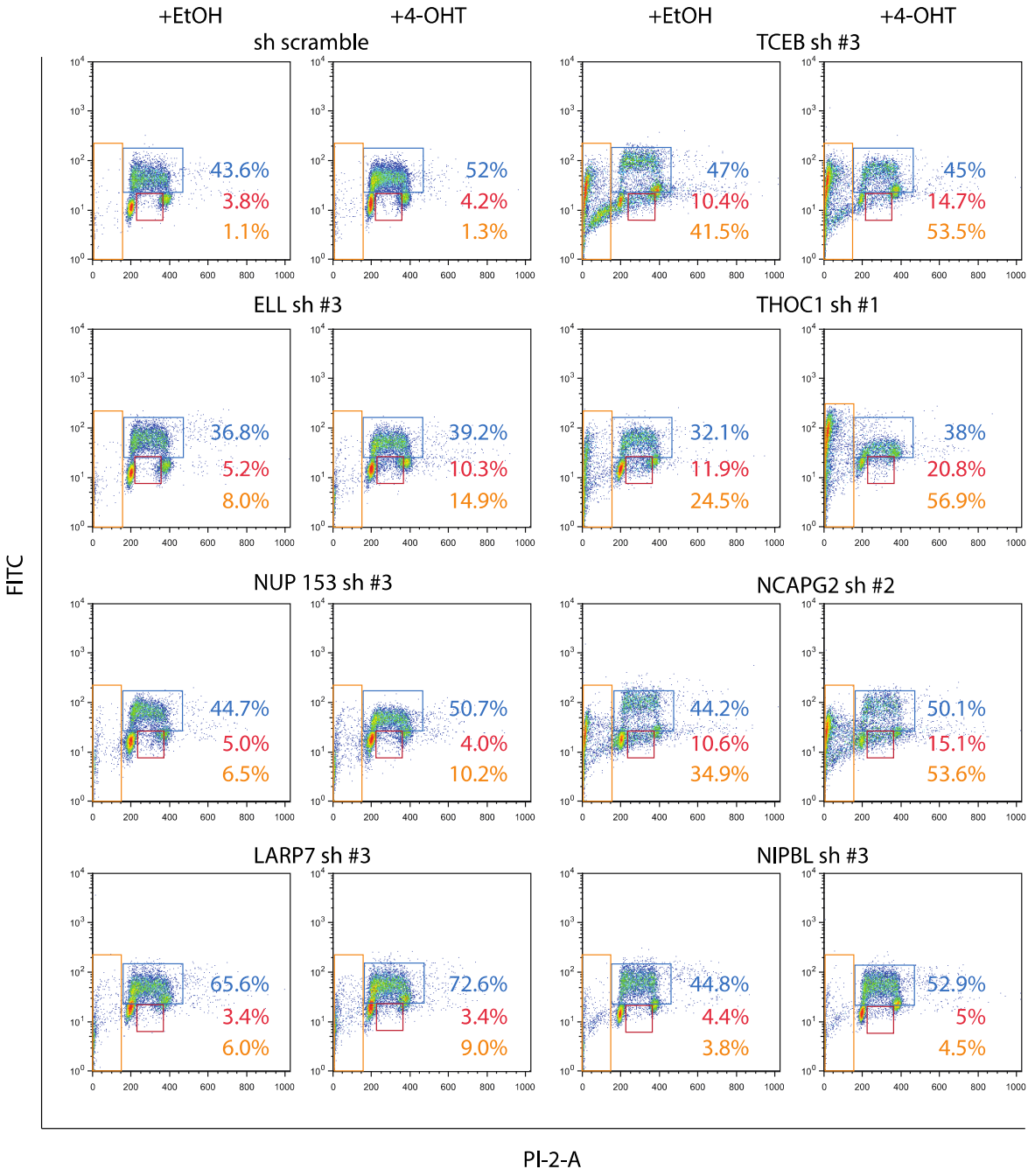

Figure 33: BrdU/PI FACS describes the S-phase problem resulted from depletion of each candidate with N-Myc activation.

One shRNA from each gene was chosen for BrdU/PI FACS. The procedure was described in Figure 13. Yellow frame enclosed the sub G1 population. Blue frame enclosed the BrdU positive population and red frame enclosed the BrdU negative population with intermediate DNA content. The quantification of blue and red frames was based on the total cell number excluding the subG1 population.

4.6.3 Investigation of DNA damage response induced by candidate genes depletion with N-Myc activation

Previous experiments refer that a N-Myc activation together with a depletion of CUL3 leads to induction of a DNA damage pathway (see Figure 27).

To investigate whether depletion of these candidates with N-Myc induces DNA damage response, histone extraction was performed to analyse the DNA damage marker γ-H2Ax (Figure 34A). Depletion of each of these genes has slightly induction of γ-H2Ax but show synergistic induction of γ-H2Ax upon N-Myc activation. To further clarify the DNA damage response, ATR downstream factor CHK1 was checked by western blot (Figure 34B). These analyses show that depletion of LARP7, THOC1 or TCEB1 synergistically induces DNA damage response upon N-Myc activation characterized by the phosphorylation of CHK1. In sum, the depletion of LARP7, THOC1 or TCEB1 leads to synergistic induction of DNA damage response.

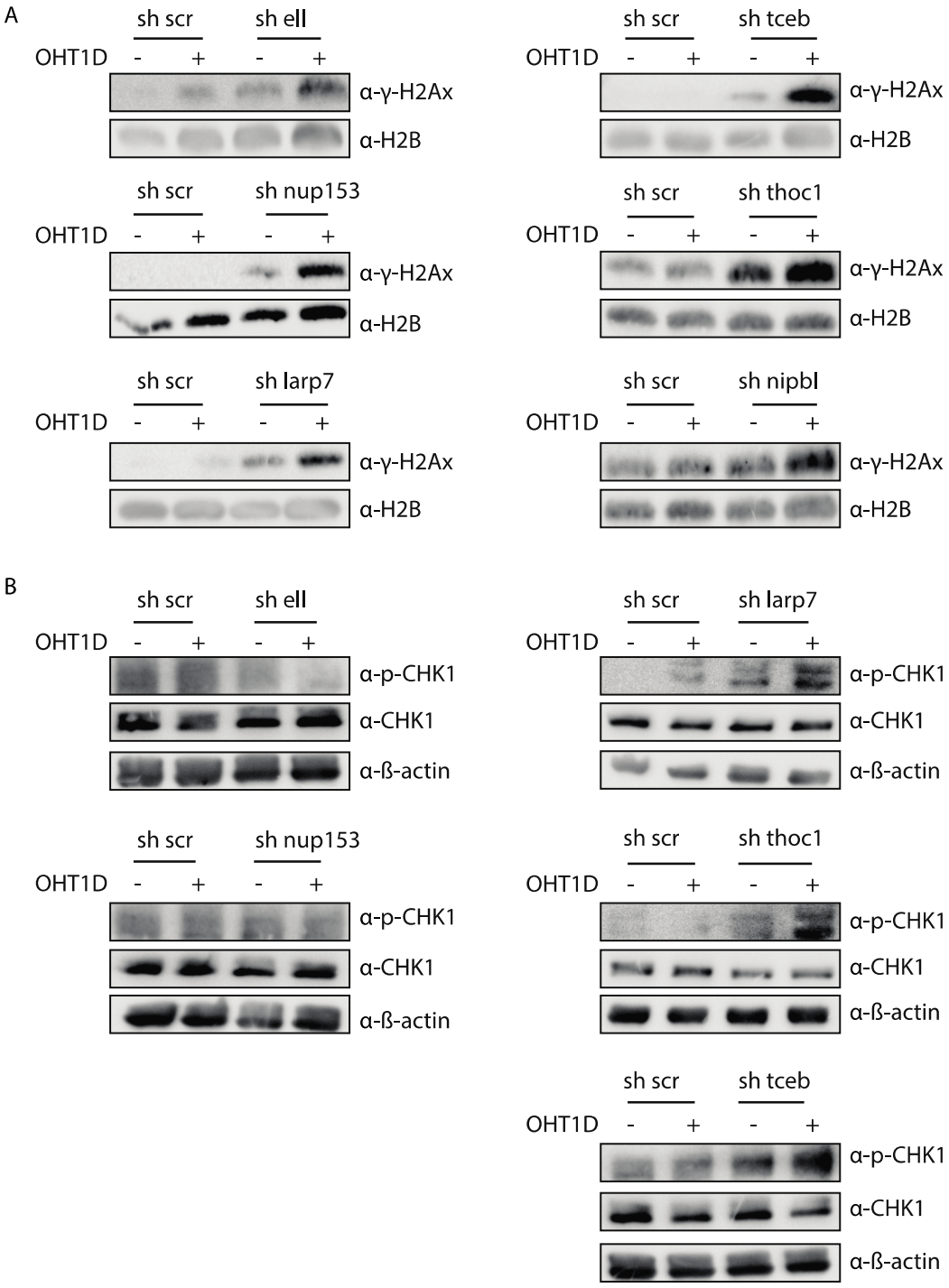

Figure 34: Analysing γ-H2Ax and p-CHK1 in cells with indicated shRNAs and N-Myc activation

(A) Depletion of indicated genes with activated N-Myc leads to a synergistic activation of γ-H2Ax. SHEP-N-MycER cells were infected with shRNAs targeting indicated genes and treated with 200nM 4-OHT for 24 hours. The cells were harvested and subjected to histone extraction. The extracted histone was analysed by western blot. H2B was used as a loading control.

(B) Depletion of LARP7 with activated N-Myc leads to a synergistic activation of p-CHK1 but not for depletion of NUP153. The cells described in (A) were harvested and lysed directly with SDS sample buffer.

4.7 MLN4924

4.7.1 Titration of MLN4924

In the previous chapter 4.3, we could show that the depletion of NAE1, CUL5 and CUL3 leads to a synthetic lethality with N-Myc. To further proof the mechanism we decided to use a NAE inhibitor to inhibit the whole neddylation pathway. NAE1 is a subunit of NAE. MLN4924 is a compound, which binds and inhibits NAE resulting in an inhibition of neddylation. A titration of MLN4924 from 1.5nM to 1000nM in SHEP-N-MycER cells was performed (Figure 35). The upper band of CUL3 which indicates neddylated CUL3 disappears while the lower band, which indicates an inactive form of CUL3 is increased. The Nedd8-Cullin complex is decreased whereas Cyclin E expression is increased with the increase of MLN4924 concentration. The role of PARP is to detect single strand break (SSB) and involved in SSB repair. As apoptosis is promoted by cleavage of PARP by preventing DNA repair-induced survival, it is used as a marker for apoptosis (D'Amours et al., 2001). At 100nM cleaved PARP is activated whereas active CUL3 is completely inhibited. We confirm that MLN4924 could inactivate CUL3-Ring-ligase and induce apoptosis. The range between 15nM and 100nM is suitable for further experiments.

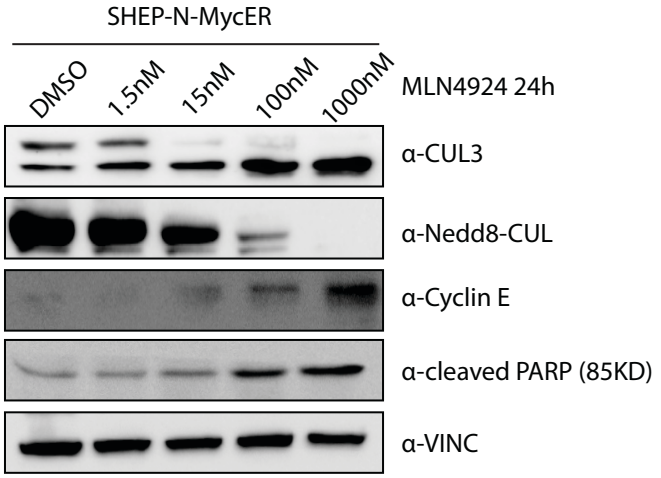

Figure 35: Titration of MLN4924 in SHEP-N-MycER cells

Titration of MLN4924 is from 1.5nM to 1000nM in SHEP-N-MycER cells. Neddylated CUL3 (upper band) is decreased and inactive CUL3 (lower band) is increased with the indicated concentration. Neddylated cullin complex is decreased. Cyclin E and cleaved-PARP are increased. The cells were treated with MLN4924 for 48 hours. The cells were lysed with RIPA buffer and the protein extracts were analysed by western blot. Vinculin was used as a loading control.

4.7.2 MLN4924 with N-Myc induces strong apoptosis and DNA damage response

To further ensure that MLN4924 induces apoptosis in SHEP-N-MycER cells, an Annexin/PI FACS was performed. The range from 25nM to 500nM was used for this experiment (Figure 36A). Apoptosis induction is correlated to the increased concentration of compound. At 100nM cells without OHT have about 20% total apoptosis whereas cells with OHT have 30% total apoptosis. In general, MLN4924 induces 10% more apoptosis with N-Myc activation than without N-Myc.

As concluded in 4.5.8 that CUL3 depletion with N-Myc activation induces synergistic DNA damage response, we asked if MLN4924 has the same effect. Therefore, a western blot was performed to analyse DNA damage response using the range from 25nM to 100nM of compound (Figure 36B). p-CHK1 is increased with the indicated concentration of compound in both N-Myc-activated and N-Myc-nonactivated cells, but it is induced more in N-Myc-activated cells. Compound treatment with OHT leads to Cyclin E accumulation. N-Myc protein level is slightly increased after compound treatment. p21 is activated p53-dependent leading to cell cycle arrest and increased upon compound treatment (el-Deiry et al., 1993; Wu et al., 2003). Therefore, MLN4924-treatment with N-Myc activation induces cell cycle arrest over p21 induction and DNA damage response.

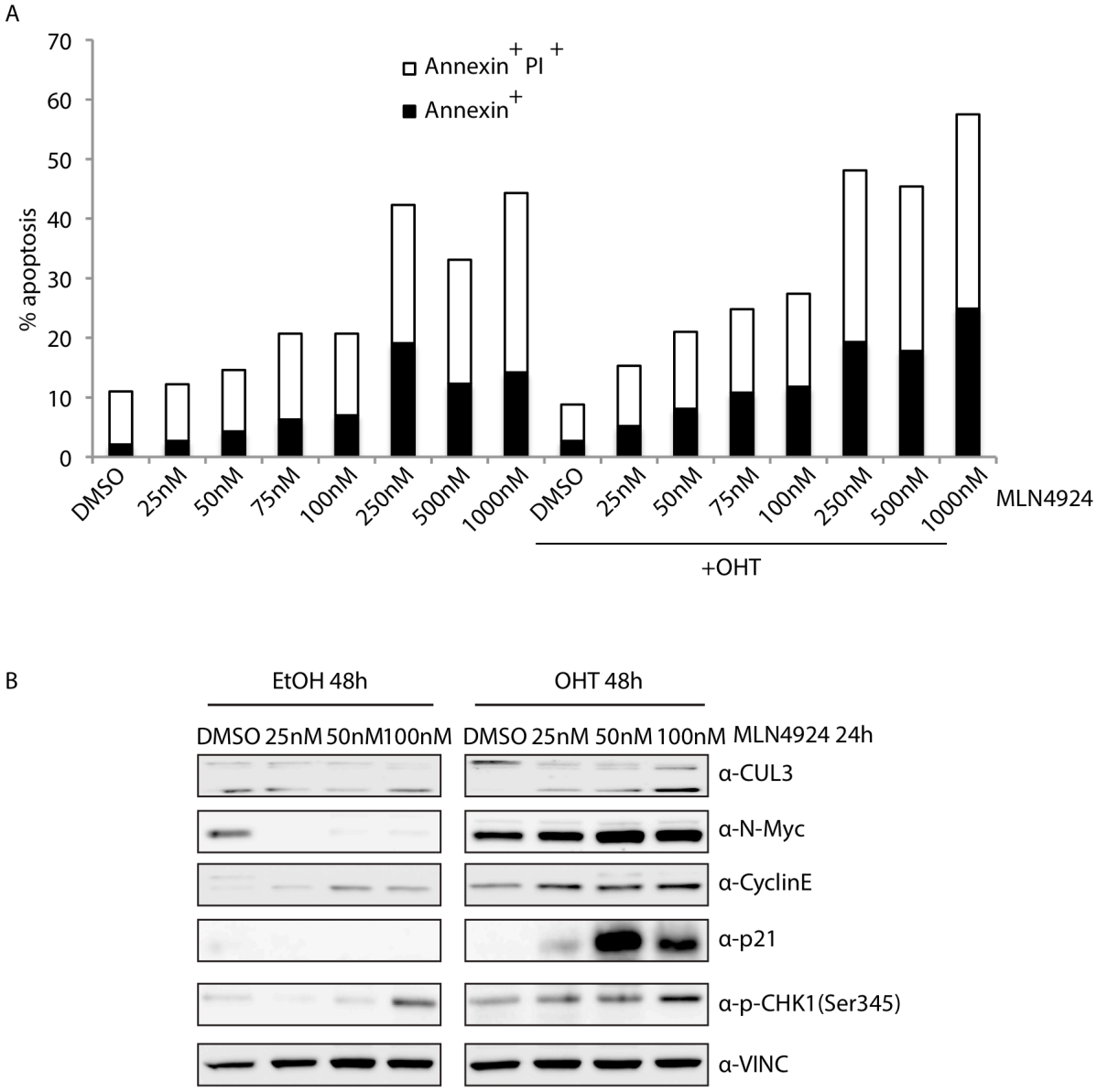

Figure 36 MLN4924-treatment induces apoptosis and DNA damage response in SHEP-N-MycER cells.

(A) MLN4924-treatment induces apoptosis of SHEP-N-MycER cells with or without 4-OHT-treatment. MLN4924 was added after 2 h OHT-treatment for 48 h. The AnnexinV/PI FACS was described in Figure 13.

(B) MLN4924-treatment leads to synergistically increase of Cyclin E and activation of CHK1 via phosphorylation at Serine 345. The increasing level correlates with compound concentration. The cells described in (A) were lysed with RIPA buffer. Protein extracts were analysed by western blot. Vinculin was used as a loading control.

4.7.3 MLN4924-treatment in *MYCN*-amplified neuroblastoma leads to cell growth arrest

To verify MLN4924 in *MYCN*-amplified neuroblastoma cells, the concentration of 75nM (median of 50nM and 100nM) MLN4924 was used for SHEP-N-MycER, SHEP, SHEP-N-Myc, IMR5 and Kelly cells. SHEP-N-Myc is a *MYCN*-nonamplified cell line stably expressing N-Myc. In SHEP-N-MycER cells, compound treatment leads to a cell growth arrest, but the effect is stronger upon N-Myc activation (Figure 37A). SHEP does not show pronounced lethal effect whereas SHEP-N-Myc presents a strong lethal effect. Both IMR5 and Kelly show a strong lethal effect. Western blot analysis shows that CUL3 is inactivated upon compound treatment and both p-CHK1 and p-p53 are activated after compound treatment and N-Myc activation (Figure 37B). We confirm that MLN4924-treatment in *MYCN*-amplified neuroblastoma leads to cell growth arrest.

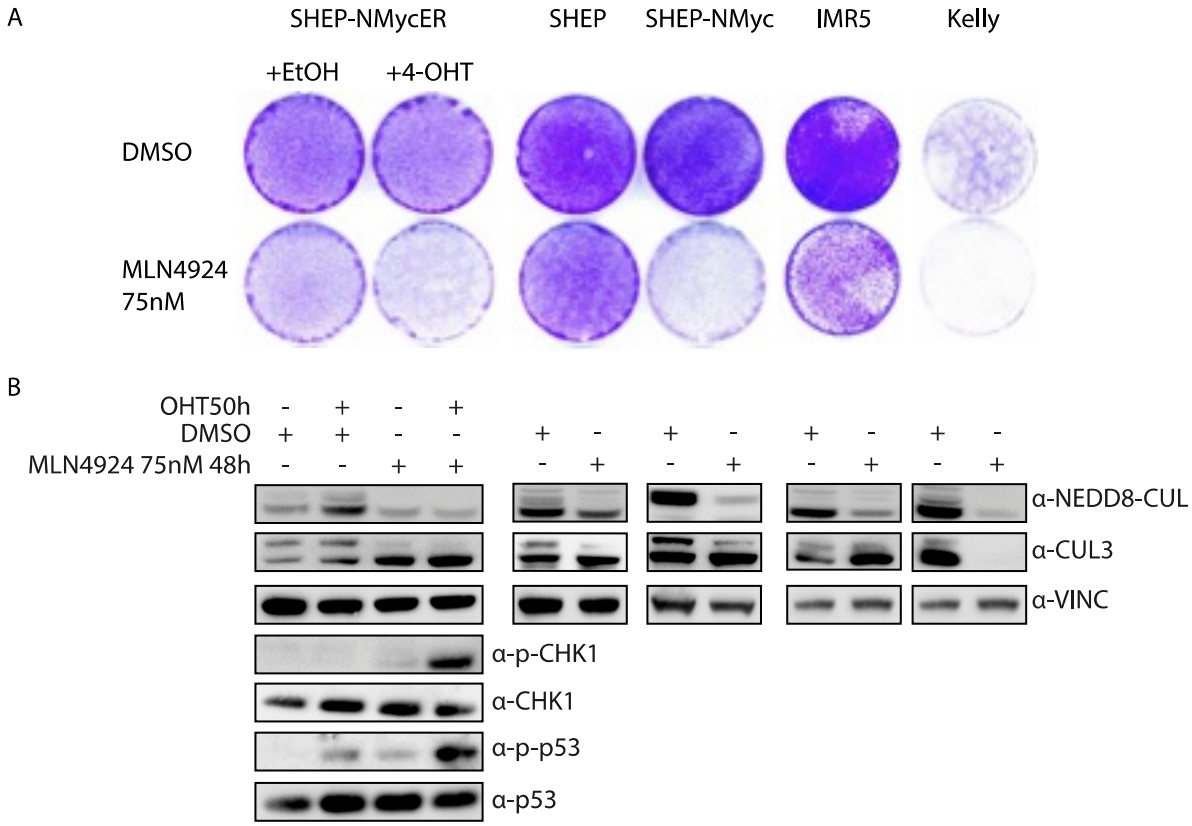

Figure 37: MLN4924-treatment in *MYCN*-amplified neuroblastoma cell lines leads to growth arrest.

(A) 75nM MLN4924 was used for SHEP-N-MycER, SHEP, SHEP-N-Myc, IMR5 and Kelly cells. All cell lines except SHEP (*MYCN*-nonamplifed) show a strong cell growth arrest. SHEP-N-MycER cells were treated with 75nM MLN4924 after 2 h OHT-treatment. The other cell lines were treated with 75nM. The colony assay was described in Figure 12.

(B) MLN4924-treatment with activated N-Myc synergistically activated phosphorylation of CHK1 and p53 (left panel). Neddylation was completely inhibited in all neuroblastoma cell lines (middle and right panels). The cells were treated with 75nM MLN-4925 after 2 h OHT-treatment for 48 h. The cells were lysed by RIPA buffer and the protein extracts were analysed by western blot.

5 Discussion

5.1 Conclusions for quality control and analysis of the high-throughput synthetic lethality screen

5.1.1 A complete representation of all shRNAs in the screened pools required a high redundancy of shRNAs in the infected cell population

A constant theoretical redundancy of each screened shRNA was predefined as one of the main screening parameters. On average, each shRNA was represented by at least 1000 cells in the overall population at the start of the screening process. A total of 100 million cells were infected with the approximately 9,000 individual lentiviral shRNAs contained in each pool. To avoid multiple infections, the multiplicity of infection (MOI) was kept as low as 0.1, resulting in approximately 10 million infected cells and therefore in an average representation of each shRNA in more than 1000 cells. To maintain this theoretical representation of all shRNAs throughout the screen, the total cell number was never allowed to drop below 10 million cells. Furthermore, shRNA sequences were recovered from at least 10 million cells for each condition and an equally high number of reads were generated by next-generation sequencing on the Illumina Genome Analyzer GAIIx.

The lack of knowledge regarding the distribution of shRNA constructs in the pooled libraries necessitated the maintenance of a high theoretical redundancy to avoid bottleneck effects for possibly underrepresented clones in the pool. Sub-populations of the commercially available genome-wide human pGIPZ shRNAmir library (Thermo Scientific / GE Healthcare) were used for the screens in the present study. Ideally, these sub-populations of pooled plasmids show an equal distribution of all individual plasmids. However, these plasmid pools had repeatedly been amplified in the past, resulting in undetermined distribution changes of individual shRNA constructs.

5.1.2 Knockdown of *PLK1* was used as a positive control to mimic a strong lethal effect

A shRNA targeting *PLK1* (sh plk1) was used as a positive control to mimic a strong lethal effect in order to answer two questions (see 4.1.2): First, how fast does a lethal shRNA disappear

completely from the cell population as a result of apoptosis induction? Second, how long after the start of the screen does a pGIPZ-based shRNA remain to be functional? PLK1 plays an important role in mitosis and throughout the cell cycle. It directly interacts with all core processes and is involved in 75% of all signal pathways. Depletion of PLK1 has a lethal effect on cells as shown in Figure 2. In the colour competition assay that was done with a shRNA targeting *PLK1* (sh #709), the ratio between green (control infected) and red (infected with sh plk1) cells on day 0 is about 1, whereas on day 9 the ratio is 10.78. This is a more than 10-fold depletion of cells infected with sh #709 during this assay (Figure 7). After 9 days the ratio between sh #709 infected and control cells did not change anymore, indicating that even lethal shRNAs may not be lost completely during a synthetic lethal screen. To determine how long the shRNA against *PLK1* is functional, *PLK1* mRNA levels were regularly determined for three weeks after infection. A prominent knockdown of plk1 was observed until approximately 18 days post infection. Based on these results for the positive control, we decided for the screening experiment to maintain pGIPZ infected and 4-OHT or ethanol treated cells in culture for 14 days. It can be expected that shRNAs are functional throughout this time and maximum depletion effects are established.

5.1.3 Limitations of the conducted large-scale shRNA screens

In the present study, a large-scale shRNA screen was performed to identify synthetic lethal interactions with deregulated N-Myc. We screened 18290 shRNAs targeting most genes in the human genome with different knockdown efficiencies in the inducible cell line SHEP-N-MycER (Figure 5B). Interestingly, genes whose knockdown was found to be synthetically lethal with an activation of N-Myc in the neuroblastoma cell line SHEP are involved in cellular processes including post-transcriptional modification and RNAPII-mediated transcriptional elongation, suggesting that N-Myc-induced transformation requires substantial buffering. Namely, some biological processes become more important to balance or compensate N-Myc-induced cell transformation.

Results from a large-scale shRNA screen need to be treated with caution due to a number of technical and biological limitations. Firstly, shRNAs that have not been functionally validated may have unpredictable target gene knockdown efficiencies. A low knockdown efficiency may not be sufficient to exert a detectable effect and thus produce false negative results. Furthermore, potential off-target effects of some shRNAs may produce false positive results. In general, RNAi results in 70-90% inhibition of the target gene expression, highlighting the possible weakness of

this tool (Unwalla and Rossi, 2008). Recently, a genome editing technology, published as CRISPR/CAS9, was developed (Marraffini and Sontheimer, 2010). This technology interferes with the target gene expression by introducing loss-of-function mutations into the genes coding sequence. This technology can be used to target many genes simultaneously in a pooled screening approach and therefore constitutes a powerful alternative to RNAi for synthetic lethal screens (Sander and Joung, 2014). Moreover, an important parameter for evaluating the relevance of an observed effect on cell viability in a screen is the percentage of individual shRNAs targeting the same gene and exerting the same effect. Unfortunately, in our synthetic lethal screen most genes were only targeted by a single shRNA, increasing the chances for false negative and false positive results.

Secondly, the SHEP-N-MycER cell line is an artificial representation of a N-Myc amplified neuroblastoma. The genetic background and cellular state of SHEP-N-MycER cells may not strictly reflect a real N-Myc addicted cancer cell. Therefore, the observed synthetic lethal interactions may not be the same as in cancer cells that naturally harbour the genetic defect.

Thirdly, hits derived from a shRNA screen become more reliable if they can be confirmed in a second related assay. Many effects observed in a large-scale screen do not strictly adhere to the definition of synthetic lethality. However, it is more convincing if a hit list generated from a shRNA screen largely overlaps with a hit list generated from another related analysis. In the present study, hit lists obtained from the synthetic lethal screen were matched with hit lists from a N-Myc proteomic analysis to identify overlapping hits. The N-Myc proteomics analysis was applied to identify N-Myc interacting proteins or differences in protein complexes between a N-Myc expressing cell line and a N-Myc non-expressing cell line. The combination of results from the two assays allow for a more reliable selection of candidates. As an example, CUL3 is one of the top candidates derived from our shRNA screen. CUL3 expression was also found to be essential in a genome-wide RAS synthetic lethal screen in a colorectal cancer cell line with RAS mutations (Luo et al., 2009). Since RAS is an upstream regulator of Myc, this is in supports with our finding that CUL3 depletion is synthetically lethal with activation of N-Myc.

Finally, a genome-wide RNAi screen might be too complex and not sufficiently specific to find each individual pathway or gene. A library which specifically targets the kinases or cancer related pathways is perhaps more suitable for a screen. We showed that most shRNAs in a genome-wide screen do not change in abundance. This is shown in the correlation dot-plot in Figure 10. Most shRNAs are plotted close to the diagonal line indicating that they behave similarly in the absence or presence of active N-Myc.

5.1.4 Final list of candidates was defined by a multi-step bioinformatics approach

Not all of the 18290 individual shRNAs that were used for the screening in a pooled format target an annotated gene in the human genome. All sequence reads generated during next generation sequencing for each screening condition were aligned with a reference dataset of 13406 unique combinations of shRNA sequences and annotated target genes. The frequency of alignments with each reference entry was counted, the count values normalized over all analysed samples and the changes in frequency of shRNAs between conditions calculated as fold change. Statistical inference, using the R implemented program edger (Mark D. Robinson, 2010), allowed us to determine the significance of the calculated fold changes.

Genes whose knockdown shows a synthetic lethal interaction with activated N-Myc in the SHEP-N-MycER cells were identified from this dataset applying the following series of criteria: 1) shRNAs significantly depleted (p-adjusted > 0.1) during the screening process independently of deregulated N-Myc were considered drop-outs and ignored in all further analyses. Target genes of these shRNAs can be expected to be involved in essential cellular processes in SHEP-N-MycER cells and their knockdown strongly effect the viability of the cells. 2) Conversely, shRNAs that were significantly depleted (p-adjusted < 0.1) only after activation of N-Myc and 3) showed a strong synthetic lethal net effect at the end of the screening procedure (at least 4-fold depletion after 14 days of 4-OHT treatment compared to ethanol treatment) were considered as targeting genes that are essential for SHEP-N-MycER cells after N-Myc activation.

Of the total of 13408 unique combinations of shRNAs and target genes screened in our approach, 148 were selected based on the above criteria. Knockdown of the target genes of these shRNAs show a strong and significant synthetic lethal interaction with active N-Myc in SHEP-N-MycER cells. This gene-set was found to be enriched for genes involved in a number of important biological processes including neddylation, RNAPII-mediated transcription elongation and mRNA export (Table 23).

5.2 Inhibition of neddylation is synthetic lethal in *MYCN*-amplified Neuroblastoma cells

5.2.1 Neddylation pathway

The neddylation pathway is a ubiquitination homologous pathway. The ubiquitination pathway is executed by a series of three distinct enzymatic steps. Ubiquitin is first 'activated' by ubiquitin-activating enzyme (E1) in an ATP-dependent reaction (Haas and Rose, 1982). In the second step, ubiquitin is transferred from E1 to a ubiquitin-conjugating enzyme (E2). The E2 then collaborates with a ubiquitin ligase enzyme (E3) to conjugate the ubiquitin to the substrate protein targeted for degradation. Neddylation pathway also involves ubiquitin ligases E1, E2, E3 and deneddylation enzymes (Hershko and Ciechanover, 1998). Nedd8 is first synthesized as a precursor that is processed at the conserved C-terminal Gly76 residue by the hydrolase activity of deneddylating enzymes exposing a glycine-glycine motif that serves as the attachment site for target substrates (Kamitani et al., 1997). Similar to ubiquitin, nedd8 is first activated by NAE (NEDD8 activating enzyme) in an ATP-dependent reaction. The activated NEDD8 is then transferred via a transthiolation reaction to the NEDD8-conjugating enzyme Ubc12 (or UBE2M). RING ubiquitin ligases are E3 ligases involved in neddylation pathway with the cullin-RING ligases (CRLs) representing the largest subfamily of RING-finger proteins. The cullin subunit is modified on a conserved lysine by NEDD8 to activate holoenzyme activity, which is passed by Ubc12. The cullin E3 ligase serves as a scaffold for the transfer of the ubiquitin molecule to the target substrate directly from ubiquitin-charged E2 (Soucy et al., 2009) (Figure 38).

Neddylation is a reversible process. The COP9 signalosome (CSN) is a zinc metalloprotease and the most studied member of the NEDD8 deconjugating enzymes. CSN is an eight subunit complex, with the CSN5 subunit possessing the catalytic activity (Lyapina et al., 2001; Schwechheimer et al., 2001). The COP9 signalosome (CSN) controls CRLs by specifically deconjugating NEDD8 (deneddylation) from cullins (Lyapina et al., 2001; Schwechheimer et al., 2001; Bondar et al., 2006; Deshaies and Joazeiro, 2009).

In addition to this catalytic mechanism, CSN can also inhibit CRL function in a noncatalytic fashion (Emberley et al., 2012; Enchev et al., 2012). The CSN-mediated inactivation of CRLs prevents the autocatalytic breakdown and enables the reassembly of the CRLs, maintaining their optimal activity (Schmidt et al., 2009). The complex stability depends further on the availability

of substrate. CAND1 is another important regulator of CRL activity maintenance in vivo. It binds to the deneddylated form of cullins and competes with substrates (Zheng et al., 2002).

Several subunits of CSN, including COPS5, COPS4 and COPS8 were found in the candidate list. Although not validated, they further imply that the neddylation pathway is synthetic lethal with active N-Myc.

CSN5 is implicated as a candidate oncogene in human breast cancer. CSN5 isopeptidase activity is essential for breast epithelial transformation and progression and amplification of CSN5 is required for transformation of primary human breast epithelial cells by defined oncogenes. The transforming effects of CSN5 require CSN subunits for assembly of the full COP9 signalosome and the isopeptidase activity of CSN5 to potentiate the transcriptional activity of Myc. Transgenic inhibition of CSN5 isopeptidase activity blocks breast cancer progression evoked by Myc and RAS *in vivo* (Adler et al., 2008), indicating the potential synthetic lethal interaction between CSN5 and high levels of N-Myc.

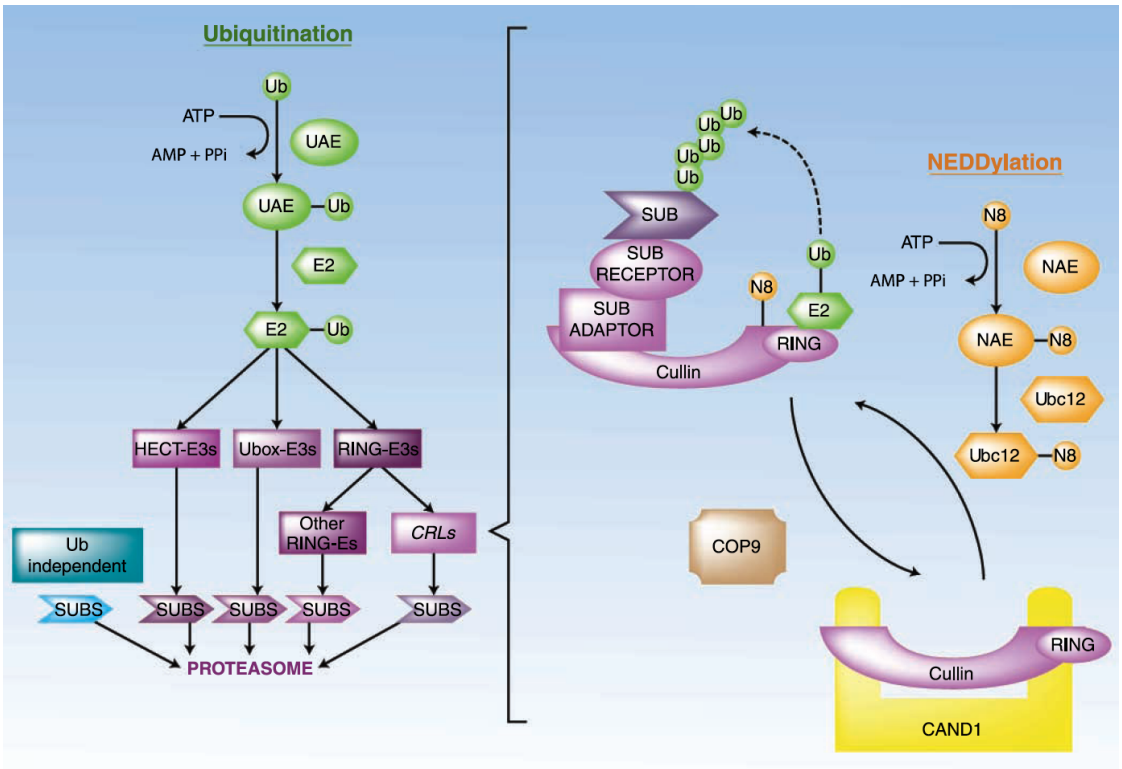

Figure 38: NEDD8 modification is required to activate the Cullin-Ring-Ligase (Soucy et al., 2009).

Proteasomes degrade proteins that are tagged with poly-ubiquitin chains. A pyramidal cascade of enzymes catalyze the formation of the polyubiquitin chain on a protein; a single E1-activating enzyme activates ubiquitin, transfers it via a transthiolation reaction to one of dozens of E2 enzymes that in turn collaborates with specific E3 ligases to catalyze the formation of a poly-ubiquitin chain on a substrate protein recruited by that E3. E3s with CRLs represent

the largest subfamily of RING-finger E3s. A key feature of CRLs is that the cullin subunit must be modified on a conserved lysine by the ubiquitin-like protein NEDD8 to activate holoenzyme activity. NEDD8 activation and conjugation to cullin proteins is catalyzed via an enzymatic cascade that is homologous to ubiquitination involving NEDD8's E1 (NAE) and E2 (Ubc12). Removal of NEDD8 from cullin is catalyzed by the COP9 signalosome. Deneddylation facilitates dissociation of CRL components. The cullin-RING core is sequestered in an inactive state by binding to CAND1 until it is recruited to form a new CRL.

5.2.2 NAE1, CUL5 and CUL3 are required for survival of *MYCN*-amplified neuroblastoma cells

NAE is an essential component of the neddylation pathway. The exposed C-terminal glycine of NEDD8 is adenylated by the NAE (E1), which is composed of NAE1 and Uba3 heterodimer, in an ATP-dependent reaction and transferred to E1 cysteine side chain via thiolester linkage (Pan et al., 2004). NAE controls the activity of the cullin-RING-ligase (CRL), thereby regulating the turnover of a subset of proteins upstream of the proteasome. Substrates of cullin-RING-ligase have important roles in cellular processes associated with cancer cell growth and survival pathways (Soucy et al., 2009).

Cullins are members of a family of scaffold proteins that assemble multisubunit ligase complexes to confer substrate specificity for the ubiquitination pathway. The substrate recognition component of CUL5 is the suppressor of cytokine signalling (SOCS) family of proteins. The C-terminal domain of SOCS has a BC box responsible for binding Elongin BC which is an adaptor between SOCS and CUL5 (Hilton, 1999). Harreman et al. reported that two distinct ubiquitin ligases, Rasp5 (human homolog of NEDD4) and Elongin C/CUL3 (human homologue of CUL5), are required for DNA damage induced polyubiquitination of RNAPII. In a first step, Rsp5 adds mono-ubiquitin or, less frequently, a ubiquitin chain linked via ubiquitin lysine 63 that does not trigger proteolysis and can be trimmed to mono-ubiquitination by a Rasp5-associated ubiquitin protease, Ubp2. Subsequently, an Elongin C/CUL3 complex produces a ubiquitin chain linked via lysine 48, which can trigger proteolysis (Harreman et al., 2009).

Another member of CRL, Cullin3, which forms a catalytically inactive BTB-CUL3-Rbx1 ubiquitin ligase sequestered by CAND1, becomes functional and is released from CAND1 upon covalent attachment of NEDD8 near the C-terminal of CUL3. CUL3-RING-ligase catalyzes the direct transfer of ubiquitin from E2 to the substrate. Alternatively, removal of NEDD8 from

cullin, catalyzed by COP9 signalosome, facilitates the dissociation of CUL3-Ring-ligase (CRL) components. The CUL3-RING core is sequestered in an inactive state by binding to CAND1 until it is recruited to form a new CRL (Furukawa et al., 2003).

In the screen, NAE1 shRNA frequency decreased only 1.2-fold in the absence of N-Myc whereas in the presence of N-Myc a remarkable 315-fold decrease was observed. Similarly, CUL5 shRNA showed a pronounced difference in abundance between the OHT-treated and the untreated culture condition. Its frequency decreased 1.6-fold in the absence of N-Myc but 18.5-fold in the presence of N-Myc (Table 23). The frequency of the higher ranked CUL3 shRNA showed a 1.2-fold decrease in the absence of N-Myc and a 8.8-fold decrease in the presence of N-Myc.

Colony assays were performed using SHEP-N-MycER cells to directly visualize the synthetic lethal effect of these shRNAs. As shown in results (Figure 12A), depletion of NAE1, CUL5 and CUL3 show a quite strong lethal effect in combination with N-Myc activation.

Both, the colony assay and the colour competition assay showed a substantially weaker lethal effect if compared to the screen. One reason could be the duration of the single experiment. The colony assay and competition assay was done for five and eight days whereas the screens took two weeks. The longer the experiment lasts, the more apparent differences between the two conditions become. Another point could be that a shRNA pool was used for screening but single shRNAs were used for the assays. Consequently, the intercellular interference caused by cells containing different shRNAs may also account for the observed effect. So far, the intercellular interference can be neither avoided during screening, nor excluded in post screen analyses. This is considered a disadvantage of large-scale screens.

The colony assay showed that depletion of NAE1, CUL3 and CUL5 had strong lethal effects on *MYCN*-amplified neuroblastoma cells, indicating these proteins to be required for survival of these cells (Figure 20). However, in *MYCN*-nonampilfied cells depletion of these proteins also showed a general effect. These neuroblastoma cell lines are very heterogeneous and harbour different mutations. In addition, they express different levels of c-Myc although they do not express N-Myc. Since c-Myc and N-Myc belong to the same protein family and share a number of targets, it is possible that depletion of these proteins in cells with high c-Myc levels also has a lethal effect (see 1.2.1). As we observed, the lethal effect in *MYCN*-amplified cells is much stronger than in *MYCN*-nonamplified cells, suggesting the lethal effect to be synthetic with active N-Myc.

Interestingly, depletion of NAE1, CUL5 and CUL3 lead to a transient accumulation of cells in the S-phase of cell cycle one hour after BrdU addition. This accumulation is stronger when N-Myc expression is switched on. The calculations from Figure 10, Figure 13 and Figure 19 showed an increase of cells in S-phase from 11.5% to 17.1% for a NAE1 knockdown, from 12.1% to 14.5% for a CUL5 knockdown and from 5% to 12% for a CUL3 knockdown.

To investigate these phenotypes in more detail, a BrdU pulse-chase experiment with a shRNA against *CUL3* was performed (Figure 24). After 6 hours the CUL3-depleted N-Myc-activated cells showed still a population within the S-phase of the cell cycle. This might be an indication that N-Myc-amplified cells need the neddylation pathway to complete the S-phase.

5.2.3 Substrate and adaptor proteins of CUL3 are implicated in different pathways

CUL3 but not other Cullins binds directly to multiple BTB domains through a conserved amino-terminal domain. The BTB domain, also known as POZ domain (poxvirus and zinc finger), is present near the N-terminus of a fraction of zinc finger proteins and in proteins that contain the Kelch motif and a family of poxvirus proteins. The core of BTB domain consists of a cluster of alpha-helix flanked by short beta-sheets at both the top and the bottom of the molecule (Pintard et al., 2003).

It has been known that the COP9 signalosome promotes deneddylation of CUL3. The signalosome is a macromolecular complex, containing eight subunits, that localizes in the nucleus and cytoplasm (5.2.1). Reducing COP9/signalosome function suppresses a partial defect in the neddylation pathway. This means deneddylation and neddylation antagonize each other. Both neddylation and deneddylation mediated by COP9 are function cycle of CUL3-RING-ligase (Pintard et al., 2003). The candidate list contains several subunits of the COP9 signalosome such as COPS4, COPS5 and COPS8, which may suggest that depleting COP9 results in a functional defect of CUL3 ligase. In the present study we could verify this by checking whether the targets of CUL3 accumulate or not. If they do, this may be a potential mechanism of synthetic lethal interaction between the neddylation pathway and N-Myc in a CUL3-dependent manner.

5.3 Cyclin E is the key player of the synthetic lethal interaction between CUL3 and N-Myc

Replication stress is defined as generation of aberrant DNA replication intermediates which lead to the accumulation of DNA damage markers at sites of active DNA replication (Felsher and Bishop, 1999). Problems in S phase are often induced by DNA replication stress. One reason for these stresses may be an overexpression of oncogenes such as CDK2 or Cyclin E. Oncogene-induced DNA replication stress activates the DNA damage response. Cyclin E is an oncogene that is frequently overexpressed in cancer tissue (Malumbres and Barbacid, 2001). It is able to induce DNA double-strand breaks, which may lead to genetic instability and aneuploid cells (Spruck et al., 1999). Consistent with the importance of Cyclin E in regulating cell proliferation and genetic stability, its expression levels are tightly controlled. In addition to transcriptional mechanisms, Cyclin E levels are also regulated by posttranslational modifications that trigger the proteolytic degradation of Cyclin E by CUL3-dependent ubiquitin ligase (Singer et al., 1999).

5.3.1 Cyclin E is a target of the CUL3-Ring-ligase

Cyclin E was identified as a target of CUL3-RING-ligase in 1999 (Singer et al., 1999). The main role of Cyclin E is promoting S-phase entry. Along with the Cyclin D complex, Cyclin E-CDK2 phosphorylates the retinoblastoma (Rb) protein to promote G1 progression (Hinds et al., 1992). Hyper-phosphorylated Rb releases the transcription factor E2F, which then promotes expression of genes that drive S-phase initiation and progression (Chellappan et al., 1991; DeGregori et al., 1995). Singer et al. found in 1999 that homozygous deletion of *CUL3* causes overexpression of the Cyclin E protein and disrupts normal cell cycle regulation *in vivo*. They performed a two-hybrid screen in which a Cyclin E mutant (R130A) was used as bait. Cyclin E (R130A) does not bind to and activate CDK2, thereby this mutant is free to be targeted for ubiquitination. They detected a single protein CUL3 that was able to bind mutant but not wild type cyclin E. The properties of this protein were shown to be consistent with its role in targeting cyclin E for ubiquitination (Singer et al., 1999).

To test whether CUL3 influences Cyclin E protein levels, SHEP-N-MycER cells were infected with a shRNA against CUL3 (Figure 26). Cyclin E levels increased 5-fold upon CUL3 depletion and the induction of N-Myc in these cells resulted in a 3-fold increase of Cyclin E. Surprisingly, the combination of CUL3 depletion and N-Myc activation increased Cyclin E levels further to 9-

fold (Figure 26). In neuroblastoma cells, Cyclin E protein runs between 40 and 55KDa instead of a regular size over 55KDa. This band (40-55kD) is increased upon N-Myc activation. This particular species of cyclin E, visible at 40-55KDa, is the active form which participates in the cell cycle regulation in breast cancer cells (Wingate et al., 2003). This isoform of cyclin E has been described as low molecular weight (LMW) Cyclin E.

LMW forms of Cyclin E are produced by proteolysis from full length Cyclin E. The protease elastase generates closely migrating doublets (Porter et al., 2001). They are specifically overexpressed in tumour tissue but not in normal tissue. The frequent appearance of the LMW form of Cyclin E and their correlation with poor prognosis in breast cancer patients suggests that they play specific roles in the development or progression of this malignancy (Wingate et al., 2003). LMW-Cyclin E clones were shown to acquire a growth advantage compared to full-length Cyclin E. LMW-Cyclin E prevents cells from cell cycle exit and entering quiescence upon growth factor deprivation. In addition, cells expressing the LMW-Cyclin E had significantly more genomic aberrations than those expressing full-length Cyclin E. Moreover, they showed that CDK2 binds 40% to 60% more of the LMW isoforms than the full-length Cyclin E, suggesting that LMW isoforms increase the kinase activity. Therefore, the overexpression of LMW-Cyclin E was claimed to result in distinct biochemical and biological characteristics, including genomic instability, in mammary epithelial cells (Wingate et al., 2009).

To date no publication reported LMW-Cyclin E in neuroblastoma cell lines. However, Cyclin E of a size of 40-55KDa is highly up-regulated either by N-Myc activation or CUL3 depletion in my study (Figure 26). Because this LMW-Cyclin E has been proposed to be an active form, we hypothesise that this observation correlates with the strong DNA damage response upon CUL3 depletion in combination with N-Myc activation.

5.3.2 Cyclin E overexpression induces replication stress

Cyclin E overexpression is associated with increased replication origin firing, impaired replication fork progression and DNA damage that activates RAD51-mediated recombination (Gorgoulis et al., 2005; Di Micco et al., 2006; Halazonetis et al., 2008). Jones et al. showed that Cyclin E-induced replication fork slowing and DNA damage are consequences of excessive origin firing via inhibiting replication initiation factors (Jones et al., 2013). Additionally, experimental overexpression of the oncogenes *Cyclin E*, *c-Myc* and *h-RAS* increases the level of replication initiation. Cyclin E directly activates CDK2. In addition, c-Myc directly interacts with replication origins and c-Myc and h-RAS promote expression of Cyclin E and other

proliferation factors. This suggests that high levels of replication initiation may contribute to oncogene-induced replication stress (Dominguez-Sola et al., 2007).

Based on this knowledge, I examined if a depletion of CUL3 induces DNA damage. For this purpose, pan-nuclear γ-H2A was analysed and shown to increase upon CUL3 depletion. Surprisingly, γ-H2Ax levels are significantly higher in cells with CUL3 depletion and N-Myc activation. This may well account for the observed synthetic lethality (Figure 27). Therefore, DNA damage response may be induced by accumulation of Cyclin E.

5.3.3 Synergistic accumulation of Cyclin E strongly induces both ATR-and ATM-dependent pathways resulting in a massive DNA damage response

ATR is activated in response to many different types of DNA damages, including double-strand breaks, base adducts, crosslinks and replication stress (Cimprich and Cortez, 2008). A single DNA structure might be responsible for ATR activation (Costanzo et al., 2003; Zou and Elledge, 2003). Replication Protein A (RPA) coats most forms of ssDNA in the cells, including the ssDNA that is formed during DNA replication and DNA repair (Fanning et al., 2006). The most common signal for ATR activation involves intrinsic replication stress in the S-phase. Cimprich et al. elucidated a model for ATR activation (Figure 39). Two complexes, RAD9-RAD1-HUS1 (9-1-1) and another one comprising ATR kinase and ATR-interacting protein (ATRIP), are independently recruited to the junction of the 5' primer with ssDNA. RPA binds ATRIP and directs the RAD17-replication factor C (RFC) clamp loader complex to load the 9-1-1-checkpoint clamp at the 5' primer junction. Loading of the 9-1-1-complex brings the ATR activator topoisomerase-binding protein-1 (TOPBP1) to the damaged site through an interaction that involves two breast cancer-1 C-terminal (BRCT) domains of TOPBP1 and the phosphorylated C-terminal tail of RAD9. TOPBP1 binds and activates ATR in an ATRIP-dependent manner, leading to phosphorylation of the downstream factor CHK1 and other ATR effectors.

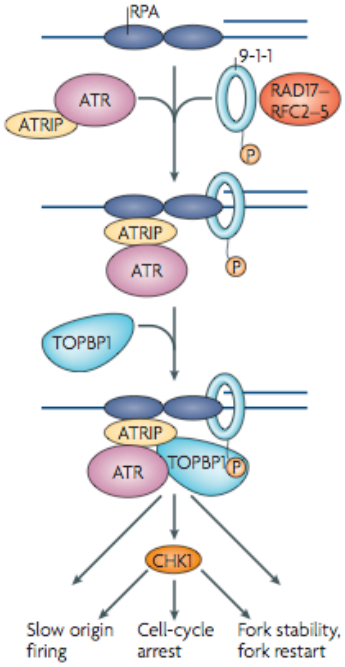

Figure 39: Simple model for ATR activation (Cimprich and Cortez, 2008)

RAD9–RAD1–HUS1 complex and one ATR kinase and ATR-interacting protein (ATRIP), are independently recruited to the junction of the 5′ primer with single-stranded DNA (ssDNA). RPA binds ATRIP and directs the RFC clamp loader complex to load the 9-1-1-checkpoint clamp at the 5′ primer junction. Loading of the RAD9–RAD1–HUS1 brings the ATR activator TOPBP1 to the damaged site through an interaction that involves two BRCT domains of TOPBP1 and the phosphorylated C-terminal tail of RAD9 (see main text). TOPBP1 binds and activates ATR in an ATRIP-dependent manner, leading to phosphorylation of the CHK1 and other ATR effectors.

CHK1 activation requires phosphorylation by ATR on Ser 317 and Ser 345, which is a reliable indicator of CHK1 activation (Walworth and Bernards, 1996). CHK1 transmits the DNA damage signal to the rest of the nucleus. CDC25 phosphatases are the key CHK1 targets for controlling cell cycle transitions. Human cells have three CDC25 proteins that regulate cell cycle transitions by removing the inhibitory phosphorylation of CDKs. CHK1 phosphorylation of CDC25A inhibits its activity and prevents CDK2 activation to avoid S to G2M transition. This promotes the replication fork stability. In response to DNA damage or replication stress, ATR and its effectors ultimately slow down the origin firing, induce cell cycle arrest and stabilize and restart stalled replication forks (Cimprich and Cortez, 2008).

As discussed above, Cyclin E overexpression induces replication stress and DNA damage. We showed that CUL3 depletion in combination with N-Myc activation leads to a 9-fold increase in Cyclin E protein levels (Figure 26). To demonstrate that this increase leads to an activation of the DNA damage response, the abundance of some targets of the ATR/ATM signalling pathway was analysed. γ-H2Ax, p-ATM, p-CHK1, p-CHK2 were induced slightly upon overexpression

of N-Myc, indicating that both ATM- and ATR- dependent DNA damage responses were activated to release the replication stress caused by N-Myc (Figure 27)(Figure 28).

It was observed that p-CHK1, p-CHK2 and γ-H2Ax are synergistically induced upon CUL3 depletion and N-Myc activation, suggesting that DNA damage response requires the induction of both ATM- and ATR- dependent pathways in these cells (Figure 28). p-RPA32 (Ser 33) which is the downstream factor of ATR is another marker for replication fork stalling besides p-CHK1. A synergistic activation of p-RPA (Ser 33) by CUL3 depletion and N-Myc overexpression suggests stalling of replication folks. This in turn may lead to collisions with many transcription complexes released by Myc (Rahl et al., 2010). We hypothesise that cells suffering from collisions of replication forks and transcriptional complexes will undergo apoptosis.

Additionally, roscovitine inhibited the activation of CHK1 upon CUL3 depletion and N-Myc activation, indicating that the DNA damage response is caused by accumulation of Cyclin E. A more specific CDK2 inhibitor, cvt-313, which prevents S-phase entry, rescues the lethal phenotype as well (Figure 31).

Moreover, Myc interacts with numerous chromatin and transcription regulation factors (Cheng et al., 1999; Cowling and Cole, 2006; Eilers and Eisenman, 2008; Rahl et al., 2010; Wasylishen and Penn, 2010). mRNA expression and DNA-binding studies have nominated an ever increasing number of genes as Myc targets including a core gene-set that constitutes a Myc signature (Shaffer et al., 2006; Margolin et al., 2009; Wasylishen and Penn, 2010; Ji et al., 2011). Myc binding is positively correlated with the expression levels of the vast majority of active genes and also with RNAPII binding in two primary cell types as well as mouse embryonic stem cells. In active B cells, Myc binding provokes a redistribution of RNAPII from promoters into gene bodies. Therefore, Myc is a universal amplifier of transcription that drives a large number of transcription complexes (Nie et al., 2012). Although this was only shown for c-Myc, both c-Myc and N-Myc are structurally highly homologous, suggesting very similar functions. They both heterodimerize with MAX, bind consensus E-box sequences (CACGTG) and have conserved regions for DNA-protein and protein-protein interactions (see 1.2.1).

In a cellular context, these findings propose the following model: N-Myc activation increases Cyclin E expression levels and drives numerous transcription units. The high level of Cyclin E increases replication origin firing. This replication stress could be normally resolved by DNA damage response. CUL3 depletion in *MYCN*-overexpressing cells leads to a further accumulation of Cyclin E. This results in a large number of replication origin firing and may conflict with the

transcription units. A strong DNA damage response resulting in a permanent replication fork stalling is induced (Figure 40).

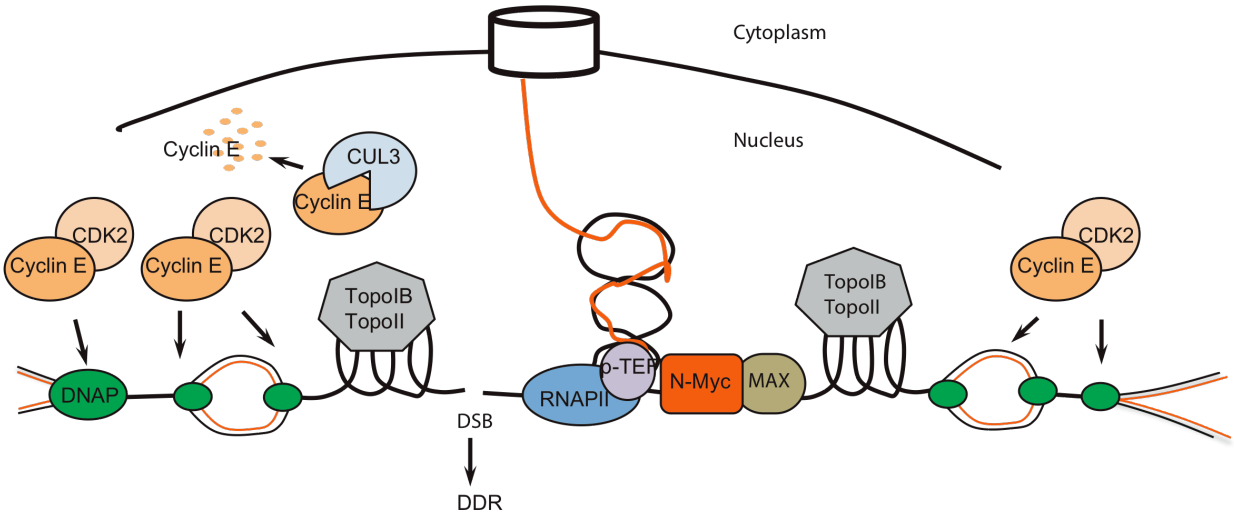

Figure 40: Model of synthetic lethal interaction between N-Myc and CUL3

Acute N-Myc activation increases Cyclin E expression, which leads to more replication origin firing. At the same time, N-Myc activation drives a large number of transcription units. CUL3 depletion in cells overexpressing N-Myc leads to accumulation of Cyclin E, which results in a collision between replication machineries and transcription units.

The fact that Myc overexpression induces DNA replication and replication stress is in support of this model. Myc promotes S-phase entry by transcriptionally regulating the cell cycle machinery. Myc is as a transcription factor that directly controls the expression of proteins of a large number of cellular pathways, which are implicated in S-phase progression. In addition, Myc promotes S-phase by directly affecting a number of active replication forks, as Myc itself can localize on active DNA replication sites. This suggests a more direct role for Myc in controlling S-phase progression by directly participating in licensing or assembly of pre-replicative complexes. Furthermore, Myc affects nucleotide biosynthetic pathways resulting in an increased nucleotide biosynthesis which also promotes the S-phase (Liu et al., 2008). Forced expression of Cyclin E in cells increases replication initiation and decreases the replication fork speed which are measured and visualised by DNA fiber experiments (Jones et al., 2013). Although Myc increases nucleotide biosynthesis, this may not completely explain the high demand of nucleotides needed during hyper-proliferative S-phase.

5.3.4 CUL3 depletion with N-Myc activation might lead to a checkpoint defect

Neelsen et al. published a study on oncogene-induced genotoxic stress by comparing Cyclin E overexpression with Cdc25A and Cyclin E overexpression. This results of this study indicated a checkpoint defect (Neelsen et al., 2013). Cdc25A is a phosphatase, a CDK activator and a key effector of the DNA damage response (Mailand et al., 2000). They proposed that nucleolytic processing of unusual replication intermediates mediates oncogene-induced genotoxicity and that limiting this processing to the mitosis is a central anti-tumourigenic function of the DNA damage checkpoints. In Cdc25A- and Cyclin E-overexpressing cells they observed that the intermediate DNA content compromised EdU incorporation and was consistently associated with pan-nuclear γ-H2Ax. In contrast, in cells overexpressing only Cyclin E, EdU was incorporated into the intermediate DNA content and an increased number of γ-H2Ax foci but no pan-nuclear γ-H2Ax was observed. RO-3306, a selective inhibitor of CDK1, can rescue the phenotype caused by Cdc25A and Cyclin E overexpression (Neelsen et al., 2013). RO-3306 inhibits CDK1/Cyclin B activity with a Ki value of 35nM. It is almost 10-fold more selective for CDK1/Cyclin B relative to CDK2/Cyclin E and >50-fold relative to CDK4/Cyclin D (Vassilev et al., 2006). Therefore, its function is highly specific for CDK1.

In the present study, a BrdU/PI FACS of cells with CUL3 depletion and N-Myc activation showed 12% BrdU negative cells with intermediate DNA content (Figure 23). This finding correlates more with the phenotypes of cells with Cdc25A and Cyclin E overexpression than with the phenotypes of cells that overexpress only Cyclin E in Neelsen's study. In order to check whether the CUL3-depleted N-Myc activated cells have a checkpoint defect, we treated the cells with RO-3306. Cells will overcome the G2M checkpoint if they have a checkpoint defect and RO-3306 is able to rescue it because it blocks the mitosis entry. As shown in Figure 30, after 5 h of RO-3306 treatment the morphology of CUL3-depleted and N-Myc activated cells became similar to the control cells. These findings suggest that CUL3 depleted and N-Myc activated cells may have also obtained a checkpoint defect to promote genome instability.

5.4 Several biological processes identified from the screen are synthetic lethal with deregulated N-Myc

5.4.1 Candidates involved in RNAPII mediated transcription elongation

Several biological processes were found to be enriched in the list of candidates: transcription elongation by RNAPII, mRNA export involving THOC1, NUP153 and ELL, DNA replication and replication checkpoints involving MCM4 and MCM6 and maintenance of chromosome integrity involving the condesin complex II subunit G2 (NCAPG2) (Figure 41). In an independent N-Myc proteomics analysis that was done by Anne Carstensen (data not shown), the proteins NUP153, NCAPG2 and THOC1 were found as new interaction partners of N-Myc. These results led us to hypothesize that knockdown of genes involved in these biological processes combined with *MYCN* overexpression result in conflicts between RNA polymerase II and the DNA replication machinery. As a result, the replication fork collapses and DNA damage responses are activated.

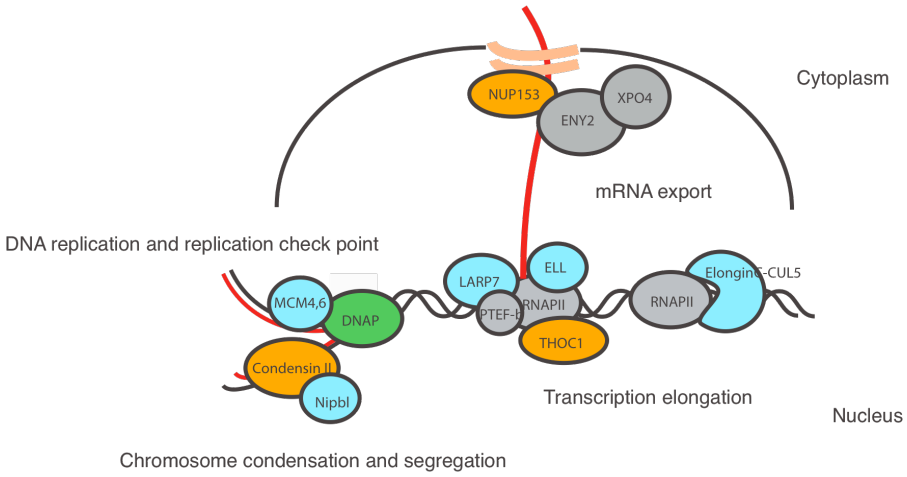

Figure 41: Schematic of candidates involved in several biological processes

The candidate genes from the screen are involved in elongation by RNA polymerase II, DNA replication and replication checkpoints, as well as maintenance of chromosome integrity. Proteins shown in blue indicate candidates from the screen. Proteins shown in orange indicate overlaps from the screen and a proteomics analysis of N-Myc associated proteins performed by A. Carstensen.

THOC1 plays an important role in coupling transcription elongation and mRNA export. As the nascent pre-mRNA emerges from the RNAPII, it is packed in a messenger ribonucleoparticle (mRNP) whose optimal configuration is critical for the normal pre-mRNA processing and

mRNA export, mRNA integrity as well as for transcription elongation efficiency. The interplay between transcription and mRNP formation feeds forward and backward and involves a number of conserved factors, ranging from THOC1 to NUP153, which additionally have a unique impact on transcription dependent genome instability. The function of THOC1 has been studied in more depth in yeast. THOC1 is a multimeric complex conserved in higher eukaryotes required for mRNP biogenesis. THOC1 is recruited to chromatin during transcription, needed for transcription elongation, mRNA export and genome integrity (Chavez et al., 2000; Strasser et al., 2002). One important feature of cells lacking the THO complex is a suboptimal mRNPs production that hinders transcription elongation and generates genome instability measured as an increase in recombination (Strasser et al., 1990). This is to some extent explained by DNA:RNA hybrid formation. In cells deprived of THOC1, the nascent RNA tends to hybridize more often or more strongly with the template DNA strand, leaving the nontranscribed strand unpaired. As a consequence, DNA:RNA hybrids (R-loops) accumulate in THOC1 mutants (Huertas and Aguilera, 2003). The displaced DNA strand is more susceptible to DNA damage and breakage, which are potential sources of genome instability. Furthermore, R-loops slow down or even completely block replication-fork progression inducing recombination (Rondon et al., 2010).

In the BrdU/PI assay of THOC1 depletion, the number of BrdU negative cells with intermediate DNA content increases 2-fold and the percentage of apoptotic cells increases from 24.5% to 56.9% in the presence of N-Myc, suggesting that synthetic lethality between THOC1 knockdown and N-Myc activation may be the result of a S-phase arrest and induction of apoptosis (Figure 33).

Colony assays show a clear lethal effect upon NUP153 depletion and N-Myc activation. The corresponding BrdU/PI assay shows that NUP153 depleted N-Myc activated cells have a lower FITC signal, which means BrdU incorporation is less and slower. NUP153 is involved in mediating the nascent mRNA transport from nucleus to cytoplasm. It interacts with the ENY2/TREX complex that couples transcription and mRNA processing with nuclear mRNA export. The successful validation of NUP153 also indicates that the defect in coupling elongation and mRNA export might be synthetic lethal with high levels of N-Myc (Figure 32).

Based on the successful functional validation, we hypothesize that defects in RNAPII-mediated transcription elongation is synthetic lethal with high levels of N-Myc (Figure 32) For this situation we suggest the following preliminary model: Normally, there are ongoing replication forks and progressing transcription bubbles. Topoisomerase can resolve the topological structure that appears between replication fork and transcription bubble. Activation of N-Myc increases

the number of ongoing replication forks and the number of RNAPII complexes since Myc binds to a number of core promoters (Rahl et al., 2010). Therefore, torsional stress largely accumulates between the replication forks and transcription bubbles. As discussed in 5.3.3, Myc promotes ongoing replication, which causes replication stress, but at the same time it decreases the replication stress via DNA damage response. Balancing the replication stress is partially achieved by topoisomerase II. On one hand, this enzyme introduces the double strand breaks in order to resolve the topological structures, on the other hand, the DNA damage response diffuses a wave of phosphorylation to the nuclear porin complex and dissembles the complex structure with gated nascent genes which bears large torsional stress potentially serving as an obstacle for approaching replication fork. If the topoisomerase adheres to its duty together with a well-coupled transcription and subsequent mRNA export, the Myc overexpressing cells should still be viability. However, if any of these important components involved in this process is missing or not functional, two consequences might occur: Firstly, if the nascent mRNA is not able to be properly gated, one end of it fixed at nuclear pore while the rest twist with the template which totally hinders the coming replications fork resulting the fork reversal. Fork reversal is lethal to the cells. Secondly, if the nascent mRNA is not gated due to a lack of components like THOC1, it may anneal with the template DNA to form a R-loop resulting in a lethal effect as well.

The underlying mechanism of the proposed model is described above and the flowchart summarizes the hypothesis (Figure 42). N-Myc activation induces S-phase progression. S-phase progression leads to replication stress. This stress can usually be decreased by DNA damage responses. In the case where all these processes are functional, including the degradation of stalled and fallen RNAPII, transcription elongation, mRNA processing and mRNA export, the cell is still viable. However, if any of these processes is not functional due to the depletion of essential proteins, the replication fork stalls and global RNA synthesis drops which leads to cell death.

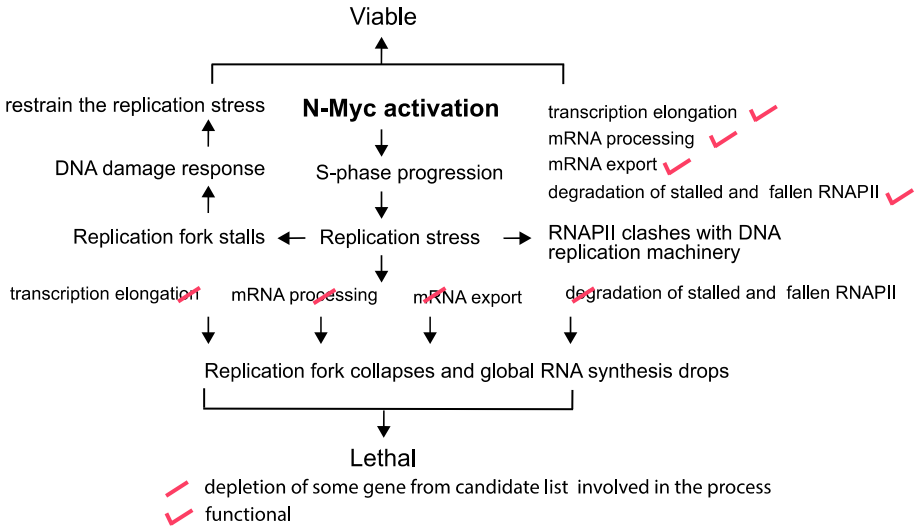

Figure 42: Summary of the synthetic lethal interaction with N-Myc in a manner of defect RNAPII mediated transcription elongation

The description of flow chart is seen in the main text.

5.4.2 Study of Condensin II complex is a new perspective of N-Myc´s role in neuroblastoma

NCAPG2, the subunit of condensin II, is a candidate from the screen that was validated (Figure 32). Although the colony formation assay of cells with a depletion of NCAPG2 did not show a pronounced synthetic lethal effect with high levels of N-Myc (Figure 32), the BrdU/PI assay showed an increase of BrdU negative cells from 10.6% to 15.1% after activation of N-Myc. Additionally, apoptotic cells are increased from 34.9% to 53.6% following N-Myc activation, suggesting a synthetic induction of apoptosis (Figure 33). Another subunit, NCAPH, is also on the list of candidates but has not yet been validated (Table 23). Additionally, NCAPG2 was also detected in two proteomic analyses of N-Myc interaction proteins, performed in Eilers' and Chesler's laboratories. However, so far almost all studies were conducted in Xenopus eggs or in the yeast system. These results draw our attention to studying function and research progress of NCAPG2 in human neuroblastoma.

During mitosis the most striking transformation of chromatin structure is observed when the cell separates its duplicated genome into daughter cells. Upon disassembly of the cell nucleus at the onset of mitosis, an amorphous mass of chromatin is converted into a discrete set of rod-shaped chromosomes in which the two sister chromatids are juxtaposed along their length. This process,

referred to as chromosome assembly or condensation, is an essential prerequisite of the faithful segregation of sister chromatids during the subsequent stages of mitosis (Hirano, 2005).

There are two kinds of condensin complexes, condensin I and condensin II. Condensin I and II have the same pair of core subunits but distinct sets of regulatory subunits. The two core subunits, SMC2 and SMC4, belong to a large family of chromosomal ATPases known as the structural maintenance of chromosomes (SMC) family. The SMC2-SMC4 heterodimer adopts a V-shaped structure, characteristic for all SMC proteins, with an ATP-binding cassette ATPase domain at the distal end of each arm, which modulates engagement and disengagement of the head domains (Melby et al., 1998; Anderson et al., 2002). The two condensin complexes are distinguished by their unique sets of non-SMC subunits. Among the three regulatory subunits of each complex, CAP-D2 and CAP-G in condensin I and CAP-D3 and CAP-G2 in condensin II contain HEAT repeats, a highly degenerate repeat motif implicated in protein-protein interactions (Neuwald and Hirano, 2000). The fifth subunits CAP-H in condensin I and CAP-H2 in condensin II belong to the kelsin family of proteins (Yoshimura et al., 2002).

In mammalian cells, condensin II is predominantly nuclear whereas condensin I is sequestered in the cytoplasm during inter-phase (Ono et al., 2004). Condensin I gains access to the chromosomes only after the nuclear envelope breaks down in the pro-metaphase, and the two complexes alternate along the chromatid axis by metaphase (Hirota et al., 2004; Ono et al., 2004). Depletion of condensin II delays prophase condensation whereas depletion of condensin I does not (Hirano, 2005).

In 2003, Maeshima et al proposed a model in which an early stage of condensation is driven by topoisomerase II-mediated axis formation and is followed by the action of condensin subunits. In this paper, topoismerase II and 13S condensin (here might indicate condensin I) were both reported to be required for mitotic chromosome assembly (Maeshima and Laemmli, 2003). This mechanism may be of major relevance for our study because topoisomerase IIA and topoisomerase IIB were found to interact with N-Myc in two independent proteomic analyses, one of which was done by Anne Carstensen (data not shown). This draws our attention to a possible cooperation between N-Myc, condensin and topoisomerase II during early mitosis and mitosis.

Very recently, Tonami et al reported that inactivation of SMC2 shows a synergistic lethal response in *MYCN*-amplified neuroblastoma cells. All the experiments in this paper were conducted in SHEP, SKN-AS and IMR32 cells. It was demonstrated that N-Myc transcriptionally up-regulates *SMC2* and interacts with SMC2 and SMC4. SMC2 was shown to

transcriptionally regulate DNA damage response genes in cooperation with N-Myc. They also found that in patients with *MYCN*-amplified tumours improved survival correlates with low SMC2 expression (Murakami-Tonami et al., 2014).

As shown in Figure 33, NCAPG2 depletion leads to a serious S-phase problem. In cells with a NCAPG2 depletion, a large population of BrdU negative S-phase cells was found. This indicates an important role of condensin II in the S-phase. This S-phase problem gets worse after activation of N-Myc, potentially due to an increased replication stress (Figure 33). Although depletion of NCAPG2 does not show a pronounced synthetic lethal effect with high levels of N-Myc in the colony assay, FACS analysis for BrdU incorporation and Annexin V staining clearly showed serious problems in the cells. All these observations led us to conclude that there may be a novel cooperation between these proteins. This cooperation may well effect late S-phase regulation, chromosome condensation and segregation.

5.5 MLN4924 is a therapeutic option in N-Myc-driven neuroblastoma

The development of inhibitors targeting Myc/N-Myc proteins is very complicated because they are basic helix-loop-helix zipper proteins with no obvious surfaces for small molecule binding (see 1.2.3). Therefore, the observation that a depletion of members of the neddylation pathway can be synthetic lethal in N-Myc amplified neuroblastoma cells may present an opportunity to target these pathways with inhibitors for therapy.

Inhibition of protein neddylation, particularly cullin neddylation, has emerged as a promising anticancer strategy, as evidenced by the anti-tumour activity of the NEDD8-activating enzyme (NAE) inhibitor MLN4924 in preclinical studies. This small molecule can block the protein neddylation pathway and is now in clinical trials.

MLN4924 was identified as an inhibitor of NAE via high throughput screens performed by Millennium Company. MLN4924 is structurally related to adenosine 5'-monophosphate (AMP) – a tight binding product of the NAE reaction. X-ray crystallography confirmed that MLN4924 bound in the nucleotide-binding site of NAE (Walden et al., 2003; Walden et al., 2003). It is already in phase III clinical trial. Treatment of tumour cells with MLN4924 increases the abundance of known CRL substrates. In the human cell lines studied, the mechanism of cell death appeared to be a consequence of uncontrolled DNA synthesis in the S-phase of the cell cycle. This results in DNA damage and the induction of apoptosis. Inhibition of neddylation via

MLN4924 accumulates CDT1, a DNA replication licensing factor, and induces DNA re-replication. *In vivo*, MLN4924 shows potent anti-tumour activity in mice with human tumour xenografts, such as large B-cell lymphoma, lung, colon and breast cancer, at drug concentrations that are well tolerated (Soucy et al., 2009).

There is no report about the application of MLN4924 in neuroblastoma. Consequently, we decided to investigate its function in neuroblastoma. First, we titrated the compound in SHEP-N-MycER cells in a range from 1.5nM to 1000nM. CUL3 was partially inhibited at a concentration of 15nM and completely inactivated at a concentration of 100nM. Cleaved PARP was significantly increased at an inhibitor concentration of 100nM. Therefore, we decided to use a range from 15nM to 100nM for all following experiments in SHEP-N-MycER cells.

A western blot analysis was performed to check DNA damage response using an inhibitor concentration range from 25nM to 100nM (Figure 36B). Generally, p-CHK1, p21 and Cyclin E are induced more in OHT-treated cells than in untreated cells within this range. The DNA damage effect, represented by signals for p-CHK1 and p21, is more pronounced at 50nM and 100nM compared to 25nM. Therefore, we concluded that a higher concentration has to be used to induce DNA damage effects and a concentration of 75nM was used for further experiments.

Treatment of the SHEP-N-MycER cells with a compound concentration of 75nM showed a stronger accumulation of DNA damage markers (Figure 37). Additionally, p21 and p-p53 are involved in p53-dependent DNA damage response and are found to be synergistically induced after MLN4924- and 4-OHT-treatment. Oncogene-induced replication appears to play a central role in tumour progression (Halazonetis et al., 2008; Evertts and Coller, 2012), suggesting that re-replication may directly challenge tumour vulnerabilities. In this study, treatment with the compound did not mitigate N-Myc-induced replication stress but further aggravated it.

However, it is not clear whether re-replication is the dominant mechanism of DNA damage in combination with other DNA damaging agents. Therefore, it is difficult to predict the best combination partner.

Recently, Garcia et al published that MLN4924 showed synergy with mitomycin C through interactions with the ATR signalling pathway. Mitomycin C is an antibiotic which alkylates DNA. About 10% of the DNA modifications result in interstrand crosslinks and the remainder being monoadduct and intrastrand crosslinks (Muniandy et al., 2010). The induction of DNA damage results in inhibition of DNA replication. The DNA damage repair is determined by the kind of detection, which is significantly influenced by the stage of the cell cycle in which the damage occurs. The combination of mitomycin C and MLN4924 was shown to be synergistic in

a melanoma mouse xenograft model. While treatment with either single agent alone results in only moderate growth inhibition, the combination keeps the tumour from growing for the entire time of treatment. Comparison of treated vs control animals at day 21 resulted in tumour volume ratios of 0.7, 0.5, and 0.17 for animals treated only with mitomycin C, only with MLN4924, and with the combination of both, respectively. They performed a screen with a siRNA pool targeting DNA damage response genes in the melanoma cell line A375 and treated the cells with MLN4924 and mitomycin C. They found that depletion of genes involved in the ATR signalling pathway, chromatin modification and transcription-coupled repair reduced the synergy between mitomycin C and MLN4924. These data suggest that mitomycin C causes stalling of the replication forks and, if combined with re-replication induced by MLN4924 results in frequent replication fork collisions followed by cell death (Garcia et al., 2014).

N-Myc acute activation largely increases the replication stress induced by MLN4924. Together with this stress leads not only to single-strand breaks but also to large amounts of double-strand breaks which further induce a strong DNA damage response. These strong DNA damage responses drive cells into apoptosis rather than inducing cell cycle arrest. The colony assays performed in other neuroblastoma cell lines showed a very convincing effect (Figure 15). Our finding that a synergistic activation of DNA damage responses by combining N-Myc activation and MLN4924-treatment results in cell death is consistent with Garcia's conclusion.

MLN8237, an Aurora A inhibitor, is currently in phase 2 clinical evaluations for childhood neuroblastoma. It is sufficient to disrupt the N-Myc/Aurora A complex without inhibiting catalytic activity of Aurora A (Matulonis et al., 2012). The evaluation of therapy efficiency in TH-*MYCN* mouse models of aggressive neuroblastoma reveals a large decrease of N-Myc protein levels and a rapid decrease in tumour volume (Brockmann et al., 2013). Topoisomerase IIA and IIB were found to interact with N-Myc in a N-Myc proteomic analysis (data not shown). Because treatment with MLN8237 in a mono-therapy has only marginal effects on neuroblastoma, a combined therapy with an inhibitor of topoisomerases may be beneficial to treating neuroblastoma patients. In fact, combining MLN8237 with a topoisomerase inhibitor is a new approach to treat neuroblastoma and is currently in a clinical trial (John Maris and Yael Mosse, personal communication, 2014).

6 Summary in English and German

6.1 Summary

In contrast to c-Myc, a deregulated expression of the *MYCN* gene is restricted to human neuroendocrine tumours. In most cases, the excessive activity of N-Myc results from a *MYCN* amplification. In neuroblastoma, amplification of *MYCN* is a predictor of poor prognosis and resistance to therapy. The inability to target the N-Myc protein directly necessitates the search for alternative targets. This project aimed at identifying genes specifically required for growth and survival of cells that express high levels of N-Myc using high-throughput shRNA screening combined with next generation sequencing. The identification and analysis of these genes will shed light on functional interaction partners of N-Myc.

We screened a shRNA library containing 18,327 shRNAs and identified 148 shRNAs, which were selectively depleted in the presence of active N-Myc. In addition, shRNAs targeting genes that are involved in p53 and ARF turnover and apoptosis were depleted in the cell population during the screen. These processes are known to affect N-Myc-mediated apoptosis. Consequently, these results biologically validated the screen. The 148 shRNAs that showed a significant synthetic lethal interaction with high levels of N-Myc expression were further analysed using the bioinformatics program DAVID. We found an enrichment of shRNAs that target genes involved in specific biological processes. For example, we validated synthetic lethal interactions for genes such as, *THOC1*, *NUP153* and *LARP7,* which play an important role in the process of RNA polymerase II-mediated transcription elongation. We also validated genes that are involved in the neddylation pathway.

In the screen we identified Cullin 3, which is a component of the BTB-CUL3-Rbx1 ubiquitin ligase that is involved in the turnover of Cyclin E. Depletion of cullin 3 and activation of N-Myc was found to synergistically increase Cyclin E expression to supraphysiological levels, inducing S-phase arrest and a strong DNA damage response.

Together with results from a proteomics analysis of N-Myc associated proteins, our results lead us to the following hypothesis:

In a neuroblastoma cell, the high levels of N-Myc result in a conflict between RNA polymerase II and the replication machinery during S-phase. The newly identified interaction partners of N-Myc are required to solve this conflict. Consequently, loss of the interaction leads to a massive

DNA damage and the induction of apoptosis. In addition, inhibition or depletion of the essential components of the neddylation pathway also results in an unresolvable problem during S-phase.

6.2 Zusammenfassung

Im Gegensatz zu c-Myc findet man eine Deregulation von N-Myc nur in einer begrenzten Anzahl maligner Tumore die neuroektodermalen Ursprungs sind. Die übermäßige Aktivität ist dabei fast immer durch eine genomische Amplifikation von N-Myc begründet. Im Neuroblastom korreliert eine *MYCN*-Amplifikation mit einer schlechten Prognose. Da es auf Grund einer fehlenden katalytischen Domäne nicht möglich ist N-Myc direkt zu inhibieren, ist die Suche nach alternativen Targets notwendig. Das Ziel dieser Arbeit war es neue Gene zu identifizieren, die notwendig für das Wachstum und Überleben von *MYCN* amplifizierten Zellen sind. Dies wurde durch eine Kombination von Hochdurchsatz-RNAi-Screens und Next-Generation-Sequenzierung erreicht.

Durch das Screenen einer shRNA-Bibliothek, die insgesamt 18327 shRNAs beinhaltet, konnten 148 shRNAs identifiziert werden, die selektiv nachteilig für das Überleben N-Myc überexpremierender Zellen sind. Die statistische Auswertung der Ergebnisse des Screens zeigte zusätzlich eine Anreichung von shRNAs gegen Gene, die p53-und ARF-abhängig Apoptose vermitteln. Da es bekannt ist, dass diese Gene in der N-Myc-vermittelten Apoptose involviert sind, konnte dadurch der Screen validiert werden. Die weitere Auswertung mit dem bioinformatischen Programm DAVID ergab, dass unter den 148 als synthetisch letal identifizierten shRNAs solche angereichert waren, die gegen Gene spezifischer biologischer Prozesse gerichtet sind. Zum einen wurden Gene wie *THOC1*, *NUP153 und LARP7* validiert, die eine Rolle im Prozeß der Elongation der RNA Polymerase II spielen. Zum anderen konnten Gene validiert werden die einen Beitrag bei der Neddylierung von Proteinen leisten.

Durch die Depletion von Cullin 3, ein Bestandteil des BTB-CUL3-Rbx1 Ubiquitin-Ligase-Komplexes, der am Abbau von Cyclin E beteiligt ist, konnte gezeigt werden, dass zusammen mit der Aktivierung von N-Myc eine supraphysiologische Erhöhung von Cyclin E induziert wird. Dies führt zu einem S-Phase Arrest in der Zelle, der die DNA-Schadens-Signalkaskade auslöst.

Zusammen mit den Ergebnissen einer Proteomanalyse, bei der neue N-Myc-assoziierte Proteine identifiziert wurden, konnte folgende Hypothese aufgestellt werden:

In einer Neuroblastomzelle helfen diese neuen Interaktionspartner den durch die N-Myc Überexpression in der S-phase entstehenden Konflikt zwischen RNA-Polymerase II und Replikationsmaschinerie zu lösen. Der Verlust dieser Interaktion führt zu einer massiven Schädigung der DNA, worauf in der Zelle Apoptose ausgelöst wird. Des Weiteren führen auch die Inhibition oder Ausschaltung wesentlicher Komponenten des Neddylierungs-Signalwegs zu unlösbaren Problemen in der S-Phase des Zellzyklus.

Bibliography

Adler, A. S., L. E. Littlepage, M. Lin, T. L. Kawahara, D. J. Wong, Z. Werb and H. Y. Chang (2008). "CSN5 isopeptidase activity links COP9 signalosome activation to breast cancer progression." Cancer Res **68**(2): 506-515.

Anderson, D. E., A. Losada, H. P. Erickson and T. Hirano (2002). "Condensin and cohesin display different arm conformations with characteristic hinge angles." J Cell Biol **156**(3): 419-424.

Bakkenist, C. J. and M. B. Kastan (2003). "DNA damage activates ATM through intermolecular autophosphorylation and dimer dissociation." Nature **421**(6922): 499-506.

Banelli, B., I. Gelvi, A. Di Vinci, P. Scaruffi, I. Casciano, G. Allemanni, S. Bonassi, G. P. Tonini and M. Romani (2005). "Distinct CpG methylation profiles characterize different clinical groups of neuroblastic tumors." Oncogene **24**(36): 5619-5628.

Barboric, M., T. Lenasi, H. Chen, E. B. Johansen, S. Guo and B. M. Peterlin (2009). "7SK snRNP/P-TEFb couples transcription elongation with alternative splicing and is essential for vertebrate development." Proc Natl Acad Sci U S A **106**(19): 7798-7803.

Bartkova, J., N. Rezaei, M. Liontos, P. Karakaidos, D. Kletsas, N. Issaeva, L. V. Vassiliou, E. Kolettas, K. Niforou, V. C. Zoumpourlis, M. Takaoka, H. Nakagawa, F. Tort, K. Fugger, F. Johansson, M. Sehested, C. L. Andersen, L. Dyrskjot, T. Orntoft, J. Lukas, C. Kittas, T. Helleday, T. D. Halazonetis, J. Bartek and V. G. Gorgoulis (2006). "Oncogene-induced senescence is part of the tumorigenesis barrier imposed by DNA damage checkpoints." Nature **444**(7119): 633-637.

Bell, E., J. Lunec and D. A. Tweddle (2007). "Cell cycle regulation targets of MYCN identified by gene expression microarrays." Cell Cycle **6**(10): 1249-1256.

Benard, J. (1995). "Genetic alterations associated with metastatic dissemination and chemoresistance in neuroblastoma." Eur J Cancer **31a**(4): 560-564.

Blasina, A., J. Hallin, E. Chen, M. E. Arango, E. Kraynov, J. Register, S. Grant, S. Ninkovic, P. Chen, T. Nichols, P. O'Connor and K. Anderes (2008). "Breaching the DNA damage checkpoint via PF-00477736, a novel small-molecule inhibitor of checkpoint kinase 1." Mol Cancer Ther **7**(8): 2394-2404.

Bondar, T., A. Kalinina, L. Khair, D. Kopanja, A. Nag, S. Bagchi and P. Raychaudhuri (2006). "Cul4A and DDB1 associate with Skp2 to target p27Kip1 for proteolysis involving the COP9 signalosome." Mol Cell Biol **26**(7): 2531-2539.

Bouwman, P. and J. Jonkers (2012). "The effects of deregulated DNA damage signalling on cancer chemotherapy response and resistance." Nat Rev Cancer **12**(9): 587-598.

Bradford, M. M. (1976). "A rapid and sensitive method for the quantitation of microgram quantities of protein utilizing the principle of protein-dye binding." Anal Biochem **72**: 248-254.

Brockmann, M., E. Poon, T. Berry, A. Carstensen, H. E. Deubzer, L. Rycak, Y. Jamin, K. Thway, S. P. Robinson, F. Roels, O. Witt, M. Fischer, L. Chesler and M. Eilers (2013). "Small molecule inhibitors of aurora-a induce proteasomal degradation of N-myc in childhood neuroblastoma." Cancer Cell **24**(1): 75-89.

Burkhart, C. A., A. J. Cheng, J. Madafiglio, M. Kavallaris, M. Mili, G. M. Marshall, W. A. Weiss, L. M. Khachigian, M. D. Norris and M. Haber (2003). "Effects of MYCN antisense oligonucleotide administration on tumorigenesis in a murine model of neuroblastoma." J Natl Cancer Inst **95**(18): 1394-1403.

Casaccia-Bonnefil, P., R. Tikoo, H. Kiyokawa, V. Friedrich, Jr., M. V. Chao and A. Koff (1997). "Oligodendrocyte precursor differentiation is perturbed in the absence of the cyclin-dependent kinase inhibitor p27Kip1." Genes Dev **11**(18): 2335-2346.

Casciano, I., B. Banelli, M. Croce, A. De Ambrosis, A. di Vinci, I. Gelvi, G. Pagnan, C. Brignole, G. Allemanni, S. Ferrini, M. Ponzoni and M. Romani (2004). "Caspase-8 gene expression in neuroblastoma." Ann N Y Acad Sci **1028**: 157-167.

Castel, V., E. Grau, R. Noguera and F. Martinez (2007). "Molecular biology of neuroblastoma." Clin Transl Oncol **9**(8): 478-483.

Charron, J., B. A. Malynn, P. Fisher, V. Stewart, L. Jeannotte, S. P. Goff, E. J. Robertson and F. W. Alt (1992). "Embryonic lethality in mice homozygous for a targeted disruption of the N-myc gene." Genes Dev **6**(12a): 2248-2257.

Chavez, S., T. Beilharz, A. G. Rondon, H. Erdjument-Bromage, P. Tempst, J. Q. Svejstrup, T. Lithgow and A. Aguilera (2000). "A protein complex containing Tho2, Hpr1, Mft1 and a novel protein, Thp2, connects transcription elongation with mitotic recombination in Saccharomyces cerevisiae." Embo j **19**(21): 5824-5834.

Chellappan, S. P., S. Hiebert, M. Mudryj, J. M. Horowitz and J. R. Nevins (1991). "The E2F transcription factor is a cellular target for the RB protein." Cell **65**(6): 1053-1061.

Chen, L., N. Iraci, S. Gherardi, L. D. Gamble, K. M. Wood, G. Perini, J. Lunec and D. A. Tweddle (2010). "p53 is a direct transcriptional target of MYCN in neuroblastoma." Cancer Res **70**(4): 1377-1388.

Chen, Y., J. Takita, Y. L. Choi, M. Kato, M. Ohira, M. Sanada, L. Wang, M. Soda, A. Kikuchi, T. Igarashi, A. Nakagawara, Y. Hayashi, H. Mano and S. Ogawa (2008). "Oncogenic mutations of ALK kinase in neuroblastoma." Nature **455**(7215): 971-974.

Cheng, S. W., K. P. Davies, E. Yung, R. J. Beltran, J. Yu and G. V. Kalpana (1999). "c-MYC interacts with INI1/hSNF5 and requires the SWI/SNF complex for transactivation function." Nat Genet **22**(1): 102-105.

Chesler, L., D. D. Goldenberg, R. Collins, M. Grimmer, G. E. Kim, T. Tihan, K. Nguyen, S. Yakovenko, K. K. Matthay and W. A. Weiss (2008). "Chemotherapy-induced apoptosis in a transgenic model of neuroblastoma proceeds through p53 induction." Neoplasia **10**(11): 1268-1274.

Cimprich, K. A. and D. Cortez (2008). "ATR: an essential regulator of genome integrity." Nat Rev Mol Cell Biol **9**(8): 616-627.

Cinatl, J., J. Cinatl, M. Mainke, A. Weissflog, H. Rabenau, B. Kornhuber and H. W. Doerr (1993). "In vitro differentiation of human neuroblastoma cells induced by sodium phenylacetate." Cancer Lett **70**(1-2): 15-24.

Cleary, M. L., S. D. Smith and J. Sklar (1986). "Cloning and structural analysis of cDNAs for bcl-2 and a hybrid bcl-2/immunoglobulin transcript resulting from the t(14;18) translocation." Cell **47**(1): 19-28.

Cohn, S. L., A. D. Pearson, W. B. London, T. Monclair, P. F. Ambros, G. M. Brodeur, A. Faldum, B. Hero, T. Iehara, D. Machin, V. Mosseri, T. Simon, A. Garaventa, V. Castel and K. K. Matthay (2009). "The International Neuroblastoma Risk Group (INRG) classification system: an INRG Task Force report." J Clin Oncol **27**(2): 289-297.

Cole, K. A., J. Huggins, M. Laquaglia, C. E. Hulderman, M. R. Russell, K. Bosse, S. J. Diskin, E. F. Attiyeh, R. Sennett, G. Norris, M. Laudenslager, A. C. Wood, P. A. Mayes, J. Jagannathan, C. Winter, Y. P. Mosse and J. M. Maris (2011). "RNAi screen of the protein kinome identifies checkpoint kinase 1 (CHK1) as a therapeutic target in neuroblastoma." Proc Natl Acad Sci U S A **108**(8): 3336-3341.

Costanzo, V., D. Shechter, P. J. Lupardus, K. A. Cimprich, M. Gottesman and J. Gautier (2003). "An ATR- and Cdc7-dependent DNA damage checkpoint that inhibits initiation of DNA replication." Mol Cell **11**(1): 203-213.

Cowling, V. H. and M. D. Cole (2006). "Mechanism of transcriptional activation by the Myc oncoproteins." Semin Cancer Biol **16**(4): 242-252.

D'Amours, D., F. R. Sallmann, V. M. Dixit and G. G. Poirier (2001). "Gain-of-function of poly(ADP-ribose) polymerase-1 upon cleavage by apoptotic proteases: implications for apoptosis." J Cell Sci **114**(Pt 20): 3771-3778.

D'Angio, G. J., A. E. Evans and C. E. Koop (1971). "Special pattern of widespread neuroblastoma with a favourable prognosis." Lancet **1**(7708): 1046-1049.

Davis, A. C., M. Wims, G. D. Spotts, S. R. Hann and A. Bradley (1993). "A null c-myc mutation causes lethality before 10.5 days of gestation in homozygotes and reduced fertility in heterozygous female mice." Genes Dev **7**(4): 671-682.

DeGregori, J., T. Kowalik and J. R. Nevins (1995). "Cellular targets for activation by the E2F1 transcription factor include DNA synthesis- and G1/S-regulatory genes." Mol Cell Biol **15**(8): 4215-4224.

Delmore, Jake E., Ghayas C. Issa, Madeleine E. Lemieux, Peter B. Rahl, J. Shi, Hannah M. Jacobs, E. Kastritis, T. Gilpatrick, Ronald M. Paranal, J. Qi, M. Chesi, Anna C. Schinzel, Michael R. McKeown, Timothy P. Heffernan, Christopher R. Vakoc, P. L. Bergsagel, Irene M. Ghobrial, Paul G. Richardson, Richard A. Young, William C. Hahn, Kenneth C. Anderson, Andrew L. Kung, James E. Bradner and Constantine S. Mitsiades (2011). "BET Bromodomain Inhibition as a Therapeutic Strategy to Target c-Myc." Cell **146**(6): 904-917.

Deshaies, R. J. and C. A. Joazeiro (2009). "RING domain E3 ubiquitin ligases." Annu Rev Biochem **78**: 399-434.

Dewitt, J., V. Ochoa, J. Urschitz, M. Elston, S. Moisyadi and R. Nishi (2014). "Constitutively active TrkB confers an aggressive transformed phenotype to a neural crest-derived cell line." Oncogene **33**(8): 977-985.

Di Micco, R., M. Fumagalli, A. Cicalese, S. Piccinin, P. Gasparini, C. Luise, C. Schurra, M. Garre, P. G. Nuciforo, A. Bensimon, R. Maestro, P. G. Pelicci and F. d'Adda di Fagagna (2006). "Oncogene-induced senescence is a DNA damage response triggered by DNA hyper-replication." Nature **444**(7119): 638-642.

Dominguez-Sola, D., C. Y. Ying, C. Grandori, L. Ruggiero, B. Chen, M. Li, D. A. Galloway, W. Gu, J. Gautier and R. Dalla-Favera (2007). "Non-transcriptional control of DNA replication by c-Myc." Nature **448**(7152): 445-451.

DuBois, S. G., Y. Kalika, J. N. Lukens, G. M. Brodeur, R. C. Seeger, J. B. Atkinson, G. M. Haase, C. T. Black, C. Perez, H. Shimada, R. Gerbing, D. O. Stram and K. K. Matthay (1999). "Metastatic sites in stage IV and IVS neuroblastoma correlate with age, tumor biology, and survival." J Pediatr Hematol Oncol **21**(3): 181-189.

Eggert, A., M. A. Grotzer, T. J. Zuzak, B. R. Wiewrodt, R. Ho, N. Ikegaki and G. M. Brodeur (2001). "Resistance to tumor necrosis factor-related apoptosis-inducing ligand (TRAIL)-induced apoptosis in neuroblastoma cells correlates with a loss of caspase-8 expression." Cancer Res **61**(4): 1314-1319.

Eilers, M. and R. N. Eisenman (2008). "Myc's broad reach." Genes Dev **22**(20): 2755-2766.

el-Deiry, W. S., T. Tokino, V. E. Velculescu, D. B. Levy, R. Parsons, J. M. Trent, D. Lin, W. E. Mercer, K. W. Kinzler and B. Vogelstein (1993). "WAF1, a potential mediator of p53 tumor suppression." Cell **75**(4): 817-825.

Elson, A., C. Deng, J. Campos-Torres, L. A. Donehower and P. Leder (1995). "The MMTV/c-myc transgene and p53 null alleles collaborate to induce T-cell lymphomas, but not mammary carcinomas in transgenic mice." Oncogene **11**(1): 181-190.

Emberley, E. D., R. Mosadeghi and R. J. Deshaies (2012). "Deconjugation of Nedd8 from Cul1 is directly regulated by Skp1-F-box and substrate, and the COP9 signalosome inhibits deneddylated SCF by a noncatalytic mechanism." J Biol Chem **287**(35): 29679-29689.

Enchev, R. I., D. C. Scott, P. C. da Fonseca, A. Schreiber, J. K. Monda, B. A. Schulman, M. Peter and E. P. Morris (2012). "Structural basis for a reciprocal regulation between SCF and CSN." Cell Rep **2**(3): 616-627.

Evan, G. I., A. H. Wyllie, C. S. Gilbert, T. D. Littlewood, H. Land, M. Brooks, C. M. Waters, L. Z. Penn and D. C. Hancock (1992). "Induction of apoptosis in fibroblasts by c-myc protein." Cell **69**(1): 119-128.

Evertts, A. G. and H. A. Coller (2012). "Back to the origin: reconsidering replication, transcription, epigenetics, and cell cycle control." Genes Cancer **3**(11-12): 678-696.

Fanning, E., V. Klimovich and A. R. Nager (2006). "A dynamic model for replication protein A (RPA) function in DNA processing pathways." Nucleic Acids Res **34**(15): 4126-4137.

Farmer, H., N. McCabe, C. J. Lord, A. N. Tutt, D. A. Johnson, T. B. Richardson, M. Santarosa, K. J. Dillon, I. Hickson, C. Knights, N. M. Martin, S. P. Jackson, G. C. Smith and A. Ashworth (2005). "Targeting the DNA repair defect in BRCA mutant cells as a therapeutic strategy." Nature **434**(7035): 917-921.

Farrell, A. S. and R. C. Sears (2014). "MYC Degradation." Cold Spring Harb Perspect Med **4**(3).

Felsher, D. W. and J. M. Bishop (1999). "Transient excess of MYC activity can elicit genomic instability and tumorigenesis." Proc Natl Acad Sci U S A **96**(7): 3940-3944.

Friend, S. H. and A. Oliff (1998). "Emerging uses for genomic information in drug discovery." N Engl J Med **338**(2): 125-126.

Fulda, S., C. Poremba, B. Berwanger, S. Hacker, M. Eilers, H. Christiansen, B. Hero and K. M. Debatin (2006). "Loss of caspase-8 expression does not correlate with MYCN amplification, aggressive disease, or prognosis in neuroblastoma." Cancer Res **66**(20): 10016-10023.

Furukawa, M., Y. J. He, C. Borchers and Y. Xiong (2003). "Targeting of protein ubiquitination by BTB-Cullin 3-Roc1 ubiquitin ligases." Nat Cell Biol **5**(11): 1001-1007.

Garcia, K., J. L. Blank, D. C. Bouck, X. J. Liu, D. S. Sappal, G. Hather, K. Cosmopoulos, M. P. Thomas, M. Kuranda, M. D. Pickard, R. Liu, S. Bandi, P. G. Smith and E. S. Lightcap (2014). "Nedd8-Activating Enzyme Inhibitor MLN4924 Provides Synergy with Mitomycin C through Interactions with ATR, BRCA1/BRCA2 and Chromatin Dynamics Pathways." Mol Cancer Ther.

Gogolin, S., V. Ehemann, G. Becker, L. M. Brueckner, D. Dreidax, S. Bannert, I. Nolte, L. Savelyeva, E. Bell and F. Westermann (2013). "CDK4 inhibition restores G(1)-S arrest in MYCN-amplified neuroblastoma cells in the context of doxorubicin-induced DNA damage." Cell Cycle **12**(7): 1091-1104.

Gomez-Casares, M. T., E. Garcia-Alegria, C. E. Lopez-Jorge, N. Ferrandiz, R. Blanco, S. Alvarez, J. P. Vaque, G. Bretones, J. M. Caraballo, P. Sanchez-Bailon, M. D. Delgado, J. Martin-Perez, J. C. Cigudosa and J. Leon (2013). "MYC antagonizes the differentiation induced by imatinib in chronic myeloid leukemia cells through downregulation of p27(KIP1.)." Oncogene **32**(17): 2239-2246.

Gonzalez-Gomez, P., M. J. Bello, J. Lomas, D. Arjona, M. E. Alonso, C. Aminoso, I. Lopez-Marin, N. P. Anselmo, J. L. Sarasa, M. Gutierrez, C. Casartelli and J. A. Rey (2003). "Aberrant methylation of multiple genes in neuroblastic tumours. relationship with MYCN amplification and allelic status at 1p." Eur J Cancer **39**(10): 1478-1485.

Goodman, L. A., B. C. Liu, C. J. Thiele, M. L. Schmidt, S. L. Cohn, J. M. Yamashiro, D. S. Pai, N. Ikegaki and R. K. Wada (1997). "Modulation of N-myc expression alters the invasiveness of neuroblastoma." Clin Exp Metastasis **15**(2): 130-139.

Gorgoulis, V. G., L. V. Vassiliou, P. Karakaidos, P. Zacharatos, A. Kotsinas, T. Liloglou, M. Venere, R. A. Ditullio, Jr., N. G. Kastrinakis, B. Levy, D. Kletsas, A. Yoneta, M. Herlyn, C. Kittas and T. D. Halazonetis (2005). "Activation of the DNA damage checkpoint and genomic instability in human precancerous lesions." Nature **434**(7035): 907-913.

Gu, L., H. Zhang, J. He, J. Li, M. Huang and M. Zhou (2012). "MDM2 regulates MYCN mRNA stabilization and translation in human neuroblastoma cells." Oncogene **31**(11): 1342-1353.

Guarente, L. (1993). "Synthetic enhancement in gene interaction: a genetic tool come of age." Trends Genet **9**(10): 362-366.

Gustafson, W. C. and W. A. Weiss (2010). "Myc proteins as therapeutic targets." Oncogene **29**(9): 1249-1259.

Haas, A. L. and I. A. Rose (1982). "The mechanism of ubiquitin activating enzyme. A kinetic and equilibrium analysis." J Biol Chem **257**(17): 10329-10337.

Halazonetis, T. D., V. G. Gorgoulis and J. Bartek (2008). "An oncogene-induced DNA damage model for cancer development." Science **319**(5868): 1352-1355.

Harreman, M., M. Taschner, S. Sigurdsson, R. Anindya, J. Reid, B. Somesh, S. E. Kong, C. A. Banks, R. C. Conaway, J. W. Conaway and J. Q. Svejstrup (2009). "Distinct ubiquitin ligases act sequentially for RNA polymerase II polyubiquitylation." Proc Natl Acad Sci U S A **106**(49): 20705-20710.

Hartman, J. L. t., B. Garvik and L. Hartwell (2001). "Principles for the buffering of genetic variation." Science **291**(5506): 1001-1004.

Hartwell, L. H., P. Szankasi, C. J. Roberts, A. W. Murray and S. H. Friend (1997). "Integrating genetic approaches into the discovery of anticancer drugs." Science **278**(5340): 1064-1068.

Hayashi, Y., N. Kanda, T. Inaba, R. Hanada, N. Nagahara, H. Muchi and K. Yamamoto (1989). "Cytogenetic findings and prognosis in neuroblastoma with emphasis on marker chromosome 1." Cancer **63**(1): 126-132.

Hershko, A. and A. Ciechanover (1998). "The ubiquitin system." Annu Rev Biochem **67**: 425-479.

Hilton, D. J. (1999). "Negative regulators of cytokine signal transduction." Cell Mol Life Sci **55**(12): 1568-1577.

Hinds, P. W., S. Mittnacht, V. Dulic, A. Arnold, S. I. Reed and R. A. Weinberg (1992). "Regulation of retinoblastoma protein functions by ectopic expression of human cyclins." Cell **70**(6): 993-1006.

Hirano, T. (2005). "Condensins: organizing and segregating the genome." Curr Biol **15**(7): R265-275.

Hirota, T., D. Gerlich, B. Koch, J. Ellenberg and J. M. Peters (2004). "Distinct functions of condensin I and II in mitotic chromosome assembly." J Cell Sci **117**(Pt 26): 6435-6445.

Ho, R., A. Eggert, T. Hishiki, J. E. Minturn, N. Ikegaki, P. Foster, A. M. Camoratto, A. E. Evans and G. M. Brodeur (2002). "Resistance to chemotherapy mediated by TrkB in neuroblastomas." Cancer Res **62**(22): 6462-6466.

Huang, M. and W. A. Weiss (2013). "Neuroblastoma and MYCN." Cold Spring Harb Perspect Med **3**(10): a014415.

Huang, R., N. K. Cheung, J. Vider, I. Y. Cheung, W. L. Gerald, S. K. Tickoo, E. C. Holland and R. G. Blasberg (2011). "MYCN and MYC regulate tumor proliferation and tumorigenesis directly through BMI1 in human neuroblastomas." Faseb j **25**(12): 4138-4149.

Huertas, P. and A. Aguilera (2003). "Cotranscriptionally formed DNA:RNA hybrids mediate transcription elongation impairment and transcription-associated recombination." Mol Cell **12**(3): 711-721.

Hurlin, P. J. (2005). "N-Myc functions in transcription and development." Birth Defects Res C Embryo Today **75**(4): 340-352.

Iolascon, A., A. Borriello, L. Giordani, V. Cucciolla, A. Moretti, F. Monno, V. Criniti, A. Marzullo, M. Criscuolo and F. D. Ragione (2003). "Caspase 3 and 8 deficiency in human neuroblastoma." Cancer Genet Cytogenet **146**(1): 41-47.

Iraci, N., D. Diolaiti, A. Papa, A. Porro, E. Valli, S. Gherardi, S. Herold, M. Eilers, R. Bernardoni, G. Della Valle and G. Perini (2011). "A SP1/MIZ1/MYCN repression complex recruits HDAC1 at the TRKA and p75NTR promoters and affects neuroblastoma malignancy by inhibiting the cell response to NGF." Cancer Res **71**(2): 404-412.

Izumi, H. and Y. Kaneko (2012). "Evidence of asymmetric cell division and centrosome inheritance in human neuroblastoma cells." Proc Natl Acad Sci U S A **109**(44): 18048-18053.

Jani, D., S. Lutz, E. Hurt, R. A. Laskey, M. Stewart and V. O. Wickramasinghe (2012). "Functional and structural characterization of the mammalian TREX-2 complex that links transcription with nuclear messenger RNA export." Nucleic Acids Res **40**(10): 4562-4573.

Ji, H., G. Wu, X. Zhan, A. Nolan, C. Koh, A. De Marzo, H. M. Doan, J. Fan, C. Cheadle, M. Fallahi, J. L. Cleveland, C. V. Dang and K. I. Zeller (2011). "Cell-type independent MYC target genes reveal a primordial signature involved in biomass accumulation." PLoS One **6**(10): e26057.

Johnsen, J. I., L. Segerstrom, A. Orrego, L. Elfman, M. Henriksson, B. Kagedal, S. Eksborg, B. Sveinbjornsson and P. Kogner (2008). "Inhibitors of mammalian target of rapamycin downregulate MYCN protein expression and inhibit neuroblastoma growth in vitro and in vivo." Oncogene **27**(20): 2910-2922.

Jones, R. M., O. Mortusewicz, I. Afzal, M. Lorvellec, P. Garcia, T. Helleday and E. Petermann (2013). "Increased replication initiation and conflicts with transcription underlie Cyclin E-induced replication stress." Oncogene **32**(32): 3744-3753.

Kaelin, W. G. (2005). "The Concept of Synthetic Lethality in the Context of Anticancer Therapy." Nature Reviews Cancer **5**(9): 689-698.

Kaelin, W. G., Jr. (1999). "Choosing anticancer drug targets in the postgenomic era." J Clin Invest **104**(11): 1503-1506.

Kamb, A. (2003). "Mutation load, functional overlap, and synthetic lethality in the evolution and treatment of cancer." J Theor Biol **223**(2): 205-213.

Kamitani, T., K. Kito, H. P. Nguyen and E. T. Yeh (1997). "Characterization of NEDD8, a developmentally down-regulated ubiquitin-like protein." J Biol Chem **272**(45): 28557-28562.

Kaneko, Y., N. Kanda, N. Maseki, M. Sakurai, Y. Tsuchida, T. Takeda, I. Okabe and M. Sakurai (1987). "Different karyotypic patterns in early and advanced stage neuroblastomas." Cancer Res **47**(1): 311-318.

Kang, J., C. M. Sergio, R. L. Sutherland and E. A. Musgrove (2014). "Targeting cyclin-dependent kinase 1 (CDK1) but not CDK4/6 or CDK2 is selectively lethal to MYC-dependent human breast cancer cells." BMC Cancer **14**: 32.

Kang, J. H., P. G. Rychahou, T. A. Ishola, J. Qiao, B. M. Evers and D. H. Chung (2006). "MYCN silencing induces differentiation and apoptosis in human neuroblastoma cells." Biochem Biophys Res Commun **351**(1): 192-197.

Kawauchi, D., G. Robinson, T. Uziel, P. Gibson, J. Rehg, C. Gao, D. Finkelstein, C. Qu, S. Pounds, David W. Ellison, Richard J. Gilbertson and Martine F. Roussel (2012). "A Mouse

Model of the Most Aggressive Subgroup of Human Medulloblastoma." Cancer Cell **21**(2): 168-180.

Kessler, J. D., K. T. Kahle, T. Sun, K. L. Meerbrey, M. R. Schlabach, E. M. Schmitt, S. O. Skinner, Q. Xu, M. Z. Li, Z. C. Hartman, M. Rao, P. Yu, R. Dominguez-Vidana, A. C. Liang, N. L. Solimini, R. J. Bernardi, B. Yu, T. Hsu, I. Golding, J. Luo, C. K. Osborne, C. J. Creighton, S. G. Hilsenbeck, R. Schiff, C. A. Shaw, S. J. Elledge and T. F. Westbrook (2012). "A SUMOylation-dependent transcriptional subprogram is required for Myc-driven tumorigenesis." Science **335**(6066): 348-353.

Kohl, N. E., N. Kanda, R. R. Schreck, G. Bruns, S. A. Latt, F. Gilbert and F. W. Alt (1983). "Transposition and amplification of oncogene-related sequences in human neuroblastomas." Cell **35**(2 Pt 1): 359-367.

Koppen, A., R. Ait-Aissa, S. Hopman, J. Koster, F. Haneveld, R. Versteeg and L. J. Valentijn (2007). "Dickkopf-1 is down-regulated by MYCN and inhibits neuroblastoma cell proliferation." Cancer Lett **256**(2): 218-228.

Koppen, A., R. Ait-Aissa, J. Koster, P. G. van Sluis, I. Ora, H. N. Caron, R. Volckmann, R. Versteeg and L. J. Valentijn (2007). "Direct regulation of the minichromosome maintenance complex by MYCN in neuroblastoma." Eur J Cancer **43**(16): 2413-2422.

Kossatz, U., K. Breuhahn, B. Wolf, M. Hardtke-Wolenski, L. Wilkens, D. Steinemann, S. Singer, F. Brass, S. Kubicka, B. Schlegelberger, P. Schirmacher, M. P. Manns, J. D. Singer and N. P. Malek (2010). "The cyclin E regulator cullin 3 prevents mouse hepatic progenitor cells from becoming tumor-initiating cells." J Clin Invest **120**(11): 3820-3833.

Laemmli, U. K., F. Beguin and G. Gujer-Kellenberger (1970). "A factor preventing the major head protein of bacteriophage T4 from random aggregation." J Mol Biol **47**(1): 69-85.

Lazcoz, P., J. Munoz, M. Nistal, A. Pestana, I. Encio and J. S. Castresana (2006). "Frequent promoter hypermethylation of RASSF1A and CASP8 in neuroblastoma." BMC Cancer **6**: 254.

Levine, A. J. (1997). "p53, the cellular gatekeeper for growth and division." Cell **88**(3): 323-331.

Li, H., B. Handsaker, A. Wysoker, T. Fennell, J. Ruan, N. Homer, G. Marth, G. Abecasis and R. Durbin (2009). "The Sequence Alignment/Map format and SAMtools." Bioinformatics **25**(16): 2078-2079.

Liu, L., J. Ulbrich, J. Muller, T. Wustefeld, L. Aeberhard, T. R. Kress, N. Muthalagu, L. Rycak, R. Rudalska, R. Moll, S. Kempa, L. Zender, M. Eilers and D. J. Murphy (2012). "Deregulated MYC expression induces dependence upon AMPK-related kinase 5." Nature **483**(7391): 608-612.

Liu, Y. C., F. Li, J. Handler, C. R. Huang, Y. Xiang, N. Neretti, J. M. Sedivy, K. I. Zeller and C. V. Dang (2008). "Global regulation of nucleotide biosynthetic genes by c-Myc." PLoS One **3**(7): e2722.

Look, A. T., F. A. Hayes, R. Nitschke, N. B. McWilliams and A. A. Green (1984). "Cellular DNA content as a predictor of response to chemotherapy in infants with unresectable neuroblastoma." N Engl J Med **311**(4): 231-235.

Look, A. T., F. A. Hayes, J. J. Shuster, E. C. Douglass, R. P. Castleberry, L. C. Bowman, E. I. Smith and G. M. Brodeur (1991). "Clinical relevance of tumor cell ploidy and N-myc gene amplification in childhood neuroblastoma: a Pediatric Oncology Group study." J Clin Oncol **9**(4): 581-591.

Luo, J., M. J. Emanuele, D. Li, C. J. Creighton, M. R. Schlabach, T. F. Westbrook, K. K. Wong and S. J. Elledge (2009). "A genome-wide RNAi screen identifies multiple synthetic lethal interactions with the Ras oncogene." Cell **137**(5): 835-848.

Lyapina, S., G. Cope, A. Shevchenko, G. Serino, T. Tsuge, C. Zhou, D. A. Wolf, N. Wei, A. Shevchenko and R. J. Deshaies (2001). "Promotion of NEDD-CUL1 conjugate cleavage by COP9 signalosome." Science **292**(5520): 1382-1385.

Ma, L., J. Young, H. Prabhala, E. Pan, P. Mestdagh, D. Muth, J. Teruya-Feldstein, F. Reinhardt, T. T. Onder, S. Valastyan, F. Westermann, F. Speleman, J. Vandesompele and R. A. Weinberg (2010). "miR-9, a MYC/MYCN-activated microRNA, regulates E-cadherin and cancer metastasis." Nature Cell Biology.

Maeshima, K. and U. K. Laemmli (2003). "A two-step scaffolding model for mitotic chromosome assembly." Dev Cell **4**(4): 467-480.

Mailand, N., J. Falck, C. Lukas, R. G. Syljuasen, M. Welcker, J. Bartek and J. Lukas (2000). "Rapid destruction of human Cdc25A in response to DNA damage." Science **288**(5470): 1425-1429.

Malumbres, M. and M. Barbacid (2001). "To cycle or not to cycle: a critical decision in cancer." Nat Rev Cancer **1**(3): 222-231.

Margolin, A. A., T. Palomero, P. Sumazin, A. Califano, A. A. Ferrando and G. Stolovitzky (2009). "ChIP-on-chip significance analysis reveals large-scale binding and regulation by human transcription factor oncogenes." Proc Natl Acad Sci U S A **106**(1): 244-249.

Maris, J. M., M. D. Hogarty, R. Bagatell and S. L. Cohn (2007). "Neuroblastoma." Lancet **369**(9579): 2106-2120.

Mark D. Robinson, D. J. M., Gordon K. Smyth (2010). "edgeR: a Bioconductor package for differential expression analysis of digital gene expression data." Bioinformatics **1; 26(1): 139,Äì140.** .

Marraffini, L. A. and E. J. Sontheimer (2010). "CRISPR interference: RNA-directed adaptive immunity in bacteria and archaea." Nat Rev Genet **11**(3): 181-190.

Matsumoto, M., T. Akiyama, S. Miyatake, Y. Oda, H. Kikuchi, M. Hanaoka and Y. Namba (1989). "Expression of proto-oncogene products during drug-induced differentiation of a neuroblastoma cell line SK-N-DZ." Acta Neuropathol **79**(2): 217-221.

Matthay, K. K., R. E. George and A. L. Yu (2012). "Promising therapeutic targets in neuroblastoma." Clin Cancer Res **18**(10): 2740-2753.

Matthay, K. K., J. G. Villablanca, R. C. Seeger, D. O. Stram, R. E. Harris, N. K. Ramsay, P. Swift, H. Shimada, C. T. Black, G. M. Brodeur, R. B. Gerbing and C. P. Reynolds (1999). "Treatment of high-risk neuroblastoma with intensive chemotherapy, radiotherapy, autologous bone marrow transplantation, and 13-cis-retinoic acid. Children's Cancer Group." N Engl J Med **341**(16): 1165-1173.

Matulonis, U. A., S. Sharma, S. Ghamande, M. S. Gordon, S. A. Del Prete, I. Ray-Coquard, E. Kutarska, H. Liu, H. Fingert, X. Zhou, H. Danaee and R. J. Schilder (2012). "Phase II study of MLN8237 (alisertib), an investigational Aurora A kinase inhibitor, in patients with platinum-resistant or -refractory epithelial ovarian, fallopian tube, or primary peritoneal carcinoma." Gynecol Oncol **127**(1): 63-69.

Meijer, L., A. Borgne, O. Mulner, J. P. Chong, J. J. Blow, N. Inagaki, M. Inagaki, J. G. Delcros and J. P. Moulinoux (1997). "Biochemical and cellular effects of roscovitine, a potent and selective inhibitor of the cyclin-dependent kinases cdc2, cdk2 and cdk5." Eur J Biochem **243**(1-2): 527-536.

Melby, T. E., C. N. Ciampaglio, G. Briscoe and H. P. Erickson (1998). "The symmetrical structure of structural maintenance of chromosomes (SMC) and MukB proteins: long, antiparallel coiled coils, folded at a flexible hinge." J Cell Biol **142**(6): 1595-1604.

Molenaar, J. J., M. E. Ebus, D. Geerts, J. Koster, F. Lamers, L. J. Valentijn, E. M. Westerhout, R. Versteeg and H. N. Caron (2009). "Inactivation of CDK2 is synthetically lethal to MYCN over-expressing cancer cells." Proc Natl Acad Sci U S A **106**(31): 12968-12973.

Mourgues, S., V. Gautier, A. Lagarou, C. Bordier, A. Mourcet, J. Slingerland, L. Kaddoum, F. Coin, W. Vermeulen, A. Gonzales de Peredo, B. Monsarrat, P. O. Mari and G. Giglia-Mari (2013). "ELL, a novel TFIIH partner, is involved in transcription restart after DNA repair." Proc Natl Acad Sci U S A **110**(44): 17927-17932.

Mueller, S. and K. K. Matthay (2009). "Neuroblastoma: biology and staging." Curr Oncol Rep **11**(6): 431-438.

Muniandy, P. A., J. Liu, A. Majumdar, S. T. Liu and M. M. Seidman (2010). "DNA interstrand crosslink repair in mammalian cells: step by step." Crit Rev Biochem Mol Biol **45**(1): 23-49.

Murakami-Tonami, Y., S. Kishida, I. Takeuchi, Y. Katou, J. M. Maris, H. Ichikawa, Y. Kondo, Y. Sekido, K. Shirahige, H. Murakami and K. Kadomatsu (2014). "Inactivation of SMC2 shows a synergistic lethal response in -amplified neuroblastoma cells." Cell Cycle **13**(7).

Muth, D., S. Ghazaryan, I. Eckerle, E. Beckett, C. Pohler, J. Batzler, C. Beisel, S. Gogolin, M. Fischer, K. O. Henrich, V. Ehemann, P. Gillespie, M. Schwab and F. Westermann (2010). "Transcriptional repression of SKP2 is impaired in MYCN-amplified neuroblastoma." Cancer Res **70**(9): 3791-3802.

Nakagawa, M., N. Takizawa, M. Narita, T. Ichisaka and S. Yamanaka (2010). "Promotion of direct reprogramming by transformation-deficient Myc." Proc Natl Acad Sci U S A **107**(32): 14152-14157.

Nakagawara, A., C. G. Azar, N. J. Scavarda and G. M. Brodeur (1994). "Expression and function of TRK-B and BDNF in human neuroblastomas." Mol Cell Biol **14**(1): 759-767.

Neelsen, K. J., I. M. Zanini, R. Herrador and M. Lopes (2013). "Oncogenes induce genotoxic stress by mitotic processing of unusual replication intermediates." J Cell Biol **200**(6): 699-708.

Negroni, A., S. Scarpa, A. Romeo, S. Ferrari, A. Modesti and G. Raschella (1991). "Decrease of proliferation rate and induction of differentiation by a MYCN antisense DNA oligomer in a human neuroblastoma cell line." Cell Growth Differ **2**(10): 511-518.

Neuwald, A. F. and T. Hirano (2000). "HEAT repeats associated with condensins, cohesins, and other complexes involved in chromosome-related functions." Genome Res **10**(10): 1445-1452.

Nie, Z., G. Hu, G. Wei, K. Cui, A. Yamane, W. Resch, R. Wang, D. R. Green, L. Tessarollo, R. Casellas, K. Zhao and D. Levens (2012). "c-Myc is a universal amplifier of expressed genes in lymphocytes and embryonic stem cells." Cell **151**(1): 68-79.

Ochiai, H., H. Takenobu, A. Nakagawa, Y. Yamaguchi, M. Kimura, M. Ohira, Y. Okimoto, Y. Fujimura, H. Koseki, Y. Kohno, A. Nakagawara and T. Kamijo (2010). "Bmi1 is a MYCN target gene that regulates tumorigenesis through repression of KIF1Bbeta and TSLC1 in neuroblastoma." Oncogene **29**(18): 2681-2690.

Ono, T., Y. Fang, D. L. Spector and T. Hirano (2004). "Spatial and temporal regulation of Condensins I and II in mitotic chromosome assembly in human cells." Mol Biol Cell **15**(7): 3296-3308.

Onyango, M., C. Ade, F. Cemic and J. Hemberger (2013). QUASI: A Pipeline for the Quality Assessment and Statistical Inference on Next Generation Sequencing Data from Pooled shRNA Library Screens. SciTePress, BIOINFORMATICS**:** 288-291.

Otto, T., S. Horn, M. Brockmann, U. Eilers, L. Schuttrumpf, N. Popov, A. M. Kenney, J. H. Schulte, R. Beijersbergen, H. Christiansen, B. Berwanger and M. Eilers (2009). "Stabilization of N-Myc is a critical function of Aurora A in human neuroblastoma." Cancer Cell **15**(1): 67-78.

Pan, Z. Q., A. Kentsis, D. C. Dias, K. Yamoah and K. Wu (2004). "Nedd8 on cullin: building an expressway to protein destruction." Oncogene **23**(11): 1985-1997.

Pei, Y., C. E. Moore, J. Wang, A. K. Tewari, A. Eroshkin, Y. J. Cho, H. Witt, A. Korshunov, T. A. Read, J. L. Sun, E. M. Schmitt, C. R. Miller, A. F. Buckley, R. E. McLendon, T. F. Westbrook, P. A. Northcott, M. D. Taylor, S. M. Pfister, P. G. Febbo and R. J. Wechsler-Reya (2012). "An animal model of MYC-driven medulloblastoma." Cancer Cell **21**(2): 155-167.

Pintard, L., T. Kurz, S. Glaser, J. H. Willis, M. Peter and B. Bowerman (2003). "Neddylation and deneddylation of CUL-3 is required to target MEI-1/Katanin for degradation at the meiosis-to-mitosis transition in C. elegans." Curr Biol **13**(11): 911-921.

Porter, D. C., N. Zhang, C. Danes, M. J. McGahren, R. M. Harwell, S. Faruki and K. Keyomarsi (2001). "Tumor-specific proteolytic processing of cyclin E generates hyperactive lower-molecular-weight forms." Mol Cell Biol **21**(18): 6254-6269.

Puissant, A., S. M. Frumm, G. Alexe, C. F. Bassil, J. Qi, Y. H. Chanthery, E. A. Nekritz, R. Zeid, W. C. Gustafson, P. Greninger, M. J. Garnett, U. McDermott, C. H. Benes, A. L. Kung, W. A. Weiss, J. E. Bradner and K. Stegmaier (2013). "Targeting MYCN in neuroblastoma by BET bromodomain inhibition." Cancer Discov **3**(3): 308-323.

Pulverer, B. J., C. Fisher, K. Vousden, T. Littlewood, G. Evan and J. R. Woodgett (1994). "Site-specific modulation of c-Myc cotransformation by residues phosphorylated in vivo." Oncogene **9**(1): 59-70.

Quinlan, A. R. and I. M. Hall (2010). "BEDTools: a flexible suite of utilities for comparing genomic features." Bioinformatics **26**(6): 841-842.

Rahl, P. B., C. Y. Lin, A. C. Seila, R. A. Flynn, S. McCuine, C. B. Burge, P. A. Sharp and R. A. Young (2010). "c-Myc regulates transcriptional pause release." Cell **141**(3): 432-445.

Rahl, P. B., C. Y. Lin, A. C. Seila, R. A. Flynn, S. McCuine, C. B. Burge, P. A. Sharp and R. A. Young (2010). "c-Myc Regulates Transcriptional Pause Release." Cell **141**(3): 432-445.

Rehman, F. L., C. J. Lord and A. Ashworth (2010). "Synthetic lethal approaches to breast cancer therapy." Nature Reviews Clinical Oncology **7**(12): 718-724.

Romero, O. A., M. Torres-Diz, E. Pros, S. Savola, A. Gomez, S. Moran, C. Saez, R. Iwakawa, A. Villanueva, L. M. Montuenga, T. Kohno, J. Yokota and M. Sanchez-Cespedes (2014). "MAX Inactivation in Small Cell Lung Cancer Disrupts MYC-SWI/SNF Programs and Is Synthetic Lethal with BRG1." Cancer Discov.

Rondon, A. G., S. Jimeno and A. Aguilera (2010). "The interface between transcription and mRNP export: from THO to THSC/TREX-2." Biochim Biophys Acta **1799**(8): 533-538.

Rondon, A. G., S. Jimeno, M. Garcia-Rubio and A. Aguilera (2003). "Molecular evidence that the eukaryotic THO/TREX complex is required for efficient transcription elongation." J Biol Chem **278**(40): 39037-39043.

Rottmann, S., Y. Wang, M. Nasoff, Q. L. Deveraux and K. C. Quon (2005). "A TRAIL receptor-dependent synthetic lethal relationship between MYC activation and GSK3beta/FBW7 loss of function." Proc Natl Acad Sci U S A **102**(42): 15195-15200.

Roussel, M. F. and G. W. Robinson (2013). "Role of MYC in Medulloblastoma." Cold Spring Harb Perspect Med **3**(11).

Sabo, A. and B. Amati (2014). "Genome Recognition by MYC." Cold Spring Harb Perspect Med **4**(2).

Sander, J. D. and J. K. Joung (2014). "CRISPR-Cas systems for editing, regulating and targeting genomes." Nat Biotechnol.

Sato, Y., T. Yoshizato, Y. Shiraishi, S. Maekawa, Y. Okuno, T. Kamura, T. Shimamura, A. Sato-Otsubo, G. Nagae, H. Suzuki, Y. Nagata, K. Yoshida, A. Kon, Y. Suzuki, K. Chiba, H. Tanaka, A. Niida, A. Fujimoto, T. Tsunoda, T. Morikawa, D. Maeda, H. Kume, S. Sugano, M. Fukayama, H. Aburatani, M. Sanada, S. Miyano, Y. Homma and S. Ogawa (2013). "Integrated molecular analysis of clear-cell renal cell carcinoma." Nat Genet **45**(8): 860-867.

Sawai, S., A. Shimono, Y. Wakamatsu, C. Palmes, K. Hanaoka and H. Kondoh (1993). "Defects of embryonic organogenesis resulting from targeted disruption of the N-myc gene in the mouse." Development **117**(4): 1445-1455.

Schleiermacher, G., V. Mosseri, W. B. London, J. M. Maris, G. M. Brodeur, E. Attiyeh, M. Haber, J. Khan, A. Nakagawara, F. Speleman, R. Noguera, G. P. Tonini, M. Fischer, I. Ambros, T. Monclair, K. K. Matthay, P. Ambros, S. L. Cohn and A. D. Pearson (2012). "Segmental chromosomal alterations have prognostic impact in neuroblastoma: a report from the INRG project." Br J Cancer **107**(8): 1418-1422.

Schmidt, M. W., P. R. McQuary, S. Wee, K. Hofmann and D. A. Wolf (2009). "F-box-directed CRL complex assembly and regulation by the CSN and CAND1." Mol Cell **35**(5): 586-597.

Schulte, J. H., S. Schulte, L. C. Heukamp, K. Astrahantseff, H. Stephan, M. Fischer, A. Schramm and A. Eggert (2013). "Targeted Therapy for Neuroblastoma: ALK Inhibitors." Klin Padiatr **225**(6): 303-308.

Schwab, M., K. Alitalo, K. H. Klempnauer, H. E. Varmus, J. M. Bishop, F. Gilbert, G. Brodeur, M. Goldstein and J. Trent (1983). "Amplified DNA with limited homology to myc cellular oncogene is shared by human neuroblastoma cell lines and a neuroblastoma tumour." Nature **305**(5931): 245-248.

Schwab, M., F. Westermann, B. Hero and F. Berthold (2003). "Neuroblastoma: biology and molecular and chromosomal pathology." Lancet Oncol **4**(8): 472-480.

Schwechheimer, C., G. Serino, J. Callis, W. L. Crosby, S. Lyapina, R. J. Deshaies, W. M. Gray, M. Estelle and X. W. Deng (2001). "Interactions of the COP9 signalosome with the E3 ubiquitin ligase SCFTIRI in mediating auxin response." Science **292**(5520): 1379-1382.

Schweigerer, L., S. Breit, A. Wenzel, K. Tsunamoto, R. Ludwig and M. Schwab (1990). "Augmented MYCN expression advances the malignant phenotype of human neuroblastoma cells: evidence for induction of autocrine growth factor activity." Cancer Res **50**(14): 4411-4416.

Sears, R., F. Nuckolls, E. Haura, Y. Taya, K. Tamai and J. R. Nevins (2000). "Multiple Ras-dependent phosphorylation pathways regulate Myc protein stability." Genes Dev **14**(19): 2501-2514.

Shaffer, A. L., G. Wright, L. Yang, J. Powell, V. Ngo, L. Lamy, L. T. Lam, R. E. Davis and L. M. Staudt (2006). "A library of gene expression signatures to illuminate normal and pathological lymphoid biology." Immunol Rev **210**: 67-85.

Sharom, J. R., D. S. Bellows and M. Tyers (2004). "From large networks to small molecules." Curr Opin Chem Biol **8**(1): 81-90.

Sherman, B. T., D. W. Huang, Q. N. Tan, Y. J. Guo, S. Bour, D. Liu, R. Stephens, M. W. Baseler, H. C. Lane and R. A. Lempicki (2007). "DAVID Knowledgebase: a gene-centered database integrating heterogeneous gene annotation resources to facilitate high-throughput gene functional analysis." Bmc Bioinformatics **8**.

Singer, J. D., M. Gurian-West, B. Clurman and J. M. Roberts (1999). "Cullin-3 targets cyclin E for ubiquitination and controls S phase in mammalian cells." Genes Dev **13**(18): 2375-2387.

Sjostrom, S. K., G. Finn, W. C. Hahn, D. H. Rowitch and A. M. Kenney (2005). "The Cdk1 complex plays a prime role in regulating N-myc phosphorylation and turnover in neural precursors." Dev Cell **9**(3): 327-338.

Slack, A., Z. Chen, R. Tonelli, M. Pule, L. Hunt, A. Pession and J. M. Shohet (2005). "The p53 regulatory gene MDM2 is a direct transcriptional target of MYCN in neuroblastoma." Proc Natl Acad Sci U S A **102**(3): 731-736.

Soucy, T. A., P. G. Smith, M. A. Milhollen, A. J. Berger, J. M. Gavin, S. Adhikari, J. E. Brownell, K. E. Burke, D. P. Cardin, S. Critchley, C. A. Cullis, A. Doucette, J. J. Garnsey, J. L. Gaulin, R. E. Gershman, A. R. Lublinsky, A. McDonald, H. Mizutani, U. Narayanan, E. J. Olhava, S. Peluso, M. Rezaei, M. D. Sintchak, T. Talreja, M. P. Thomas, T. Traore, S. Vyskocil, G. S. Weatherhead, J. Yu, J. Zhang, L. R. Dick, C. F. Claiborne, M. Rolfe, J. B. Bolen and S. P. Langston (2009). "An inhibitor of NEDD8-activating enzyme as a new approach to treat cancer." Nature **458**(7239): 732-736.

Soucy, T. A., P. G. Smith and M. Rolfe (2009). "Targeting NEDD8-Activated Cullin-RING Ligases for the Treatment of Cancer." Clinical Cancer Research **15**(12): 3912-3916.

Spruck, C. H., K. A. Won and S. I. Reed (1999). "Deregulated cyclin E induces chromosome instability." Nature **401**(6750): 297-300.

Stanton, B. R., A. S. Perkins, L. Tessarollo, D. A. Sassoon and L. F. Parada (1992). "Loss of N-myc function results in embryonic lethality and failure of the epithelial component of the embryo to develop." Genes Dev **6**(12a): 2235-2247.

Stanton, L. W., M. Schwab and J. M. Bishop (1986). "Nucleotide sequence of the human N-myc gene." Proc Natl Acad Sci U S A **83**(6): 1772-1776.

Strasser, A., A. W. Harris, M. L. Bath and S. Cory (1990). "Novel primitive lymphoid tumours induced in transgenic mice by cooperation between myc and bcl-2." Nature **348**(6299): 331-333.

Strasser, K., S. Masuda, P. Mason, J. Pfannstiel, M. Oppizzi, S. Rodriguez-Navarro, A. G. Rondon, A. Aguilera, K. Struhl, R. Reed and E. Hurt (2002). "TREX is a conserved complex coupling transcription with messenger RNA export." Nature **417**(6886): 304-308.

Stupack, D. G., X. S. Puente, S. Boutsaboualoy, C. M. Storgard and D. A. Cheresh (2001). "Apoptosis of adherent cells by recruitment of caspase-8 to unligated integrins." J Cell Biol **155**(3): 459-470.

Stupack, D. G., T. Teitz, M. D. Potter, D. Mikolon, P. J. Houghton, V. J. Kidd, J. M. Lahti and D. A. Cheresh (2006). "Potentiation of neuroblastoma metastasis by loss of caspase-8." Nature **439**(7072): 95-99.

Swartling, F. J., V. Savov, A. I. Persson, J. Chen, C. S. Hackett, P. A. Northcott, M. R. Grimmer, J. Lau, L. Chesler, A. Perry, J. J. Phillips, M. D. Taylor and W. A. Weiss (2012). "Distinct neural stem cell populations give rise to disparate brain tumors in response to N-MYC." Cancer Cell **21**(5): 601-613.

Tanaka, N. and M. Fukuzawa (2008). "MYCN downregulates integrin alpha1 to promote invasion of human neuroblastoma cells." Int J Oncol **33**(4): 815-821.

Teitz, T., M. Inoue, M. B. Valentine, K. Zhu, J. E. Rehg, W. Zhao, D. Finkelstein, Y. D. Wang, M. D. Johnson, C. Calabrese, M. Rubinstein, R. Hakem, W. A. Weiss and J. M. Lahti (2013). "Th-MYCN mice with caspase-8 deficiency develop advanced neuroblastoma with bone marrow metastasis." Cancer Res **73**(13): 4086-4097.

Teitz, T., T. Wei, M. B. Valentine, E. F. Vanin, J. Grenet, V. A. Valentine, F. G. Behm, A. T. Look, J. M. Lahti and V. J. Kidd (2000). "Caspase 8 is deleted or silenced preferentially in childhood neuroblastomas with amplification of MYCN." Nat Med **6**(5): 529-535.

Thiele, C. J., C. P. Reynolds and M. A. Israel (1985). "Decreased expression of N-myc precedes retinoic acid-induced morphological differentiation of human neuroblastoma." Nature **313**(6001): 404-406.

Traxler, P., G. Bold, E. Buchdunger, G. Caravatti, P. Furet, P. Manley, T. O'Reilly, J. Wood and J. Zimmermann (2001). "Tyrosine kinase inhibitors: from rational design to clinical trials." Med Res Rev **21**(6): 499-512.

Tsujimoto, Y., L. R. Finger, J. Yunis, P. C. Nowell and C. M. Croce (1984). "Cloning of the chromosome breakpoint of neoplastic B cells with the t(14;18) chromosome translocation." Science **226**(4678): 1097-1099.

Tweddle, D. A., A. J. Malcolm, M. Cole, A. D. Pearson and J. Lunec (2001). "p53 cellular localization and function in neuroblastoma: evidence for defective G(1) arrest despite WAF1 induction in MYCN-amplified cells." Am J Pathol **158**(6): 2067-2077.

Unwalla, H. and J. J. Rossi (2008). "Tat-regulated expression of RNA interference: triggers for the treatment of HIV infection." Curr HIV/AIDS Rep **5**(1): 40-43.

Valli, E., S. Trazzi, C. Fuchs, D. Erriquez, R. Bartesaghi, G. Perini and E. Ciani (2012). "CDKL5, a novel MYCN-repressed gene, blocks cell cycle and promotes differentiation of neuronal cells." Biochim Biophys Acta **1819**(11-12): 1173-1185.

van Golen, C. M., M. E. Soules, A. R. Grauman and E. L. Feldman (2003). "N-Myc overexpression leads to decreased beta1 integrin expression and increased apoptosis in human neuroblastoma cells." Oncogene **22**(17): 2664-2673.

Varlakhanova, N. V., R. F. Cotterman, W. N. deVries, J. Morgan, L. R. Donahue, S. Murray, B. B. Knowles and P. S. Knoepfler (2010). "myc maintains embryonic stem cell pluripotency and self-renewal." Differentiation **80**(1): 9-19.

Vassilev, L. T., C. Tovar, S. Chen, D. Knezevic, X. Zhao, H. Sun, D. C. Heimbrook and L. Chen (2006). "Selective small-molecule inhibitor reveals critical mitotic functions of human CDK1." Proc Natl Acad Sci U S A **103**(28): 10660-10665.

Vermes, I., C. Haanen, H. Steffens-Nakken and C. Reutellingsperger (1995). "A novel assay for apoptosis Flow cytometric detection of phosphatidylserine expression on early apoptotic cells using fluorescein labelled Annexin V." Journal of Immunological Methods **184**(1): 39-51.

Wakamatsu, Y., Y. Watanabe, H. Nakamura and H. Kondoh (1997). "Regulation of the neural crest cell fate by N-myc: promotion of ventral migration and neuronal differentiation." Development **124**(10): 1953-1962.

Walden, H., M. S. Podgorski, D. T. Huang, D. W. Miller, R. J. Howard, D. L. Minor, Jr., J. M. Holton and B. A. Schulman (2003). "The structure of the APPBP1-UBA3-NEDD8-ATP complex reveals the basis for selective ubiquitin-like protein activation by an E1." Mol Cell **12**(6): 1427-1437.

Walden, H., M. S. Podgorski and B. A. Schulman (2003). "Insights into the ubiquitin transfer cascade from the structure of the activating enzyme for NEDD8." Nature **422**(6929): 330-334.

Walworth, N. C. and R. Bernards (1996). "rad-dependent response of the chk1-encoded protein kinase at the DNA damage checkpoint." Science **271**(5247): 353-356.

Wang, Y., I. H. Engels, D. A. Knee, M. Nasoff, Q. L. Deveraux and K. C. Quon (2004). "Synthetic lethal targeting of MYC by activation of the DR5 death receptor pathway." Cancer Cell **5**(5): 501-512.

Wasylishen, A. R. and L. Z. Penn (2010). "Myc: the beauty and the beast." Genes Cancer **1**(6): 532-541.

Weinberg, R. A. (2007). The biology of cancer, Garland Science, Taylor & Francis Group, LLC.

Welcker, M., A. Orian, J. Jin, J. E. Grim, J. W. Harper, R. N. Eisenman and B. E. Clurman (2004). "The Fbw7 tumor suppressor regulates glycogen synthase kinase 3 phosphorylation-dependent c-Myc protein degradation." Proc Natl Acad Sci U S A **101**(24): 9085-9090.

Westermann, F. and M. Schwab (2002). "Genetic parameters of neuroblastomas." Cancer Lett **184**(2): 127-147.

Wingate, H., I. Bedrosian, S. Akli and K. Keyomarsi (2003). "The low molecular weight (LMW) isoforms of cyclin E deregulate the cell cycle of mammary epithelial cells." Cell Cycle **2**(5): 461-466.

Wingate, H., A. Puskas, M. Duong, T. Bui, D. Richardson, Y. Liu, S. L. Tucker, C. Van Pelt, L. Meijer, K. Hunt and K. Keyomarsi (2009). "Low molecular weight cyclin E is specific in breast cancer and is associated with mechanisms of tumor progression." Cell Cycle **8**(7): 1062-1068.

Wu, S., C. Cetinkaya, M. J. Munoz-Alonso, N. von der Lehr, F. Bahram, V. Beuger, M. Eilers, J. Leon and L. G. Larsson (2003). "Myc represses differentiation-induced p21CIP1 expression via Miz-1-dependent interaction with the p21 core promoter." Oncogene **22**(3): 351-360.

Yaari, S., J. Jacob-Hirsch, N. Amariglio, R. Haklai, G. Rechavi and Y. Kloog (2005). "Disruption of cooperation between Ras and MycN in human neuroblastoma cells promotes growth arrest." Clin Cancer Res **11**(12): 4321-4330.

Yada, M., S. Hatakeyama, T. Kamura, M. Nishiyama, R. Tsunematsu, H. Imaki, N. Ishida, F. Okumura, K. Nakayama and K. I. Nakayama (2004). "Phosphorylation-dependent degradation of c-Myc is mediated by the F-box protein Fbw7." Embo j **23**(10): 2116-2125.

Yang, D., H. Liu, A. Goga, S. Kim, M. Yuneva and J. M. Bishop (2010). "Therapeutic potential of a synthetic lethal interaction between the MYC proto-oncogene and inhibition of aurora-B kinase." Proc Natl Acad Sci U S A **107**(31): 13836-13841.

Yoshimura, S. H., K. Hizume, A. Murakami, T. Sutani, K. Takeyasu and M. Yanagida (2002). "Condensin architecture and interaction with DNA: regulatory non-SMC subunits bind to the head of SMC heterodimer." Curr Biol **12**(6): 508-513.

Zaizen, Y., S. Taniguchi, S. Noguchi and S. Suita (1993). "The effect of N-myc amplification and expression on invasiveness of neuroblastoma cells." J Pediatr Surg **28**(6): 766-769.

Zhang, C., Z. Yan, C. L. Painter, Q. Zhang, E. Chen, M. E. Arango, K. Kuszpit, K. Zasadny, M. Hallin, J. Hallin, A. Wong, D. Buckman, G. Sun, M. Qiu, K. Anderes and J. G. Christensen (2009). "PF-00477736 mediates checkpoint kinase 1 signaling pathway and potentiates docetaxel-induced efficacy in xenografts." Clin Cancer Res **15**(14): 4630-4640.

Zhao, X., D. D' Arca, W. K. Lim, M. Brahmachary, M. S. Carro, T. Ludwig, C. C. Cardo, F. Guillemot, K. Aldape, A. Califano, A. Iavarone and A. Lasorella (2009). "The N-Myc-DLL3 Cascade Is Suppressed by the Ubiquitin Ligase Huwe1 to Inhibit Proliferation and Promote Neurogenesis in the Developing Brain." Developmental Cell **17**(2): 210-221.

Zheng, J., X. Yang, J. M. Harrell, S. Ryzhikov, E. H. Shim, K. Lykke-Andersen, N. Wei, H. Sun, R. Kobayashi and H. Zhang (2002). "CAND1 binds to unneddylated CUL1 and regulates the formation of SCF ubiquitin E3 ligase complex." Mol Cell **10**(6): 1519-1526.

Zou, L. and S. J. Elledge (2003). "Sensing DNA damage through ATRIP recognition of RPA-ssDNA complexes." Science **300**(5625): 1542-1548.

Zuin, J., V. Franke, W. F. van Ijcken, A. van der Sloot, I. D. Krantz, M. I. van der Reijden, R. Nakato, B. Lenhard and K. S. Wendt (2014). "A Cohesin-Independent Role for NIPBL at Promoters Provides Insights in CdLS." PLoS Genet **10**(2): e1004153.

Appendix A

List of abbreviations

A selection of abbreviations that can be found in this thesis are explained below. Furthermore the abbreviations of the IUPAC (International union of pure und applied Chemistry) and of the SI-System (Système international d'unités) were used.

A.1 Prefixes

Table 25: Abbreviation for prefixes and multiplication factors

Abbreviation	Prefix	Factor
p	Pico-	10^{-12}
n	Nano-	10^{-9}
µ	Micro-	10^{-6}
m	Mili-	10^{-3}
c	Centi-	10^{-2}

A.2 Units

A ampere

Da dalton

g gram

h hour

J joule

l liter

m meter

min minute

M mol/l mol mol

OD optical density

s second

U unit

vol volume

v/v volume per volume

w/v weight per volume

°C degree celsius

A.3 Proteins, protein domains and other biomolecules

A adenine

ATP adenosine-5'-triphosphate

A alanine

aa amino acid

bp basepair (s)

BTB broad-complex, tramtrack and bric à brac

C cytosine

cDNA complementary DNA

DNA deoxyribonucleic acid

dNTPs deoxyribonucleoside-5'-triphosphate (dATP, dCTG, dGTP, dTTP)

G guanine

GFP green fluorescent protein

GTP guanosine-5'-triphosphate

HRP horseradish peroxidase

K lysine

nt nucleotide(s)

POZ pox virus and zinc finger

R arginine

Rb Retinoblastoma

RFP red fluorescent protein

RNA ribonucleic acid

RNAPII RNA polymerase II

T thymine

TopBP topoisomerase-binding protein

ZF zinc finger

A.4 Chemicals and solutions

APS ammoniumpersulfate

ddH2O bidestilled water

DMEM Dulbeccos Modified Eagle-Medium

DMSO dimethylsulfoxide

DTT dithiothreitol

EDTA ethylendiamintetraacetate

FCS fetal calf serum

FBS fetal bovine serum

NEM N-ethylmaleimide

PBS phosphate-buffered saline

PVDF polyvinylidenfluoride

SDS sodium dodecyl sulfate

TBE Tris-borate-EDTA-buffer

TBS Tris-buffered saline

TBS-T Tris-buffered saline with tween-20

TE Tris-EDTA-buffer

TEMED N,N,N',N'-tetramethylethylendiamine

Tris Tris-(hydroxymethyl)-aminomethan

A.5 Other abbreviations

abs. absolute

approx. approximately

ATCC American Type Culture Collection

ChIP chromosome immunoprecipitation

ECL enhanced chemoluminescence

E. coli Escherichia coli

Inc. Incorporated

IP immunoprecipitation

PAGE polyacrylamide-gelelectrophoresis

PCR polymerase chain reaction

qPCR quantitative PCR

rpm rotations per minute

RT room temperature

o./n. over night; 16-20 h

S1 security level 1

S2 security level 2

wt wild type

Appendix B

Acknowledgements

I would like to express the deepest appreciation to my committee chair Professor Dr. Martin Eilers, who has the attitude and the substance of a genius. He continually and convincingly conveyed a spirit of adventure in regard to research and an excitement in regard to teaching. Without his guidance and persistent help this dissertation would not have been possible.

I would also like to thank my committee member, professor Dr. Manfred Schartl for serving as my committee member, his encouragement, insightful comments and hard questions.

I especially thank Dr. Steffi Herold and Dr. Carsten Ade who corrected my thesis and supported me all the time. I would like to thank you all the members of Group Eilers, Gallant and Wiegering, also former members of laboratory: Joachim, Nikita and Group Murphy. I would also thank Francesca L, Francesca D, Eva, Anne, Maria, Kartrin, Laura, Jing for the moral support and friendship－ I am so glad we had each other.

I want to express my gratitude towards the Graduate School of Life Science for their support and providing soft skill trainings. I also like to thank Federal Ministry of Education and Research for their financial support granted through my predoctoral research.

A special thanks to my family. Words can not express how grateful I am to my mother and father for all of the sacrifices that you've made on my behalf. Your prayer for me was what sustained me thus far. They were always my support in the moments when there was no one to answer my queries.

Appendix C

Curriculum vitae

Appendix D

Affidavit

I hereby confirm that my thesis entitled “A high-complexity lentiviral shRNA screen identifies synthetic lethal interactions with deregulated N-Myc in neuroblastoma cells” is the result of my own work. I did not receive any help or support from commercial consultants. All sources and/or materials applied are listed and speci ed in the thesis.

Furthermore, I confirm that this thesis has not yet been submitted as part of another examination process neither in identical nor in similar form.

Würzburg, May 15, 2014